High-Pressure Catalytic Reactions of C_6 Hydrocarbons on Platinum Single-Crystals and Nanoparticles: A Sum Frequency Generation Vibrational Spectroscopic and Kinetic Study

By

Kaitlin Bratlie

B.S. (University of Minnesota, Twin Cities) 2003

A dissertation submitted in partial fulfillment of the

requirements for the degree of

Doctor of Philosophy

In

Chemistry

in the

Graduate Division

of the

University of California, Berkeley

Committee in charge:

Professor Gabor A. Somorjai
Professor Heino Nitsche
Professor Kyriakos Komvopoulos

Fall 2007

The dissertation of Kaitlin Bratlie is approved:

_____

Chair Date

_____

Date

_____

Date

University of California, Berkeley

2007

High-Pressure Catalytic Reactions of C_6 Hydrocarbons on Platinum Single-Crystals and Nanoparticles: A Sum Frequency Generation Vibrational Spectroscopic and Kinetic Study

by

Kaitlin Bratlie

Abstract

High-Pressure Catalytic Reactions of C_6 Hydrocarbons on Platinum Single-Crystals and Nanoparticles: A Sum Frequency Generation Vibrational Spectroscopic and Kinetic Study

by

Kaitlin Bratlie

Doctor of Philosophy in Chemistry

University of California, Berkeley

Professor Gabor A. Somorjai, Chair

Catalytic reactions of cyclohexene, benzene, *n*-hexane, 2-methylpentane, 3-methylpentane, and 1-hexene on platinum catalysts were monitored *in situ* via sum frequency generation (SFG) vibrational spectroscopy and gas chromatography (GC). SFG is a surface specific vibrational spectroscopic tool capable of monitoring sub-monolayer coverages under reaction conditions without gas-phase interference.

SFG was used to identify the surface intermediates present during catalytic processes on Pt(111) and Pt(100) single-crystals and on cubic and cuboctahedra Pt nanoparticles in the Torr pressure regime and at high temperatures (300K – 450K). At low pressures ($<10^{-6}$ Torr), cyclohexene hydrogenated and dehydrogenates to form cyclohexyl (C_6H_{11}) and π-allyl C_6H_9, respectively, on Pt(100). Increasing pressures to 1.5 Torr form cyclohexyl, π-allyl C_6H_9, and 1,4-cyclohexadiene, illustrating the necessity to investigate catalytic reactions at high-pressures. Simultaneously, GC was used to

acquire turnover rates that were correlated to reactive intermediates observed spectroscopically.

Benzene hydrogenation on Pt(111) and Pt(100) illustrated structure sensitivity via both vibrational spectroscopy and kinetics. Both cyclohexane and cyclohexene were produced on Pt(111), while only cyclohexane was formed on Pt(100). Additionally, π-allyl c-C_6H_9 was found only on Pt(100), indicating that cyclohexene rapidly dehydrogenates on the (100) surface. The structure insensitive production of cyclohexane was found to exhibit a compensation effect and was analyzed using the selective energy transfer (SET) model. The SET model suggests that the Pt-H system donates energy to the E_{2u} mode of free benzene, which leads to catalysis.

Linear C_6 (*n*-hexane, 2-methylpentane, 3-methylpentane, and 1-hexene) hydrocarbons were also investigated in the presence and absence of excess hydrogen on Pt(100). Based on spectroscopic signatures, mechanisms for catalytic isomerization and dehydrocyclization of *n*-hexane were identified.

The structure sensitivity of benzene hydrogenation on shape controlled platinum nanoparticles was also studied. The nanoparticles showed similar selectivities to those found for Pt(111) and Pt(100) single-crystals. Additionally, the nanoparticles have lower activation energies than their single-crystal counterparts.

_____

Professor Gabor A. Somorjai
Dissertation Committee Chair

Table of Contents

List of Figures

Acknowledgments

First and foremost, I would like to thank my advisors Prof. Gabor Somorjai and Prof. Kyriakos Komvopoulos for the opportunity to work on this project. Of course Inger Coble also deserves thanks for all of her assistance over the last four years.

Thanks to Keng Chou and Keith McCrea for providing excellent training on the SFG laser system. Minchul Yang also showed me the ins and outs of traditional surface science techniques. Sasha Kweskin definitely provided enthusiasm towards SFG. Hyunjoo Lee and Susan Habas definitely are in need of thanks for providing so many nanoparticle samples at the drop of a hat. I leave my project in the more than capable hands of Cesar Aliaga, who I have enjoyed working with during the past few months.

Time at the ALS would have been much more painful (and completely unnecessary) without Derek Butcher, Michael Grass, Jeong Park, and Matthias Kobel. I also thank Yimin Li for his tireless efforts on the compensation effect. George Holinga, Will Browne, and Elad Harel definitely made life in and out of the lab much more entertaining. Without equivocation I can say that Lucio Flores made my first two years in graduate school more interesting.

Somorjai group members Chris Kliewer, Russ Renzas, Leonid Belau, Marco Bieri, Yuri Borodko, Wenyu Huang, Feng Tao, Tianfu Zhang, Yawen Zhang, Louis Jones, Anthony Contreras, Max Montano, Diana Phillips, Ozzy Mermut, Mike Ferguson, Staffan Westerberg, David Tang, Rob Rioux, Xiaoming (Mike) Yan, Eric Ji, James Hoefelmeyer, and Mario Farias kept daily life at LBL interesting.

I should thank my parents: Steve and Cindy Bratlie. I probably wouldn't have gone to college, much less to grad school, without their help. My sisters, Meghan and

Kelsey, also deserve some thanks for their support over the years. My grandparents Otto and Glenice Bratlie who unfortunately are no longer here along with my grandparents Ardee and Eunice Johnson are always been a source of inspiration.

Finally, I should thank Roger York. Anyone who knows Roger knows that there is never a dull moment around him. Despite my protest, he did push me into competition throughout grad school. Our "discussions" about chemistry and spectroscopy are some of my fondest scientific memories. Of course our personal interactions have kept me sane.

In addition, this work was supported by the Berkeley-ITRI Research Center (BIRC) under Fund No. 46101-23845-44-EKMAJ, and the Director, Office of Energy Research, Office of Basic Energy Sciences, and Materials Science Division of the U.S. Department of Energy under Contract No. DE-AC02-05CH11231.

Chapter 1

Introduction

Model catalysts have largely been used to reduce the complexities of real catalyst systems. Many ultra-high vacuum (UHV) techniques have been employed to investigate these model systems, such as low-energy electron diffraction (LEED), Auger electron spectroscopy (AES), X-ray photoelectron spectroscopy (XPS), high-resolution electron energy loss spectroscopy (HREELS), and other techniques.[1-6] The major drawback to these studies lies in the limitation of the techniques to low pressure environments due to the large mean free path required for the electrons to reach the sample or detector. Extrapolation of these low-pressure experiments to industrially relevant conditions is not possible since the surface compositions can be significantly different under high-pressure conditions. Photon based techniques are not limited by a mean free path and can be performed at high-pressures. Additionally, vibrational spectroscopies such as Fourier transform infrared (FTIR) and Raman provide molecular information on the surface adsorbates.[6-8] Complications arise in using these techniques as both the bulk material and the gas-phase reactants can contribute to the signal. A relatively new vibrational spectroscopic tool referred to as sum frequency generation (SFG) vibrational spectroscopy has been shown to be surface specific. [9-14] Additionally, the signal is unaffected by gas-phase molecules.[9-14] SFG is a non-linear optical process in which two beams, typically one infrared and one visible, are overlapped temporally and spatially on a surface whereupon a third beam is generated at the sum frequency of the incoming two beams. Tuning the infrared frequency while monitoring the intensity of the sum

frequency results in a vibrational spectrum. The vibrational mode must be both infrared and Raman active. This requirement is only met in matter with no inversion symmetry, which excludes most bulk materials and isotropic phases. This symmetry is necessarily broken at interfaces resulting in a surface sensitive signal.

Gaining molecular information of catalytic reactions *in situ* has been the aim of the studies presented in this thesis. Ideally, a better understanding of catalytic reactions will translate to improvements in industrial processes. Several reactions and specific problems have been investigated. Simultaneous SFG spectroscopic and gas chromatographic measurements are obtained so kinetics can be calculated and correlated to surface intermediates.

Several reactions were studied to determine the effect of structure on reactions and surface adsorbates. The first case is cyclohexene hydrogenation and dehydrogenation on Pt(100). This reaction is known to be structure sensitive and the effects were studied under both UHV and high-pressure conditions. Pressure studies show that the surface adsorbates are different in UHV and high-pressure regimes, illustrating the need to investigate reactions at high-pressures.

The next reaction studied is benzene hydrogenation on both Pt(111) and Pt(100). The hydrogenation of benzene to cyclohexane is found to be structure insensitive while the hydrogenation to cyclohexene is structure sensitive. Spectroscopic studies are able to correlate these differences with surface intermediates formed during reaction. A Langmuir-Hinshelwood mechanism is employed to model the kinetics of cyclohexane production based on a rate-determining step of the addition of the first hydrogen. This assumption is verified by spectroscopic studies that find adsorbed benzene to be the most

abundant surface intermediate. A compensation effect between the pre-exponential and the activation energy for cyclohexane production is also observed and is analyzed using the selective energy transfer model. This model suggests that the Pt-H system donates energy to the E_{2u} mode of free benzene, which leads to catalysis.

The adsorption geometries and surface reactions of various C_6 hydrocarbons (*n*-hexane, 2-methylpentane, 3-methylpentane, and 1-hexene) on Pt(100) are also examined. Different conformations of these various hydrocarbons are explored in the presence and absence of excess hydrogen. The mechanisms for catalytic isomerization and dehydrocyclization of *n*-hexane are elucidated on the basis of these results.

Benzene hydrogenation is also examined on shape controlled platinum nanoparticles. Cubic particles produced only cyclohexane, while cuboctahedral particles produced both cyclohexene and cyclohexane. This result was inline with the single crystal studies. Furthermore, the activation energies on the platinum nanoparticles are lower and corresponding turnover rates are three times higher than those obtained with single-crystal Pt surfaces.

References

(1) Somorjai, G. A. *Introduction to Surface Science Chemistry and Catalysis*; Wiley: New York, 1994.

(2) Contreras, A. M.; Montano, M.; Kweskin, S. J.; Koebel, M. M.; Bratlie, K.; Becraft, K.; Somorjai, G. A. *Topics in Catalysis* **2006**, *40*, 19-34.

(3) Somorjai, G. A.; Bratlie, K. M.; Montano, M. O.; Park, J. Y. *Journal of Physical Chemistry B* **2006**, *110*, 20014-20022.

(4) Goodman, D. W. *Chemical Reviews* **1995**, *95*, 523-536.

(5) Ertl, G. *Surface Science* **1994**, *299*, 742-754.

(6) Woodruff, D. P.; Delchar, T. A. *Modern Techniques of Surface Science*; Cambridge University Press: New York, 1986.

(7) Roberts, N. K. In *Surface Analysis Methods in Material Science*; Springer Series in Surface Sciences ed.; O'Conner, D. J., Sexton, B. A., Smart, R. S. C., Eds.; Springer-Verlag: Berlin, 1992; Vol. 23.

(8) Chabal, Y. J. *Surface Science Reports* **1988**, *8*, 211-357.

(9) Shen, Y. R. *Surface Science* **1994**, *299/300*, 551-562.

(10) Du, Q.; Superfine, R.; Freysz, E.; Shen, Y. R. *Physical Review Letters* **1996**, *70*, 2313-2316.

(11) Johal, M. S.; Ward, R. N.; Davies, P. B. *Journal of Physical Chemistry* **1996**, *100*, 274-279.

(12) Conboy, J. C.; Messmer, M. C.; Richmond, G. L. *Journal of Physical Chemistry* **1996**, *100*, 7617-7622.

(13) Shen, Y. R. *Nature* **1989**, *337*, 519-525.

(14) Buck, M.; Himmelhaus, M. *Journal of Vacuum Science and Technology A-Vacuum Surfaces and Films* **2001**, *19*, 2717-2736.

Chapter 2

Experimental Methods

Two catalytic systems were studied throughout this dissertation: platinum single-crystals and nanoparticles. Both of these systems require characterization techniques and unique reaction cells. Through detailed studies of single-crystals and nanoparticles, a more comprehensive understanding of catalytic processes can be achieved.

2.1. Introduction

In order to conduct a detailed study of atomically clean surfaces, we must work under ultra high vacuum (UHV) conditions. A rough estimate using the following equation illustrates the importance of maintaining a UHV environment.

$$F = \frac{N_A P}{\sqrt{2\pi MRT}} \tag{2.1}$$

or

$$F(molecules \cdot cm^{-2} \cdot s^{-1}) = 3.51 \times 10^{22} \frac{P(Torr)}{\sqrt{M(g/mole)T}} \tag{2.2}$$

where F is the flux of molecules striking the surface of unit area, P is the pressure of the gas in Torr, N_A is Avogadro's number, R is the gas constant, M is the average molar weight of the gas, and T is the temperature. Substituting the molecular weight of carbon monoxide for M, room temperature for T, and assuming a pressure of 3×10^{-6} Torr yields a flux of $\sim 10^{15}$ molecules $\cdot$ cm^{-2} $\cdot$ s^{-1}. Since 1 cm^2 of the surface has approximately 10^{15} atoms, the amount of time necessary to cover the surface with 1 monolayer (ML) of CO is about 1 s at these pressures. From this basis, the Langmuir (1L

= 1 × 10^{-6} Torr · s) unit is defined as the exposure corresponding to one monolayer of coverage assuming a sticking coefficient of unity. Pressures on the order of 10^{-9} Torr will result in a monolayer in 10^3 s. Current surface analytical techniques are capable of detecting 1% of a monolayer of contamination on a surface meaning that at UHV conditions (~10^{-9} Torr) a clean surface may be maintained for approximately one hour.

2.2. Sample Preparation

The single-crystals used were Pt(100) and Pt(111) cut within 0.3° of accuracy from Matek Corporation. The crystal was mounted in Koldmount epoxy and polished using Metadi diamond paste polishing compound on Buehler Microcloth polishing cloths. Starting with a grit size of 15 micron, the grit size was deduced to 6 microns, then 1 micron, and finally 0.25 microns. After satisfactorily polishing the crystal, the epoxy was removed by sonication in acetone. Once the crystal was removed from the epoxy, it was etched in room temperature aqua regia to remove surface defects caused by the polishing process. The crystal was then sonicated in deionized water to remove residual acid.

The Pt(100) and Pt(111) crystals were cleaned by sputtering with Ar^+ ions (1 keV) for 20 minutes, heating to 1123 K in the presence of 5 × 10^{-7} Torr O_2 for 2 minutes, and then annealing at 1123 K for 2 minutes. Auger electron spectrosocpy was used to verify the cleanliness of the Pt(100) or Pt(111) surface after several cleaning cycles.

2.3. Auger Electron Spectroscopy (AES)

Auger electron spectroscopy (AES) is an electron-in-electron-out process employed to monitor the cleanliness of a surface. The surface sensitivity of this

technique results from the limited depth penetration of electrons. The mean free path of electrons is the average distance a particle travels between collisions with other particles that can be calculated from the following equation:

$$\lambda = (n\sigma)^{-1} \tag{2.3}$$

where λ is the mean free path, n is the number of particles per unit volume, and σ is the effective cross sectional area for collision.

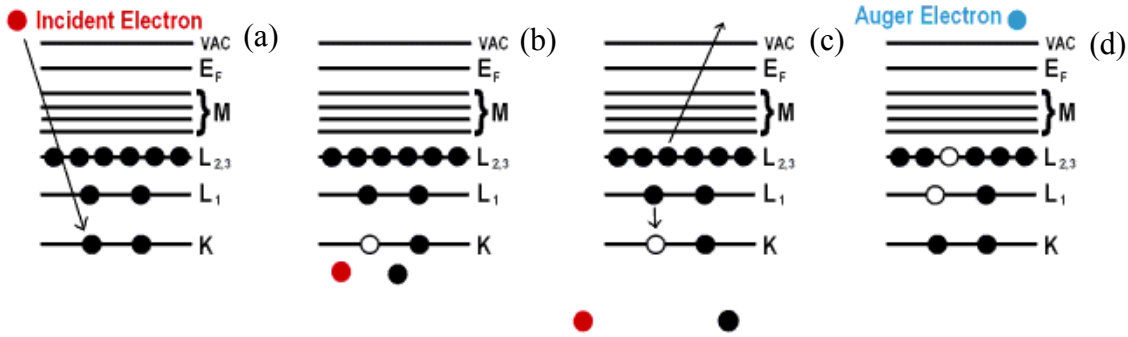

Figure 2.1. Diagram of the four step Auger process: (a) high energy electrons bombard the surface atoms, (b) atomic ionization results from the removal of a core electron, (c) a higher shell electron collapses to fill a core vacancy, and (d) energy released from collapse results in the emission of an outer shell electron known as the Auger electron.

AES uses the Auger process, illustrated in figure 2.1, to detect atomic species present on the surface. To accomplish this, high energy electrons (3 keV) impact the surface and eject a core electron. An outer shell electron then decays to fill the inner core hole allowing an Auger electron to be ejected. The Auger process is nonradiative and depends on electrostatic forces between a hole and the surrounding electron cloud. The ejected Auger electron has a characteristic kinetic energy (KE) that can be calculated from the following equation:

$$KE = E_a - E_b - E_c \tag{2.4}$$

where E_a is the energy of the core electron that was removed, E_{bc} is the energy of the electron that fills the empty orbital, and E_c is the energy of the outer shell electron ejected.

Auger electron spectroscopy can also be used as a quantitative technique for chemical analysis and has a sensitivity of about 1% of a monolayer.[1] A method[2] consisting of plotting the Auger peak-to-peak signal intensity from the substrate against the similar signal from the adsorbate yields the following equation:

$$\theta_1^0 = \left(1 + \frac{I_S I_{A_1}}{I_A I_{S_1}} \alpha_S^A - \alpha_S^A \right)^{-1} \tag{2.5}$$

where θ_1^0 is the coverage as the first layer forms, I_S and I_A are the Auger peak intensities corresponding to this coverage, $\alpha_S^A = \frac{I_{S_1}}{I_S}$ is the coefficient of attenuation of the substrate Auger peak due to the presence of a monolayer or adsorbate, and I_{S_1} is the peak-to-peak intensity of the Auger signal due to the substrate covered with a monolayer, and I_{A_1} is the Auger peak intensity due to a monolayer of adsorbate. After determining α_S^A, I_{S_1}, and I_{A_1}, equation 2.5 becomes:

$$\theta_1^0 = \left(0.4 + 1.92 \frac{I_{Pt_{237}}}{I_{C_{272}}} \right)^{-1} . \tag{2.6}$$

Where $I_{Pt_{237}}$ and $I_{C_{272}}$ are the intensities of the Pt peak at a kinetic energy of 237 eV and of the C peak at a kinetic energy of 272 eV, respectively. Using equation 2.4, the surface coverage of carbon on platinum single crystals can be determined.

A representative Auger spectrum is shown in figure 2.2. The bottom spectrum shows the Pt(100) surface before the previously discussed sputtering and annealing cleaning procedure. Using equation 2.6, a carbon surface coverage of 13% is found. After three cycles of the cleaning procedure this peak has been largely removed (carbon surface coverage <1%) and only the signature platinum peaks remain.

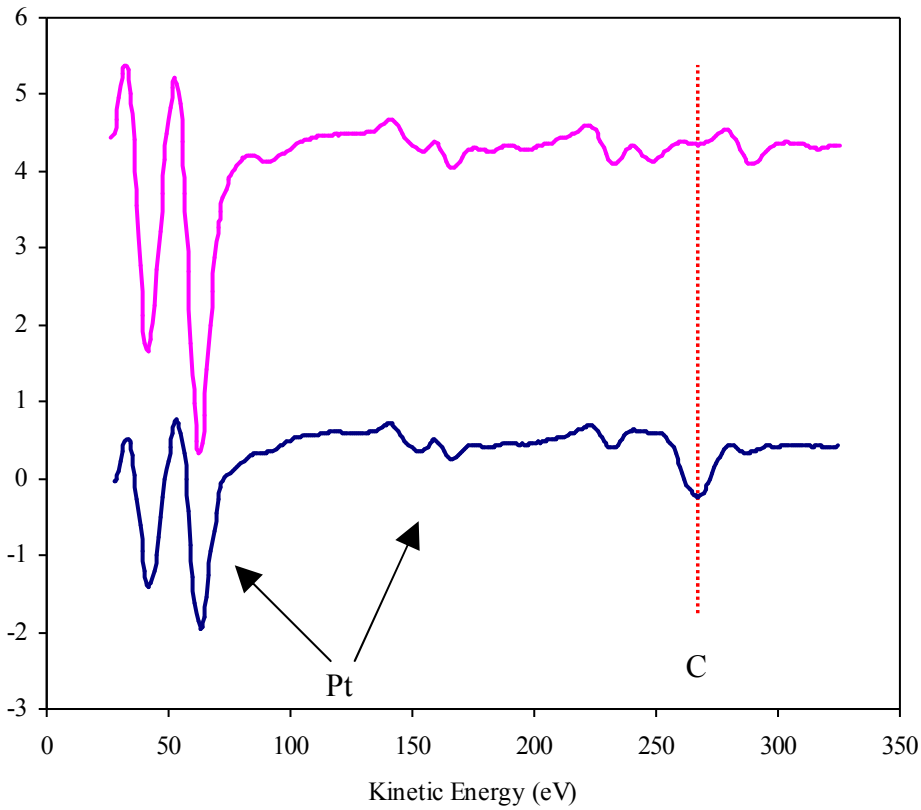

Figure 2.2. Sample Auger spectra of Pt(100). The carbon peak is clearly visible in the bottom spectrum and yields a surface coverage of 13%. After three cleaning cycles, the top spectrum shows the carbon is removed from the surface with a surface coverage of <1%.

2.4. Scanning Electron Microscopy

Scanning electron microscopy (SEM) is a powerful imaging technique that is capable of producing high resolution images of surfaces. Characterizing nanoparticle surfaces before and after reaction is important to ensure the particles have not aggregated and also for determining surface coverages to normalize kinetic results for sample-to-sample deviations. In SEM, a stream of electrons are emitted from an electron gun and accelerated at a surface of interest. The electrons pass through several metal apertures and magnetic lenses to produce a tightly focused high energy electron beam. The electron beam is raster scanned across the surface via electromagnetic deflection coils. The backscattered and secondary electrons emitted from the surface are collected and converted into an image of the surface.[3-5] The set-up of an SEM is shown in figure 2.3.

Two different types of interactions result from exposure of the surface to the electron beam: elastic and inelastic. Backscattered electrons result from elastic processes while inelastic processes generate secondary electrons, Auger electrons, characteristic and bremsstrahlung x-rays, and cathodoluminescence. While backscattered electrons are the dominant feature, at lower energies (<50 eV) the number of electrons emitted sharply increases to levels far above the expected contribution from backscattered electrons; this rise is attributed to the secondary electrons. Secondary electrons result from interactions between energetic electrons and the loosely bound conduction band electrons in metal or outer-shell valence electrons in semi-conductors and insulators. The energy transfer of this process is not efficient due to the energy difference between the incident electrons and the sample electrons. Both secondary and backscattered electrons are collected and processed to produce and image with SEM. Both surface topography and chemical

composition influence the intensities of the backscattered and secondary electrons. Since most secondary electrons have low kinetic energies (~10 eV), these electrons typically originate within a few nanometers from the surface and are very sensitive to topographical variations allowing for higher resolution images. The more energetic backscattered electrons are more chemically sensitive resulting from the Z^2 (Z = atomic number) dependence of the event.

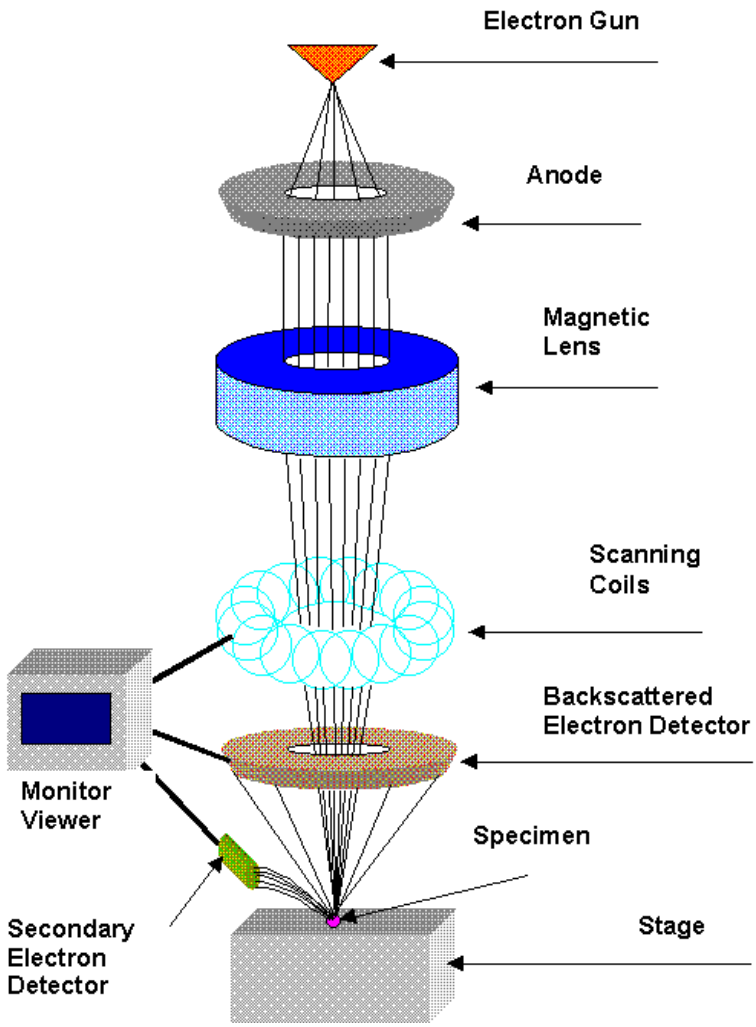

Figure 2.3. Schematic of scanning electron microscope.

The SEM images presented in this thesis were taken with a Zeiss Gemini Ultra-55 field emission SEM. The typical experimental parameters used were 5 – 10 keV acceleration voltage, 12 μA emission current, and a working distance of 3 – 4 mm.

2.5. High Pressure Reaction Cell

The 600-mL stainless steel high pressure (HP) cell for single-crystal catalysis has several ports and is electroplated with gold to reduce catalytic reactivity. A leak valve connects the gas line to the UHV chamber/quadrupole mass spectrometer and can be used to sample the gas products during reaction. Two CaF_2 conflat windows on the HP cell are mounted 120° with respect to one another allowing transmission of infrared (IR), visible (VIS), and sum frequency beams during experiments. The HP cell is equipped with a re-circulation loop that includes a diaphragm pump and inlet for gas chromatographic (GC) (Hewlett Packard 6890) analysis. In GC analysis, a gaseous mobile phase flows under pressure through a heated packed column. Once on the column separation of a mixture occurs according to the relative lengths of time spent by its components in the stationary phase. The reactant and product gases were constantly mixed via the recirculation pump while kinetics were determined by periodically sampling the reaction mixture and measuring mole% gas phase composition using flame ionization detection and a packed column (0.1% AT-1000 on Graphpac GC 80/100 Alltech). The operating pressure in the HP cell is measured with two capacitance manometers (MKS, 722A), for pressure ranges between 0.1 and 1000 mTorr and between 0.1 and 1000 Torr. The high pressure cell is illustrated in figure 2.4.

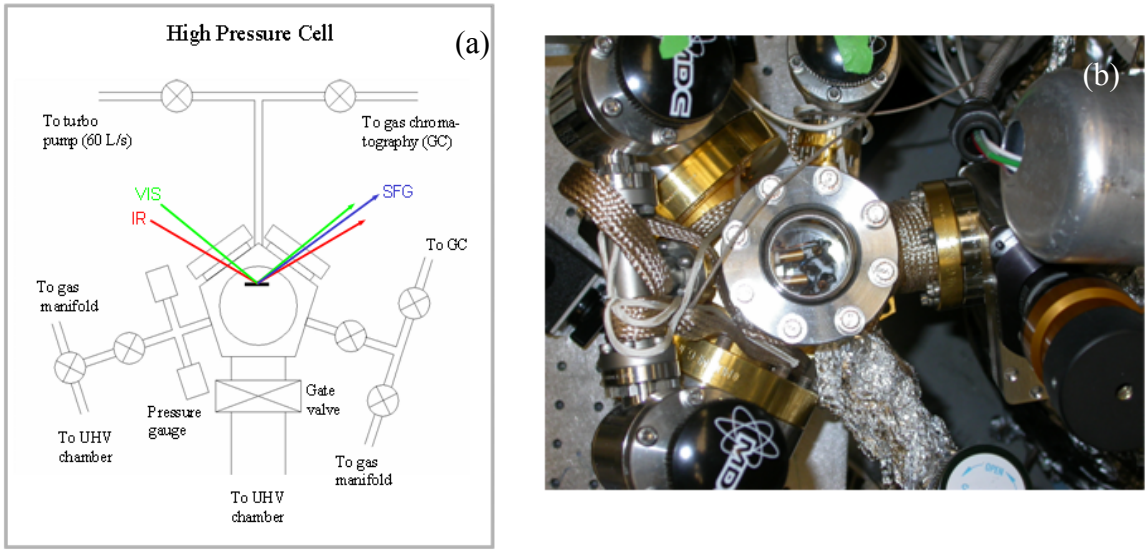

Figure 2.4. (a) Schematic and (b) photograph of the *in situ* SFG high pressure reaction cell.

2.6. Nanoparticle Reaction Cell

Nanoparticle catalytic studies were carried out in a custom-made reaction cell under continuous batch reactor conditions, shown in figure 2.5. A silicon wafer or quartz prism coated with a nanoparticle monolayer was pressed against a rubber O-ring by tightening a teflon block with two set screws. The temperature at the wafer surface was measured with a thermocouple placed directly onto the sample. Heating was applied at the top of the wafer by a Kapton resistive element (Omega Engineering). Temperature variations across the 20 × 20 mm^2 wafer area were insignificant. The reaction cell was connected to a stainless steel tubing gas manifold of diameter equal to 0.3175 cm. A vacuum pressure of less than 1 mTorr was maintained in the reaction cell by mechanical and turbomolecular pumps.

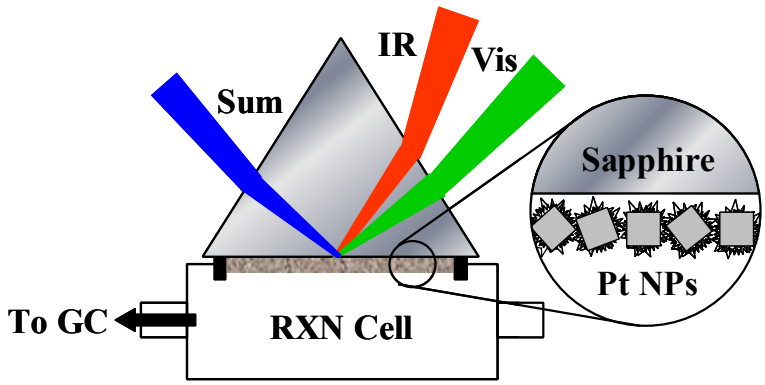

Figure 2.5. Schematic of the *in situ* SFG reaction cell with a monolayer of Pt nanoparticles.

The reaction cell is equipped with a recirculation loop that includes a diaphragm pump and a septum for GC analysis. The reactant and product gases were constantly mixed by the recirculation pump, while kinetic data were acquired periodically by sampling the reaction mixture and measuring the relative gas phase composition. Kinetic measurements were obtained with GC system (Hewlett Packard 6890) using flame ionization detection and a 0.1% AT-1000 on Graphpac GC 80/100 packed column of 180 m length and 0.3175 cm outside diameter (Alltech). Helium was used as carrier gas and the oven temperature was maintained at 413 K.

References

(1) Somorjai, G. A. *Introduction to Surface Science Chemistry and Catalysis*; Wiley: New York, 1994.

(2) Biberian, J. P.; Somorjai, G. A. *Applications of Surface Science* **1979**, *2*, 352-358.

(3) Flefler, S. L.; Heckman, J. W.; Klomparens, K. L. *Scanning and Transmission Electron Microscopy: An Introduction*; Oxford University Press: New York, 1993.

(4) Hayat, M. A. *Principles and Techniques of Scanning Electron Microscopy*; Van Nostrand Reinhold: New York, 1974.

(5) Goldstein, J. I.; Newbury, D. E.; Echlin, P.; D.C., J.; Romig, A. D.; Lyman, C. E.; Fiori, C.; Lifshin, E. *Scanning Electron Microscopy and X-Ray Microanalysis: A Text for Biologists, Materials Scientists, and Geologists*; 2nd ed.; Plenum Press: New York, 1992.

Chapter 3

Sum Frequency Generation

Sum frequency generation is a powerful surface-specific vibrational spectroscopy with sub-monolayer sensitivity. Isotropic materials, such as the gas phase, do not produce sum frequency signal, allowing only adsorbates present on the surface to contribute to the spectrum. This allows SFG to be an extremely useful tool for vibrational studies of catalytic reactions performed at high pressures.

3.1. Sum Frequency Generation Theory

Sum frequency generation vibrational spectroscopy (SFG) was first observed[1] and described[2] in the 1960s. However, the technique was not developed and shown to be surface-specific until the 1980s by Y.R. Shen.[3] Since then, SFG as a technique for vibrational spectroscopy has been extensively described.[4-12] The principle of SFG is regulated by second-order nonlinear optics, and the technique itself is permitted by high-energy electric fields, in this case pulsed lasers. Under weak electric fields, the polarization $\vec{P}$ expansion has two terms as shown in equation 3.1, where $\vec{P}^{(0)}$ is the static polarization, $\vec{P}^{(1)}$ is the first-order linear polarization, ε_0 is the permittivity of free space, $\vec{\chi}^{(1)}$ is the linear susceptibility, t is time, and $\vec{E}(r)\cos(\omega t)$ describes the electric field.

$$\vec{P} \approx \vec{P}^{(0)} + \vec{P}^{(1)} = \vec{P}^{(0)} + \varepsilon_0 \vec{\chi}^{(1)} \vec{E}(r)\cos(\omega t) \qquad (3.1)$$

For linear optics, this equation shows that the frequency of the light is invariant as it passes through a medium.

Under strong electric fields, the polarization can be further expanded to include higher-order terms.

$$\vec{P} \approx \vec{P}^{(0)} + \vec{P}^{(1)} + \vec{P}^{(2)} + \vec{P}^{(3)} + ... \tag{3.2}$$

The second-order polarization, $P_i^{(2)}$, where $\chi_{ijk}^{(2)}$ is the second-order nonlinear susceptibility and $\vec{E}_j(r)\cos(\omega_1 t)$ and $\vec{E}_k(r)\cos(\omega_2 t)$ are the two input fields at different frequencies is given by equation 3.3

$$P_i^{(2)} = \varepsilon_0 \sum_{j,k} \chi_{ijk}^{(2)} \vec{E}_j(r)\cos(\omega_1 t)\vec{E}_k(r)\cos(\omega_2 t) \tag{3.3}$$

Which can be rearranged to form

$$P_i^{(2)} = \tfrac{1}{2}\varepsilon_0 \sum_{j,k} \chi_{ijk}^{(2)} \vec{E}_j(r)\vec{E}_k(r)\left[\cos(\omega_1 + \omega_2)t + \cos(\omega_1 - \omega_2)t\right]. \tag{1.4}$$

Equation 3.4 illustrates how the frequency of light can change after passing through a medium, resulting in a SFG and difference frequency generation (DFG). In SFG vibrational spectroscopy, ω_1 is typically chosen to be in the visible region of the spectrum while ω_2 is in the infrared.

The sum frequency radiation is strongly peaked in one direction determined by phase matching conditions. Efficient energy transfer from the ω_{vis} and ω_{IR} to the sum frequency ω_{SF} occurs when both energy and momentum are conserved. Energy conservation requires that $\omega_{SF} = \omega_{vis} + \omega_{IR}$, while momentum conservation requires

$$\vec{k}_{SF} = \vec{k}_{vis} + \vec{k}_{IR}. \tag{3.5}$$

Equation 3.5 can be rewritten for the angles of incidence for the visible and infrared beams.

$$k_{SF}\sin\theta_{SF} = k_{vis}\sin\theta_{vis} + k_{IR}\sin\theta_{IR} \tag{3.6}$$

where k_{SF}, k_{vis}, and k_{IR} are the three wavenumbers ($2\pi/\lambda$), θ_{vis} and θ_{IR} are the angles of incidence compared to the surface normal of the visible and IR laser beams, and θ_{SF} is the angle of the sum frequency radiation. From this equation, it can be noted that the angle of emission changes as ω_{IR} is scanned over the spectrum.

The magnitude of the SFG signal is proportional to the absolute square of $\chi_{eff}^{(2)}$ shown in equation 3.7.

$$I(\omega_{SF}) \propto \left|\chi_{eff}^{(2)}\right|^2 = \left|\chi_{NR}^{(2)} + \chi_{R}^{(2)}\right|^2 \tag{3.7}$$

$\chi_{eff}^{(2)}$ is comprised of both a non-resonant susceptibility term, $\chi_{NR}^{(2)}$, and a resonant susceptibility term, $\chi_{R}^{(2)}$. The non-resonant susceptibility term arises from the substrate surface and is typically invariant as the IR beam is scanned over the spectrum.

The surface specificity in SFG arises from the fact that $\chi^{(2)}$ is a third rank tensor whose element values depend on the properties of the medium under investigation. For centrosymmetric media, $\chi^{(2)}$ should be invariant under inversion symmetry, however, the electric field and the polarization must change signs as vectors. From equation 3.3, one can see that the inversion operator will result in $\chi^{(2)} = -\chi^{(2)}$ or $\chi^{(2)} = 0$, thus yielding no SFG signal from media with inversion symmetry. For centrosymmetric media to generate SFG signal, the inversion symmetry must be broken, which is only necessarily true at an interface or surface.

The resonant susceptibility, which originates from vibrational modes on the surface, can be described by equation 3.8.

$$\chi_R^{(2)} = N\chi_{ijk}^{(2)} \sum_{i,j,k} \langle (\hat{i}\cdot\hat{l})(\hat{j}\cdot\hat{m})(\hat{k}\cdot\hat{n})\rangle \frac{A_q}{\omega_{IR} - \omega_q + i\Gamma_q} \Delta\rho_{gq} \qquad (3.8)$$

where A_q is the strength of the q[th] vibrational mode, N is the number density of molecules on the surface, ω_{IR} is the frequency of the infrared laser beam, ω_q is the frequency of the q[th] vibrational mode, Γ_q is the damping constant of the q[th] vibrational mode, and $\Delta\rho_{gq}$ is the population difference between the ground and first excited states. The subscripts l, m, and n refer to the axes for the molecular coordinate system and so the average, $\langle (\hat{i}\cdot\hat{l})(\hat{j}\cdot\hat{m})(\hat{k}\cdot\hat{n})\rangle$, is the coordination transformation from molecular fixed coordinates to laboratory fixed coordinates averaged over molecular orientations. Since this average is over all of the molecular orientations, the adsorbates must have some ordering to produce a sum frequency signal. Additionally, isotropic media are also SFG forbidden. From equation 1.8, one can see that $\chi_R^{(2)}$ reaches a maximum when $\omega_{IR} = \omega_q$, and hence a vibrational spectrum is acquired by scanning the IR frequency.

Selection rules for the SFG process can be inferred from equation 3.9.

$$A_q = \frac{1}{2\omega_q} \frac{\partial\mu_n}{\partial q} \frac{\partial\alpha_{lm}^{(1)}}{\partial q} \qquad (3.9)$$

where μ_n is the dipole moment and $\alpha_{lm}^{(1)}$ is the polarizability. Hence, in order for $\chi_R^{(2)}$ to be non-zero, the vibrational mode of interest must be both IR and Raman active.

3.2. Sum Frequency Generation from a Surface

In general, the surface susceptibility $\chi^{(2)}$ is a 27-element tensor, however, it can often be reduced to several non-vanishing elements by symmetry constraints. Interfaces are isotropic in the plane of the surface. The symmetry constraints for an in-plane isotropic surface reduces $\chi^{(2)}$ to the following four independent non-zero elements

$$\chi^{(2)}_{zzz}; \chi^{(2)}_{xxz} = \chi^{(2)}_{yyz}; \chi^{(2)}_{xzx} = \chi^{(2)}_{yzy}; \chi^{(2)}_{zxx} = \chi^{(2)}_{zyy} \tag{3.10}$$

Where z is defined to be the direction normal to the surface. These four independent elements contribute to the SFG signal under four different polarization conditions: ppp, ssp, sps, and pss, where the polarizations are listed in order of decreasing frequency (SF, vis, IR). P polarization occurs when the electrical field vector is parallel to the plane of incidence, which contains the surface normal and the incident beam. The vector is perpendicular to the plane of incidence in s polarization.

Information about molecular orientation of the adsorbate on the surface may be determined using different polarization combinations of IR, vis, and SF radiation on non-metal surfaces.[13] Different susceptibility components are measured for each polarization combination used during an SFG experiment. These polarization combinations determine the ratios of the different tensor elements, which provides molecular orientation information. The orientation of adsorbates can be extracted through modeling of the susceptibility components. However, this characterization technique is not possible on single-crystals due to the metal-surface-selection-rule (MSSR). Due to the freedom of the conduction electrons to respond to electric fields, the charge above the surface of a metal produces lines of force as if there was a negative charge at an equal distance below the surface, known as an image charge. Ergo, dipoles parallel to the

surface will become invisible while dipole perpendicular to the surface will become enhanced, as seen in figure 3.1.

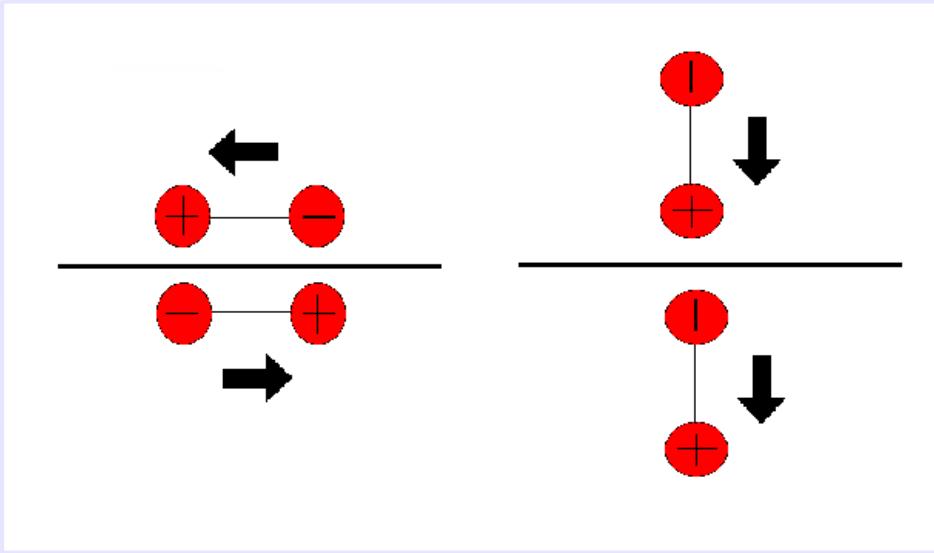

Figure 3.1. The electrical image resulting during the vibration of a dipole parallel and perpendicular to the surface of the metal.

3.3. Sum Frequency Generation Experimental Setup

All SFG spectra were obtained using a mode-locked Nd:YAG laser (Leopard D20, Continuum) (1064 nm fundamental having a 20 ps long pulse with a 20 Hz repetition rate). The 1064 nm beam was frequency doubled to 532 nm in a β-BaB_2O_4 (BBO) crystal. The tunable IR beam was generated in a $LiNbO_3$ or a $AgGaS_2$ by difference frequency mixing of the 1064 nm beam with the output of a $KTiOPO_4$ (KTP) optical parametric generator/amplifier (OPA/OPG) pumped by the 532 nm beam. A schematic of the OPA/OPG is illustrated in figure 3.2. The VIS beam (200 μJ) and the IR (200 μJ) beams were spatially and temporally overlapped on the Pt(100) surface with incident angles of 55º and 60º, respectively, with respect to the surface normal. All

single-crystal spectra were taken using a ppp polarization combination (SFG, VIS, and IR beams were all p-polarized) while the nanoparticle spectra were taken in ppp and ssp polarizations. The generated SFG beam was sent through a monochromator and the signal intensity was detected with a photomultiplier tube (Hamamatsu) and a gated integrator (Stanford Research) as the IR beam was scanned over the range of interest.

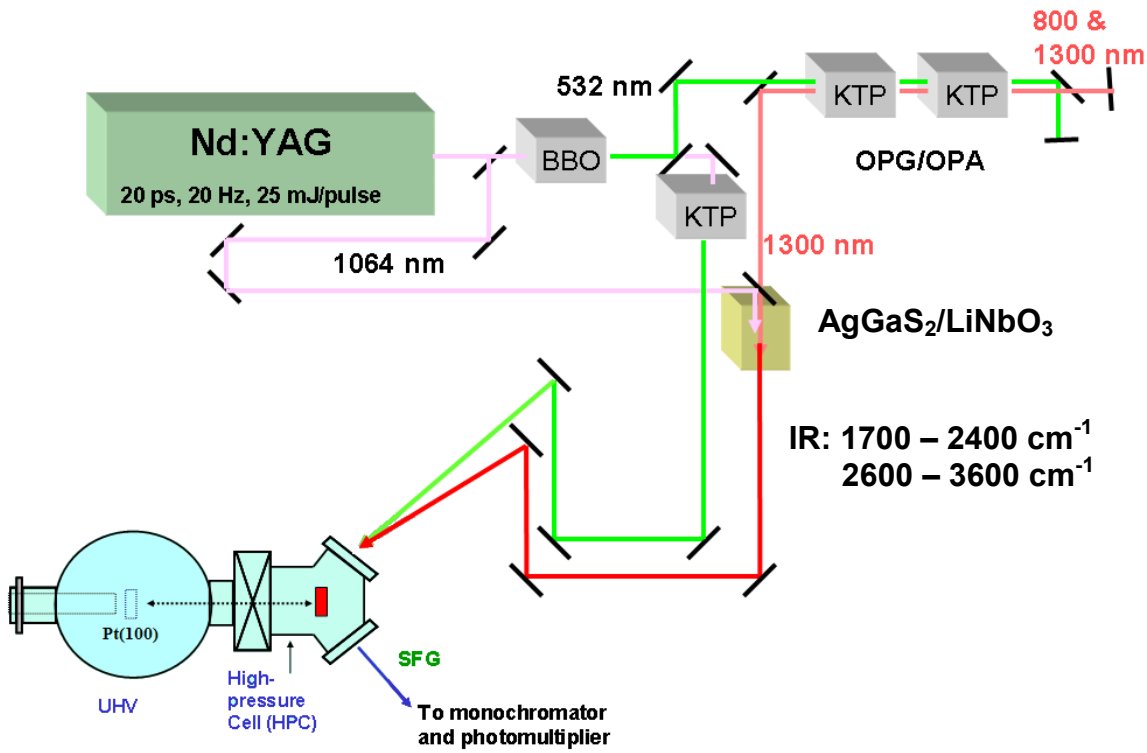

Figure 3.2. Schematic of OPG/OPA system to generate laser beams used for SFG experiments. Tuning range is between 1700 – 2400 cm^{-1} and 2600 - 3600 cm^{-1}.

References

(1) Bass, M.; Franken, P. A.; Hill, A. E.; Peters, C. W.; Wieinreich, G. *Physical Review Letters* **1962**, *8*, 18-18.

(2) Bloembergen, N. *Nonlinear Optics*; Benjamin: New York, 1965.

(3) Hunt, J. H.; Guyot-Sionnest, P.; Shen, Y. R. *Chemical Physics Letters* **1987**, *133*, 189-192.

(4) Shen, Y. R. *Nature* **1989**, *337*, 519-525.

(5) Shen, Y. R. *Annual Review of Physical Chemistry* **1989**, *40*, 327-350.

(6) Shen, Y. R. *Surface Science* **1994**, *299/300*, 551-562.

(7) Shen, Y. R. *The Principles of Nonlinear Optics*; Wiley: New York, 2003.

(8) Du, Q.; Superfine, R.; Freysz, E.; Shen, Y. R. *Physical Review Letters* **1996**, *70*, 2313-2316.

(9) Johal, M. S.; Ward, R. N.; Davies, P. B. *Journal of Physical Chemistry* **1996**, *100*, 274-279.

(10) Conboy, J. C.; Messmer, M. C.; Richmond, G. L. *Journal of Physical Chemistry* **1996**, *100*, 7617-7622.

(11) Buck, M.; Himmelhaus, M. *Journal of Vacuum Science and Technology A-Vacuum Surfaces and Films* **2001**, *19*, 2717-2736.

(12) Hirose, C.; Akamatsu, N.; Domen, K. *Applied Spectroscopy* **1992**, *46*, 1051-1072.

(13) Hirose, C.; Yamamoto, H.; Akamatsu, N.; Domen, K. *Journal of Chemical Physics* **1993**, *97*, 10064-10069.

Chapter 4

Hydrogenation and Dehydrogenation of Cyclohexene on Pt(100): A Sum Frequency Generation Vibrational Spectroscopic and Kinetic Study

This chapter illustrates the use of sum frequency generation (SFG) vibrational spectroscopy to study the hydrogenation/dehydrogenation of cyclohexene on Pt(111). SFG vibrational spectroscopy and kinetic measurements were performed during cyclohexene hydrogenation/dehydrogenation over a range of pressures (10^{-8}-5 Torr) and temperatures (300-500 K) on the Pt(100) surface. Upon adsorption at pressures below 1.5 Torr and at 300 K, cyclohexene dehydrogenates to form π-allyl c-C_6H_9 and hydrogenates to form cyclohexyl (C_6H_{11}) surface intermediates. Increasing the pressure to 1.5 Torr produces adsorbed 1,4-cyclohexadiene, π-allyl c-C_6H_9, and cyclohexyl species. These adsorbed molecules are found both in the absence and presence of excess hydrogen on the Pt(100) surface at high pressures and up to 380 K and 360 K, respectively. π-Allyl c-C_6H_9 and cyclohexyl are adsorbed on the surface up to 440 K in the absence of excess hydrogen and 460 K in the presence of excess hydrogen, at which point they are no longer detectable by SFG. Kinetic studies in the absence of excess hydrogen show that the apparent activation energy for the dehydrogenation pathway (14.3 ± 1.2. kcal/mol) is similar to that of the hydrogenation pathway (12.9 ± 0.6 kcal/mol). Different apparent activation energies are observed for the dehydrogenation

pathway (22.4 ± 1.6 kcal/mol) and the hydrogenation pathway (18.8 ± 0.9 kcal/mol) in the presence of excess hydrogen.

4.1. Introduction

(a) π-allyl c-C_6H_9 (b) quadra-σ 1,4-cyclohexadiene (C_6H_8)

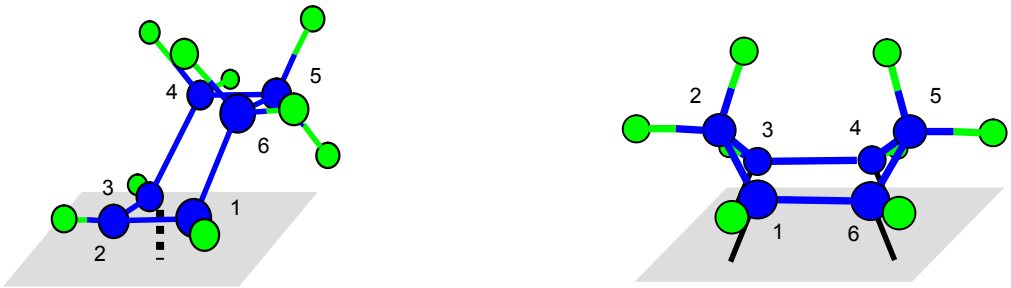

(c) cyclohexyl (C_6H_{11})

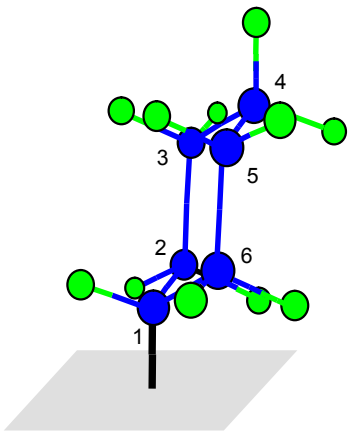

Scheme 4.1 Schematic diagram of (a) π-allyl c-C_6H_9, (b) quadra-σ 1,4-cyclohexadiene (C_6H_8), and (c) cyclohexyl (C_6H_{11}) intermediates.

Cyclohexene surface chemistry on single crystal platinum has received significant attention since it is considered prototypical of cyclic hydrocarbon conversion processes during naphtha reforming.[1] Cyclohexene is not only one of the possible reaction intermediates when cyclohexane (C_6H_{10}) is dehydrogenated to benzene (C_6H_6), but also a

reactant molecule that can be either hydrogenated to cyclohexane or dehydrogenated to benzene. Cyclohexene hydrogenation/dehydrogenation on the platinum surface is found to be structure sensitive[2, 2] since its turnover rates are sensitive to surface structure.

Cyclohexene adsorption on Pt(100) at low pressures ($\leq 10^{-6}$ Torr) has been studied using thermal desorption spectroscopy (TDS),[3-5] RAIRS,[3] and EEL spectroscopy.[3] Briefly, cyclohexene exists in a di-σ form on Pt(100) at 100 K. As the surface temperature is increased to 200 K, di-σ cyclohexene is converted to π-allyl c-C_6H_9. Further increasing the surface temperature leads to dehydrogenation and benzene desorption.[3] The surface species present at low pressures/temperatures under UHV may not necessarily be the same as those species that are adsorbed under catalytically relevant conditions found at high pressures/temperatures or under an excess of hydrogen. The observed surface species at various temperatures at low pressures are summarized in scheme 4.2(e)

Cyclohexene adsorption on the Pt(111) surface has been studied using various techniques such as TDS,[5] bismuth post dosing TDS (BPTDS),[5,6] laser-induced thermal desorption (LITD),[4] high-resolution electron energy loss spectroscopy (HREELS),[3,4] RAIRS,[7] and SFG[8-13] under a broad range of pressure (10^{-8}-5 Torr). Briefly, at low pressures ($\leq 10^{-6}$ Torr) on Pt(111) cyclohexene adsorbs molecularly in a di-σ form at 100 K and is dehydrogenated to π-allyl c-C_6H_9 as the surface temperature is increased to 200 K.[6,7] π-Allyl c-C_6H_9 further dehydrogenates to benzene as the surface temperature is increased up to 300 K and desorption and decomposition of benzene at temperatures ≥300 K.[4,6,7] Increasing the cyclohexene pressure to 1.5 Torr at 298 K interestingly results in the dehydrogenation of π-allyl c-C_6H_9 to 1,4-cyclohexadiene. Increasing the surface

temperature in the absence of excess hydrogen results in hydrogenation of 1,4-cyclohexadiene to π-allyl c-C_6H_9 at 323 K. Similarly, π-Allyl c-C_6H_9 dehydrogenates to benzene as the temperatures increase s to 453 K.[8] The observed surface species at various temperatures and pressures on Pt(111) are summarized in scheme 4.2(b), (d), and(f).

In the presence of excess hydrogen (15 Torr), it was found that 1,4-cyclohexadiene and 1,3-cyclohexadiene co-exist on Pt(111) at 303 K and subsequently hydrogenate to π-allyl c-C_6H_9 at 323 K. As the surface temperature is increased to 400 K, π-allyl c-C_6H_9 dehydrogenates to 1,3-cyclohexadiene.[8] Kinetic measurements of cyclohexene hydrogenation/dehydrogenation have also be investigated on the Pt(111) surface. Yang *et al.*[11] have reported that cyclohexene hydrogenation occurs through two reaction pathways: disproportionation (R4.1) or reductive hydrogen addition (R4.3) by adsorbed hydrogen. The dehydrogenation of cyclohexene was reported to occur through stepwise dehydrogenation (R4.2) or disproportionation (R4.1).

$$3C_6H_{10} \rightarrow 2\,C_6H_{12} + C_6H_6 \qquad \text{(R4.1)}$$

$$C_6H_{10} \rightarrow C_6H_6 + 4H \qquad \text{(R4.2)}$$

$$C_6H_{10} + 2H \rightarrow C_6H_{12} \qquad \text{(R4.3)}$$

In this chapter, I investigate catalytic reactions of cyclohexene on the Pt(100) single crystal surface with SFG vibrational spectroscopy and gas chromatography (GC) in a range of pressures (10^{-6} – 5 Torr cyclohexene) and temperatures (298-500 K) in the presence and absence of excess hydrogen (15 Torr). SFG measurements show the existence of three distinct surface intermediates on Pt(100): π-allyl c-C_6H_9, 1,4-cyclohexadiene (C_6H_8), and cyclohexyl (C_6H_{11}) (see scheme 4.1). I find that cyclohexene

forms both hydrogenated and dehydrogenated products in the presence and absence of excess hydrogen. Differences between the Pt(100) and Pt(111) surfaces exist as the pressure of cyclohexene and surface temperature in the presence and absence of excess hydrogen are varied. On the Pt(100) surface, π-allyl c-C_6H_9 and cyclohexyl exist on the surface until the pressure of cyclohexene is increased to 1.5 Torr at which point 1,4-cyclohexadiene is co-adsorbed with π-allyl c-C_6H_9 and cyclohexyl. π-Allyl c-C_6H_9 is the dominant surface species until the cyclohexene pressure is increased to 1.5 Torr upon which π-allyl c-C_6H_9 is dehydrogenated to 1,4-cyclohexadiene. The major difference between the Pt(100) and Pt(111) surface as the temperature is increased in the absence of hydrogen is the lack of benzene on the Pt(100) surface. In the presence of excess hydrogen, 1,3-cyclohexadiene is co-adsorbed with 1,4-cyclohexadiene on Pt(111). 1,4-Cylcohexadiene is co-adsorbed with π-allyl c-C_6H_9 and cyclohexyl on Pt(100). Herein, I discuss the temperature, pressure, and excess hydrogen dependent surface chemistry of cyclohexene.

4.2. Experimental

4.2.1. High-Pressure/Ultrahigh-Vacuum (HP/UHV) System

All experiments were carried out on a Pt(100) single-crystal surface in a high-pressure/ultrahigh-vacuum (HP/UHV) system. The HP/UHV system is composed of a UHV chamber with a base pressure of 2 x 10^{-9} Torr and a HP cell isolated from the UHV chamber by a gate valve. The UHV chamber is equipped with an Auger electron spectrometer (AES), quadrupole mass spectrometer (QMS) and Ar^+ ion sputter gun . The sample is transferred along a horizontal linear path between the UHV chamber and the

HP cell using a magnetically coupled transfer arm. The 600-mL stainless steel HP cell has several ports and is electroplated with gold to reduce catalytic reactivity. A leak valve connects the gas line to the UHV chamber/ QMS and can be used to sample the gas products during reaction. Two CaF_2 conflat windows on the HP cell are mounted 120^o with respect to one another allowing transmission of infrared (IR), visible (VIS), and sum frequency beams during experiments. The HP cell is equipped with a re-circulation loop that includes a diaphragm pump and inlet for gas chromatographic analysis. In GC analysis, a gaseous mobile phase flows under pressure through a heated packed column. Once on the column separation of a mixture occurs according to the relative lengths of time spent by its components in the stationary phase. The reactant and product gases were constantly mixed via the recirculation pump while kinetics were determined by periodically sampling the reaction mixture and measuring mol% gas phase composition using flame ionization detection and a packed column (0.1% AT-1000 on Graphpac GC 80/100 Alltech). The operating pressure in the HP cell is measured with two capacitance manometers, for pressure ranges between 0.1 and 1000 mTorr and between 0.1 and 1000 Torr.

The Pt(100) crystal was cleaned by sputtering with Ar^+ ions (1 keV) for 20 minutes, heating to 1123 K in the presence of 5 x 10^{-7} Torr O_2 for 2 minutes, and then annealing at 1123 K for 2 minutes. Surface cleanliness of the Pt(100) sample was verified by AES and low energy electron diffraction (LEED). The Pt(100) sample was transferred to the HP cell for SFG and GC experiments after several cleaning cycles and was routinely monitored for cleanliness by AES. Cyclohexene ($\geq$ 99.5 %, Aldrich) was purified by several freeze-pump-thaw cycles before introduction to the HP cell.

Cyclohexene impurities were routinely checked using GC. The impurities were below 0.5 % and all of the impurities were light alkanes below C_6.

4.2.2. Sum Frequency Generation Vibrational Spectroscopy

A Nd:YAG laser (1064 nm fundamental having a 20 ps long pulse with a 20 Hz repetition rate) was used to perform the SFG experiments. The 1064 nm beam was frequency doubled to 532 nm in a $KTiOPO_4$ (KTP) crystal. The tunable IR beam was generated in a $LiNbO_3$ by difference frequency mixing of the 1064 nm beam with the output of a β-BaB_2O_4 (BBO) optical parametric generator/amplifier (OPA/OPG) pumped by the 532 nm beam. The VIS beam (200 μJ) and the IR (200 μJ) beams were spatially and temporally overlapped on the Pt(100) surface with incident angles of 55º and 60º, respectively, with respect to the surface normal. All spectra were taken using a ppp polarization combination (SFG, VIS, and IR beams were all p-polarized). The generated SFG beam was sent through a monochromator and the signal intensity was detected with a photomultiplier tube and a gated integrator as the IR beam was scanned over the range of interest.

SFG technique and theory have been described in detail previously.[14-16] Briefly, SFG is a second-order nonlinear optical process in which an IR beam at ω_{IR} is spatially and temporally overlapped with a VIS beam at ω_{VIS} to generate a sum frequency beam at $\omega_{SF} = \omega_{IR} + \omega_{VIS}$. In this study, the IR beam was tuned while the VIS beam remained at 532 nm. When the IR energy matches the vibrational energy of an interfacial molecule, the SFG signal is resonantly enhanced. Isotropic gases in the HP cell do not generate SFG. Under the electric dipole approximation, media with centrosymmetry are not

susceptible to SFG. Platinum bulk has a center of inversion and its contribution to the SFG signal will usually be negligable. This center of inversion is broken at the surface, giving rise to a surface specific signal. The SFG signal, I_{SF}, is related to the incident visible (I_{VIS}) and infrared (I_{IR}) beam intensities, and second-order susceptibility of the media ($\chi^{(2)}$) as

$$I_{SF} \propto \left|\chi^{(2)}\right|^2 I_{VIS} I_{IR}. \tag{4.1}$$

To analyze our SFG spectra, the SFG signal was normalized to the IR intensity (I_{IR}) incident on the surface by the following expression

$$I_{SFG,norm} = \frac{I_{SFG}}{\sqrt{I_{IR,before} I_{IR,after}}} \tag{4.2}$$

where $I_{SFG,norm}$ is the normalized SFG signal, I_{SFG} is the measured SFG signal, $I_{IR,before}$ is the IR signal measured before the HP cell, and $I_{IR,after}$ is the IR signal measured after the HP cell. This was necessary because gas molecules in the HP cell absorb some of the incoming radiation. Detailed descriptions on the HP/UHV system and SFG measurement can be found elsewhere.[17,18]

4.3. Results

4.3.1. Pressure dependence (<10^{-6} – 5 Torr) of major surface species upon cyclohexene adsorption on Pt(100)at 298 K: SFG results and peak assignments

Figure 4.1 shows the SFG spectra of the major surface species on the Pt(100) surface at 298K at various pressures. The vibrational spectrum at a 10 L (Langmuir, 1 L = 10^{-6} Torr · s) exposure shows three major bands centered at 2935, 2870, and 2830 cm^{-1}. The position of the three major bands shifts to 2940, 2865, and 2805 cm^{-1} and a shoulder

at 2780 cm^{-1} appears as the cyclohexene pressure is increased to 10 mTorr. The peak at 2780 cm^{-1} is assigned to the CH_2 stretch of 1,4-cyclohexadiene. 1,4-Cyclohexadiene has been shown to adsorb in a boat conformation by SFG,[12,13] RAIRS,[7] and density functional studies[19] (see scheme 4.1(b)). The C=C-H bonds (C_1, C_3, C_4, and C_6 in scheme 4.1(b)) are in the molecular plane and parallel to the surface, therefore, giving no SFG signal under the MSSR.[20,21] The observed mode is assigned to the symmetric-symmetric C-H stretch of the CH_2 group. This assignment is in accordance with RAIRS and SFG results of 1,4-cyclohexadiene adsorption on Pt(111) in UHV and high pressure environments.[13,22,23] The red shift from the typical CH_2 stretching range (2840-2940 cm^{-1}) is due in part to the strong electron withdrawal effect from the surface platinum atoms.[19] Consequently, the electron density in the two C-H bonds is reduced resulting in a less energetic vibrational mode.

It should be noted from figure 4.1 that the SFG spectrum at pressures about 10 mTorr is clearly different from the SFG and RAIR spectra of di-σ-type cyclohexene (C_6H_{10}) and cyclohexadienes (C_6H_8). Literature addressing cyclic C_6 hydrocarbon chemistry on the Pt(111) surface will be used for comparison of the surface species formed on the Pt(100) surface. The RAIR[7] (SFG[13]) spectrum of di-σ-type cyclohexene on Pt(111) is distinguished by three bands at $\nu(CH_{2,distal})$ = 2938 (2958), $\nu_{asym}(CH_2)$ = 2902 (2918), and $\nu_{sym}(CH_2)$ = 2864 (2875) cm^{-1} and the relative intensities of the bands are found to be equivalent. The RAIR[7] (SFG[13]) of 1,3-cyclohexadiene exhibits modes at $\nu_{sym}(CH_2)$ = 2816, $\nu_{sym}(CH_2)$ = 2825 (2830), $\nu_{sym}(CH_2)$ = 2859 (2875), and $\nu_{asym}(CH_2)$ = 2881 (2900) cm^{-1} and the relative intensities of the bands are also comparable.

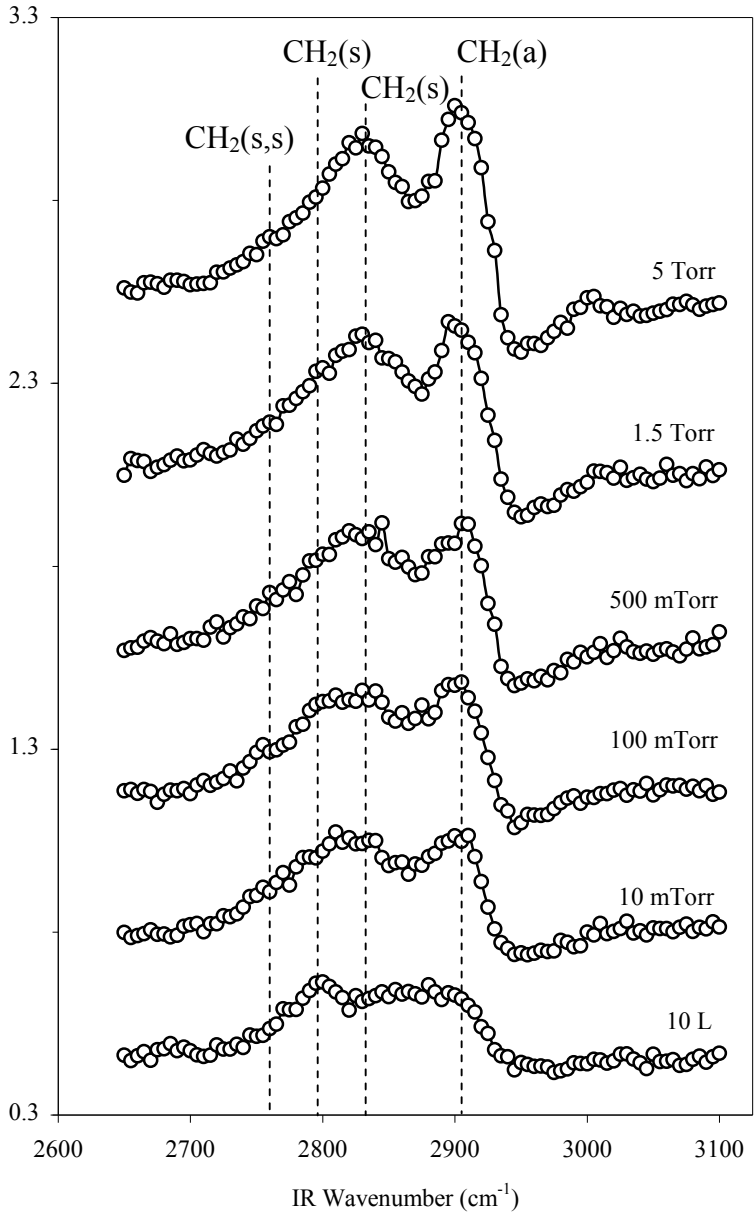

Figure 4.1 SFG spectra of surface species on Pt(100) at 298K at various pressures of cyclohexene: 10 L, 10 mTorr, 100 mTorr, 500 mTorr, 1.5 Torr, and 5 Torr, from the bottom. For an exposure of 10 L (Langmuir, 1 L = 10^{-6} Torr · s), cyclohexene was dosed for 100 seconds at 1 x 10^{-7} Torr. Symmetric (s), asymmetric (a), and symmetric-symmetric (s,s) bands are identified. Lines were drawn for visual aides.

The following assignments were given to the three bands observed in figure 4.1: $\nu_{asym}(CH_2)$ = 2940, $\nu_{sym}(CH_2)$ = 2865, and $\nu_{sym}(CH_2)$ = 2805 cm^{-1}. The RAIRS[3] spectrum of cyclohexene on Pt(100) is distinguished by three bands at $\nu_{asym}(CH_2)$ = 2944, $\nu_{sym}(CH_2)$ = 2872, and $\nu_{sym}(CH_2)$ = 2811 cm^{-1}. The geometry of the dehydrogenated cyclohexene surface species was found to be the π-allyl c-C_6H_9 species shown in scheme 4.1(a). The SFG[10] spectrum of π-allyl c-C_6H_9 has transitions at $\nu_{sym}(CH_2)$ = 2845 and $\nu_{asym}(CH_2)$ = 2920 cm^{-1} with the $\nu_{asym}(CH_2)$ peak much larger than the $\nu_{sym}(CH_2)$ peak (~5:1, respectively). The SFG[9] spectrum of cyclohexyl on Pt(111) shows peaks at $\nu_{sym}(CH_2)$ = 2850 and $\nu_{asym}(CH_2)$ = 2915 cm^{-1} with similar intensities. The close proximity of the $\nu_{asym}(CH_2)$, $\nu_{sym}(CH_2)$ = 2872 cm^{-1}, and $\nu_{sym}(CH_2)$ = 2811 cm^{-1} peak positions and their relative intensities (~4.5:2:1, respectively), suggests that the surface may have co-adsorbed cyclohexyl and π-allyl c-C_6H_9 species. The observed surface species at various pressures are summarized in scheme 4.2(e).

4.3.2. Temperature dependence of major surface species under 1.5 Torr cyclohexene on Pt(100) in the absence of excess H_2: SFG results and peak assignments

Figure 4.2 shows the temperature dependent SFG spectra of the surface species on Pt(100) under 1.5 Torr cyclohexene in the absence of H_2. At 300 K, the four modes at $\nu_{sym,\ sym}(CH_2)$ = 2780, $\nu_{sym}(CH_2)$ = 2815, $\nu_{sym}(CH_2)$ = 2854, and $\nu_{asym}(CH_2)$ = 2940 cm^{-1} were assigned to π-allyl c-C_6H_9 and 1,4-cyclohexadiene co-adsorbed on the Pt(100) surface. It should be noted that the SFG spectrum at 300 K is quite different from the SFG and RAIR spectra of di-σ-type cyclohexene (C_6H_{10}) and cyclohexadienes (C_6H_8) on Pt(111) (table 4.1b). As noted in a previous section, the close proximity in peak positions

and their relative intensities suggests co-adsorbed π-allyl c-C_6H_9 and cyclohexyl. Upon heating to 360 K, the band at $\nu_{sym,\ sym}(CH_2)$ = 2780 cm^{-1} completely disappears while the bands at $\nu_{sym}(CH_2)$ = 2815, $\nu_{sym}(CH_2)$ = 2865, and $\nu_{asym}(CH_2)$ = 2940 cm^{-1} reach a maximum intensity. As the surface temperature is further increased, the bands at $\nu_{sym}(CH_2)$ = 2815, $\nu_{sym}(CH_2)$ = 2865, and $\nu_{asym}(CH_2)$ = 2940 cm^{-1} decrease in intensity until they completely disappear at 440 K. Upon subsequent cooling to 300 K, three modes at $\nu_{sym}(CH_2)$ = 2815, $\nu_{sym}(CH_2)$ = 2865, and $\nu_{asym}(CH_2)$ = 2940 cm^{-1} reappear. The intensities of these three modes $\nu_{sym}(CH_2)$ = 2815, $\nu_{sym}(CH_2)$ = 2865, and $\nu_{asym}(CH_2)$ = 2940 cm^{-1} now appear noticeably decreased if one compares the spectra before and after increasing the surface temperature. The absence of a stretch at 2780 cm^{-1} indicates that 1,4-cyclohexadiene is not present on the surface after cooling the sample from 440 K to 300 K. The observed surface species and modes at various temperatures are summarized in scheme 4.2(a) and table 4.1, respectively.

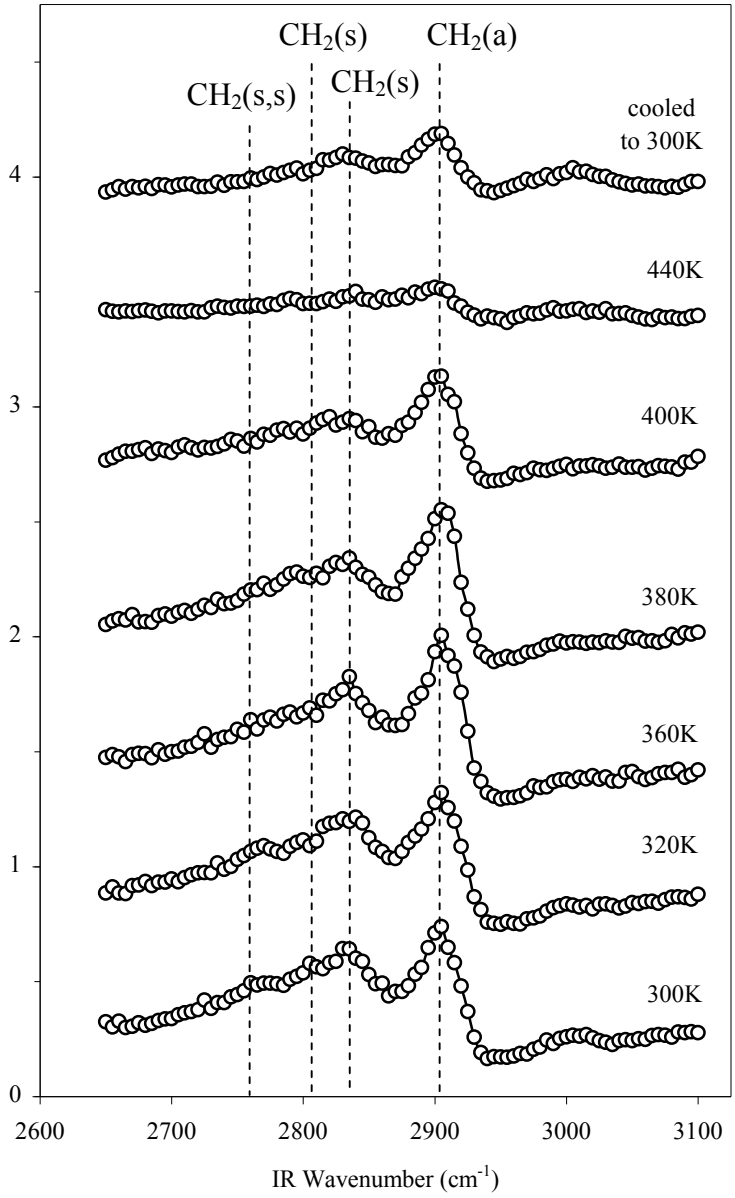

Figure 4.2 Temperature dependent SFG spectra of surface species on Pt (100) under 1.5 Torr cyclohexene in the range of 300-440 K. The top SFG spectrum was taken after the metal surface was cooled from 440 K to 300 K. Symmetric (s), asymmetric (a), and symmetric-symmetric (s,s) bands are identified. Lines were drawn for visual aides.

(a)

Assignments	Temperature						
	300 K	320 K	360 K	380 K	400 K	440 K	Cooled to 300 K
$\nu_{sym,\ sym}(CH_2)$ †	2780	2780					
$\nu_{sym}(CH_2)$‡/*	2815	2815	2815	2815	2815		2815
$\nu_{sym}(CH_2)$‡/*	2854‡	2854	2865	2865*	2865		2865
$\nu_{asym}(CH_2)$‡/*	2940	2940	2940	2940	2940		2940

(b)

Assignments	Temperature					
	303 K	323 K	333 K	363 K	423 K	453 K
$\nu_{sym,\ sym}(CH_2)$†	2760					
$\nu_{sym}(CH_2)$‡		2840	2840	2840	2840	2840
$\nu_{sym}(CH_2)$§						2865
$\nu_{asym}(CH_2)$ ‡		2920	2920	2920	2920	2910
$\nu_{asym}(CH_2)$§						2895
$\nu_{aromatic}(CH)$					2990	2990

Table 4.1. Frequencies (in cm^{-1}) and mode assignments for SFG spectra of 1.5 Torr cyclohexene on (a) Pt(100) and (b) Pt(111)[8] ‡ = π-allyl c-C_6H_9, † =1,4-cyclohexadiene, § = 1,3-cyclohexadiene, * = C_6H_{11}cyclohexyl

(a) At high pressures without H_2 on Pt(100)

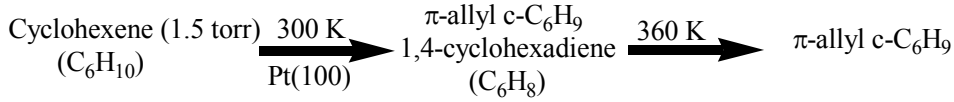

(b) At high pressures without H_2 on Pt(111)

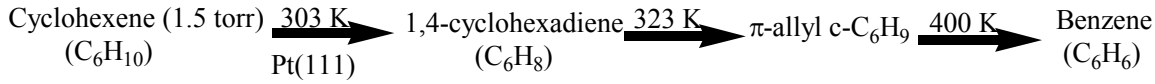

(c) At high pressures with 15 Torr H_2 on Pt(100)

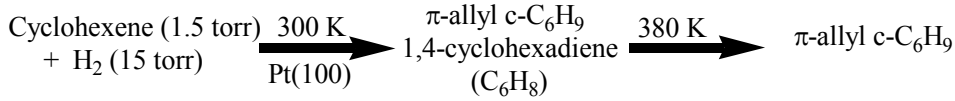

(d) At high pressures with 15 Torr H_2 on Pt(111)

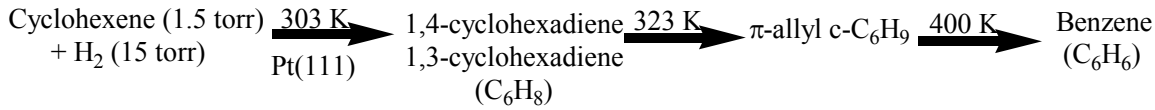

(e) Under UHV conditions ($\leq 10^{-6}$ Torr cyclohexene) on Pt(100)

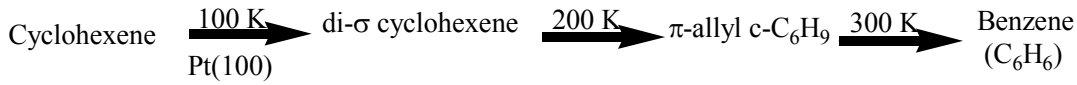

(f) Under UHV conditions ($\leq 10^{-6}$ Torr cyclohexene) on Pt(111)

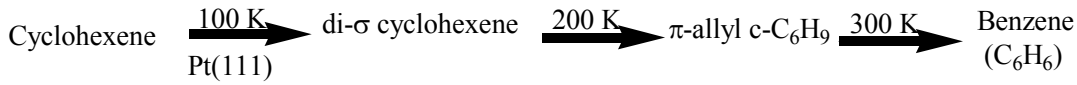

Scheme 4.2 Schematic diagram of observed surface species under 1.5 Torr cyclohexene (a) without H_2 on Pt(100), (b) without H_2 on Pt(111)[8], (c) with 15 Torr H_2 on Pt(100), and (d) with 15 Torr H_2 on Pt(111)[8] and under UHV conditions ($\leq 10^{-6}$ Torr cyclohexene) on (e) Pt(100)[4] and (f) Pt(111)[7].

4.3.3. Temperature dependence of major surface species under 1.5 Torr cyclohexene on Pt(100) in the presence of 15 Torr H_2: SFG results and peak assignments

The temperature dependent SFG spectra of the surface species on Pt(100) under 1.5 Torr cyclohexene and 15 Torr H_2 are shown in figure 4.3 and summarized in table 4.2(a). At 300 K, four modes at $\nu_{sym,\ sym}(CH_2)$ = 2780, $\nu_{sym}(CH_2)$ = 2815, $\nu_{sym}(CH_2)$ = 2865, and $\nu_{asym}(CH_2)$ = 2940 cm^{-1} are observed. These peaks were assigned to π-allyl c-C_6H_9 and 1,4-cyclohexadiene co-adsorbed on the Pt(100) surface. It should be noted that the SFG spectrum at 300 K is quite different from the SFG and RAIR spectra of di-σ-type cyclohexene (C_6H_{10}) and cyclohexadienes (C_6H_8) on Pt(111) as described in the previous section. The relative intensity of the peak at $\nu_{sym,\ sym}(CH_2)$ = 2780 cm^{-1} in the presence of 15 Torr H_2 is much larger than the relative intensity in the absence of H_2.

As the temperature is increased to 380 K, the intensity of the band at 2780 cm^{-1} completely disappears while the bands at $\nu_{sym}(CH_2)$ = 2815, $\nu_{sym}(CH_2)$ = 2865, and $\nu_{asym}(CH_2)$ = 2940 cm^{-1} reach a maximum. This transition temperature is 20 K higher in the presence of 15 Torr H_2 than in the absence of H_2. As the surface temperature is further increased, the bands at $\nu_{sym}(CH_2)$ = 2815, $\nu_{sym}(CH_2)$ = 2865, and $\nu_{asym}(CH_2)$ = 2940 cm^{-1} decrease in intensity until they completely disappear at 460 K. The intensities of the three bands are very similar to the bands observed before the surface temperature was increased. Upon cooling to 300 K, three bands at $\nu_{sym}(CH_2)$ = 2815, $\nu_{sym}(CH_2)$ = 2865, and $\nu_{asym}(CH_2)$ = 2940 cm^{-1} appear. The absence of a mode at $\nu_{sym,\ sym}(CH_2)$ = 2780 cm^{-1} indicates that 1,4-cyclohexadiene is not present on the surface after cooling the sample from 460 K to 300 K. The observed surface species and modes at various temperatures are summarized in scheme 4.2(b) and table 4.2, respectively.

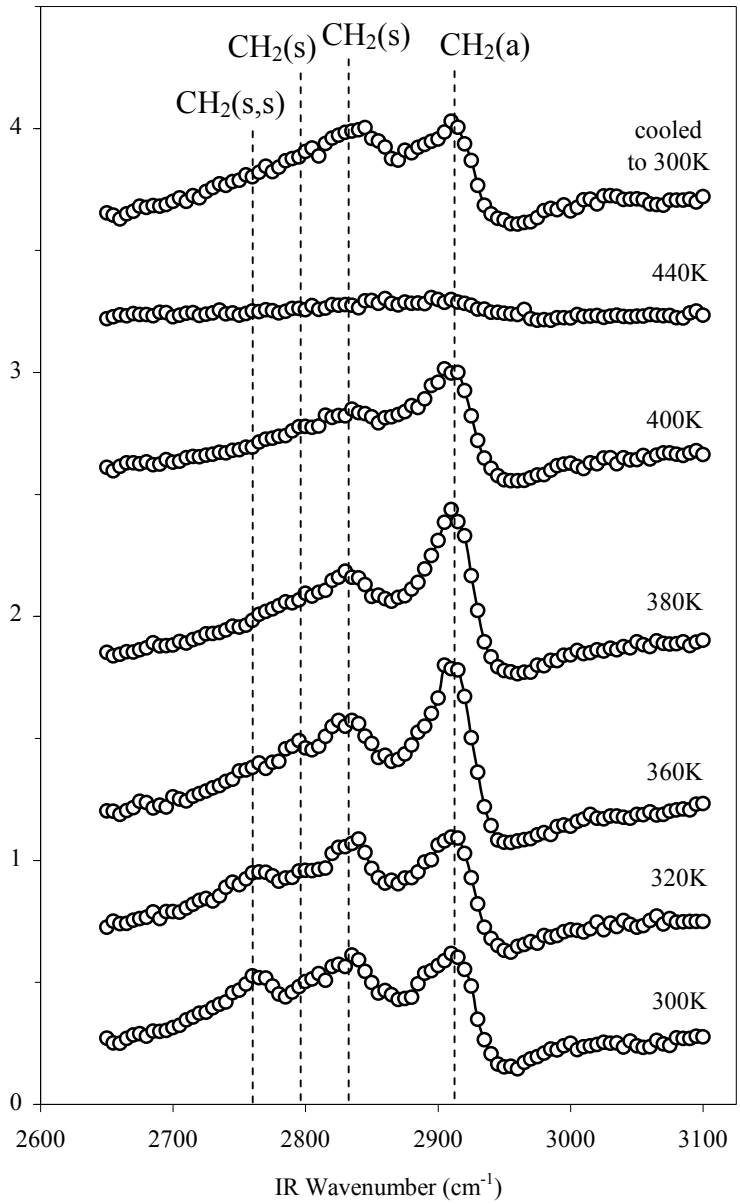

Figure 4.3 Temperature dependent SFG spectra of surface species on Pt(100) under 1.5 Torr cyclohexene and 15 Torr H_2 in the range of 300-460 K. The top SFG spectrum was taken after the metal surface was cooled from 460 K to 300 K. Symmetric (s), asymmetric (a), and symmetric-symmetric (s,s) bands are identified. Lines were drawn for visual aides.

(a)

Assignments	Temperature						
	300 K	320 K	360 K	380 K	400 K	460 K	Cooled to 300 K
$\nu_{sym,\ sym}(CH_2)^{\dagger}$	2780	2780	2780				
$\nu_{sym}(CH_2)^{\ddagger/*}$	2815	2815	2815	2815	2815		2815
$\nu_{sym}(CH_2)^{\ddagger/*}$	2854	2854	2865	2865	2865		2865
$\nu_{asym}(CH_2)^{\ddagger/*}$	2940	2940	2940	2940	2940		2940

(b)

Assignments	Temperature						
	303 K	323 K	343 K	373 K	403 K	453 K	483 K
$\nu_{sym,\ sym}(CH_2)^{\dagger}$	2760						
$\nu_{sym}(CH_2)^{\ddagger}$	2855	2840	2840	2840	2840	2840	2840
$\nu_{sym}(CH_2)^{\S}$	2880				2870	2870	2870
$\nu_{asym}(CH_2)^{\ddagger}$		2920	2920	2920	2920	2920	2920
$\nu_{asym}(CH_2)^{\S}$	2900				2900	2900	2900

Table 4.2 Frequencies (in cm^{-1}) and mode assignments for SFG spectra of 1.5 Torr cyclohexene in the presence of 15 Torr H_2 on (a) Pt(100) and (b) Pt(111)[8] ‡ = π-allyl c-C_6H_9 species, † =1,4-cyclohexadiene, § = 1,3-cyclohexadiene

4.3.4. Turnover rates and activation energies to form the products (cyclohexane and benzene) under 1.5 Torr cyclohexene on Pt(100) in the absence and presence of 15 Torr H_2

In figure 4.4 are the kinetic studies carried out in the absence of excess hydrogen using gas chromatography detection over the 320-500 K temperature range using 1.5 Torr cyclohexene as reactant. Estimated turnover rates (TORs), in molecules per Pt atom per second, are shown in Figure 4.4(a) giving the production of cyclohexane and benzene as a function of temperature. Arrhenius plots of the kinetics are given in figure 4.4(b). The production of cyclohexane and benzene reaches a maximum at 375 K and then decreases with increasing temperature. The apparent activation energy of the hydrogenation pathway was 12.9 ± 0.6 kcal/mol over the temperature range 320-350 K while the apparent activation energy for the dehydrogenation pathway was 14.3 ± 1.2 kcal/mol over the 320-370 K temperature range.

The non-Arrhenius behavior at temperatures above 375 K can be explained in terms of a change in the surface coverage of adsorbed species. Surface coverage, σ (in molecules $\cdot$ cm^{-2}), is defined as the product of the incident flux, F (in molecules $\cdot$ cm^{-2} $\cdot$ s^{-1}), and the residence time, τ (in sec^{-1}).

$$\sigma = F\tau \tag{4.3}$$

Flux, F, can further be defined as

$$F = \frac{N_A P}{\sqrt{2\pi MRT}} \tag{4.4}$$

where N_A is Avogadro's number, P is the pressure, M is the average molar weight of the gaseous species, T is the temperature, and R is the gas constant. Residence time, τ, is given by

$$\tau = \tau_0 \exp\left(\frac{\Delta H_{ads}}{RT}\right) \tag{4.5}$$

where τ_0 is correlated to the surface atom vibration times (typically 10^{-12} s), ΔH_{ads} is the heat of adsorption, T is the temperature, and R is the gas constant. Using equations 3.4 and 3.5 we can rewrite surface coverage (equation 4.3) as

$$\sigma = \frac{N_A P}{\sqrt{2\pi MRT}} \tau_0 \exp\left(\frac{\Delta H_{ads}}{RT}\right) \tag{4.6}$$

The surface coverage decreases as the temperature increases causing the turnover to decrease as seen in figure 4.4.

The kinetic results given in figure 4.5 were performed with 1.5 Torr cyclohexene in the presence of 15 Torr H_2 over the 300-500 K temperature range. Figure 4.5(a) shows the initial TORs for the production of cyclohexane and benzene as a function of temperature. The cyclohexane and benzene products both reach maxima at 375 K and 425 K, respectively. The non-Arrhenius behavior at temperatures above 375 K and 425 K for cyclohexane and benzene production, respectively, can be explained in terms of a change in the surface coverage of adsorbed species as discussed previously. The Arrhenius plots for the TORs are shown in figure 4.5(b). The apparent activation energy obtained for the hydrogenation pathway in the temperature range 310-350 K was 18.8 ± 0.9 kcal/mol. For the dehydrogenation pathway, the apparent activation energy obtained for the temperature range 340-400 K was 22.4 ± 1.6 kcal/mol.

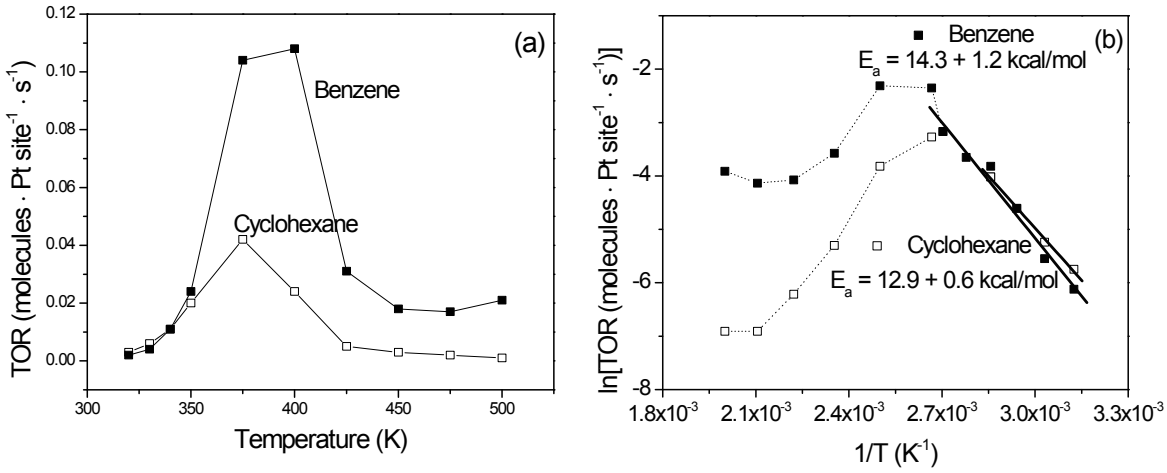

Figure 4.4 (a) Turnover rates (TORs), in molecules per Pt atom per second, for cyclohexene (at 1.5 Torr) hydrogenation to cyclohexane and dehydrogenation to benzene, and (b) Arrhenius plots of the TORs. Apparent activation energies are 12.9 ± 0.6 kcal/mol for the hydrogenation pathway and 14.3 ± 1.2 kcal/mol for the dehydrogenation pathway. The apparent activation energies on the Pt(111) surface are 14.0 ± 0.4 kcal/mol for the production of cyclohexane and 13.5 ± 0.8 kcal/mol for the production of benzene.[8] The non-Arrhenius behavior above 375 K is explained in terms of changes in the surface coverage of the adsorbates. Dotted lines were drawn for visual aides.

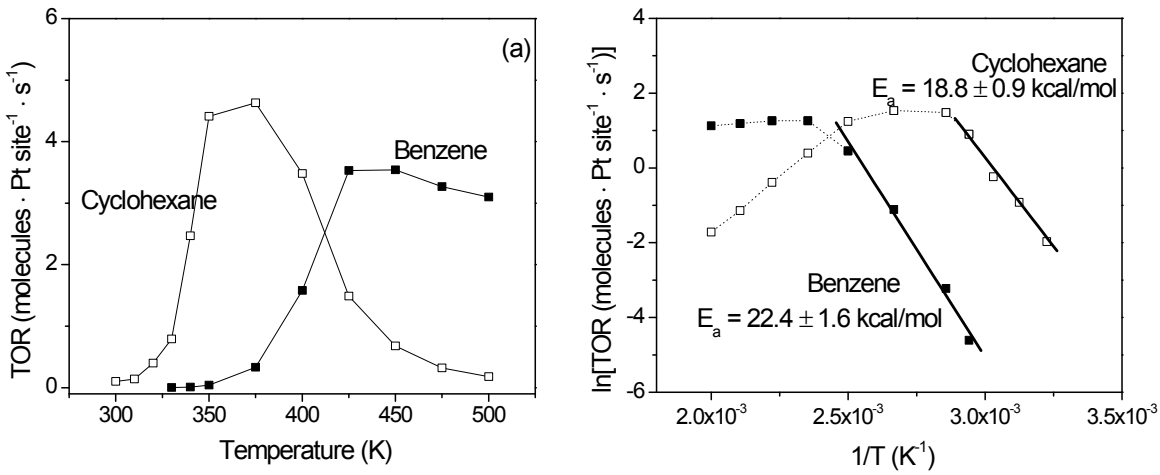

Figure 4.5 (a) Turnover rates (TORs) for the hydrogenation to cyclohexane and dehydrogenation to benzene under 1.5 Torr cyclohexene and 15 Torr H_2 and (b) Arrhenius plots for the TORs. Apparent activation energies are 18.8 ± 0.9 kcal/mol for the hydrogenation pathway and 22.4 ± 1.6 kcal/mol for the dehydrogenation pathway. The apparent activation energies on the Pt(111) surface are 8.6 ± 0.1 kcal/mol for the production of cyclohexane and 17.9 ± 0.2 kcal/mol for the production of benzene.[8] The non-Arrhenius behavior above 375 K for hydrogenation and 425 K for dehydrogenation is explained in terms of changes in the surface coverage of the adsorbates. Dotted lines were drawn for visual aides.

4.4. Discussion

4.4.1. The effects of temperature and pressure on the surface chemistry of cyclohexene on Pt(100) as monitored by SFG

In figure 4.1, π-allyl c-C_6H_9 is a major surface species upon cyclohexene adsorption on Pt(100) at low cyclohexene pressure ($\leq$ 0.5 Torr) and low surface temperature (298 K). As the pressure is increased to 1.5 Torr at 298 K, π-allyl c-C_6H_9 and 1,4-cyclohexadiene are co-adsorbed on the surface. At low pressures ($\leq 10^{-6}$ Torr) cyclohexene exists in a di-σ form on Pt(100) at 100K. When the surface temperature is increased to 200K, the di-σ cyclohexene is converted to π-allyl c-C_6H_9.[4] This result is similar to our spectra at low pressures and increased temperatures. However, the di-σ cyclohexene species that is observed at low temperatures and pressures is not seen at increased temperature and pressure. Increasing the temperature of the metal surface causes the 1,4-cyclohexadiene to disappear and π-allyl c-C_6H_9 becomes the dominant surface species. π-Allyl c-C_6H_9 may occur through the formation of di-σ C_6H_{10} and its dehydrogenation.

$$C_6H_{10} \rightarrow C_6H_9 + H \qquad \text{(R4.4)}$$

As seen in figure 4.1, π-allyl c-C_6H_9 and 1,4-cyclohexadiene are co-adsorbed species at 298 K as the pressure was increased to 1.5 Torr. Cyclohexene and π-allyl c-C_6H_9 undergo hydrogen transfer and give rise to the formation of 1,4-cyclohexadiene and cyclohexyl radical (C_6H_{11}).

$$C_6H_9 + C_6H_{10}\,(\text{excess}) \rightarrow C_6H_8 + C_6H_{11} \qquad \text{(R4.5)}$$

The cyclohexyl radical dehydrogenates in the absence of hydrogen. Unsaturated cyclic hydrocarbons have distinctive capacities as hydrogen donor/acceptors on a Pt surface,

which allows for the proposal of a bi-molecular reaction between π-allyl c-C_6H_9 and excess cyclohexene. As the temperature is increased, the 1,4-cyclohexadiene, co-adsorbed with π-allyl c-C_6H_9, converts to π-allyl c-C_6H_9. Using a bimolecular reaction scheme, cyclohexene and 1,4-cyclohexadiene undergo hydrogen transfer to produce π-allyl c-C_6H_9.

$$C_6H_8 + C_6H_{10}\,(\text{excess}) \rightarrow 2C_6H_9 \qquad \text{(R4.6)}$$

On Pt(111) and Pt(100), other than the C_6H_8 species no other intermediates with stoichiometries between C_6H_9 and benzene have been observed.[3,4,6,7,24]

4.4.2. Comparison of the surface chemistry on Pt(100) and Pt(111) as monitored by SFG: Pressure and temperature dependence

As discussed in a previous section, π-allyl c-C_6H_9 is the major surface species on Pt(100) at low pressures of cyclohexene (≤ 0.5 Torr) and low surface temperatures. As the pressure is increased to 1.5 Torr, 1,4-cyclohexadiene appears to be co-adsorbed with π-allyl c-C_6H_9. Increasing the pressure to 1.5 Torr led to the conversion of 1,4-cyclohexadiene to π-allyl c-C_6H_9 and co-adsorbed cyclohexyl (table 4.1a).

Yang *et al.*[11] reported that π-allyl c-C_6H_9 is the major surface species upon cyclohexene adsorption on Pt(111) at low pressures (≤ 0.1 Torr) and low surface temperature (298 K). As the pressure is increased to 1.5 Torr, π-allyl c-C_6H_9 is converted into 1,4-cyclohexadiene at 298 K. In the presence of excess hydrogen and under 1.5 Torr cyclohexene, 1,3-cyclohexadiene is co-adsorbed with 1,4-cyclohexadiene (table 4.1b). Increasing the surface temperature led to the conversion of 1,4-cyclohexadiene to π-allyl c-C_6H_9 in the presence and absence of excess hydrogen (table 4.1b and table 4.2b).

Similarly, 1,3-cyclohexadiene appears on the Pt(111) surface when the metal surface temperature is increased to 400 K with and without hydrogen. The observed surface species at various temperatures in the absence and presence of excess hydrogen are summarized in scheme 4.2(c) and 2(b), respectively.

4.4.3. Kinetics and suggested reaction pathways of cyclohexene in the absence and presence of excess hydrogen: Step-wise dehydrogenation/hydrogenation vs. disproportionation

Kinetic measurements in the absence of excess hydrogen gave similar apparent activation energies for dehydrogenation (14.3 ± 1.2 kcal/mol) and hydrogenation (12.9 ± 0.6 kcal/mol) on Pt(100). Moreover, in the 333-373 K temperature range the apparent activation energies for dehydrogenation/hydrogenation on Pt(111) are 13.5 ± 0.8 kcal/mol and 14.0 ± 0.4 kcal/mol, respectively.[10] This result is supportive of dehydrogenation and hydrogenation sharing analogous reaction pathways on both the Pt(100) and Pt(111) surfaces. In the presence of excess hydrogen on Pt(100), similar apparent activation energies (22.4 ± 1.6 kcal/mol for dehydrogenation and 18.8 ± 0.9 kcal/mol for hydrogenation) suggest two distinctive reaction pathways.

Yang et.al.[11] have suggested that the cyclohexane production can be accessed through two different reactions. One reaction is the step-wise hydrogenation, whereby adsorbed cyclohexene reacts with adsorbed hydrogen to form cyclohexyl and subsequently cyclohexane evolves (R4.3). Boudart and Djega-Mariadassou[25] have reported that the reaction order varies between 0.5 and 1 with respect to hydrogen

pressure. The other possible reaction pathway suggested by Yang et al.[11] is disproportionation (R4.1), which is normally independent of hydrogen pressure.

In figure 4.4, the reactions were conducted in the absence of excess hydrogen, which implies that the production of cyclohexane occurred primarily through disproportionation. Given that the cyclohexane and benzene productions took place through the same reaction pathway, we conclude disproportionation is the main reaction responsible for the cyclohexane and benzene productions in the temperature range 320-370 K and 320-350 K for dehydrogenation and hydrogenation, respectively.

4.4.4. Comparison of the dehydrogenation/hydrogenation pathways on Pt(100) and Pt(111)

Similar apparent activation energies for dehydrogenation/hydrogenation reactions on Pt(111)[10] and Pt(100) suggest that the disproportionation reaction is not structure sensitive over these surfaces. However, in the presence of added hydrogen there is notable structure sensitivity during cyclohexene hydrogenation/dehydrogenation for the Pt(100) and Pt(111) surfaces. Similarly, Yang *et al.*[10] reported apparent activation energies of 17.9 ± 0.2 kcal/mol for the dehydrogenation pathway and 8.6 ± 0.1 kcal/mol for the hydrogenation pathway on Pt(111). Activation energies for the Pt(100) surface (22.4 ± 1.6 kcal/mol for dehydrogenation and 18.8 ± 0.9 kcal/mol for hydrogenation), the Pt(111) apparent activation energies are quite different.

A possible explanation for the structure insensitivity in the absence of H_2 and the structure sensitivity under excess H_2 for the Pt(100) and Pt(111) surfaces is that the surface intermediates responsible for the hydrogenation and dehydrogenation pathways

under excess H_2 are not present without H_2. This effect may be due to a lack of hydrogen adsorbed on the platinum surfaces. Furthermore, the TORs in the presence of H_2 are about forty times greater than that without H_2; this may indicate that the reactive surface intermediates in the presence of H_2 react very quickly, which explains the similarity in the SFG spectra with and without H_2.

An understanding of the activation energies measured for catalytic dehydrogenation/hydrogenation on platinum is obtainable through the semiempirical thermodynamic analysis of Koel et al.[26] Calculations show that C-H cleavage from π-allyl c-C_6H_9 is a slow step with an activation energy of 22 kcal/mol to benzene formation on the surface, which agrees our measured activation energy for the dehydrogenation pathway on Pt(100). 1,3-Cyclohexadiene has been observed on the Pt(111) surface and has a calculated activation energy of only 7 kcal/mol. If 1,3-cyclohexadiene and π-allyl c-C_6H_9 are co-adsorbed on the Pt(111) surface, we would expect the apparent activation energy for dehydrogenation to be a weighted average of the activation energies of both π-allyl c-C_6H_9 and 1,3-cyclohexadiene. The absence of 1,3-cyclohexadiene on the Pt(100) surface may explain the increased apparent activation energy for dehydrogenation.

Koel et al.[26] shows that hydrogenation of the cyclohexyl radical has an activation energy of 17 kcal/mol, which is in agreement with the apparent activation energy for hydrogenation on Pt(100) (18.8 ± 0.9 kcal/mol). The SFG spectra on Pt(111) show that π-ally c-C_6H_9 is found on the surface.[8] In section 3.1, we give evidence that π-ally c-C_6H_9 is co-adsorbed with the cyclohexyl C_6H_{11}on Pt(100). The difference in the SFG spectra on Pt(100) and Pt(111) may explain the discrepancy between the apparent activation energies and implies that different binding sites are favored in the hydrogenation

pathway. The activation energy of dehydrogenating adsorbed cyclohexene to π-ally c-C_6H_9 is 9 kcal/mol, which agrees with the measured activation energy on Pt(111) (8.6 ± 0.1 kcal/mol). This step may be important in the hydrogenation pathway since an adsorbed hydrogen atom will be left on the metal surface.

4. 5. Conclusions

Kinetic measurements and SFG vibrational spectroscopy have allowed clarification of the reaction pathways during cyclohexene hydrogenation/dehydrogenation at various temperatures and pressures on Pt(100). Cyclohexene adsorption under ≤ 1.5 Torr at 300 K gives π-allyl c-C_6H_9 and cyclohexyl on the surface. As the pressure of cyclohexene is increased to 1.5 Torr, π-allyl c-C_6H_9 and cyclohexyl become adsorbed with 1,4-cyclohexadiene. Raising the surface temperature changes in the surface spectra until complete molecular desorption. In the absence of excess hydrogen, 1,4-cyclohexadiene is no longer visible on the surface at 360 K while the other species have reduced intensities. No spectral features are observed past a temperature of 440 K. In the presence of hydrogen, 1,4-cyclohexadiene disappears at 380 K leaving π-allyl c-C_6H_9 and cyclohexyl as the dominant surface species up to 460 K. Kinetic measurements show that in the absence of hydrogen, the apparent activation energies for hydrogenation (12.9 ± 0.6 kcal/mol) and dehydrogenation (14.3 ± 1.2. kcal/mol) are very similar suggesting a disproportionation mechanism. However, in the presence of hydrogen, the apparent activation energies yield unique values (18.8 ± 0.9 kcal/mol for hydrogenation and for 22.4 ± 1.6 kcal/mol dehydrogenation) suggesting different reaction pathways.

Difference between the Pt(100) and Pt(111) surfaces arise as the pressures of cyclohexene and the surface temperatures in the absence and presence of excess hydrogen are varied. Briefly, cyclohexyl is found to be co-adsorbed with π-allyl c-C_6H_9 on Pt(100) and is not seen on Pt(111).[8] 1,4-Cyclohexadiene is found to be the dominant surface species at pressures greater than 1.5 Torr on Pt(111)[8] whereas 1,4-cyclohexadiene is co-adsorbed with π-allyl c-C_6H_9 and cyclohexyl on Pt(100). When excess hydrogen is presence, 1,4-cyclohexadiene and 1,3-cyclohexadiene are co-adsorbed on Pt(111) whereas on Pt(100), 1,4-cyclohexadiene is co-adsorbed with π-allyl c-C_6H_9 and cyclohexyl.

References

(1) *Catalytic naphtha reforming: science and technology*; 2nd ed.; Antos, G. J.; Aitani, A. M.; Parera, J. M., Eds.; Marcel Dekker: New York, 1995.

(2) McCrea, K. R.; Somorjai, G. A. *Journal of Molecular Catalysis A: Chemical* **2000**, *163*, 43-53.

(3) Lamont, C. L. A., Borbach, M., Marin, R., Gardner, P., Jones, T. S., Conrad, H., Bradshaw, A. M. *Surface Science* **1997**, *374*, 215-228.

(4) Pettiette-Hall, C. L.; Land, D. P.; McIver, R. T.; Hemminger, J. C. *Journal of the American Chemical Society* **1991**, *113*, 2755-2756.

(5) Rodriguez, J. A.; Campbell, C. T. *Journal of Catalysis* **1989**, *115*, 500-520.

(6) Henn, F. C.; Diaz, A. L.; Bussel, M. E.; Huggenschmidt, M. B.; Domagala, M. E.; Campbell, C. T. *Journal of Physical Chemistry* **1992**, *96*, 5965-5974.

(7) Manner, W. L., Girolami, G. S., Nuzzo, R. G. *Journal of Physical Chemistry B* **1998**, *102*, 10295-10306.

(8) Yang, M.; Chou, K. C.; Somorjai, G. A. *Journal of Physical Chemistry B* **2003**, *107*, 5267-5272.

(9) Yang, M.; Somorjai, G. A. *Journal of the American Chemical Society* **2003**, *125*, 11131-11135.

(10) Yang, M.; Chou, K. C.; Somorjai, G. A. *Journal of Physical Chemistry B* **2004**, *108*, 14766-14779.

(11) Yang, M.; Dunietz, B.; Head-Gordon, M.; Somorjai, G. A. *in publication* **2005**.

(12) Su, X.; Shen, Y. R.; Somorjai, G. A. *Chemical Physics Letters* **1997**, *280*, 302-307.

(13) Su, X.; Kung, K.; Lahtinen, J.; Shen, Y. R.; Somorjai, G. A. *Journal of Molecular Catalysis A: Chemical* **1999**, *141*, 9-19.

(14) Shen, Y. R. *Nature* **1989**, *337*, 519-525.

(15) Shen, Y. R. *The Principles of Nonlinear Optics*; Wiley: New York, 2003.

(16) Shen, Y. R. *Annual Review of Physical Chemistry* **1989**, *40*, 327-350.

(17) Kung, K. Y.; Chen, P.; Wei, F.; Rupprechter, G.; Shen, Y. R.; Somorjai, G. A. *Review of Scientific Instruments* **2001**, *72*, 1806-1809.

(18) Yang, M.; Tang, D. C.; Somorjai, G. A. *Review of Scientific Instruments* **2003**, *74*, 4554-4557.

(19) Saeys, M.; Reyniers, M.; Marin, G. B.; Neurock, M. *Surface Science* **2002**, *513*, 315-327.

(20) Dignam, M. J.; Moskovits, M.; Stobie, R. W. *Transactions of the Faraday Society* **1971**, *67*, 3306-3317.

(21) Pearce, H. A.; Sheppard, N. *Surface Science* **1976**, *59*, 205-217.

(22) Manner, W. L.; Bishop, A. R.; Girolami, G. S.; Nuzzo, R. G. *Journal of Physical Chemistry B* **1998**, *102*, 8816-8824.

(23) Carriera, L. A.; Carter, R. O.; Durig, J. R. *Journal of Chemical Physics* **1973**, *59*, 812-816.

(24) Martin, R.; Gardner, P.; Tushaus, M.; Bonev, C.; Bradshaw, A. M. *Journal of Electron Spectroscopy and Related Phenomena* **1990**, *54*, 773-778.

(25) Boudart, M. E.; Djega-Mariadassou, G. *Kinetics of heterogeneous catalytic reactions*; Princeton Univ.: Princeton, 1984.

(26) Koel, B. E.; Blank, D. A.; Carter, E. A. *Journal of Molecular Catalysis A: Chemical* **1998**, *131*, 39-53.

Chapter 5

In-Situ Sum Frequency Generation Vibrational Spectroscopy Observation of a Reactive Surface Intermediate During High-Pressure Benzene Hydrogenation

Sum frequency generation (SFG) surface vibrational spectroscopy and kinetic measurements using gas chromatography (GC) have been used to identify a reactive surface intermediate *in-situ* during hydrogenation of benzene (C_6H_6) on a Pt(111) single crystal surface at Torr pressures. Upon adsorption at 310 K, both chemisorbed and physisorbed benzene coexist on the surface; a result which has not previously been observed. Kinetic measurements show a linear compensation effect for both the production of cyclohexane and cyclohexene. From this data the isokinetic temperature was identified and correlated to the chemisorbed benzene species, which were probed by means of vibrational spectroscopy. Additionally, chemisorbed benzene was determined to be a reactive intermediate, which is critical for hydrogenation.

5.1. Introduction

Catalytic reactions involving aromatic molecules are important in the chemical industry for both fuel reforming and environmental concerns.[1] In order to better understand industrial catalytic processes, we carry out model studies using platinum single crystal surfaces at pressures and temperatures used in the chemical technologies. In the case of benzene hydrogenation, earlier studies have shed light on the adsorption

and reaction mechanism: 1,3- as well as 1,4- cyclohexadiene, cyclohexane, and cyclohexene have been postulated as possible surface species[2-17]. The large number of possible reaction pathways (based on the surface species given above), has led to numerous studies probing adsorption and isolated reactions (hydrogenation / dehydrogenation) of these species. Despite the vast quantity of data published on these cyclic hydrocarbons, very little is known regarding the surface chemistry at ambient pressures and the nature of reactive surface intermediates. This results from a paucity of techniques that are capable of probing surface intermediates at ambient pressures.

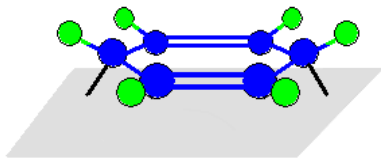

Scheme 5.1. Schematic diagram of dienyl chemisorbed benzene (C_6H_6) intermediate.

Various surface analytical techniques have led to the characterization of thermally stable adsorbates during exposure of Pt(111) to benzene at low pressure (<10^{-6} Torr) and low temperatures (<300K). Among the most prominent techniques used are: low energy electron diffraction (LEED),[18] near edge X-ray absorption spectroscopy (NEXAFS),[10] calorimetry,[6] thermal desorption spectroscopy (TDS),[7,12] electron energy loss spectroscopy (EELS),[9,19] and reflection-absorption infrared spectroscopy (RAIRS).[5,8] Density functional theory (DFT)[2-4] provides possible adsorption energies for different sites and chemical species. Taken together, the various techniques show benzene preferentially adsorbs to bridge sites in the low coverages limit whereas for high coverages adsorption onto three-fold hollow sites is observed.[3] EELS studies display two

distinct vibrational signatures in the cases of both low and high coverages, chemisorbed and physisorbed benzene.[3,19] The chemisorbed species is thought of as the dienyl benzene illustrated in scheme 5.1, while physisorbed benzene is thought of as flat lying.[3,20]

In this study, sum frequency generation (SFG) vibrational spectroscopy is employed to identify the surface intermediates during high-pressure (7.5, 10, 12.5, and 15 Torr) benzene reactions in the presence of hydrogen on Pt(111) at high temperatures (310 – 440 K). Under the electric dipole approximation, media with centrosymmetry and isotropic gases do not appear in the SFG spectrum. Bulk platinum has a center of inversion and its contribution to the SFG signal can therefore be neglected. At the surface, the symmetry is broken, giving rise to the surface specific signal. This explains why SFG is a more sensitive tool to study interfaces via vibrational spectroscopies in comparison to infrared absorption and Raman spectroscopies. Typically, electron spectroscopies cannot be employed under ambient pressure conditions necessary to perform catalytic reactions.

Here, I report evidence for chemisorbed dienyl benzene (C_6H_6) as the reactive surface intermediate for benzene hydrogenation on Pt(111) at high pressures (100 Torr H_2 with 7.5, 10, 12.5, and 15 Torr benzene and 10 Torr benzene with 10, 50, and 150 Torr H_2) and at high temperatures (310 – 440 K). At low temperatures we find that chemisorbed and physisorbed benzene coexist on the surface. This is the first study to show both chemisorbed and physisorbed benzene on Pt(111) simultaneously. At low pressures and temperatures, EELS studies of submonolayer coverages of benzene on

Pt(111) produced chemisorbed dienyl benzene whereas saturation doses (1L) led to physisorption of the benzene.[21] Herein, I discuss the temperature and pressure dependent surface chemistry of benzene on Pt(111) in the presence of hydrogen.

5.2. Experimental

All experiments were carried out in a high-pressure/ultrahigh-vacuum (HP/UHV) system on a prepared Pt(111) single-crystal surface. The HP/UHV system consists of a UHV chamber operating at a base pressure of 2×10^{-9} Torr and a high-pressure (HP) cell isolated from the UHV chamber by a gate valve. The UHV chamber is equipped with an Auger electron spectrometer (AES), quadrupole mass spectrometer (QMS) and Ar^+ ion sputter gun. Two CaF_2 conflat windows on the HP cell allow transmission of infrared (IR), visible (VIS), and sum frequency radiation for SFG experiments. The HP cell is equipped with a re-circulation loop that includes a diaphragm pump and a septum for gas chromatographic analysis. The reactant and product gases are constantly mixed via a recirculation pump while kinetics data is acquired by periodically sampling the reaction mixture and measuring the relative gas phase composition (FID detection and 0.1% AT-1000 on Graphpac GC 80/100 packed column (Alltech)).

The Pt(111) crystal was cleaned by sputtering with Ar^+ ions (1 keV) for 20 minutes, heating to 1123 K in the presence of 5×10^{-7} Torr O_2 for 2 minutes, and then annealing at 1123 K for 2 minutes. AES and LEED were used to verify the cleanliness of the Pt(111) surface after several cleaning cycles. The Pt(111) sample was then transferred into the HP cell for SFG reaction studies. Benzene ($\geq$ 99.0 %, EM Science)

was purified by several freeze-pump-thaw cycles before introduction into the HP cell. Prior to the experiment, benzene was checked for impurities by means of GC. Such impurities were below 0.5 % and consisted of mostly light alkanes below C_6.

A Nd:YAG laser (1064 nm fundamental having a 20 ps pulse width operating at a 20 Hz repetition rate) was used to create a tunable IR (1800-4000 cm^{-1}) and a second harmonic VIS (532 nm) beam. The VIS beam (200 μJ) and the IR (200 μJ) beams were spatially and temporally overlapped on the Pt(111) surface with incident angles of 55º and 60º, with respect to the surface normal. All spectra were taken using a ppp polarization combination (SFG, VIS, and IR beams were all p-polarized). The generated SFG beam was sent through a monochromator and the signal intensity was detected with a photomultiplier tube and a gated integrator as the IR beam was scanned over the range of interest. Spectra were curve fit using a previously reported procedure[20,22] to a form of the equation

$$I_{SFG} \propto \left| \chi_{NR}^{(2)} e^{i\phi_{NR}} + \sum_q \frac{A_q}{\omega_{IR} - \omega_q + i\Gamma_q} e^{i\gamma_q} \right|^2 \qquad (5.1)$$

where $\chi_{NR}^{(2)}$ is the nonresonant nonlinear susceptibility, $e^{i\phi_{NR}}$ is the phase associated with the nonresonant background, A_q is the strength of the qth vibrational mode, ω_{IR} is the frequency of the incident infrared laser beam, ω_q is the frequency of the qth vibrational mode, Γ_q is the natural line width of the qth vibrational transition, and $e^{i\gamma_q}$ is the phase associated with the qth vibrational transition. Detailed descriptions on the HP/UHV system and SFG measurement can be found elsewhere.[11,13,23-26]

5.3. Results

5.3.1. Turnover rates, reaction orders, and activation energies to form the products (cyclohexane and cyclohexene) under varied pressures of benzene and hydrogen on Pt(111)

Figure 5.1 shows the kinetic data for 100 Torr hydrogen and 7.5, 10, 12.5, and 15 Torr benzene pressures, respectively, over a temperature range from 310K to 440 K. Estimated turnover rates (TORs) [molecules · Pt site^{-1} · s^{-1}] are shown in figure 5.1(a) illustrating the production of cyclohexane at different temperatures. The TORs are calculated assuming that every platinum surface atom is an active site. Errors associated with these measurements are given as error bars. Arrhenius plots of the TORs are given in figure 5.1(b). This reaction also produces cyclohexene at higher temperatures. The TORs for cyclohexene formation are shown in figure 5.2(a) along with the corresponding Arrhenius plots in figure 5.2(b). In a second experiment, the benzene pressure was held constant at 10 Torr and the H_2 pressure was adjusted to 10, 50, 100, and 150 Torr. The corresponding cyclohexane and cyclohexene TORs are shown in figures 5.3(a) and 5.4(a) with the matching Arrhenius plots being displayed in figures 5.3(b) and 5.4(b), respectively. Above 370 K and 420 K, the observed turnover rates for cyclohexane and cyclohexene deviate from the linear Arrhenius regression line. This is due to a change in the surface coverage of adsorbed species as previously discussed.[11] Apparent activation energies and pre-exponentials for cyclohexane and cyclohexene are listed in tables 5.1 and 5.2. The apparent activation energies depend upon the pressure of each reactant. In many hydrogenation reactions (e.g. ethylene, propylene, n-hexene, cyclohexene etc.), H_2

is more strongly adsorbed than the hydrocarbon reactant and has a dominant effect on the apparent activation energies.[27] Benzene, in contrast, binds very strongly to the Pt(111) surface and large changes in the apparent activation energies are expected upon varying its partial pressure. This change in activation energy is more noticeable in cyclohexene producing hydrogenation pathway as illustrated in tables 5.1 and 5.2.

The rate law for benzene hydrogenation can be described by a standard empirical power law

$$r = kP_{Bz}{}^{a}P_{H_2}{}^{b} \tag{5.2}$$

where r is the rate of reaction, P_{Bz} and P_{H_2} are the pressures of the reactant gases (benzene and H_2, respectively), a and b are the reaction order with respect to the reactant species, and *k* is the rate constant. The rate constant can be expressed as

$$k = Ae^{-E_a / RT} \tag{5.3}$$

where A is the pre-exponential factor, E_a is the activation energy, R is the gas constant, and T is temperature. The exponents a and b are determined over a range of reaction temperatures (310 – 360 K for cyclohexane and 370 – 400 K for cyclohexene) using

$$a = \left[\frac{\partial \ln r}{\partial \ln P_{Bz}}\right]_{P_{H_2}} . \tag{5.4}$$

The benzene and H_2 reaction orders for both cyclohexane and cyclohexene production are listed in tables 5.1 and 5.2.

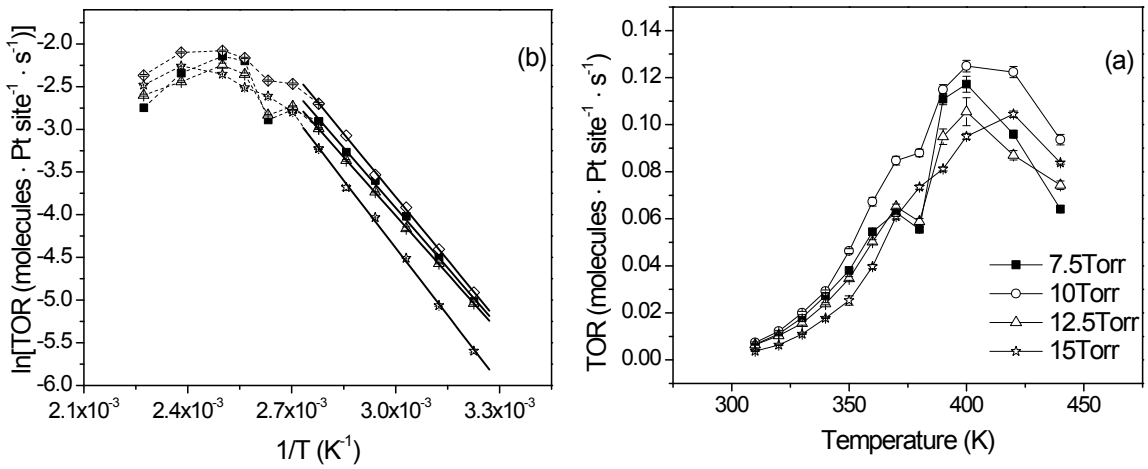

Figure 5.1. (a) Turnover rates (TORs), in molecules per Pt atom per second, for benzene (at 7.5, 10, 12.5, and 15 Torr) hydrogenation to cyclohexane in the presence of H_2 (100 Torr), and (b) Arrhenius plots of the TORs. Apparent activation energies and pre-exponentials are listed in table 5.1. The decrease in TOR at 380 K followed by a sharp increase at 390 K is attributed to the onset of cyclohexene production (See figure 5.2(a)). Cyclohexene has a higher sticking probability on platinum resulting in further hydrogenation to cyclohexane. The non-Arrhenius behavior above 370 K is explained in terms of changes in the surface coverage of the adsorbates. Dotted lines were drawn for visual aides.

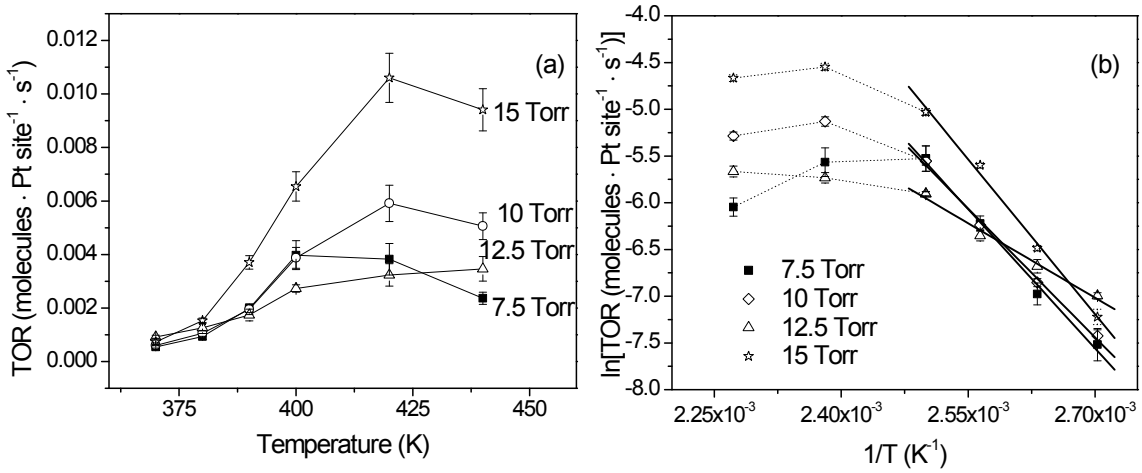

Figure 5.2. (a) Turnover rates (TORs), in molecules per Pt atom per second, for benzene (7.5, 10, 12.5, and 15 Torr) hydrogenation to cyclohexene in the presence of H_2(100 Torr), and (b) Arrhenius plots of the TORs. Apparent activation energies and pre-exponentials are listed in table 5.2. The non-Arrhenius behavior above 420 K is explained in terms of changes in the surface coverage of the adsorbates. Dotted lines were drawn for visual aides.

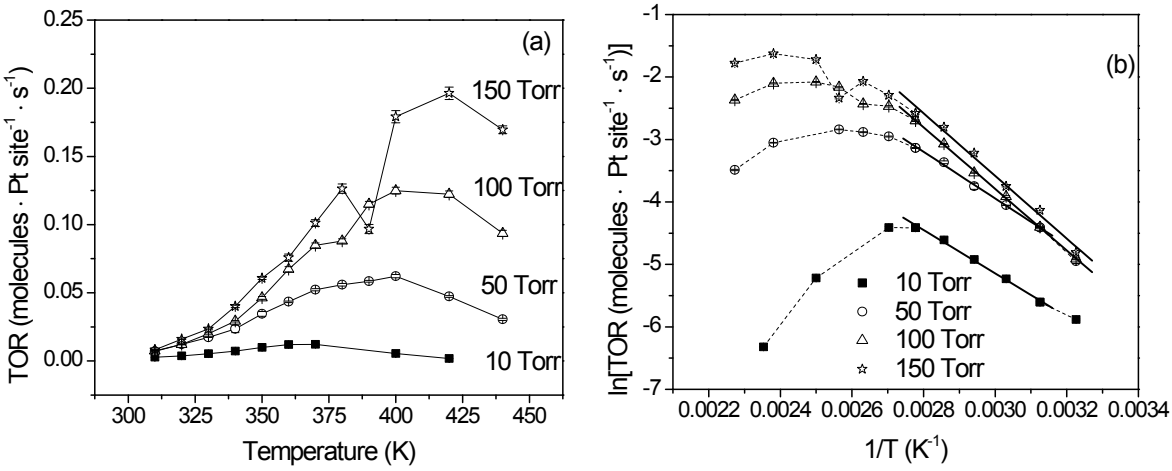

Figure 5.3. (a) Turnover rates (TORs), in molecules per Pt atom per second, for benzene (10 Torr) hydrogenation to cyclohexane in the presence of H_2 (at 10, 50, 100, and 150 Torr), and (b) Arrhenius plots of the TORs. Apparent activation energies and pre-exponentials are listed in table 5.1. The decrease in TOR at 380 K followed by a sharp increase at 390 K is attributed to the onset of cyclohexene production (see figure 5.4(a)). Cyclohexene has a higher sticking probability on platinum resulting in further hydrogenation to cyclohexane. The non-Arrhenius behavior above 370 K is explained in terms of changes in the surface coverage of the adsorbates. Dotted lines were drawn for visual aides.

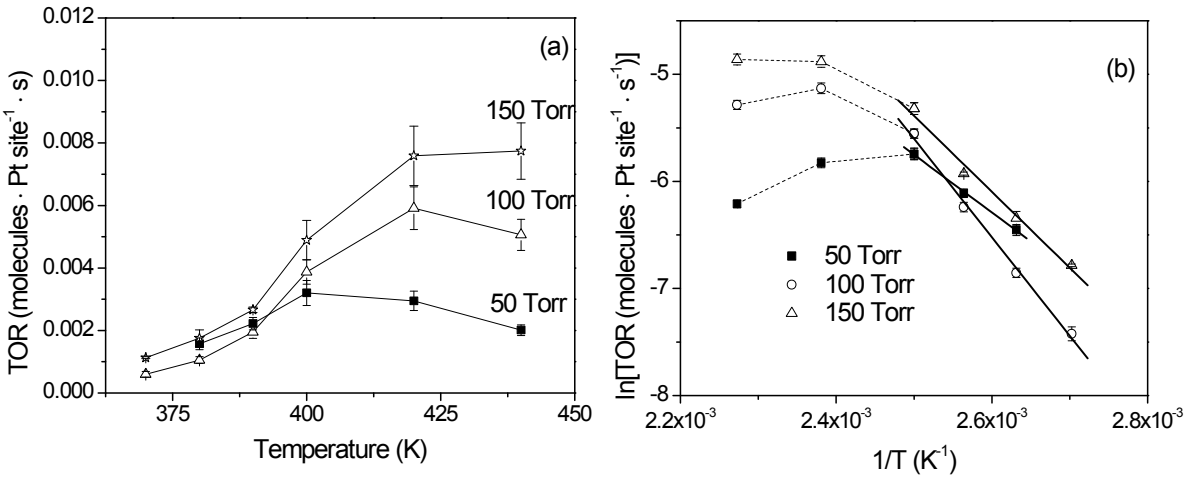

Figure 5.4. (a) Turnover rates (TORs), in molecules per Pt atom per second, for benzene (10 Torr) hydrogenation to cyclohexene in the presence of H_2 (at 50, 100, and 150 Torr), and (b) Arrhenius plots of the TORs. Apparent activation energies and pre-exponentials are listed in table 5.2. The non-Arrhenius behavior above 420 K is explained in terms of changes in the surface coverage of the adsorbates. Dotted lines were drawn for visual aides.

	ln (A)	E_a
10.5 Torr Benzene		
11.2 Torr H_2	3.93 ± 0.33	6.95 ± 0.22
52 Torr H_2	5.62 ± 0.49	7.95 ± 0.33
105 Torr H_2	8.17 ± 0.18	9.79 ± 0.12
158 Torr H_2	9.43 ± 0.65	10.6 ± 0.4
105 Torr H_2		
7.9 Torr Bz	6.97 ± 0.33	9.31 ± 0.22
10.5 Torr Bz	8.17 ± 0.18	9.79 ± 0.12
13.3 Torr Bz	7.10 ± 0.18	9.06 ± 0.05
16.5 Torr Bz	9.07 ± 0.65	10.5 ± 0.2

	T_i/(K)	υ/(cm^{-1})
CHA	317 ± 16	443 ± 22

	order
Benzene	-1.1 ± 0.1
H_2	0.6 ± 0.01

Table 5.1. Pre-exponentials (in molecules per Pt atom per second), apparent activation energies (in kcal/mol), orders for both H_2 and benzene, isokinetic temperature (in K), and the critical vibration (in cm^{-1}) for cyclohexane production under a constant pressure of 10 Torr benzene varying H_2 and under constant pressure of 100 Torr H_2 while varying benzene.

	ln (A)	E_a
10.5 Torr Benzene		
52 Torr H_2	13.0 ± 0.6	10.7 ± 0.4
105 Torr H_2	22.3 ± 1.1	18.3 ± 0.8
158 Torr H_2	17.0 ± 1.4	14.1 ± 1.1
105 Torr H_2		
7.9 Torr Bz	24.4 ± 1.5	19.7 ± 1.2
10.5 Torr Bz	22.3 ± 1.1	18.3 ± 0.8
13.3 Torr Bz	12.1 ± 1.1	10.6 ± 0.8
16.5 Torr Bz	26.3 ± 0.9	21.2 ± 0.7

	T_i/(K)	υ/(cm^{-1})
CHE	317 ± 16	443 ± 22

	order
Benzene	-0.7 ± 0.1
H_2	0.6 ± 0.1

Table 5.2. Pre-exponentials (in molecules per Pt atom per second), apparent activation energies (in kcal/mol), orders for both H_2 and benzene, isokinetic temperature (in K), and the critical vibration (in cm^{-1}) for cyclohexene production under a constant pressure of 10 Torr benzene varying H_2 and under constant pressure of 100 Torr H_2 while varying benzene.

In figures 5.1(a) and 5.3(a) one observes a sharp dip in the reaction rate plot for cyclohexane formation at approximately 380K. We assign this feature to the onset of cyclohexene formation. Cyclohexene formation is observed at 370 K but increases significantly above 390 K. Because of its larger sticking coefficient compared to cyclohexane (<0.1[6]), we expect cyclohexene (0.2[28]), once formed, to be an intermediate on the surface, which remains adsorbed until it is further hydrogenated to cyclohexane.

5.3.2. Temperature dependence of the major surface species under varied pressures of benzene and hydrogen on Pt(111): SFG vibrational spectroscopy results and peak assignments

SFG spectra of the surface species on Pt(111) at 15 Torr benzene and 100 Torr H_2 at various temperatures are shown in figure 5.5. At 300 K, peaks are observed at 2945, 3030, and 3060 cm^{-1}. As the temperature is increased to 360 K the peak intensity at 3060 cm^{-1} drops until it completely disappears at 400 K. The peaks at 2945 and 3030 cm^{-1}, on the other hand, increase over the temperature range from 310 – 420 K. Cooling the surface from 440 K to 300 K reveals reversible behavior of the surface composition. The peak at 3060 cm^{-1} is assigned to physisorbed benzene.[19] Benzene has been shown to adsorb parallel to the Pt(111) surface by EELS,[19,21] NEXAFS,[10] RAIRS,[5] and DFT.[3,4] The molecule is still intact since it is physisorbed and the six carbons and hydrogens are assumed to be roughly equivalent giving rise to only one peak in the region the spectra were taken as observed by EELS.[19,21] Furthermore, gas phase benzene exhibits an aromatic C-H stretch at 3068 cm^{-1} which corresponds quite well to the surface vibrational spectra,[19] justifying the assignment of physisorbed benzene.

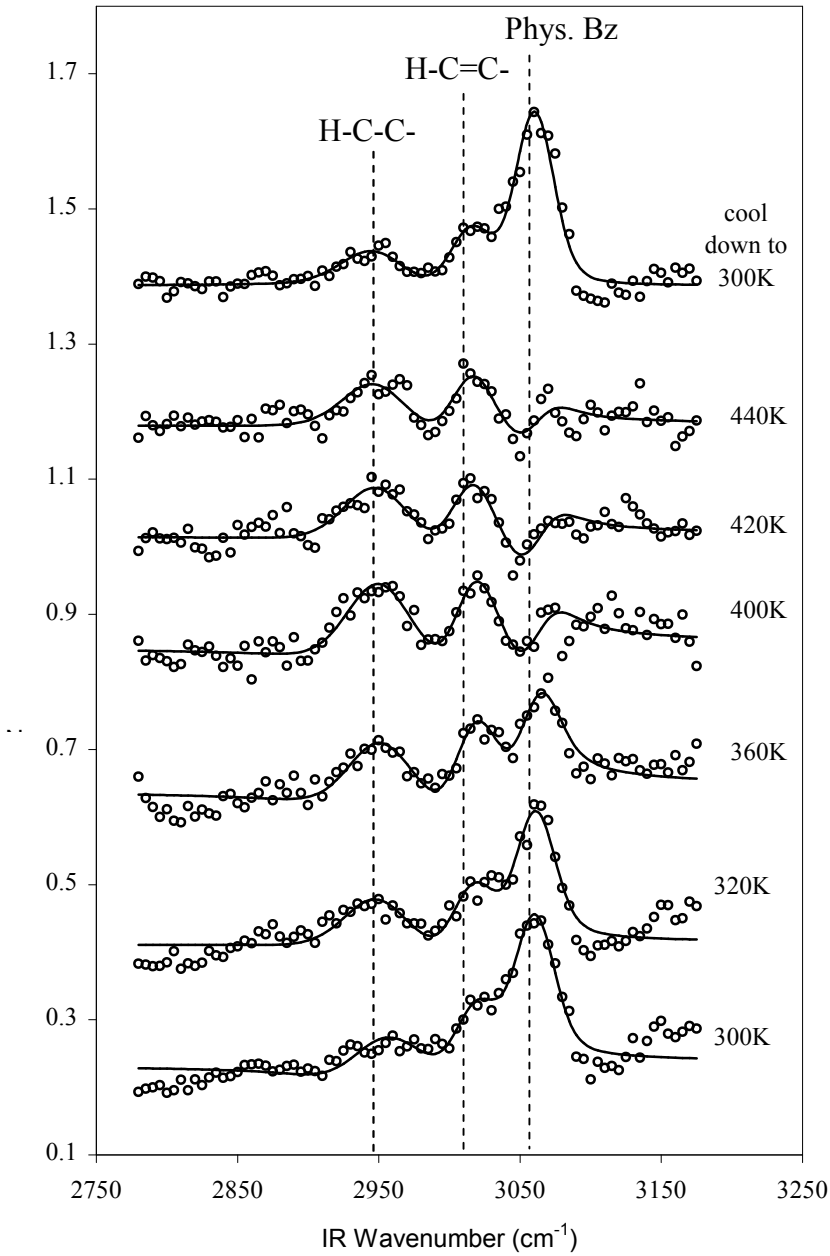

Figure 5.5. Temperature dependent SFG spectra of surface species on Pt(111) under 15 Torr benzene and 100 Torr H_2 in the range of 300-440 K. The top SFG spectrum was taken after the metal surface was cooled from 440 K to 300 K. H-C-C-, vinylic (H-C=C-), and physisorbed benzene (phys. Bz) bands are identified. Markers represent experimental data and solid lines represent the curve fits to equation 5.1.

It becomes clear by comparison that the SFG spectra in figure 5.5 are different from the SFG and RAIRS data of di-σ-type cyclohexene (C_6H_{10}), π-allyl c-C_6H_9, cyclohexyl (C_6H_{11}), and cyclohexadienes (C_6H_8). Literature on cyclic C_6 hydrocarbon chemistry on the Pt(111) surface will be used for comparing surface species found on the Pt(111) surface. The RAIRS[29] (SFG[30]) spectrum of di-σ-type cyclohexene on Pt(111) is distinguished by three bands at $\nu(CH_{2,distal})$ = 2938 (2958), $\nu_{asym}(CH_2)$ = 2902 (2918), and $\nu_{sym}(CH_2)$ = 2864 (2875) cm^{-1} of equal intensity. The RAIRS[29] (SFG[14]) spectrum of π-allyl c-C_6H_9 shows $\nu_{sym}(CH_2)$ = 2846 (2845) and $\nu_{asym}(CH_2)$ = 2930 (2925) cm^{-1}. The cyclohexyl SFG[15] spectrum exhibits two equally intense vibrational signatures at $\nu_{sym}(CH_2)$ = 2850 and $\nu_{asym}(CH_2)$ = 2915 cm^{-1}. The RAIRS[29] (SFG[30]) of 1,3-cyclohexadiene reveals modes at $\nu_{sym}(CH_2)$ = 2816, $\nu_{sym}(CH_2)$ = 2825 (2830), $\nu_{sym}(CH_2)$ = 2859 (2875), and $\nu_{asym}(CH_2)$ = 2881 (2900) cm^{-1} and the relative intensities of the bands are again similar. Finally, the RAIRS[29] (SFG[30]) spectrum of 1,4-cyclohexadiene has only one mode at $\nu_{sym,\ sym}(CH_2)$ = 2763 (2770) cm^{-1}. Presumably, the absence of a symmetric CH_2 stretch in figure 5.5 indicates that the adsorbate is some C_6H_6 or more dehydrogenated species (e.g. polyaromatics).

Previous infrared/high resolution electron energy loss spectroscopy (IR/HREELS)[21,31] studies on benzene adsorption at low coverages (0.2 L, Langmuir, 1 L = 10^{-6} Torr · s) have revealed two peaks centered around 2960 and 3020 cm^{-1}. The 2960 cm^{-1} peak suggests the presence of some sp^3 hybridized carbon. Moreover, Thomas *et al.*[21] did not detect the presence of the 1815 and 1960 cm^{-1} peaks indicating that the adsorbed benzene is of a dienyl chemisorbed nature (see scheme 5.1). Grassian and Muetterties[31] have also presented a similar chemisorbed structure. According to those

two groups, the adsorbate has six carbon-carbon bonds, two double and four single. The two singly bonded carbons are also bonded to the platinum surface, explaining the sp^3 hybridization character in the spectral signature. These results are further corroborated in figure 5.5 by the apparent simultaneous growth and decay variation of the temperature. Hence, the modes in figure 5.5 have been assigned as follows: ν(H-C-C-) = 2945 cm^{-1}, ν(C-H)(vinylic) = 3030 cm^{-1}, and ν(C-H)(aromatic) = 3060 cm^{-1}.

Figure 5.6 shows the SFG spectra of 7.5 Torr benzene and 100 Torr H_2 on Pt(111) as the temperature is varied. The results are strikingly similar to the previously discussed 15 Torr benzene case (figure 5.5). Both chemisorbed and physisorbed benzene are observed at 300 K. The physisorbed benzene slowly desorbs as the surface temperature is increased to 360 K and vanishes completely at 400 K. Both peaks responsible for the chemisorbed benzene increase in intensity as the surface temperature is raised to 420 K. Upon cooling the surface, the physisorbed benzene, once again, becomes the dominant surface species displaying that the reaction is reversible.

Experiments on other pressure combinations (10 Torr benzene under 10, 50, 100, and 150 Torr H_2 and 12.5 Torr benzene under 100 Torr H_2) exhibited the same pattern of chemisorbed and physisorbed benzene co-existing on the platinum surface until the temperature was increased to 360 K, at which point only chemisorbed benzene is present. The chemisorbed dienyl has a maximum intensity at 420 K. Cooling the surface reverses the reaction resulting in physisorbed benzene being the dominant surface species.

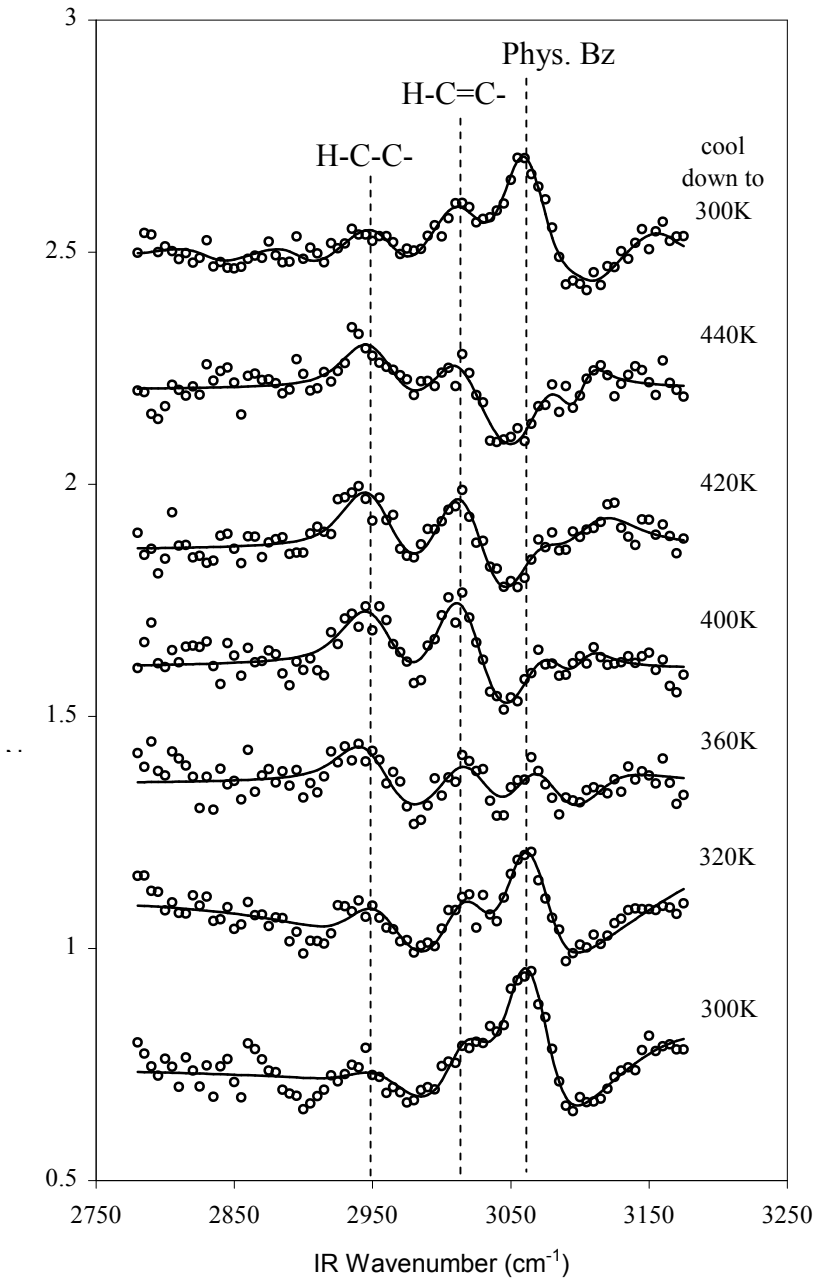

Figure 5.6. Temperature dependent SFG spectra of surface species on Pt(111) under 7.5 Torr benzene and 100 Torr H_2 in the range of 300-440 K. The top SFG spectrum was taken after the metal surface was cooled from 440 K to 300 K. H-C-C-, vinylic (H-C=C-), and physisorbed benzene (phys. Bz) bands are identified. Markers represent experimental data and solid lines represent the curve fits to equation 5.1.

5.4. Discussion

5.4.1. Compensation effect and isokinetic temperature

The Arrhenius plots for both cyclohexane and cyclohexene production (figures 5.1(b), 5.2(b), 5.3(b), and 5.4(b)) have yielded apparent activation energies and pre-exponential factors for all pressure variations. The resulting Arrhenius plot parameter pairs form a straight line, as presented in figure 5.7, and exhibit compensation behavior. The isokinetic temperature is derived from the natural logarithm of equation 5.3

$$\ln A = \frac{E_a}{RT} + \ln k \qquad (5.5)$$

and is related to the slope of the compensation effect. The isokinetic temperature (T_{iso}) is 317 ± 15 K for both cyclohexane and cyclohexene formation. This temperature seems to agree with the point at which the Arrhenius plots intersect. A possible explanation of the isokinetic temperature, as explained by Molinari,[32] is the existence of an equilibrium between adsorption and desorption at T_{iso}. An alternative model proposed by Larsson[33] is based on "selective energy transfer at the active site" which he further explains as a particular transfer of "energy into the vibrational mode of the reactant that most effectively takes the system to the activated state." Larsson[34] has treated the system as a "coupled, damped, oscillation system of classical physics" and derives the following equation

$$T_{iso} = NhcR^{-1}\left(v^2 - \omega^2\right)\omega^{-1}\left\{\pm\frac{1}{2}\pi - arctg\left[0.5v\omega\left(v^2 - \omega^2\right)\right]^{-1}\right\}^{-1} \qquad (5.6)$$

where v is the vibrational mode leading toward reaction, ω is the frequency of the heat bath, N is Avogadro's number, h is Planck's constant, and c is the speed of light. For maximum efficacy of resonance energy transfer, ω = v, equation 5.6 becomes

$$T_{iso} = \frac{Nhc}{2Rv} = 0.719v. \qquad (5.7)$$

Based on the above equation, a critical frequency of vibration for cyclohexane and cyclohexene production is found to be 443 ± 22 cm^{-1}. This corresponds to a metal-carbon stretching vibrational mode,[19,21] which facilitates the $sp^2 \rightarrow sp^3$ reaction.

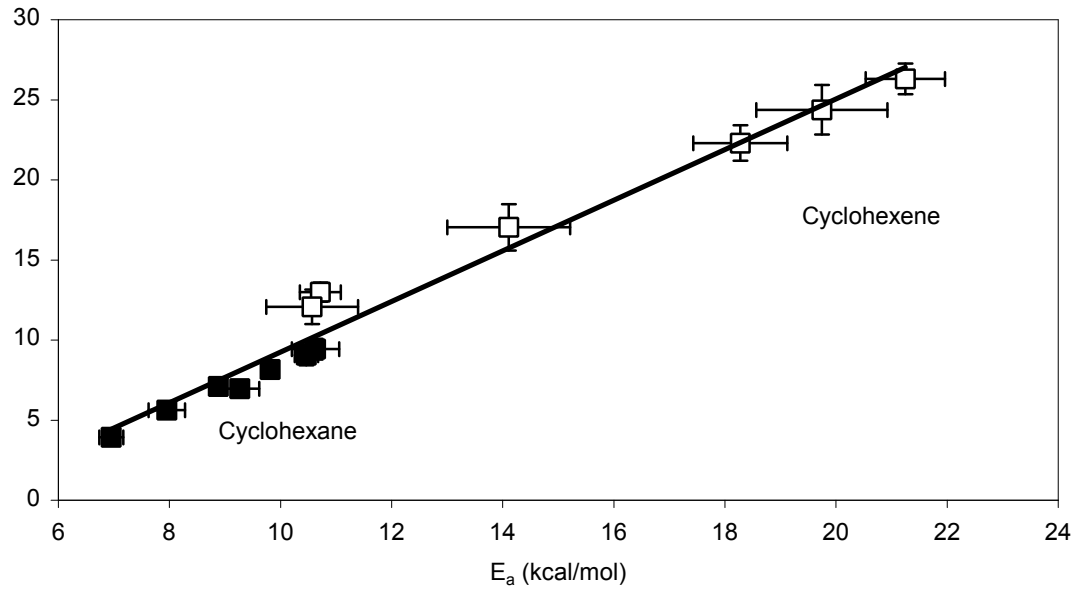

Figure 5.7. Constable plot for the hydrogenation of benzene to cyclohexane and cyclohexene. Open symbols represent cyclohexene and closed denote cyclohexane.

5.4.2. Kinetics and suggested reaction pathways of benzene hydrogenation

Kinetic results have shown the formation of two products during the hydrogenation of benzene: cyclohexane and cyclohexene. The onset of cyclohexane production occurs at a lower temperature compared to that of cyclohexene. The surface concentration of cyclohexene, increases with temperature and is an endothermic process. However, both cyclohexane and cyclohexene production appear to be intimately tied with the dienyl chemisorbed benzene species since its peaks follow the rise and fall of the turnover rate (of both products) as the surface temperature is varied. This implies that there are at least two reaction mechanisms

According to Koel *et al.,*[35] the most favorable pathway for benzene hydrogenation to cyclohexane occurs in a Horiuti-Polanyi mechanism[36] involving cyclohexene as an intermediate. The likely observable intermediates for this pathway would be η^5-cyclohexadienyl, π-allyl c-C_6H_9, and di-σ cyclohexene. As stated previously, these species are unlikely to be on the platinum surface at high pressures since the absence of symmetric CH_2 modes indicates that the molecule does not have any CH_2 groups. Furthermore, chemisorbed benzene is not likely to be an abundant surface intermediate for this pathway since adsorbed benzene immediately hydrogenates to η^5-cyclohexadienyl.

Saeys *et al.*[3] have developed another possible reaction pathway via DFT. Instead of using chemical intuition to determine a rate determining step and pathway, 14 possible reaction paths were proposed for the six sequential hydrogenation steps. The dominant pathway does not proceed through cyclohexene, as Koel *et al.*[35] have proposed, favoring this as the most probable mechanism for benzene hydrogenation to cyclohexane at low

temperatures. Saeys *et al.*[3] also conclude that "the thermodynamic sink of the energy profile is clearly the adsorbed benzene and hydrogen. They are likely to be the most-abundant reaction intermediates." Adsorbed benzene in the "thermodynamic sink" may be attributed to dienyl chemisorbed benzene, as proposed based on the SFG results in figures 5.5 and 5.6, a finding which is consistent with the mechanism proposed by Saeys *et al.*[3]. However, there is no spectroscopic evidence of any hydrogenated benzene species confirming the plausibility of this pathway, probably due to the short lifetime and small coverages of such species. In the DFT study presented by Saeys *et al.*[3], it was assumed that benzene adsorbs on the three-fold hollow site; this seems preferable at low temperatures and coverages.[4] Higher temperatures favor the bridge site,[37] which, in this work, we assumed to correspond to the dienyl-type chemisorbed benzene. Bonding type effects (bridge versus three-fold hollow) are not explored in the mechanism proposed by Saeys *et al.*[3]

The previously mentioned compensation effect indicates that the critical vibrational frequencies at 443 ± 22 cm^{-1} for cyclohexane and cyclohexene production could be attributed to a metal-carbon stretch, thus facilitating the $sp^2 \rightarrow sp^3$ reaction. In addition, Thomas *et al.*[21] have reported a vibrational mode for chemisorbed benzene at 475 cm^{-1}, which was assigned to metal-carbon stretches. The metal-carbon stretching frequency for physisorbed benzene was reported at 550 cm^{-1}, excluding the physisorbed species as the reactive intermediate by this model. The suggested structure for the dienyl species is clearly the product of the $sp^2 \rightarrow sp^3$ reaction and is likely to be the reactive surface intermediate in the benzene hydrogenation for both cyclohexane and cyclohexene.

5.5. Conclusions

Surface intermediates at various temperatures during high-pressure catalytic reactions of benzene on Pt(111) using SFG surface vibrational spectroscopy have been identified. Chemisorbed and physisorbed benzene were found to coadsorb at 310 K. Heating to 360 K made the physisorbed species disappear and resulted in only chemisorbed benzene on the surface. At 400K the coverage of chemisorbed benzene reaches a maximum and decays as the temperatures is further raised to 440K. When the surface was subsequently cooled from 440 K to 310 K, the observed SFG spectrum was identical to that obtained before reaction indicating complete reversibility of the surface composition. Kinetic studies identified chemisorbed dienyl benzene as a possible critical vibration intermediate to form cyclohexane and cyclohexene. Resonance vibrational frequencies were extracted from the isokinetic temperature and agreed reasonably well with ones expected from a dienyl benzene – type surface species. To conclude, chemisorbed dienyl benzene is a reactive surface intermediate during benzene hydrogenation.

References

(1) Cooper, B. H.; Donnis, B. B. L. *Applied Catalysis A* **1996**, *137*, 203-223.

(2) Saeys, M.; Reyniers, M.; Marin, G. B.; Neurock, M. *Surface Science* **2002**, *513*, 315-327.

(3) Saeys, M.; Reyniers, M.; Marin, G. B. *Journal of Physical Chemistry B* **2002**, *106*, 7489-7498.

(4) Morin, C.; Simon, D.; Sautet, P. *Journal of Physical Chemistry B* **2004**, *108*, 5653-5665.

(5) Haq, S.; King, D. A. *Journal of Physical Chemistry* **1996**, *100*, 16957-16965.

(6) Ihm, H.; Ajo, H. M.; Gottfried, J. M.; Bera, P.; Campbell, C. T. *Journal of Physical Chemistry B* **2004**, *108*, 14627-14633.

(7) Lutterloh, C.; Biener, L.; Pohlmann, K.; Schenk, A.; Kuppers, J. *Surface Science* **1996**, *352-354*, 133-137.

(8) Haaland, D. M. *Surface Science* **1981**, *102*, 405-423.

(9) Abon, M.; Bertolini, J. C.; Billy, J.; Massardier, J.; Tardy, B. *Surface Science* **1985**, *162*, 395-401.

(10) Horsley, J. A.; Stohr, J.; Hitchcock, A. P.; Newbury, D. C.; Johnson, A. L.; Sette, F. *Journal of Chemical Physics* **1985**, *83*, 6099-6107.

(11) Bratlie, K. M.; Flores, L. D.; Somorjai, G. A. *Surface Science* **2005**, *599*, 93-106.

(12) Tsai, M.-C.; Muetterties, E. L. *Journal of the American Chemical Society* **1982**, *104*, 2534-2539.

(13) Yang, M.; Tang, D. C.; Somorjai, G. A. *Review of Scientific Instruments* **2003**, *74*, 4554-4557.

(14) Yang, M.; Chou, K. C.; Somorjai, G. A. *Journal of Physical Chemistry B* **2003**, *107*, 5267-5272.

(15) Yang, M.; Somorjai, G. A. *Journal of the American Chemical Society* **2003**, *125*, 11131-11135.

(16) Yang, M.; Chou, K. C.; Somorjai, G. A. *Journal of Physical Chemistry B* **2004**, *108*, 14766-14779.

(17) Yang, M.; Dunietz, B.; Head-Gordon, M.; Somorjai, G. A. *in publication* **2005**.

(18) Ogletree, D. F.; Van Hove, M. A.; Somorjai, G. A. *Surface Science* **1987**, *183*, 1-20.

(19) Lehwald, S.; Ibach, H.; Demuth, J. E. *Surface Science* **1978**, *78*, 577-590.

(20) Bain, C. D.; Davies, P. B.; Ong, T. H.; Ward, R. N.; Brown, M. A. *Langmuir* **1991**, *7*, 1563-1566.

(21) Thomas, F. S.; Chen, N. S.; Ford, L. P.; Masel, R. I. *Surface Science* **2001**, *486*, 1-8.

(22) Moore, F. G.; Becraft, K. A.; Richmond, G. L. *Applied Spectroscopy* **2002**, *56*, 1575-1578.

(23) Kung, K. Y.; Chen, P.; Wei, F.; Rupprechter, G.; Shen, Y. R.; Somorjai, G. A. *Review of Scientific Instruments* **2001**, *72*, 1806-1809.

(24) Shen, Y. R. *The Principles of Nonlinear Optics*; Wiley: New York, 2003.

(25) Shen, Y. R. *Annual Review of Physical Chemistry* **1989**, *40*, 327-350.

(26) Shen, Y. R. *Nature* **1989**, *337*, 519-525.

(27) Bond, G. C.; Keane, M. A.; Kral, H.; Lercher, J. A. *Catalysis Review* **2000**, *42*, 323-383.

(28) Henn, F. C.; Diaz, A. L.; Bussel, M. E.; Huggenschmidt, M. B.; Domagala, M. E.; Campbell, C. T. *Journal of Physical Chemistry* **1992**, *96*, 5965-5974.

(29) Manner, W. L., Girolami, G. S., Nuzzo, R. G. *Journal of Physical Chemistry B* **1998**, *102*, 10295-10306.

(30) Su, X.; Kung, K.; Lahtinen, J.; Shen, Y. R.; Somorjai, G. A. *Journal of Molecular Catalysis A: Chemical* **1999**, *141*, 9-19.

(31) Grassian, V. H.; Muetterties, E. L. *Journal of Physical Chemistry* **1987**, *91*, 389-396.

(32) Molinari, E. *Z. Phys. Chem.* **1956**, *6*, 1.

(33) Larsson, R. *Catalysis Today* **1987**, *1*, 93-99.

(34) Lomot, D.; Juszczyk, W.; Karpinski, Z.; Larsson, R. *Journal of Molecular Catalysis A: Chemical* **2002**, *186*, 163-172.

(35) Koel, B. E.; Blank, D. A.; Carter, E. A. *Journal of Molecular Catalysis A: Chemical* **1998**, *131*, 39-53.

(36) Horiuti, J.; Polanyi, M. *Transactions of the Faraday Society* **1934**, *30*, 1164-1172.

(37) Weiss, P. S.; Eigler, D. M. *Physical Review Letters* **1993**, *71*, 3139-3142.

Chapter 6

Sum Frequency Generation Vibrational Spectroscopic and High-Pressure Scanning Tunneling Microscopic Studies of Benzene Hydrogenation on Pt(111)

Sum frequency generation (SFG) vibrational spectroscopy and high-pressure scanning tunneling microscopy (HP-STM) have been used in combination for the first time to study a catalytic reaction. These techniques have been able to identify surface intermediates *in situ* during benzene hydrogenation on a Pt(111) single crystal surface at Torr pressures. In a background of 10 Torr benzene STM is able to image small ordered regions corresponding to the c(2√3 x 3)*rect* structure in which each molecule is chemisorbed at a bridge site. In addition, individual benzene molecules are also observed between the ordered regions. These individual molecules are assumed to be physisorbed benzene based on the SFG results showing both chemisorbed and physisorbed molecules. The surface becomes too mobile to image upon addition of hydrogen but is determined to have physisorbed and chemisorbed benzene present by SFG. It was spectroscopically determined that heating the platinum surface after poisoning with CO displaces benzene molecules. The high-coverage pure CO structure of (√19 x √19) *R*23.4° imaged with STM is a verification of spectroscopic measurements.

6.1. Introduction

High-pressure scanning tunneling microscopy (HP-STM) and sum frequency generation (SFG) vibrational spectroscopy have been widely used to study high-pressure reactions by means of atomically resolved images of surfaces and chemical information of adsorbates.[1-7] However, these techniques have never been combined to investigate catalytic reactions. Using these techniques to study benzene hydrogenation leads to better understanding of surface adsorbate chemical composition, bonding, and structure during reaction.

Traditionally, benzene has been studied at low pressure ($<10^{-6}$ Torr) and low temperatures (<300K), which are far removed from catalytically relevant conditions. Briefly, benzene has been shown to preferentially adsorb to bridge sites at low coverages and to three-fold hollow sites at high coverages by STM[8] and density functional theory (DFT).[9] Electron energy loss spectroscopy (EELS)[10-12] studies have shown two distinct vibrational signatures for low and high coverages, chemisorbed and physisorbed benzene. Taken together, the various techniques show benzene preferentially adsorbs to bridge sites in the low coverages limit whereas for high coverages adsorption onto three-fold hollow sites is observed.[13] Scheme 6.1 depicts the chemisorbed species, which is thought to be dienyl in nature. Physisorbed benzene is thought to be flat-lying by EELS[12,14] and near edge X-ray absorption spectroscopy (NEXAFS).[15]

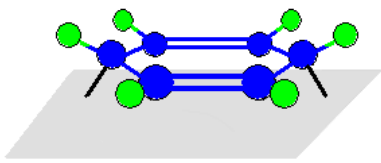

Scheme 6.1. Schematic diagram of dienyl chemisorbed benzene (C_6H_6) intermediate.

In this study, SFG vibrational spectroscopy, high-pressure STM, and reaction turnover studies are used for the first time to investigate and identify the surface species present during benzene hydrogenation (10 Torr benzene) in the presence of excess hydrogen (100 Torr) and in a range of temperatures (300 – 440 K). This reaction is also studied by poisoning the platinum surface with 5 Torr CO. The electric dipole approximation forbids centrosymmetric media and isotropic gases from appearing in the SFG spectrum. Since bulk platinum has a center of inversion, its contribution to the SFG signal is negligible. This symmetry is broken at the surface allowing for a surface specific signal. For these reasons SFG is an ideal tool to probe single-crystal surfaces for chemical functionalities at high-pressures. High-pressure STM has the ability to monitor adsorbates and metal atoms provided their mobility occurs at speeds comparable to or less than the scan rate of approximately 10 μm/sec. The unique ability to detect surface dynamics complements the time-averaged spectroscopic information obtained from SFG. High-pressure STM is also capable of accessing structure and bonding information.

My findings show that both physisorbed and chemisorbed benzene are present on the surface in a background of 10 Torr benzene by SFG. Small ordered regions are observed by STM and identified as the c(2√3 x 3)*rect* structure in which each molecule is chemisorbed at a bridge site. Individual benzene molecules are also observed between the ordered regions that likely correspond to the physisorbed benzene identified by SFG. Adding hydrogen to the system mobilizes the surface by STM. SFG is able to detect physisorbed and chemisorbed benzene. Heating the platinum surface after poisoning with CO displaces benzene molecules evidenced by SFG. STM is able to verify this after

imaging the (√19 x √19) *R*23.4° structure after cooling to room temperature, corresponding to the high-coverage pure CO structure.

6.2. Experimental

6.2.1 Sum Frequency Generation Vibrational Spectroscopy

All sum frequency generation experiments were carried out in a high-pressure/ultrahigh-vacuum (HP/UHV) system on a prepared Pt(111) single-crystal surface. The HP/UHV system consists of a UHV chamber operating at a base pressure of 2×10^{-9} Torr and a high-pressure (HP) cell isolated from the UHV chamber by a gate valve. The UHV chamber is equipped with an Auger electron spectrometer (AES), quadrupole mass spectrometer (QMS), and Ar^+ ion sputter gun. Two CaF_2 conflat windows on the HP cell allow transmission of infrared (IR), visible (VIS), and sum frequency radiation for SFG experiments. The HP cell is equipped with a re-circulation loop that includes a diaphragm pump and a septum for gas chromatographic analysis. The reactant and product gases are constantly mixed via a recirculation pump while kinetics data is acquired by periodically sampling the reaction mixture and measuring the relative gas phase composition with gas chromatography (GC) (flame ionization detection and 0.1% AT-1000 on Graphpac GC 80/100 packed column (Alltech)).

The Pt(111) crystal was cleaned by sputtering with Ar^+ ions (1 keV) for 20 minutes, heating to 1123 K in the presence of 5×10^{-7} Torr O_2 for 2 minutes, and then annealing at 1123 K for 2 minutes. AES and LEED were used to verify the cleanliness of the Pt(111) surface after several cleaning cycles. The Pt(111) sample was then transferred into the HP cell for SFG reaction studies. Benzene ($\geq$ 99.0 %, EM Science)

was purified by several freeze-pump-thaw cycles before introduction into the HP cell. Prior to the experiment, benzene was checked for impurities by means of GC. Such impurities were below 0.5 % and consisted of mostly light alkanes below C_6. During poisoning experiments, CO was introduced after the Pt(111) single crystal was exposed to benzene and hydrogen.

A Nd: YAG laser (1064 nm fundamental having a 20 ps pulse width operating at a 20 Hz repetition rate) was used to create a tunable IR (1800-4000 cm^{-1}) and a second harmonic VIS (532 nm) beam. The VIS beam (200 μJ) and the IR (200 μJ) beams were spatially and temporally overlapped on the Pt(111) surface with incident angles of 55º and 60º, with respect to the surface normal. All spectra were taken using a ppp polarization combination (SFG, VIS, and IR beams were all p-polarized). The generated SFG beam was sent through a monochromator and the signal intensity was detected with a photomultiplier tube and a gated integrator as the IR beam was scanned over the spectral range of interest. Spectra were curve fit using a previously reported procedure[16,17] to a form of the equation

$$I_{SFG} \propto \left| \chi_{NR}^{(2)} e^{i\phi_{NR}} + \sum_q \frac{A_q}{\omega_{IR} - \omega_q + i\Gamma_q} e^{i\gamma_q} \right|^2 \qquad (6.1)$$

where $\chi_{NR}^{(2)}$ is the nonresonant nonlinear susceptibility, $e^{i\phi_{NR}}$ is the phase associated with the nonresonant background, A_q is the strength of the qth vibrational mode, ω_{IR} is the frequency of the incident infrared laser beam, ω_q is the frequency of the qth vibrational mode, Γ_q is the natural line width of the qth vibrational transition, and $e^{i\gamma_q}$ is the phase

associated with the qth vibrational transition. Detailed descriptions on the HP/UHV system and SFG measurement can be found elsewhere.[1,5,18-21]

6.2.2 High Pressure Scanning Tunneling Microscopy

Scanning tunneling microscopy experiments were performed in a high-pressure, high-temperature STM that has been described in detail elsewhere.[22] The system combines a UHV surface analysis/preparation chamber with a variable temperature (298K - 675K) and pressure (10^{-10} - 10^{3} Torr) scanning tunneling microscope from RHK (model VT-UHV 300). The base pressure of the system was 1 x 10^{-10} Torr with a background mostly made up of H_2, CO and H_2O. Using three gate valves, the STM chamber can be isolated from the rest of the system and filled with any gas mixture up to a total pressure of 1 atm.

The sample was a platinum single crystal of (111) orientation from Matek Corporation with a miscut angle of $< 0.3^{\circ}$. Before each experiment the sample was sputtered in 5 x 10^{-6} Torr Ar^{+} for 15 minutes at an ion energy of 500 eV and current of 4 μA. After sputtering the sample was heated with an electron beam to 1073 K for 10 min. The sample was then sputtered again and annealed at 1073 K for 4 min before being transferred to the STM chamber. Sample composition was monitored using AES and its cleanliness / flatness checked with STM prior to gas introduction.

During experiments, the STM chamber was isolated from the rest of the system while combinations of benzene, hydrogen, argon, and carbon monoxide were introduced. The hydrogen, argon, and CO were of ultrahigh purity grade, while the benzene (>99.5%, Aldrich) was further purified by freeze-pump-thaw cycles prior to use. If the experiment

involved CO it was introduced after the sample had reached experimental temperature. A 150 W quartz projector bulb positioned just below the sample without making mechanical contact accomplished sample heating. A type K thermocouple spot-welded to the side of the crystal monitored sample temperature. The sample was always allowed to equilibrate at least 5 min prior to imaging. Images were taken with electrochemically etched tungsten tips, following the technique described by Klein *et al*.[23] STM settings during image acquisition were I = 0.05 - 0.2 nA and V = 50 - 100 mV. An MKS Instrument Baratron model 122A was used for 0.1mTorr - 10 Torr and model 722A for experiments exceeding 10 Torr.

6.3. Results and Discussion

6.3.1 *In-situ* SFG vibrational spectroscopy and HP- STM of surface species present on Pt(111) at 300 K under 10 Torr benzene

The SFG spectrum of the surface species adsorbed on Pt(111) at 10 Torr benzene at 300 K is presented in figure 6.1. Three peaks are observed at 2945, 3030, and 3060 cm^{-1}. The peak at 3060 cm^{-1} has been assigned to physisorbed benzene.[2,11] Previous studies using EELS[11,12], NEXAFS[15], RAIRS[24], and DFT[13,25] have shown that benzene adsorbs parallel to the surface on platinum. Since the molecule physisorbs intact, the six carbons and hydrogens are assumed to be roughly equivalent resulting in only one peak in the C-H stretching region as observed by EELS.[11,12] This assignment can be further substantiated by referencing the aromatic C-H stretch at 3068 cm^{-1} present in the gas phase IR spectrum.[11]

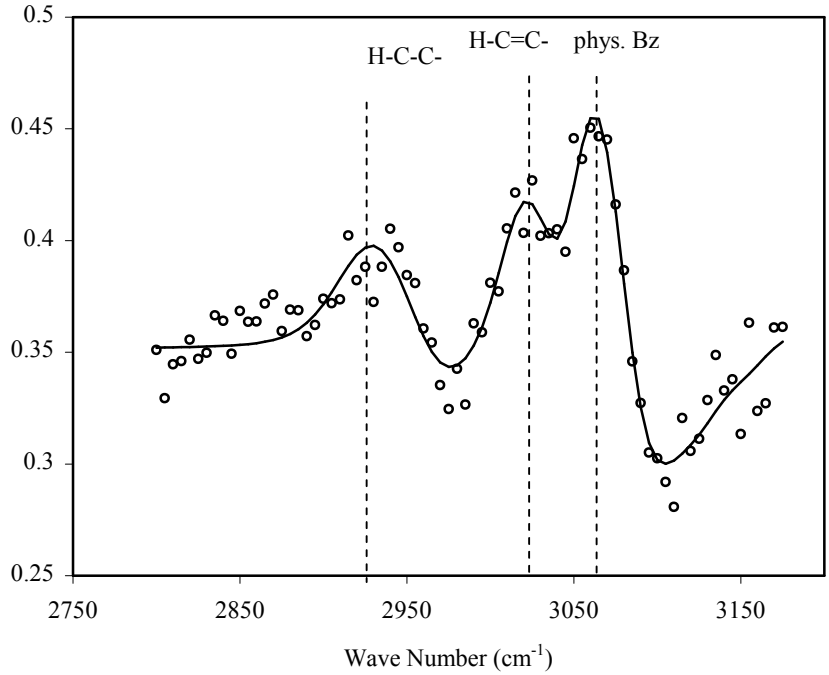

Figure 6.1. SFG spectra of surface species on Pt(111) under 10 Torr benzene at 300K. H-C-C-, vinylic (H-C=C-), and physisorbed benzene (phys. Bz) bands are identified. Markers represent experimental data and solid lines represent the curve fits to equation 6.1.

Two peaks centered around 2960 and 3020 cm^{-1} have been reported by infrared/high resolution electron energy loss spectroscopy (IR/HREELS)[12,14] for low coverages (0.2 L, Langmuir, 1 L = 10^{-6} Torr · s) of benzene. Thomas *et al.*[12] have suggested that the peak at 2960 cm^{-1} arises from an sp^3-hybridized carbon. The absence of modes at 1815 and 1960 cm^{-1} led Thomas *et al.*[12] to propose a structure of a dienyl nature for chemisorbed benzene (see scheme 6.1). Grassian and Muetterties have also proposed a similar chemisorption structure.[14] The proposed structure has two double and four single carbon-carbon bonds. The singly bonded carbons are bound to the platinum surface resulting in the sp^3-hybridized character of the vibrational signature. The

apparent simultaneous growth and decay of both the 2945 and 3030 cm^{-1} peaks with variation of temperature observed by SFG[2] corroborates this assignment. Hence, the modes in figure 6.1 have been assigned as follows: ν(H-C-C-) = 2945 cm^{-1}, ν(C-H)(vinylic) = 3030 cm^{-1}, and ν(C-H)(aromatic) = 3060 cm^{-1}. The absence of a symmetric CH_2 stretch in figure 6.1 indicated that the adsorbate is some C_6H_6 or more dehydrogenated species (e.g. polyaromatics).

Imaging the surface with HP-STM reveals a surface covered with immobile adsorbed benzene, as shown in figure 6.2. The surface is largely disordered with patches of short-range order composed of 15-30 adsorbed molecules. Previous studies of Pt(111) electrodes in a benzene solution by Yau *et al.*[26] yields very similar results with small ordered regions separated by disordered areas. These small patches appear to be the c(2√3 x 3)*rect* structure reported by Yau *et al.,*[26] in which each molecule is chemisorbed at a bridge site. Between the patches of order, easily resolved individual benzene molecules are also bound, which are likely bound to the 3-fold hollow site and are responsible for the physisorbed species observed in the SFG spectrum (see figure 6.1). In addition, several six member hexagonal rings (see figure 6.2(a)) form, in which all benzene molecules are adsorbed at 2-fold bridge sites.[26] Yau *et al.*[26] concluded that the "chemisorbed benzene at 2-fold sites is greatly distorted toward the boat-like structure" and that these structures appear to be (√21 x √21)*R*10.9°. These hexagonal rings have an apparently hollow center that most likely contains a weakly bound physisorbed species that is difficult to image due to its shorter residence time, as concluded by Yau *et al.*[26] who found that "an additional benzene molecule can be squeezed into the unit cell." Furthermore, Saeys *et al.*[13] found that the tilted geometry is energetically feasible through

DFT studies. Zebisch *et al.*[27] were able to observe the tilted adsorption of benzene on Pt(110) 1 × 2 with angle-resolved UV photoemission (ARUPS) and NEXAFS.

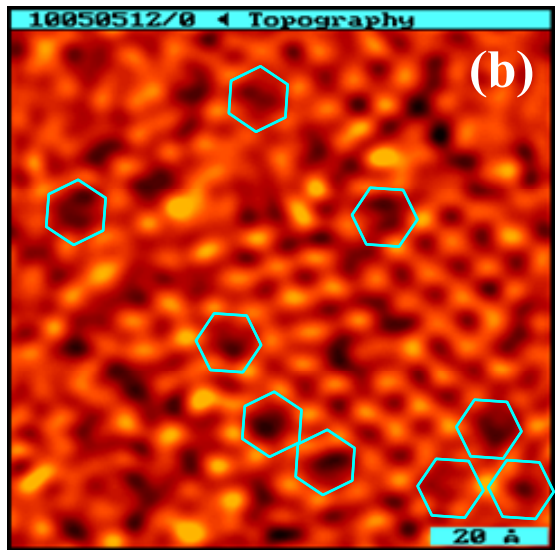

Figure 6.2. STM images of Pt(111) in the presence of 10 Torr benzene at 298K with a scan area of (a) 300Å × 300Å and (b) 95Å × 95Å. Hexagons represent six benzene molecules forming a hexagonal ring with an apparently hollow center, most likely containing a weakly bound physisorbed species.

6.3.2. Temperature dependence of the major surface species under 10 Torr benzene and 100 Torr H_2 as studied by HP-STM and SFG vibrational spectroscopy

Upon the addition of 100 Torr H_2 and 630 Torr Ar the surface changes dramatically, as evidenced by STM (see figure 6.3(a)). The patches of ordered benzene disappear and only a few isolated benzene molecules are visible on the largely mobile adsorbate layer. A few of the benzene molecules that can still be imaged are highlighted in figure 6.3(a). This is not entirely surprising as excess hydrogen is known to weaken

the surface bonding of adsorbed organic species and increase their mobility.[4] When the surface is heated to 353 K, all surface ordering of the resolved adsorbed molecules is lost as the adsorbed monolayer becomes too mobile to be imaged by our STM, as seen in figure 6.3(b).

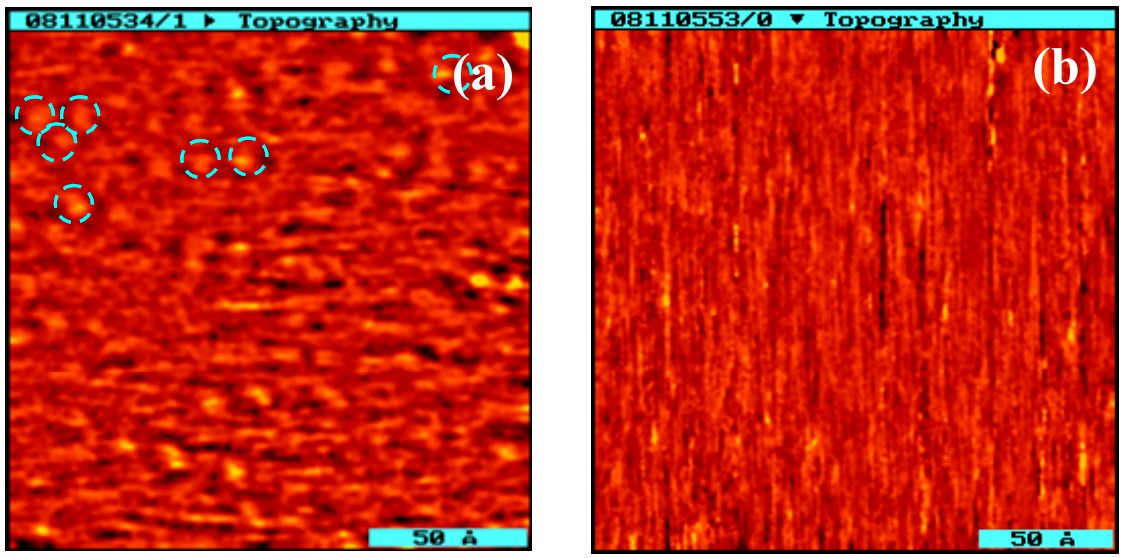

Figure 6.3. 200Å × 200Å STM images of Pt(111) in the presence of 10 Torr benzene, 100 Torr H_2, and 650 Torr Ar at (a) 298 K and (b) heated to 353 K. Rings represent adsorbed benzene.

The surface chemistry of adsorbed benzene in the presence of excess H_2 at elevated temperatures not visible by STM can be studied by SFG vibrational spectroscopy. Figure 6.4 shows the SFG spectra of 10 Torr benzene and 100 Torr H_2 on Pt(111) as the surface temperature is varied from 300 K to 440 K. Like the spectrum of 10 Torr benzene, these spectra exhibit three bands at 2945, 3030, and 3060 cm^{-1}. These bands are attributed to the chemisorbed and physisorbed species as discussed in the

previous section. Increasing the temperature to 320 K desorbs the physisorbed benzene, leaving the chemisorbed species as the dominant surface species. Chemisorbed benzene reaches a maximum surface coverage at 400 K based on the SFG signal intensity reaching a maximum at that temperature. Cooling the surface to 300 K allows physisorbed benzene to readsorb and shows that a carbonaceous layer does not poison the surface.

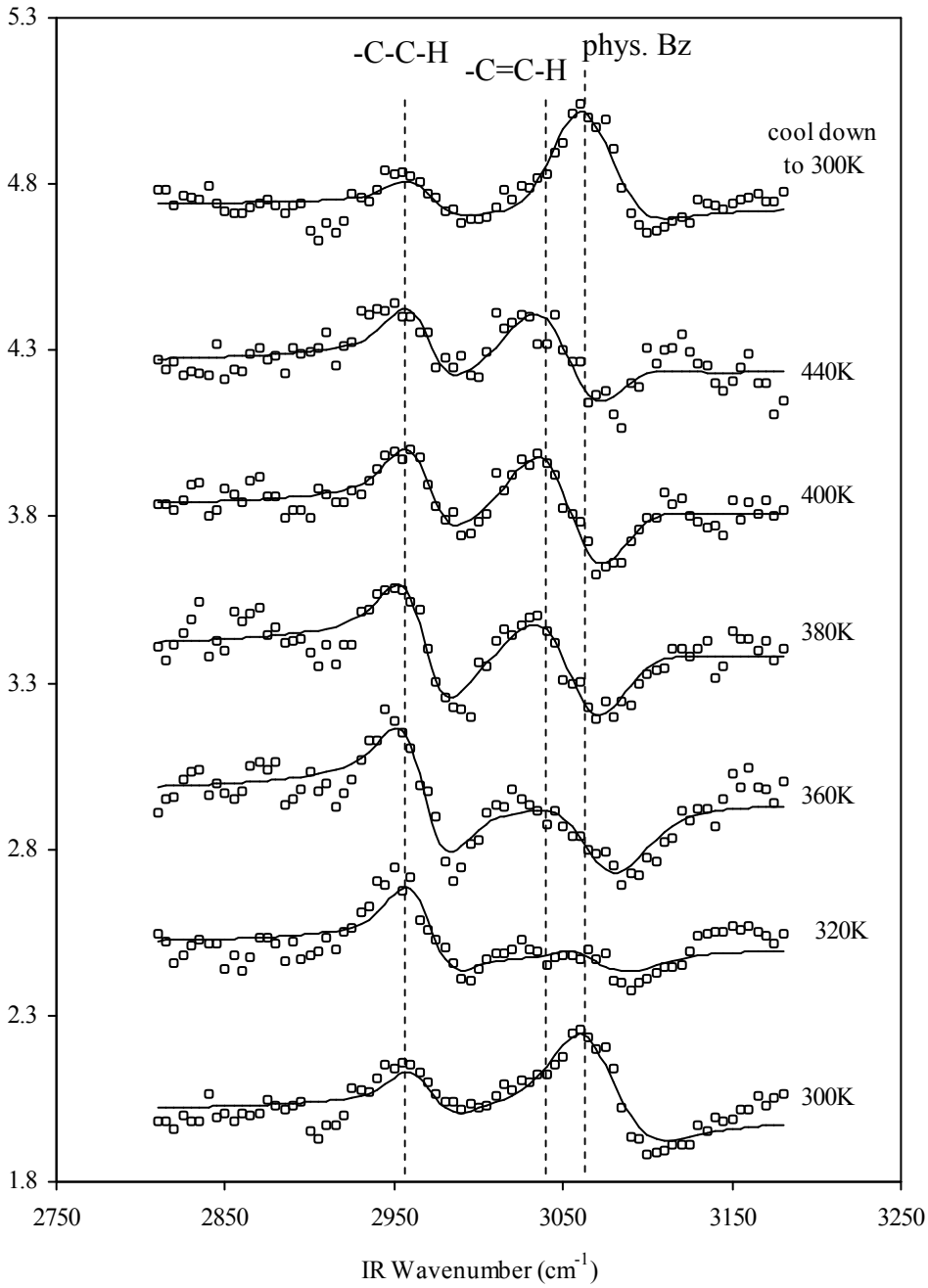

Figure 6.4. Temperature dependent SFG spectra of surface species on Pt(111) under 10 Torr benzene and 100 Torr H_2 in the range of 300-440 K. The top SFG spectrum was taken after the metal surface was cooled from 440 K to 300 K. H-C-C-, vinylic (H-C=C-), and physisorbed benzene (phys. Bz) bands are identified. Markers represent experimental data and solid lines represent the curve fits to equation 6.1.

6.3.3. Turnover rates and activation energies to form cyclohexane and cyclohexene under 10 Torr benzene on Pt(111) in the presence of 100 Torr H_2

Figure 6.5 displays the kinetic studies carried out in the presence of 10 Torr benzene and 100 Torr H_2 using gas chromatography detection over the 310 – 440 K temperature range. Estimated turnover rates (TORs) [molecules · Pt site^{-1} · s^{-1}] are shown in figure 6.5(a) giving production of cyclohexane and cyclohexene as a function of temperature. The corresponding Arrhenius plots of the TORs are given in figure 6.5(b). Above 370 K, the observed turnover frequencies for cyclohexane deviate from the linear Arrhenius regression line. This is explained by a change in the surface coverage of the adsorbed species as previously discussed.[1] The apparent activation energies for the hydrogenation to cyclohexane is 9.8 ± 0.1 kcal/mol. A maximum of cyclohexane turnover is observed at 400 K, corresponding to the maximum surface coverage of chemisorbed benzene as seen with SFG vibrational spectroscopy. In a previous study, Bratlie *et al.*[2] concluded that chemisorbed benzene is a reactive surface intermediate critical to benzene hydrogenation. This conclusion is further supported by our kinetic and vibrational studies.

Perhaps the most noticeable feature observed in figure 6.5(a) is the dip in cyclohexane formation at 380 K. This feature has been attributed to the onset of cyclohexene formation, which is initially observed at 370 K but significantly increases with surface temperature. Previous studies[2] have ascribed this to the larger sticking coefficient of cyclohexene (0.2[28]) as compared to cyclohexane (<0.1[29]). This larger sticking coefficient allows for further hydrogenation of cyclohexene.

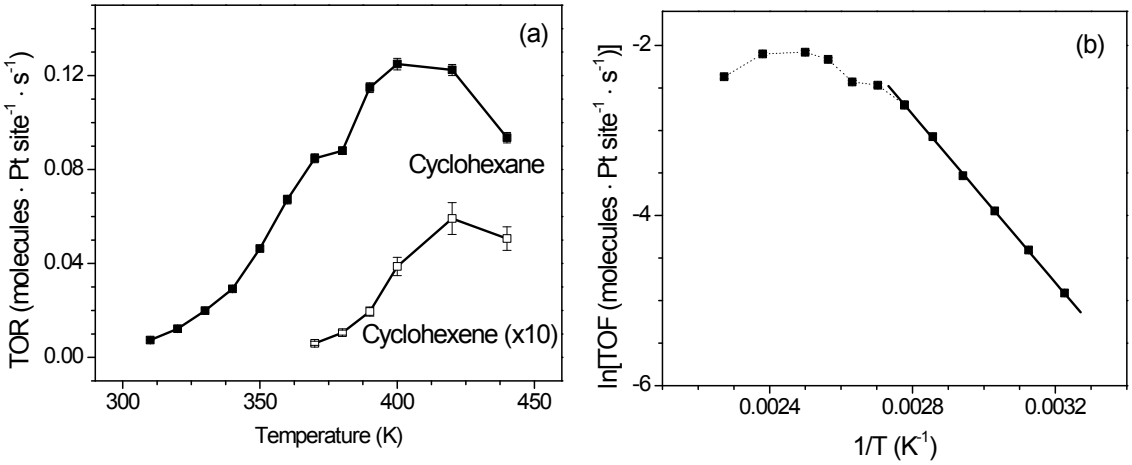

Figure 6.5. (a) Turnover rates (TORs) for the hydrogenation to cyclohexane and cyclohexene under 10 Torr benzene and 100 Torr H_2 and (b) Arrhenius plots for the TORs of cyclohexane. Apparent activation energies are 9.8 ± 0.1 kcal/mol for cyclohexane formation. The non-Arrhenius behavior above 370 K is explained in terms of changes in the surface coverage of the adsorbates. The dotted line was drawn for visual aide.

6.3.4. Major surface species present under 10 Torr benzene and 100 Torr H_2 after poisoning with 5 Torr CO as studied by HP- STM and SFG vibrational spectroscopy: Temperature effects

Previous studies by Ogletree *et* al.[30] show that adsorbing CO molecules first creates a very large work function for the hydrocarbon to overcome in order to adsorb on the surface. For this reason, CO was introduced after benzene and H_2 addition. The presence of CO has no effect on the surface structure of the system as observed by STM at 353 K. Again, this is attributed to the fact that although CO is now present on the

surface its high mobility makes imaging with STM difficult. This is also observed previously under lower pressure conditions.[4,8] When the mobile CO dominated surface is cooled to 298K, the increase in CO surface coverage forms an immobile surface structure as can be seen in figure 6.6. This high-coverage pure CO structure was first reported by the Besenbacher group[31] and observed in our laboratory as well.[3] The structure corresponds to the (√19 x √19) *R*23.4˚ structure with a total coverage of ~0.7 monolayers. As observed with STM that benzene no longer remains on the surface, as all physisorbed and chemisorbed species are displaced by the stronger bound and closer packed CO molecules.

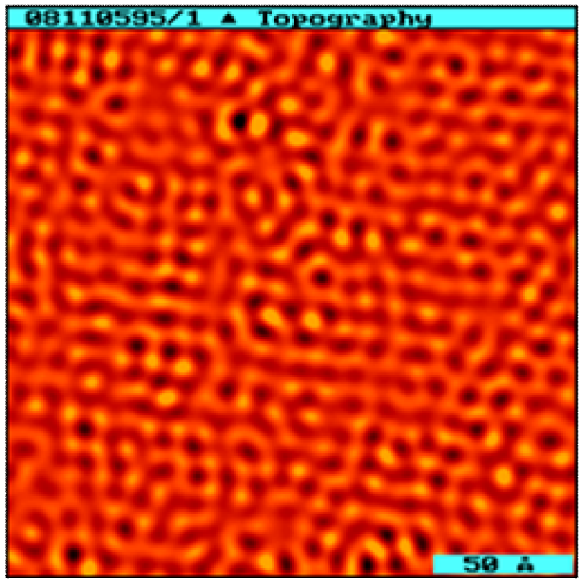

Figure 6.6. 200Å × 200Å STM image of Pt(111) in the presence of 10 Torr benzene, 100 Torr H_2, and 630 Torr Ar heated to 353 K, 5 Torr CO added, and cooled to 298 K. The high-coverage pure CO structure corresponds to the (√19 x √19) R23.4˚ structure. All benzene adsorbates have been displaced by the strongly bound and closely packed CO molecules.

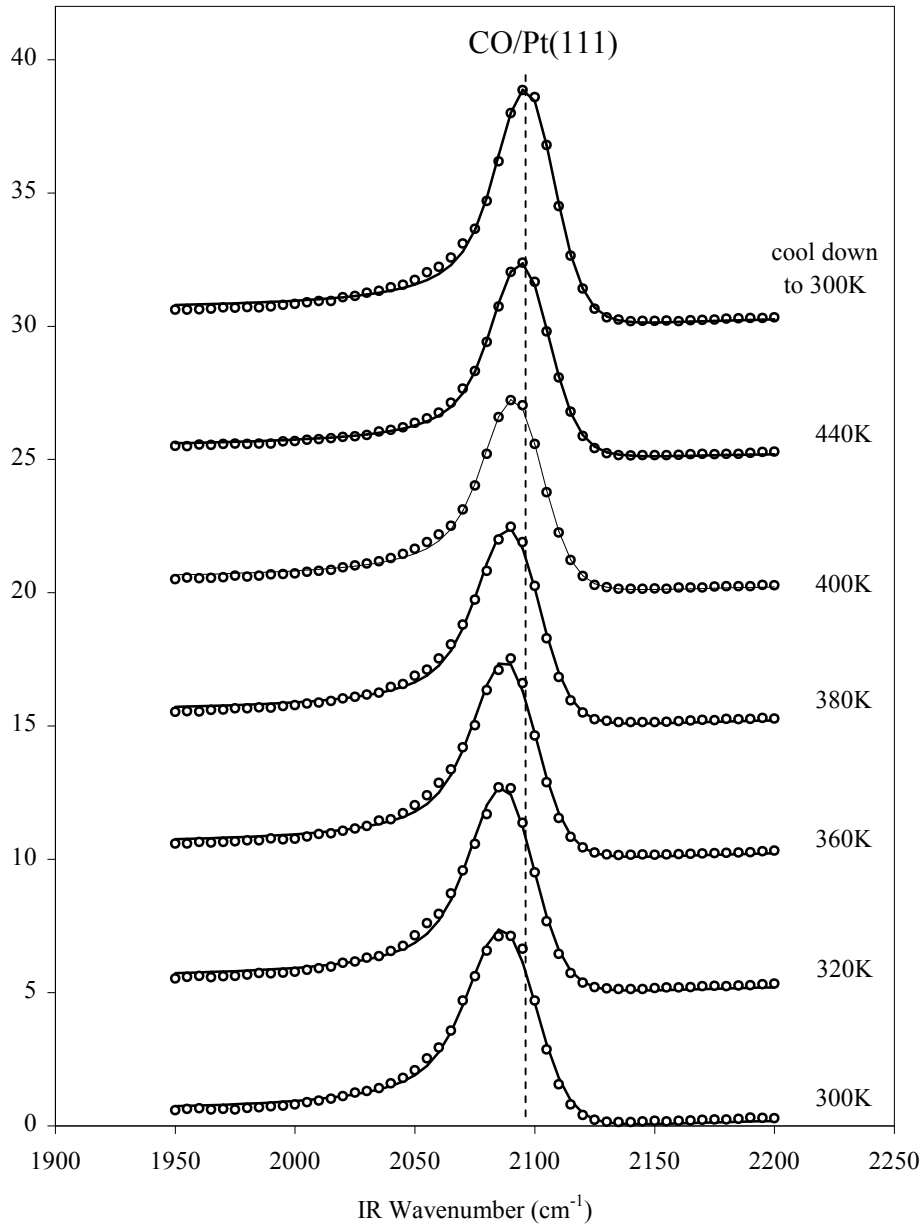

Figure 6.7. Temperature dependent SFG spectra of surface species on Pt(111) under 10 Torr benzene, 100 Torr H_2, and 5 Torr CO in the range of 300-440 K. The top SFG spectrum was taken after the metal surface was cooled from 440 K to 300 K. The band for the C-O stretch adsorbed on clean Pt(111) is identified. Markers represent experimental data and solid lines represent the curve fits to equation 6.1.

In order to understand how CO affects adsorbates at elevated temperatures, SFG is used to monitor the system under identical conditions. McCrea *et al.*[32] have reported that CO adsorbed on clean Pt(111) has a C-O stretch at 2094 cm^{-1}. Upon CO co-adsorption with benzene and H_2, the C-O stretch appears at 2090 cm^{-1}, as given figure 6.7. The red shifting of the C-O stretch results from a weakening of the C-O bond, which may be due to an interaction with the adsorbed benzene. According to Jasen *et al.,*[33] the red shift results from a "charge transfer from benzene via the substrate to CO," which strengthens the CO-Pt bond. Increasing the surface temperature to 440 K blue shifts the C-O band to 2094 cm^{-1} (illustrated in figure 6.8), which remains on the surface as it is cooled to 300 K displaying the irreversibility of the system. Presumably, the blue shift of the C-O band results from displacement of the benzene molecules, as observed with STM.

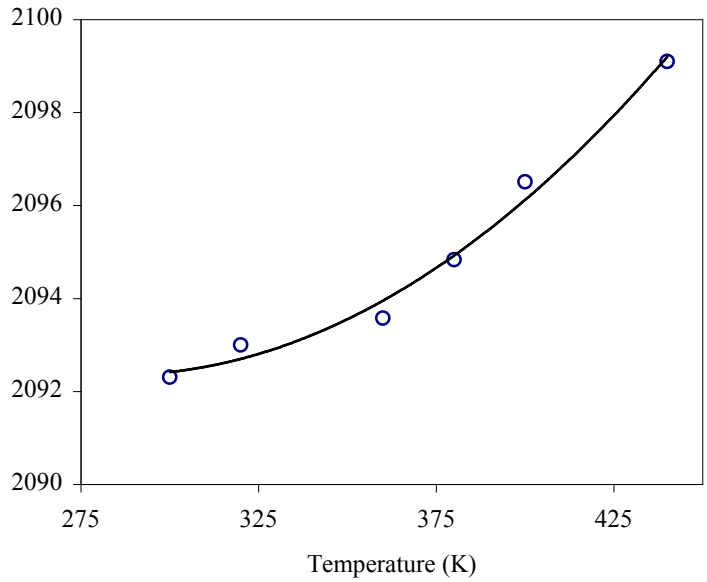

Figure 6.8. CO vibrational resonance frequency, ω_{CO}, plotted against the metal surface temperature. Solid line drawn as a visual aide.

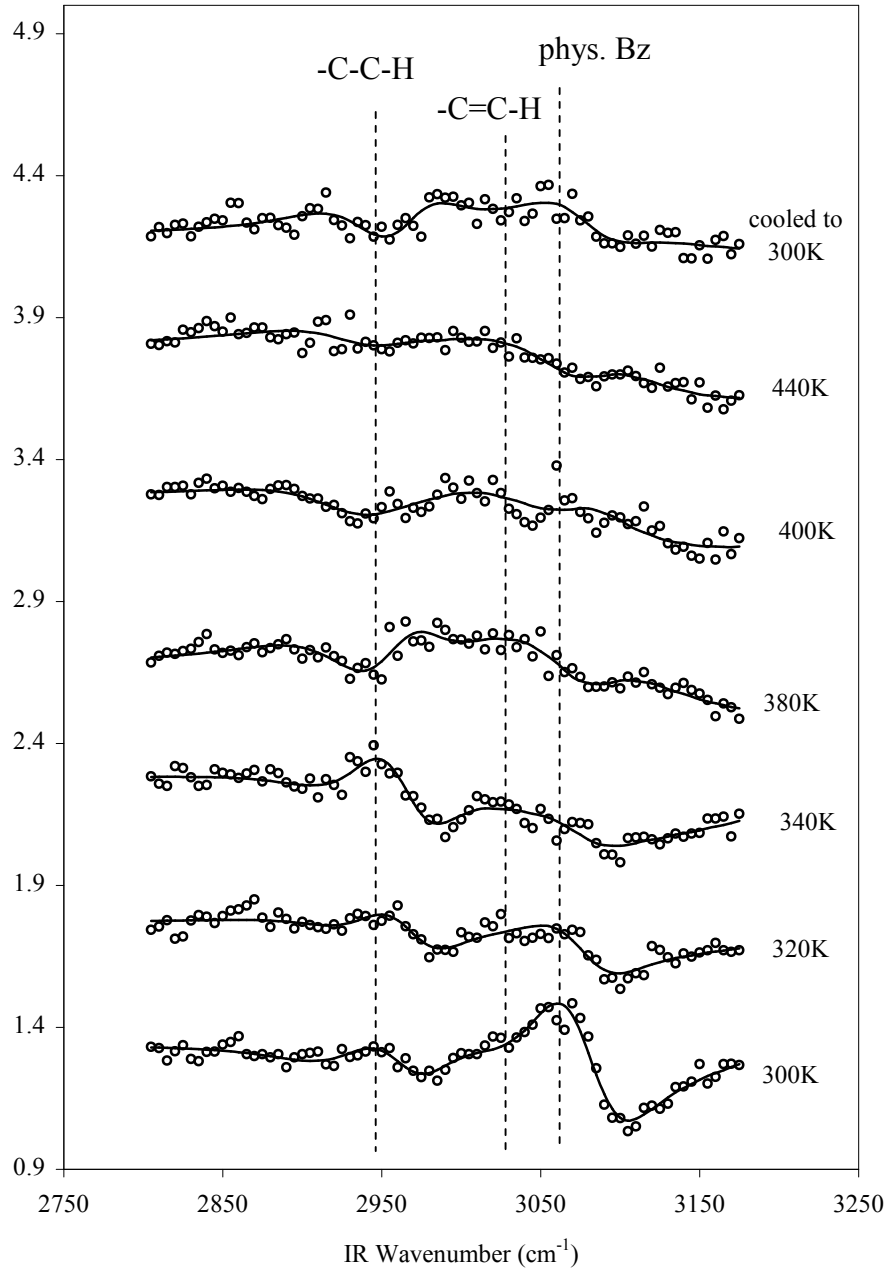

Figure 6.9. Temperature dependent SFG spectra of surface species on Pt(111) under 10 Torr benzene, 100 Torr H_2, and 5 Torr CO in the range of 300-440 K. The top SFG spectrum was taken after the metal surface was cooled from 440 K to 300 K. H-C-C-, vinylic (H-C=C-), and physisorbed benzene (phys. Bz) bands are identified. Markers represent experimental data and solid lines represent the curve fits to equation 6.1.

SFG vibrational spectroscopy is also used to probe this system in the C-H stretching region, as shown in figure 6.9. Co-adsorption of CO with benzene and H_2 reveals a similar spectrum with and without H_2 at 300 K (see figures 6.1 and 6.4). Heating the surface led to the eventual desorption of physisorbed and chemisorbed benzene. Neither of these surface species readsorb after cooling the surface to 300 K. Based on the results from STM and the SFG spectra of the C-O stretching region we conclude that CO displaces any hydrocarbon previously on the surface. Furthermore, since the C-O vibration after cooling from 440 K to 300 K is so similar to CO on clean platinum, we assert that benzene desorbs intact and does not dehydrogenate to form a carbonaceous layer.

6.4. Conclusions

The chemical composition and adsorption structures of the surface species are measured during benzene hydrogenation on Pt(111) by SFG vibrational spectroscopy and high-pressure STM. Small ordered regions corresponding to the c(2√3 x 3)*rect* structure, in which each molecule is chemisorbed at a bridge site, are imaged in a 10 Torr background of benzene. Individual physisorbed benzene molecules are observed between these ordered regions. Several six member hexagonal rings with a seemingly hollow center are imaged. The hollow center most likely contains a physisorbed species. Upon the addition of hydrogen, SFG is necessary to characterize the surface as it has become too mobile to image. Both physisorbed and chemisorbed benzene are present under 100 Torr hydrogen. Raising the temperature desorbs physisorbed benzene and leaves the chemisorbed species on the surface. Spectroscopic evidence shows that

poisoning the reaction with CO displaces the adsorbed benzene molecules. This assertion is validated by the (√19 x √19) *R*23.4˚ structure imaged after cooling the surface, which corresponds to pure CO at high-coverages.

References

(1) Bratlie, K. M.; Flores, L. D.; Somorjai, G. A. *Surface Science* **2005,** *599*, 93-106.

(2) Bratlie, K. M.; Flores, L. D.; Somorjai, G. A. *Journal of Physical Chemistry B* **2006,** *110*, 10051-10057.

(3) Montano, M. O.; Braltie, K. M.; Salmeron, M. B.; Somorjai, G. A. *Journal of the American Chemical Society* **2006,** *128*, 13229-13234.

(4) Montano, M. O., Salmeron, M.B., Somorjai, G.A. *Surface Science* **2006,** *600*, 1809-1816.

(5) Yang, M.; Tang, D. C.; Somorjai, G. A. *Review of Scientific Instruments* **2003,** *74*, 4554-4557.

(6) Yang, M.; Chou, K. C.; Somorjai, G. A. *Journal of Physical Chemistry B* **2003,** *107*, 5267-5272.

(7) Yang, M.; Somorjai, G. A. *Journal of the American Chemical Society* **2003,** *125*, 11131-11135.

(8) Weiss, P. S.; Eigler, D. M. *Physical Review Letters* **1993,** *71*, 3139-3142.

(9) Sautet, P.; Bocquet, M.-L. *Physical Review B* **1996,** *53*, 4910-4925.

(10) Abon, M.; Bertolini, J. C.; Billy, J.; Massardier, J.; Tardy, B. *Surface Science* **1985,** *162*, 395-401.

(11) Lehwald, S.; Ibach, H.; Demuth, J. E. *Surface Science* **1978,** *78*, 577-590.

(12) Thomas, F. S.; Chen, N. S.; Ford, L. P.; Masel, R. I. *Surface Science* **2001,** *486*, 1-8.

(13) Saeys, M.; Reyniers, M.; Marin, G. B. *Journal of Physical Chemistry B* **2002,** *106*, 7489-7498.

(14) Grassian, V. H.; Muetterties, E. L. *Journal of Physical Chemistry* **1987,** *91*, 389-396.

(15) Horsley, J. A.; Stohr, J.; Hitchcock, A. P.; Newbury, D. C.; Johnson, A. L.; Sette, F. *Journal of Chemical Physics* **1985,** *83*, 6099-6107.

(16) Bain, C. D.; Davies, P. B.; Ong, T. H.; Ward, R. N.; Brown, M. A. *Langmuir* **1991,** *7*, 1563-1566.

(17) Moore, F. G.; Becraft, K. A.; Richmond, G. L. *Applied Spectroscopy* **2002,** *56*, 1575-1578.

(18) Kung, K. Y.; Chen, P.; Wei, F.; Rupprechter, G.; Shen, Y. R.; Somorjai, G. A. *Review of Scientific Instruments* **2001,** *72*, 1806-1809.

(19) Shen, Y. R. *The Principles of Nonlinear Optics*; Wiley: New York, **2003.**

(20) Shen, Y. R. *Annual Review of Physical Chemistry* **1989,** *40*, 327-350.

(21) Shen, Y. R. *Nature* **1989,** *337*, 519-525.

(22) Jenson, J. A.; Rider, K. B.; Chen, Y.; Salmeron, M. B.; Somorjai, G. A. *Journal of Vacuum Science and Technology B* **1999,** *17*, 1080-1084.

(23) Klein, M.; Schwitzgebel, G. *Review of Scientific Instruments* **1997,** *68*, 3099-3103.

(24) Haq, S.; King, D. A. *Journal of Physical Chemistry* **1996,** *100*, 16957-16965.

(25) Morin, C.; Simon, D.; Sautet, P. *Journal of Physical Chemistry B* **2004,** *108*, 5653-5665.

(26) Yau, S.-L.; Kim, Y.-G.; Itaya, K. *Journal of the American Chemical Society* **1996,** *118*, 7795-7803.

(27) Zebisch, P.; Stichler, M.; Trischberger, P.; Weinelt, M.; Steinruck, H.-P. *Surface Science* **1998,** *396*, 61-77.

(28) Henn, F. C.; Diaz, A. L.; Bussel, M. E.; Huggenschmidt, M. B.; Domagala, M. E.; Campbell, C. T. *Journal of Physical Chemistry* **1992,** *96*, 5965-5974.

(29) Ihm, H.; Ajo, H. M.; Gottfried, J. M.; Bera, P.; Campbell, C. T. *Journal of Physical Chemistry B* **2004,** *108*, 14627-14633.

(30) Ogletree, D. F.; Van Hove, M. A.; Somorjai, G. A. *Surface Science* **1987,** *183*, 1-20.

(31) Longwitz, S. R.; Schnadt, J.; Vestergaard, E. K.; Vang, R. T.; Laegagaard, E.; Stensgaard, I.; Brune, H.; Besenbacher, F. *Journal of Physical Chemistry B* **2004,** *108*, 14497-14502.

(32) McCrea, K. R.; Parker, J. S.; Somorjai, G. A. *Journal of Physical Chemistry B* **2002,** *106*, 10854-10863.

(33) Jasen, P. V.; Brizuela, G.; Padin, Z.; Gonzalez, E. A.; Juan, A. *Applied Surface Science* **2004,** *236*, 394-405.

Chapter 7

Structure Effects of Benzene Hydrogenation Studied with Sum Frequency Generation Vibrational Spectroscopy and Kinetics on Pt(111) and Pt(100) Single Crystal Surfaces

Sum frequency generation (SFG) surface vibrational spectroscopy and kinetic measurements using gas chromatography (GC) have identified at least two reaction pathways for benzene hydrogenation on the Pt(100) and Pt(111) single crystal surfaces at Torr pressures. Kinetic studies at low temperatures (310 – 370 K) show that benzene hydrogenation does not proceed through cyclohexene. A Langmuir-Hinshelwood type rate law for the low temperature reaction pathway is identified. The rate-determining step for this pathway is the addition of the first hydrogen atom to adsorbed benzene for both surfaces, which is verified by the spectroscopic observation of adsorbed benzene at low temperatures on both the Pt(100) and Pt(111) crystal faces. Low temperature SFG studies reveal chemisorbed and physisorbed benzene on both surfaces. At higher temperatures (370 – 440 K), hydrogenation of benzene to π-allyl c-C_6H_9 is observed only on the Pt(100) surface. Previous single crystal studies have identified π-allyl c-C_6H_9 as the rate-determining step for cyclohexene hydrogenation to cyclohexane.

7.1. Introduction

Benzene hydrogenation is an industrially relevant reaction for several essential steps in petroleum refining and downstream chemical processing.[1] Identifying reactive

surface intermediates and rate laws is a key issue in understanding the mechanism of benzene hydrogenation. Furthermore, understanding how these surface intermediates and rate laws are affected by surface structure is of importance to extend our knowledge of single-crystals to industrial catalysts.

Benzene adsorption on platinum at low pressures (< 10^{-6} Torr) has been studied using various surface-analytical techniques, including low energy electron diffraction (LEED),[2] near edge X-ray absorption fine structure spectroscopy (NEXAFS),[3] calorimetry,[4] thermal desorption spectroscopy (TDS),[5,6] electron energy loss spectroscopy (EELS),[7-9] scanning tunneling microscopy (STM),[10] and reflection-absorption infrared spectroscopy (RAIRS).[11,12] In addition, possible adsorption energies for different adsorption sites and surface species have been studied by density function theory (DFT).[13-15] STM[10] and DFT[15] studies show that benzene preferentially adsorbs to bridge sites in the low coverage limit and to the three-fold hollow at high coverages on the Pt(111) crystal face. The low and high coverage species have two distinct vibrational signatures, as studied by EELS,[8,9] which correspond to chemisorbed and physisorbed benzene. Thomas *et al*.[9] proposed the chemisorbed species is a dienyl benzene, illustrated in scheme 7.1(a). Physisorbed benzene, on the other hand, is thought of as flat lying based on NEXAFS studies.[3]

High-pressure reactions of benzene on Pt(111) have been investigated using sum frequency generation (SFG) vibrational spectroscopy[16,17] and high-pressure STM.[16] These studies observe both chemisorbed and physisorbed benzene under high-pressure conditions. STM observed small ordered regions corresponding to the *c*($2\sqrt{3} \times 3$)*rect* structure in a background of 10 Torr benzene.[16] Between the ordered regions, individual

benzene molecules were observed by STM.[16] Based on the SFG results, the individual molecules were assumed to be physisorbed benzene, while the ordered regions correspond to the chemisorbed benzene. Conducting these experiments on Pt(100) will further our knowledge of this reaction, in particular how structure affects the reaction pathway.

(a) dienyl chemisorbed benzene (b) π-allyl c-C_6H_9

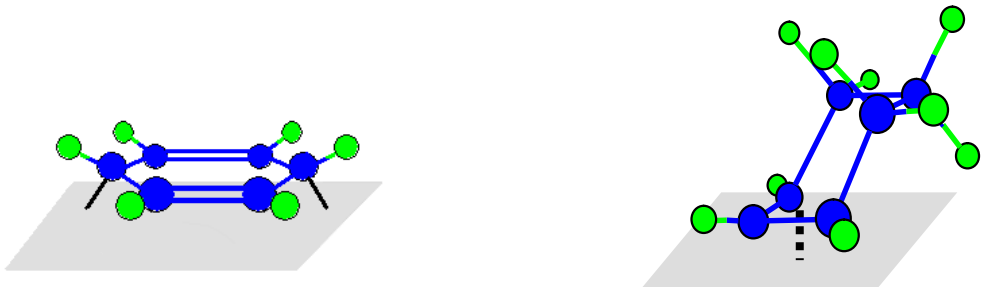

Scheme 7.1. Schematic diagram of (a) dienyl chemisorbed benzene (C_6H_6) and (b) π-allyl c-C_6H_9 intermediates.

In this study, sum frequency generation (SFG) vibrational spectroscopy and gas chromatography (GC) are used to investigate benzene hydrogenation at high temperatures (310 – 440 K) to elicit structure effect information. Media with centrosymmetry and isotropic gases do not appear in the SFG spectrum under the electric dipole approximation. Since bulk platinum has a center of inversion, its contribution to the SFG signal is negligible. The symmetry at the surface of the platinum crystal is broken, giving rise to a surface specific signal. Because the SFG signal arises solely from the adsorbates, SFG is a more sensitive tool to study interfaces than infrared absorption and Raman spectroscopies. Electron spectroscopies typically cannot be employed under ambient pressure conditions necessary to perform catalytic reactions.

Here, I report evidence for chemisorbed dienyl benzene (C_6H_6) as the reactive surface intermediate for benzene hydrogenation on both the Pt(100) and Pt(111) surfaces at high pressures (7.5, 10, 12.5, and 15 Torr benzene and 10, 50, 100, and 150 Torr H_2) and at high temperatures (310 – 440 K). Both surfaces exhibit co-adsorbed chemisorbed and physisorbed benzene at low temperatures. Differences arise as the temperature is increased: π-allyl c-C_6H_9 (see scheme 7.1(b))is observed on the Pt(100) surface at high temperatures and not on the Pt(111) surface. Previous studies show that π-allyl c-C_6H_9 is the most abundant surface intermediate during cyclohexene hydrogenation.[18,19] These studies also suggest that the hydrogenation of π-allyl c-C_6H_9 is the rate determining step (RDS) in forming cyclohexane. Kinetic studies on benzene hydrogenation to cyclohexane at low temperatures have identified a rate law where the RDS is the addition of the first hydrogen to benzene. Herein, we discuss the temperature, pressure, and structure dependent surface chemistry of benzene hydrogenation on Pt(100) and Pt(111).

7.2. Experimental

All experiments were carried out in a high-pressure/ultrahigh-vacuum (HP/UHV) system on a prepared Pt(100) or Pt(111) single-crystal surface. The HP/UHV system consists of a UHV chamber operating at a base pressure of 2×10^{-9} Torr and a high-pressure (HP) cell isolated from the UHV chamber by a gate valve. The UHV chamber is equipped with an Auger electron spectrometer (AES), quadrupole mass spectrometer (QMS) and Ar^+ ion sputter gun. Two CaF_2 conflat windows on the HP cell allow transmission of infrared (IR), visible (VIS), and sum frequency radiation for SFG experiments. The HP cell is equipped with a re-circulation loop that includes a

diaphragm pump and a septum for gas chromatographic analysis. The reactant and product gases are constantly mixed via a recirculation pump while kinetic data is acquired by periodically sampling the reaction mixture and measuring the relative gas phase composition (flame ionization detection and 0.1% AT-1000 on Graphpac GC 80/100 packed column (Alltech)).

The Pt(100) and Pt(111) crystals were cleaned by sputtering with Ar^+ ions (1 keV) for 20 minutes, heating to 1123 K in the presence of 5×10^{-7} Torr O_2 for 2 minutes, and then annealing at 1123 K for 2 minutes. AES and LEED were used to verify the cleanliness of the Pt(100) or Pt(111) surface after several cleaning cycles. The Pt(100) or Pt(111) sample was then transferred into the HP cell for SFG reaction studies. Benzene ($\geq$ 99.0 %, EM Science) was purified by several freeze-pump-thaw cycles before introduction into the HP cell. Prior to the experiment, benzene was checked for impurities by means of GC. Such impurities were below 0.5 % and consisted of mostly light alkanes below C_6.

SFG measurements were performed using a mode locked Nd:YAG laser (1064 nm fundamental having a 20 ps pulse width operating at a 20 Hz repetition rate) to create a tunable IR (1800-4000 cm^{-1}) and a second harmonic VIS (532 nm) beam. The VIS beam (200 μJ) and the IR (200 μJ) beams were spatially and temporally overlapped on the Pt(111) surface with incident angles of 55º and 60º, with respect to the surface normal. All spectra were taken using a ppp polarization combination (SFG, VIS, and IR beams were all p-polarized). The generated SFG beam was sent through a monochromator and the signal intensity was detected with a photomultiplier tube and a gated integrator as the IR beam was scanned over the frequency range of interest. The

sum frequency output was normalized by the intensity of the incident infrared beam at the surface. This is necessary because gas molecules absorb some of the incoming radiation. Spectra were curve fit using a previously reported procedure[20,21] to a form of the equation

$$I_{SFG} \propto \left| \chi_{NR}^{(2)} e^{i\phi_{NR}} + \sum_q \frac{A_q}{\omega_{IR} - \omega_q + i\Gamma_q} e^{i\gamma_q} \right|^2 \qquad (7.1)$$

where $\chi_{NR}^{(2)}$ is the nonresonant nonlinear susceptibility, $e^{i\phi_{NR}}$ is the phase associated with the nonresonant background, A_q is the strength of the qth vibrational mode, ω_{IR} is the frequency of the incident infrared laser beam, ω_q is the frequency of the qth vibrational mode, Γ_q is the natural line width of the qth vibrational transition, and $e^{i\gamma_q}$ is the phase associated with the qth vibrational transition. Detailed descriptions on the HP/UHV system and SFG measurement can be found elsewhere.[19,22-26]

7.3. Results

7.3.1. Turnover rates, reaction orders, and Arrhenius parameters for benzene hydrogenation to cyclohexane under varied pressures of benzene and hydrogen on Pt(100) and Pt(111)

Figure 7.1 shows the kinetic data obtained for 100 Torr H_2 and 7.5, 10, 12.5, and 15 Torr benzene over a range of temperatures (310-440 K). The production of cyclohexane is displayed at different temperatures by the turnover rates (TORs) [molecules · Pt site^{-1} · s^{-1}] shown in figure 7.1(a). The TORs are calculated based on the assumption that every platinum atom is an active site. The errors associated with the measurements are shown as error bars in figure 7.1(a). The corresponding Arrhenius

plots of the TORs are given in figure 7.1(b). TORs were also collected for a constant benzene pressure (10 Torr) with a varied H_2 pressure (10, 50, 100, and 150 Torr). The TORs for cyclohexane formation are shown in figure 7.2(a) with the resultant Arrhenius plots in figure 7.2(b). Above 370 K, the observed TORs for cyclohexane deviate from the linear Arrhenius line; this results from a change in the surface coverage of the adsorbed species, as previously discussed.[19] Apparent activation energies and pre-exponentials for hydrogenation to cyclohexane are listed in table 7.1. These experiments have been carried out on the Pt(111) surface previously[17] and are summarized in table 7.1.

	Pt(111)		Pt(100)	
	ln(A)	E_a	ln(A)	E_a
10.5 Torr Benzene				
11.2 Torr H_2	3.0 ± 0.3	7.0 ± 0.2	5.4 ± 0.8	8.7 ± 0.5
52 Torr H_2	4.7 ± 0.5	8.0 ± 0.3	6.3 ± 0.3	9.4 ± 0.2
105 Torr H_2	7.3 ± 0.1	9.8 ± 0.1	14.9 ± 0.2	15.7 ± 0.1
158 Torr H_2	8.5 ± 0.7	10.6 ± 0.4	11.2 ± 0.1	12.5 ± 0.1
105 Torr H_2				
7.9 Torr Bz	6.0 ± 0.3	9.3 ± 0.3	20.0 ± 0.2	18.9 ± 0.1
10.5 Torr Bz	7.3 ± 0.1	9.8 ± 0.1	17.1 ± 1.2	16.8 ± 0.8
13.3 Torr Bz	5.9 ± 0.1	8.9 ± 0.1	14.9 ± 0.2	15.7 ± 0.1
16.5 Torr Bz	8.1 ± 0.7	10.5 ± 0.2	12.4 ± 0.2	13.6 ± 0.1

	order Pt(111)	order Pt(100)
Benzene	-1.1 ± 0.1	-1.1 ± 0.3
H_2	0.6 ± 0.01	0.6 ± 0.02

	T_i/(K)	υ/(cm^{-1})
C_6H_{12}	358 ± 5	501 ± 7

Table 7.1. Pre-exponentials (in molecules per Pt atom per second), apparent activation energies (in kcal/mol), orders for both H_2 and benzene, isokinetic temperature (in K), and the critical vibration (in cm^{-1}) for C_6H_{12} production under a constant pressure of 10 Torr benzene varying H_2 and under constant pressure of 100 Torr H_2 while varying benzene.

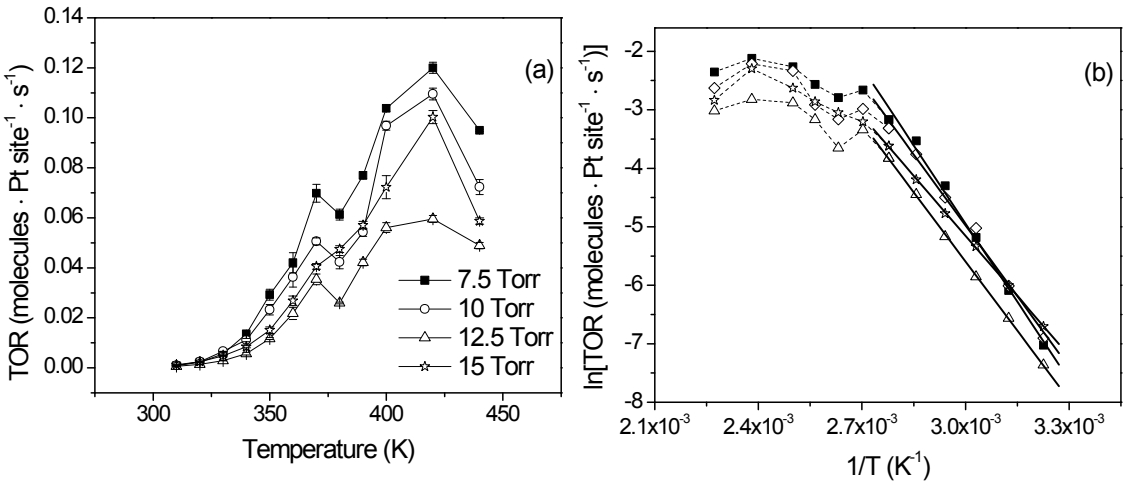

Figure 7.1. (a) Turnover rates (TORs), in molecules per Pt atom per second, for benzene (7.5, 10, 12.5, and 15 Torr) in the presence of H_2 (100 Torr) on Pt(100) to form CHA. (b) Arrhenius plots of the corresponding TORs. The decrease in the TOR for cyclohexane production at 380 K followed by a sharp increase at 390 K is attributed to the onset of cyclohexene production. Cyclohexene has a higher sticking probability on platinum resulting in further hydrogenation to cyclohexane. The non-Arrhenius behavior above 370 K is explained in terms of changes in the surface coverage of the adsorbates. Apparent activation energies and pre-exponentials are listed in table 7.1. Dotted lines were drawn for visual aides.

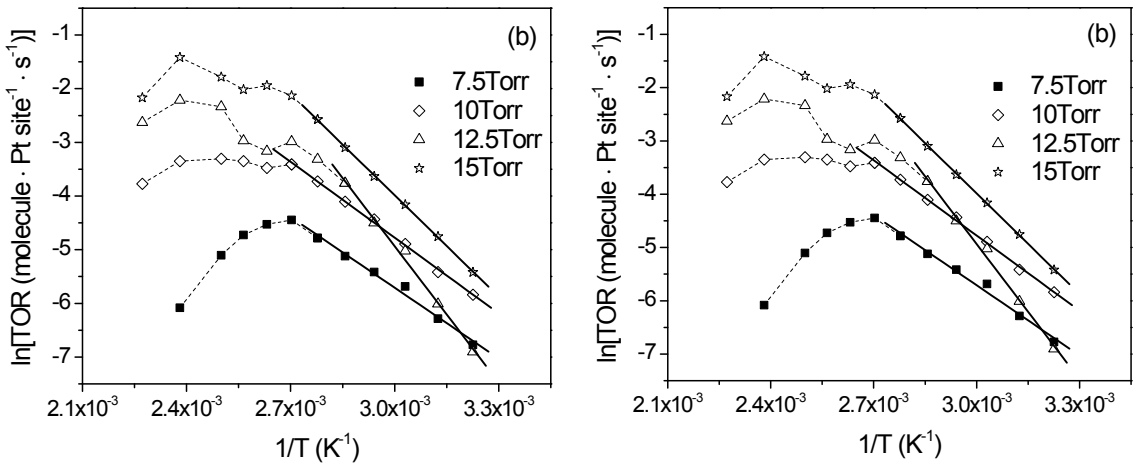

Figure 7.2. (a) Turnover rates (TORs), in molecules per Pt atom per second, for benzene (10 Torr) in the presence of H_2 (10, 50, 100, and 150 Torr) on Pt(100) to form CHA. (b) Arrhenius plots of the corresponding TORs. The decrease in the TOR for cyclohexane production at 380 K followed by a sharp increase at 390 K is attributed to the onset of cyclohexene production. Cyclohexene has a higher sticking probability on platinum resulting in further hydrogenation to cyclohexane. The non-Arrhenius behavior above 370 K is explained in terms of changes in the surface coverage of the adsorbates. Apparent activation energies and pre-exponentials are listed in table 7.1. Dotted lines were drawn for visual aides.

The rate law for benzene hydrogenation can be described by a standard empirical power law

$$r = k p_{C_6H_6}{}^{a} p_{H_2}{}^{b} \tag{7.2}$$

where r is the rate of reaction, $p_{C_6H_6}$ and p_{H_2} are the pressures of the reactant gases (benzene and H_2, respectively), a and b are the reaction order with respect to the reactant species, and *k* is the rate constant. The rate constant can be expressed as

$$k = Ae^{-E_a / RT} \tag{7.3}$$

where A is the pre-exponential factor, E_a is the activation energy, R is the gas constant, and T is temperature. The exponents a and b are determined over a range of reaction temperatures (310 – 370 K using

$$a = \left[\frac{\partial \ln r}{\partial \ln p_{C_6H_6}} \right]_{p_{H_2}} . \tag{7.4}$$

The benzene and H_2 reaction orders for cyclohexane production on both the Pt(111) and Pt(100) surfaces are listed in table 7.1.

The most noticeable feature visible in figures 7.1(a) and 7.2(a) is the sharp dip in the turnover plot at approximately 390 K. This is attributed to the onset of cyclohexene formation on the surface resulting from a competing pathway. Cyclohexene production is observed at 370 K for benzene hydrogenation on Pt(111).[17] Cyclohexene has a larger sticking coefficient (0.2[27]) than cyclohexane (<0.1[4]) on Pt(111) which allows the gas phase precursor to remain on the surface and further hydrogenate.[17] We presume that adsorbed cyclohexene is formed on Pt(100) during the reaction at high temperatures based on these results.

7.3.2. Temperature dependence of the major surface species under varied pressures of benzene and hydrogen on Pt(100) and Pt(111): SFG vibrational spectroscopy results and peak assignments

Figure 7.3 shows the SFG spectra of the surface species present on Pt(100) at 15 Torr benzene and 100 Torr H_2 at various temperatures. At 300 K, three peaks are observed at 2945, 3030, and 3060 cm^{-1}. The mode at 3060 cm^{-1} decreases in intensity as the temperature is increased and disappears completely at 380 K. This peak has been previously identified by SFG[17] and EELS[9] as the aromatic C-H stretch of the physisorbed benzene. The intensity of the peak at 3030 cm^{-1} neither increases nor decreases as the temperature is increased. This mode is also present on the Pt(111) surface and is assigned by SFG[17] to the vinylic stretch of a dienyl chemisorbed benzene (see scheme 7.1(a)). The mode at 2945 cm^{-1} is also observed on the Pt(111) surface and assigned to the sp^3 hybridized C-H stretch of the dienyl chemisorbed benzene. Dienyl chemisorbed benzene is composed of four single and two double carbon-carbon bonds. The two singly bound carbon atoms are also bound to the platinum surface, giving rise to the sp^3 hybridization character in the spectral signature. Unlike the Pt(111) surface, the peaks at 2945 and 3030 cm^{-1} do not simultaneously grow and decay with temperature variations. Furthermore, the peak at 2945 cm^{-1} red shifts to 2940 cm^{-1} as the temperature is increased and a new peak appears at 2865 cm^{-1}. It becomes clear by comparison that the SFG spectra in figure 3 are similar to previous SFG data of π-allyl c-C_6H_9 on Pt(100)[19]. The SFG[19] spectrum of π-allyl c-C_6H_9 on Pt(100) is characterized by two peaks at $\nu_{sym}(CH_{2,})$ = 2865 and $\nu_{asym}(CH_2)$ = 2940 cm^{-1} with the $\nu_{asym}(CH_2)$ peak approximately twice as intense as the $\nu_{sym}(CH_{2,})$ peak. Hence, the modes in figure 3 are assigned as follows: $\nu_{sym}(CH_{2,})$ = 2865 cm^{-1}, $\nu_{asym}(CH_2)$ = 2940 cm^{-1}, ν(H-C-C-) = 2945 cm^{-1}, ν(C-H)(vinylic) = 3030 cm^{-1}, and ν(C-H)(aromatic) = 3060 cm^{-1}. Cooling the platinum surface

temperature from 440 K to 300 K reveals the reversible behavior of the surface composition.

The same surface species are present at other pressure combination (7.5 and 12.5 Torr benzene under 100 Torr H_2 and 10 Torr benzene under 10, 50, 100, and 150 Torr H_2) on the Pt(100) surface. Both chemisorbed and physisorbed benzene are co-adsorbed at 300 K. Heating the crystal surface to 340 K forms π-allyl c-C_6H_9 on the surface, which is co-adsorbed with physisorbed and chemisorbed benzene. Further increasing the temperature to 380 K desorbs the physisorbed benzene, leaving π-allyl c-C_6H_9 and chemisorbed benzene on the surface. Cooling the surface reverses the reaction, resulting in physisorbed benzene being the dominant surface species.

Figure 7.4 shows the SFG spectra of the surface species present on Pt(111) under 10 Torr benzene and 10 Torr H_2 at varied temperatures. Much like the benzene hydrogenation on Pt(100) the spectrum at 300 K exhibits three peaks at 2945, 3030, and 3060 cm^{-1}. These three peaks represent physisorbed and dienyl chemisorbed benzene. As the surface temperature is increased to 380 K the physisorbed benzene desorbs. The two peaks that are assigned to the dienyl chemisorbed benzene simultaneously increase in intensity as the surface temperature is increased to 420 K. Based on these peaks growing and decaying in unison as the temperature is varied coupled with the notable absence of a $\nu_{sym}(CH_2)$ peak, we conclude that π-allyl c-C_6H_9 is not present on the Pt(111) surface. Cooling the surface reveals that, like that on Pt(100), the benzene hydrogenation reaction is reversible on Pt(111).

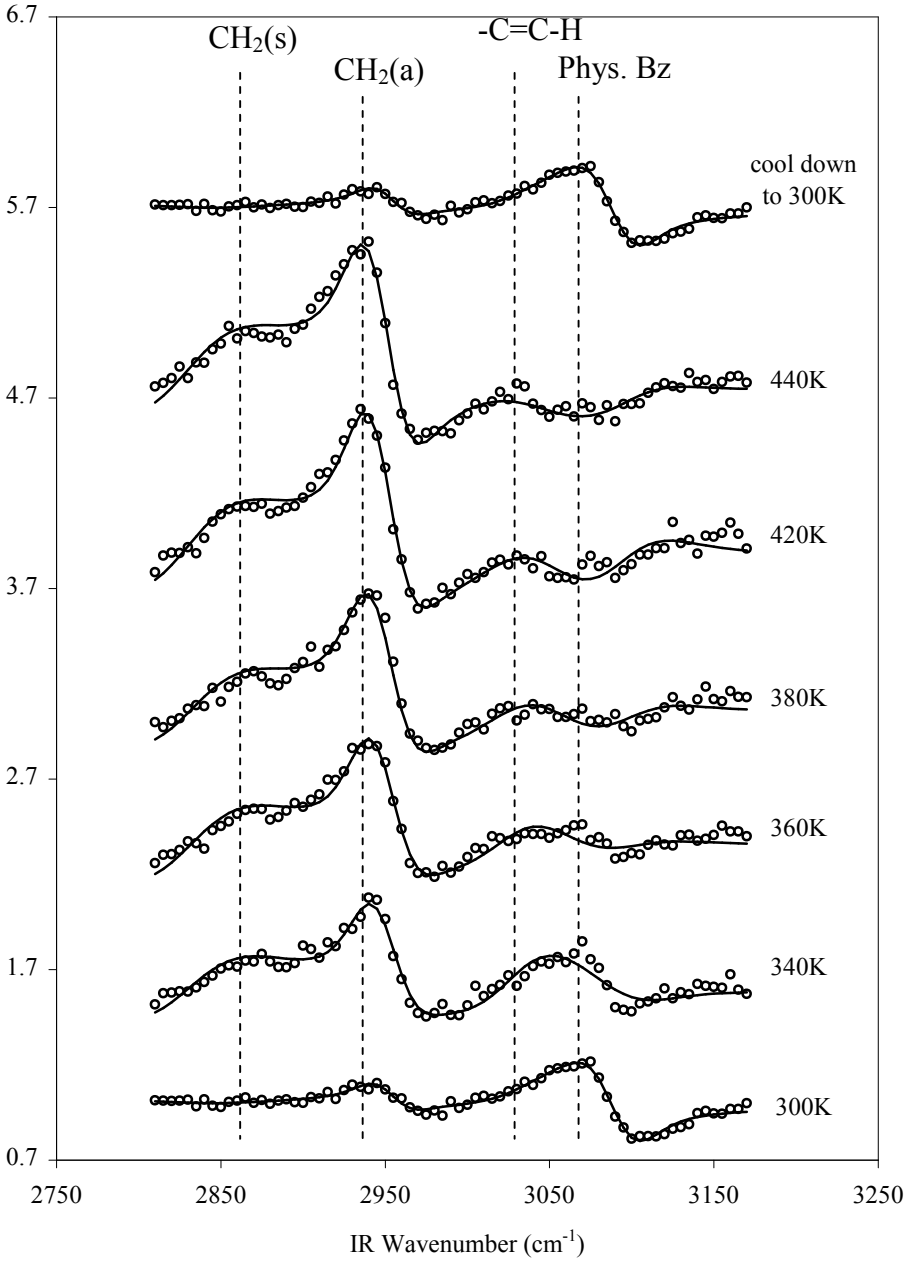

Figure 7.3. Temperature dependent SFG spectra of surface species on Pt(100) under 15 Torr benzene and 100 Torr H_2 in the range of 300-440 K. The top SFG spectrum was taken after the metal surface was cooled from 440 K to 300 K. CH_2(s), CH_2(a), vinylic (H-C=C-), and physisorbed benzene (phys. Bz) bands are identified. Markers represent experimental data and solid lines represent the curve fits to equation 7.1.

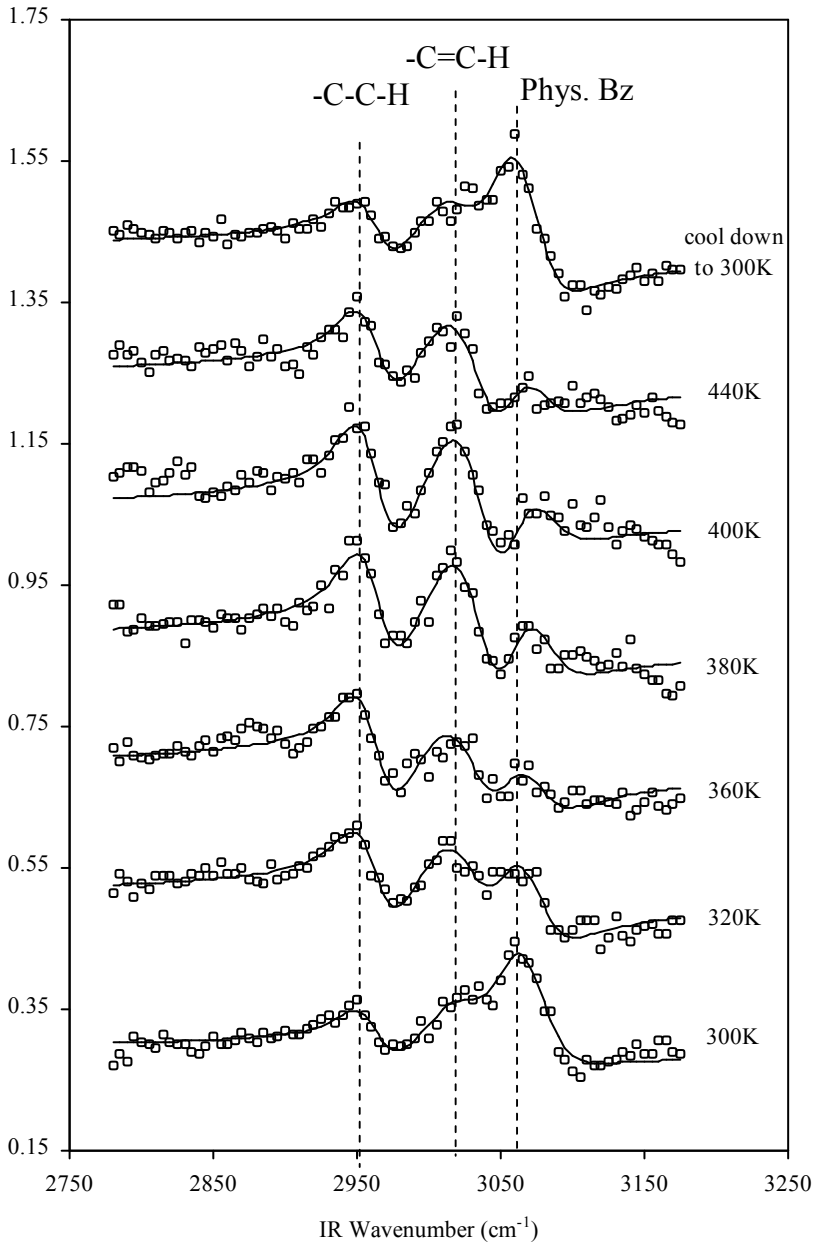

Figure 7.4. Temperature dependent SFG spectra of surface species on Pt(111) under 10 Torr benzene and 10 Torr H_2 in the range of 300-440 K. The top SFG spectrum was taken after the metal surface was cooled from 440 K to 300 K. H-C-C-, vinylic (H-C=C-), and physisorbed benzene (phys. Bz) bands are identified. Markers represent experimental data and solid lines represent the curve fits to equation 7.1.

7.4. Discussion

7.4.1. Langmuir-Hinshelwood mechanism and suggested reaction pathways for benzene hydrogenation to cyclohexane on Pt(111) and Pt(100)

The reaction orders found in table 7.1 for hydrogenation of benzene on both Pt(111) and Pt(100) corresponds to a Langmuir-Hinshelwood type mechanism where the RDS is the surface reaction between an adsorbed benzene molecule and one adsorbed hydrogen atom. The proposed mechanism for benzene hydrogenation to cyclohexane involves the following elementary reaction steps:

$$H_2 + 2* \underset{}{\overset{K_{H_2}}{\rightleftharpoons}} 2H* \qquad \text{(R7.1)}$$

$$C_6H_6 + * \underset{}{\overset{K_1}{\rightleftharpoons}} *C_6H_6* \qquad \text{(R7.2)}$$

$$C_6H_6* + * \xrightarrow{k_2} HC*C_6H_7* + * \qquad \text{(R7.3)}$$

According to Saeys *et al.*,[14] C_6H_6* is the most stable adsorbed C_6 species in the conversion of benzene to cyclohexane. This choice of RDS is in agreement with the spectroscopic evidence that shows only adsorbed benzene present on both the Pt(111) and Pt(100) crystal surfaces at low temperatures. The rate of benzene hydrogenation to cyclohexane can be written as

$$r_{C_6H_6} = k_2 \theta_{C_6H_6*} \theta_{H*} \qquad (7.5)$$

where the coverage of adsorbed hydrogen, θ_{H*}, is determined from the equilibrium of gas phase H_2 and adsorbed hydrogen,

$$\theta_{H*} = \sqrt{K_{H_2} p_{H_2}}\, \theta_* \qquad (7.6)$$

where p_{H_2} is the pressure of the gas phase H_2. The coverage of benzene, $\theta_{C_6H_6*}$, is also determined by the equilibrium of gas phase benzene and adsorbed benzene

$$\theta_{C_6H_6*} = K_1 p_{C_6H_6} \theta_* \tag{7.7}$$

where $p_{C_6H_6}$ is the pressure of gas phase benzene. Inserting equations 7.6 and 7.7 into equation 7.5 becomes

$$r_{C_6H_6} = k_2 K_1 \sqrt{K_{H_2}}\, p_{C_6H_6} \sqrt{p_{H_2}}\, \theta_*^2 \tag{7.8}$$

The site balance for the system is given by

$$1 = \theta_* + \theta_{C_6H_6*} + \theta_{H*} \tag{7.9}$$

which leads to a Langmuir-Hinshelwood type rate expression for benzene hydrogenation to cyclohexane

$$r_{C_6H_6} = \frac{k_{app} p_{C_6H_6} \sqrt{p_{H_2}}}{\left(1 + K_1 p_{C_6H_6} + \sqrt{K_{H_2} p_{H_2}}\right)^2} \tag{7.10}$$

where $k_{app} = K_1 k_2 \sqrt{K_{H_2}}$. The rate expression allows the order of benzene to vary from –1 to first order and the order of H_2 from -½ to half-order. Since benzene adsorption at low temperatures (300 K ≤ T ≤ 400 K) is favorable and there is a high gas phase pressure of benzene, $K_1 p_{C_6H_6}$ is much larger than $1 + \sqrt{K_{H_2} p_{H_2}}$ and the rate expression becomes

$$r_{C_6H_6} = \frac{k_{app} \sqrt{p_{H_2}}}{K_1^2 p_{C_6H_6}}. \tag{7.11}$$

This low temperature rate expression shows the dependence on benzene is –1 and for hydrogen it is half-order, which are strikingly similar to the experimentally obtained reaction orders listed in table 7.1 for both Pt(111) and Pt(100). The theoretical rate expression in eqns. 6.10 and 6.11 were verified by fitting to the experimentally obtained rates.

Previous reaction studies of benzene hydrogenation on Pt(111) concluded that at least two reaction pathways exist since gas phase cyclohexene evolves only at high temperatures.[17] Furthermore, a decrease and sudden increase in turnover at 370K coincides with the onset of cyclohexene formation and, hence, another reaction pathway. A similar trend is presumed to also occur on the Pt(100) surface since the turnover plots display similar features as Pt(111). Sayes *et al.*[14] have developed a possible reaction pathway by DFT that does not proceed through cyclohexene, as the experimental data implies. The proposed reaction pathway occurs in a Horiuti-Polanyi scheme[28] that adds hydrogens to benzene adsorbed to the platinum surface in an ortho fashion. Saeys *et al.*[14] also find that "the thermodynamic sink of the energy profile is clearly the adsorbed benzene and hydrogen. They are likely to be the most-abundant reaction intermediates." Again, this pathway is consistent with the spectral evidence showing only adsorbed benzene at low temperatures and the rate expression that arises from the addition of the first hydrogen.

One of the reaction pathways at higher temperatures is the hydrogenation of cyclohexene to cyclohexane. Previous investigations into this reaction by Bratlie *et al.*[19] on the Pt(100) surface and by by Yang *et al.*[18] on the Pt(111) surface identified π-allyl c-C_6H_9 as the most abundant reactive intermediate and its hydrogenation a likely RDS

for cyclohexene hydrogenation. The spectrum in figure 7.3 clearly shows π-allyl c-C_6H_9 on the Pt(100) surface in the presence of benzene, however, π-allyl c-C_6H_9 is not visible on the Pt(111) surface. This indicates that adsorbed cyclohexene more readily dehydrogenates to form π-allyl c-C_6H_9 on the Pt(100) surface than on the Pt(111) surface.

7.4.2. Compensation effect and isokinetic temperature

Apparent activation energies and pre-exponential factors for all pressure combinations on both the Pt(100) and Pt(111) surfaces are listed in table 7.1. Plotting these Arrhenius parameter pairs forms a straight line, presented in figure 7.5, which is attributed to the compensation effect. Taking the natural logarithm of equation 7.3 yields

$$\ln A = \frac{E_a}{RT} + \ln k \,. \tag{7.12}$$

Based on equation 7.12, the slope of figure 7.5 is related to the isokinetic temperature (T_{iso}). For cyclohexane formation on both Pt(100) and Pt(111), T_{iso} is 358 ± 5 K, which corresponds reasonably well with the temperature that the Arrhenius plots intersect. Possible explanations for the compensation effect have been explored extensively and are reviewed by Bond *et al.*[29] One of the interpretations of the isokinetic temperature cited by Bond *et al.*[29] is a model proposed by Larsson[30] which assumes there is a transfer of "energy into the vibrational mode of the reactant that most effectively takes the system to the activated site" from the active site. Based on this model, Larsson[30] derives the following equation

$$T_{iso} = \frac{Nhcv}{2R} = 0.719v \tag{7.13}$$

where *v* is the vibrational mode leading toward reaction, N is Avogadro's number, h is Planck's constant, and c is the speed of light. Using equation 7.13 to interpret T_{iso} in terms of wave numbers, the critical frequency of vibration is 501 ± 7 cm^{-1}. Difficulties arise in assigning this critical vibration to an adsorbed surface species. Thomas *et al.*[9] find that physisorbed and chemisorbed benzene both exhibit Pt-C stretches at 550 and 475 cm^{-1}, respectively. Lamont *et al.*[31] report a ring deformation for cyclohexene at 539 cm^{-1} and a CCC deformation for cyclohexane at 515 cm^{-1}. These are just three of the possible adsorbed molecules that may be present on the platinum surface illustrating how the critical vibration could belong to any number of adsorbed C_6 surface species.

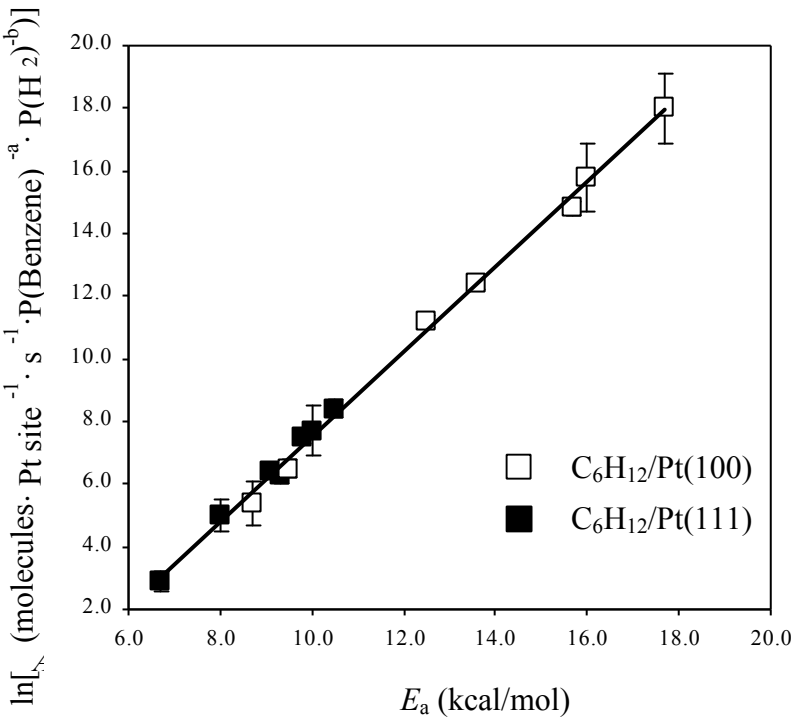

Figure 7.5. Constable plot for the hydrogenation of benzene to cyclohexane on Pt(111) and Pt(100).

7.5. Conclusions

The low temperature reaction pathway for benzene hydrogenation has been clarified through kinetic measurements, SFG vibrational spectroscopy, and parameters obtained from fits to the experimentally determined turnover rates on both the Pt(100) and Pt(111) single crystal surfaces. A Langmuir-Hinshelwood type rate expression for the low temperature reaction pathway was identified and its rate-determining step is the addition of the first hydrogen to adsorbed benzene. The rate expression was experimentally verified by the reaction orders for benzene and hydrogen obtained from kinetic measurements and by SFG measurements. At 300 K, physisorbed and chemisorbed benzene were observed on both single crystal surfaces. Increasing the temperature desorbed the physisorbed benzene from both surfaces and produced π-allyl c-C_6H_9 on the Pt(100) surface only. Heating the single crystal surfaces to 440 K and subsequently cooling to 300 K resulted in SFG spectra that were identical to those obtained before reaction, indicating complete reversibility of the surface composition for both Pt(100) and Pt(111). Chemisorbed benzene was determined to be the reactive surface intermediate responsible for the rate-determining step in the Langmuir-Hinshelwood type rate expression. Based on previous studies, π-allyl c-C_6H_9 was concluded as the rate-determining step in cyclohexene hydrogenation on both platinum crystal surfaces, a reaction that occurs at higher temperatures.

References

(1) Cooper, B. H.; Donnis, B. B. L. *Applied Catalysis A* **1996**, *137*, 203-223.

(2) Ogletree, D. F.; Van Hove, M. A.; Somorjai, G. A. *Surface Science* **1987**, *183*, 1-20.

(3) Horsley, J. A.; Stohr, J.; Hitchcock, A. P.; Newbury, D. C.; Johnson, A. L.; Sette, F. *Journal of Chemical Physics* **1985**, *83*, 6099-6107.

(4) Ihm, H.; Ajo, H. M.; Gottfried, J. M.; Bera, P.; Campbell, C. T. *Journal of Physical Chemistry B* **2004**, *108*, 14627-14633.

(5) Lutterloh, C.; Biener, L.; Pohlmann, K.; Schenk, A.; Kuppers, J. *Surface Science* **1996**, *352-354*, 133-137.

(6) Tsai, M.-C.; Muetterties, E. L. *Journal of the American Chemical Society* **1982**, *104*, 2534-2539.

(7) Abon, M.; Bertolini, J. C.; Billy, J.; Massardier, J.; Tardy, B. *Surface Science* **1985**, *162*, 395-401.

(8) Lehwald, S.; Ibach, H.; Demuth, J. E. *Surface Science* **1978**, *78*, 577-590.

(9) Thomas, F. S.; Chen, N. S.; Ford, L. P.; Masel, R. I. *Surface Science* **2001**, *486*, 1-8.

(10) Weiss, P. S.; Eigler, D. M. *Physical Review Letters* **1993**, *71*, 3139-3142.

(11) Haq, S.; King, D. A. *Journal of Physical Chemistry* **1996**, *100*, 16957-16965.

(12) Haaland, D. M. *Surface Science* **1981**, *102*, 405-423.

(13) Saeys, M.; Reyniers, M.; Marin, G. B.; Neurock, M. *Surface Science* **2002**, *513*, 315-327.

(14) Saeys, M.; Reyniers, M.; Marin, G. B. *Journal of Physical Chemistry B* **2002**, *106*, 7489-7498.

(15) Morin, C.; Simon, D.; Sautet, P. *Journal of Physical Chemistry B* **2004**, *108*, 5653-5665.

(16) Bratlie, K. M.; Montano, M. O.; Flores, L. D.; Paajanen, M.; Somorjai, G. A. *Journal of the American Chemical Society* **2006**, *128*, 12810-12816.

(17) Bratlie, K. M.; Flores, L. D.; Somorjai, G. A. *Journal of Physical Chemistry B* **2006**, *110*, 10051-10057.

(18) Yang, M.; Chou, K. C.; Somorjai, G. A. *Journal of Physical Chemistry B* **2003**, *107*, 5267-5272.

(19) Bratlie, K. M.; Flores, L. D.; Somorjai, G. A. *Surface Science* **2005**, *599*, 93-106.

(20) Bain, C. D.; Davies, P. B.; Ong, T. H.; Ward, R. N.; Brown, M. A. *Langmuir* **1991**, *7*, 1563-1566.

(21) Moore, F. G.; Becraft, K. A.; Richmond, G. L. *Applied Spectroscopy* **2002**, *56*, 1575-1578.

(22) Kung, K. Y.; Chen, P.; Wei, F.; Rupprechter, G.; Shen, Y. R.; Somorjai, G. A. *Review of Scientific Instruments* **2001**, *72*, 1806-1809.

(23) Yang, M.; Tang, D. C.; Somorjai, G. A. *Review of Scientific Instruments* **2003**, *74*, 4554-4557.

(24) Shen, Y. R. *The Principles of Nonlinear Optics*; Wiley: New York, 2003.

(25) Shen, Y. R. *Annual Review of Physical Chemistry* **1989**, *40*, 327-350.

(26) Shen, Y. R. *Nature* **1989**, *337*, 519-525.

(27) Henn, F. C.; Diaz, A. L.; Bussel, M. E.; Huggenschmidt, M. B.; Domagala, M. E.; Campbell, C. T. *Journal of Physical Chemistry* **1992**, *96*, 5965-5974.

(28) Horiuti, J.; Polanyi, M. *Transactions of the Faraday Society* **1934**, *30*, 1164-1172.

(29) Bond, G. C.; Keane, M. A.; Kral, H.; Lercher, J. A. *Catalysis Review* **2000**, *42*, 323-383.

(30) Larsson, R. *Catalysis Today* **1987**, *1*, 93-99.

(31) Lamont, C. L. A., Borbach, M., Marin, R., Gardner, P., Jones, T. S., Conrad, H., Bradshaw, A. M. *Surf. Sci.* **1997**, *374*, 215.

Chapter 8

Compensation Effect of Benzene Hydrogenation on Pt(111) and Pt(100) Analyzed by the Selective Energy Transfer Model

Kinetic measurements at low temperatures (310 – 360 K) using gas chromatography (GC) for benzene hydrogenation on Pt(100) and Pt(111) single crystal surfaces have been carried out at Torr pressures. These kinetic measurements demonstrated a linear compensation effect for the production of cyclohexane. A detailed application of the model of selective energy transfer to the experimentally obtained results yields the vibrational frequency of the adsorbate leading to reaction. This frequency is attributed to ring distortion modes. The vibrational frequency of the heat bath, or catalyst, is ascribed to a Pt-H mode. An approximate heat of adsorption of the reacting molecule is also calculated from the model.

8.1. Introduction

Benzene hydrogenation is an industrially relevant reaction for several essential steps in petroleum refining and downstream chemical processing.[1] Understanding how energy is transferred to facilitate reactions and identifying the reactive surface intermediates are central issues in understanding the mechanism of benzene hydrogenation and heterogeneous catalysis.

The rate law for benzene hydrogenation (and nearly all simple, thermally activated processes) can be described by a standard empirical power law

$$r = kP_{Bz}{}^{a} P_{H_2}{}^{b} \tag{8.1}$$

where r is the rate of reaction, P_{Bz} and P_{H_2} are the pressures of the reactant gases (benzene and H_2, respectively, in this case), a and b are the reaction order with respect to the reactant species, and *k* is the rate constant. The rate constant can be expressed as

$$k = Ae^{-E_a / RT} \tag{8.2}$$

where *A* is the pre-exponential factor, E_a is the activation energy, *R* is the gas constant, and T is temperature. For some classes of systems with varying activation energies, a compensation effect exists such that as the apparent activation energy changes, so does the pre-exponential factor as demonstrated in the following equation:

$$\ln A = bE_a + c \tag{8.3}$$

where $b = \dfrac{1}{RT_{iso}}$ (8.3a)

and $c = \ln k_{iso}$ (8.3b)

The compensation effect was first observed by Constable[2] in heterogeneous catalysis and has been found to hold true for a whole host of chemical reactions.[3-6] An isokinetic temperature (T_{iso}) is defined by the slope of the relation (8.3), at which all the considered reactions have the same rate constant. Possible explanations for the compensation effect have been explored extensively and are reviewed by Bond *et al.*[7] One of the interpretations of the compensation effect cited by Bond *et al.*[7] is a model proposed by Larsson[8] which assumes there is a transfer of energy into the vibrational mode of the reactant that "most effectively distorts the molecule towards the structure it has in the 'activated complex' of the reaction." In another interpretation, Norskov and co-workers[9] suggest the compensation effect arises from "a switching of kinetic

regimes," meaning that there is a monotonic relationship between "the activation energy of the rate-limiting step and the stability of the reaction intermediates on the surface."

Here, we consider the compensation effect of benzene hydrogenation to cyclohexane on Pt(111) and Pt(100) using the selective energy transfer (SET) model proposed by Larsson.[10,11] Kinetic measurements of benzene hydrogenation to cyclohexane on Pt(111) and Pt(100) at low temperatures (310 – 360 K) and Torr pressures show a linear compensation effect between activation energy and the pre-exponential factor. Employing the SET model to the experimentally obtained Arrhenius parameters generates vibrational frequencies of the adsorbate leading to reaction along with the vibrational frequencies of the heat bath, or catalyst. The heat of adsorption of the reacting adsorbate is also determined from the SET model.

8.2. Experimental

All experiments were carried out in a high-pressure/ultrahigh-vacuum (HP/UHV) system on prepared Pt(111) and Pt(100) single-crystal surfaces. The HP/UHV system consists of a UHV chamber operating at a base pressure of 2×10^{-9} Torr and a high-pressure (HP) cell isolated from the UHV chamber by a gate valve. The UHV chamber is equipped with an Auger electron spectrometer (AES), quadrupole mass spectrometer (QMS) and Ar^+ ion sputter gun. The HP cell is equipped with a re-circulation loop that includes a diaphragm pump and a septum for gas chromatographic (GC) analysis. The reactant and product gases are constantly mixed via a recirculation pump while kinetic data is acquired by periodically sampling the reaction mixture and measuring the relative

gas phase composition (flame ionization detection and 0.1% AT-1000 on Graphpac GC 80/100 packed column (Alltech)).

The Pt(111) and Pt(100) crystals were cleaned by sputtering with Ar^+ ions (1 keV) for 20 minutes, heating to 1123 K in the presence of 5×10^{-7} Torr O_2 for 2 minutes, and then annealing at 1123 K for 2 minutes. AES and LEED were used to verify the cleanliness of the Pt(111) and Pt(100) surfaces after several cleaning cycles. The Pt(111) or Pt(100) crystal was then transferred into the HP cell for reaction studies. Benzene ($\geq$ 99.0 wt-%, EM Science) was purified by several freeze-pump-thaw cycles before introduction into the HP cell. Prior to the experiment, benzene was checked for impurities by means of GC. Such impurities were below 0.5 % and consisted of mostly light alkanes below C_6.

8.3. Results and Discussion

8.3.1. Apparent activation energies and compensation effect to form cyclohexane under varied pressures of benzene and hydrogen on Pt(111) and Pt(100)

Figure 8.1 shows the Arrhenius plot for 11 Torr benzene and 11, 52, and 158 Torr hydrogen, respectively, and 105 Torr hydrogen and 8, 11, 13, and 17 Torr benzene pressures, respectively, over a temperature range from 310K to 360 K on Pt(111) and Pt(100). The rate constants (k) [molecules $\cdot$ site^{-1} $\cdot$ s^{-1} $\cdot$ P(benzene)$^{-a}$ $\cdot$ P(H_2)$^{-b}$] are calculated from the turnover rates using the empirical equation 8.1, with the reaction orders listed in table 8.1, assuming that every platinum surface atom is an active site. Apparent activation energies and pre-exponentials for cyclohexane formation are listed in table 8.2.

	order Pt(111)	order Pt(100)
Benzene	-1.1 ± 0.1	-1.1 ± 0.3
H_2	0.6 ± 0.01	0.6 ± 0.02

Table 8.1. Orders for both H_2 and benzene on Pt(111) and Pt(100).

The apparent activation energies depend upon the pressure of each reactant. In many hydrogenation reactions (e.g. ethylene, propylene, n-hexene, cyclohexene etc.), H_2 is more strongly adsorbed than the hydrocarbon reactant and has a dominant effect on the apparent activation energies.[7] Benzene, in contrast, binds very strongly to the Pt(111) surface and large changes in the apparent activation energies are expected upon varying its partial pressure. The exponents a and b in equation 8.1 are determined over a range of reaction temperatures (310 – 360 K) using

$$a = \left[\frac{\partial \ln r}{\partial \ln p_{C_6H_6}} \right]_{p_{H2}} . \qquad (4)$$

The benzene and H_2 reaction orders for cyclohexane production on both the Pt(111) and Pt(100) surfaces are – as said above - listed in table 8.1.

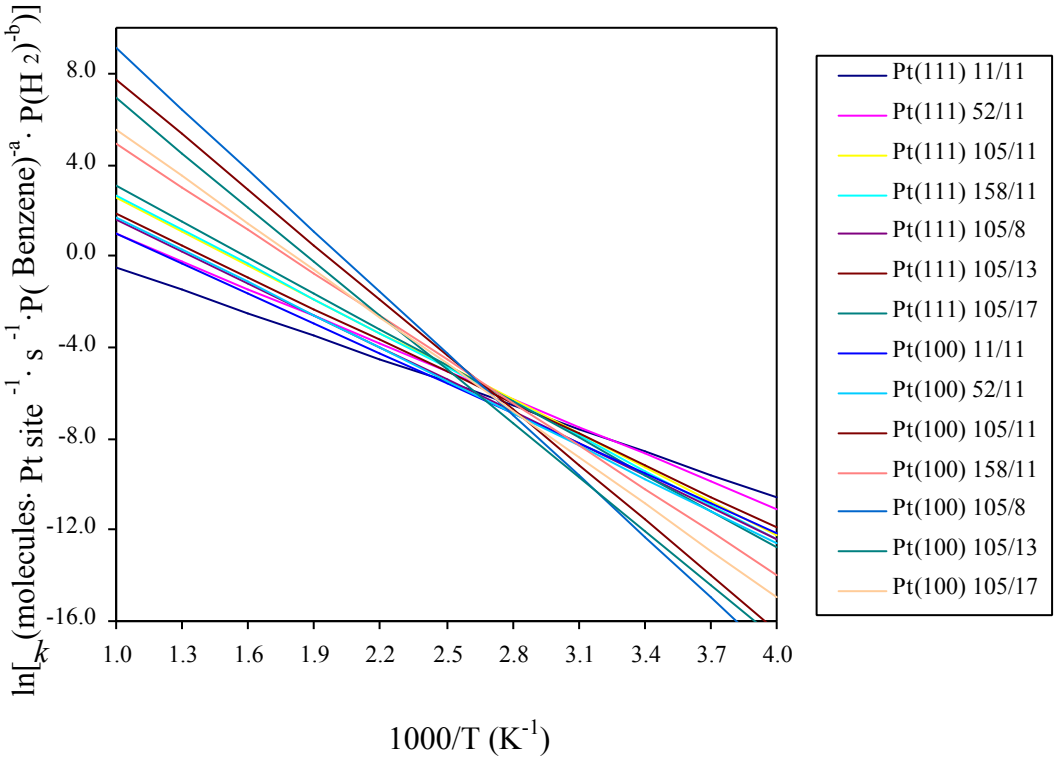

Figure 8.1. Arrhenius plots of rate constants (k) (in molecules · Pt site^{-1} · s^{-1} · P(benzene)$^{-a}$ · P(H_2)$^{-b}$) on Pt(111) and Pt(100) for benzene (7.5, 10, 12.5, and 15 Torr) hydrogenation to cyclohexane in the presence of H_2 (10, 50, 100, and 150 Torr). Apparent activation energies and pre-exponentials are listed in table 8.2.

System $P(C_6H_6)/P(H_2)$	$\ln(A)$	E_a	ΔE_a	n'	$E_a - RT$	n
			Pt(111)			
11/11	2.9 ± 0.3	6.7 ± 0.2			6.0 ± 0.2	5
11/52	5.0 ± 0.5	8.0 ± 0.3	1.3 ± 0.4	1	7.3 ± 0.3	6
11/105	7.5 ± 0.2	9.8 ± 0.1	1.8 ± 0.3	2	9.1 ± 0.1	8
11/158	7.7 ± 0.8	10.0 ± 0.5	0.2 ± 0.5	0	9.3 ± 0.4	8
8/105	6.3 ± 0.3	9.3 ± 0.2	-0.7 ± 0.5	1	8.6 ± 0.3	8
13/105	6.4 ± 0.1	9.1 ± 0.1	-0.2 ± 0.2	0	8.4 ± 0.1	7
17/105	8.4 ± 0.3	10.5 ± 0.2	1.4 ± 0.2	1	9.8 ± 0.2	9
			Pt(100)			
11/11	5.4 ± 0.7	8.7 ± 0.5	-1.8 ± 0.5	2	8.0 ± 0.5	7
11/52	6.5 ± 0.3	9.5 ± 0.2	0.8 ± 0.5	1	8.7 ± 0.2	8
11/105	15.8 ± 1.1	16.0 ± 0.7	6.5 ± 0.7	6	15.0 ± 0.2	14
11/158	11.2 ± 0.2	12.5 ± 0.1	-3.5 ± 0.7	3	11.8 ± 0.1	10
8/105	18.0 ± 1.1	17.7 ± 0.8	5.2 ± 0.8	5	18.2 ± 0.1	15
13/105	14.8 ± 0.2	15.7 ± 0.8	-2.0 ± 0.8	2	16.1 ± 0.8	13
17/105	12.4 ± 0.2	13.6 ± 0.1	-2.1 ± 0.2	2	12.9 ± 0.8	11
			-6.9 ± 0.2	7		

Table 8.2. Pre-exponentials (in molecules · site^{-1} · s^{-1} ·P(benzene)$^{-a}$ · P$(H_2)^{-b}$); $\Delta E_a = E_{a_i} - E_{a_{i+1}}$; *n'* is the number of a least common factor in the absolute values of the preceding column; apparent activation energies (in kcal · mol^{-1}); activation energies corrected for temperature, $E_a - RT$; and $E_a - RT$ divided by the self-consistent least common factor giving the corresponding vibrational quantum numbers.

8.3.2. Selective Energy Transfer Model

One notes that the Arrhenius lines in Figure 8.1 intersect in a temperature region of about $1000/T = 2.6 - 2.8\ \ K^{-1}$. This means that the isokinetic temperature is T_{iso} = 1000/(2.7± 0.1) = 370 ± 14 K. This relatively good agreement between the experimental data for Pt(111) and Pt(100) makes it reasonable to use all the data in one and the same "compensation plot"; i.e. ln(A) versus E_a .

Plotting the Arrhenius parameter pairs listed in table 8.2 forms a straight line, presented in figure 8.2. Based on equation 8.3, the slope of the line in figure 8. 2 is related to the isokinetic temperature (T_{iso}). For cyclohexane formation on both Pt(100) and Pt(111), T_{iso} is 370 ± 6 K, which corresponds well with the temperature at which the Arrhenius plots intersect, 370 ± 14 K.

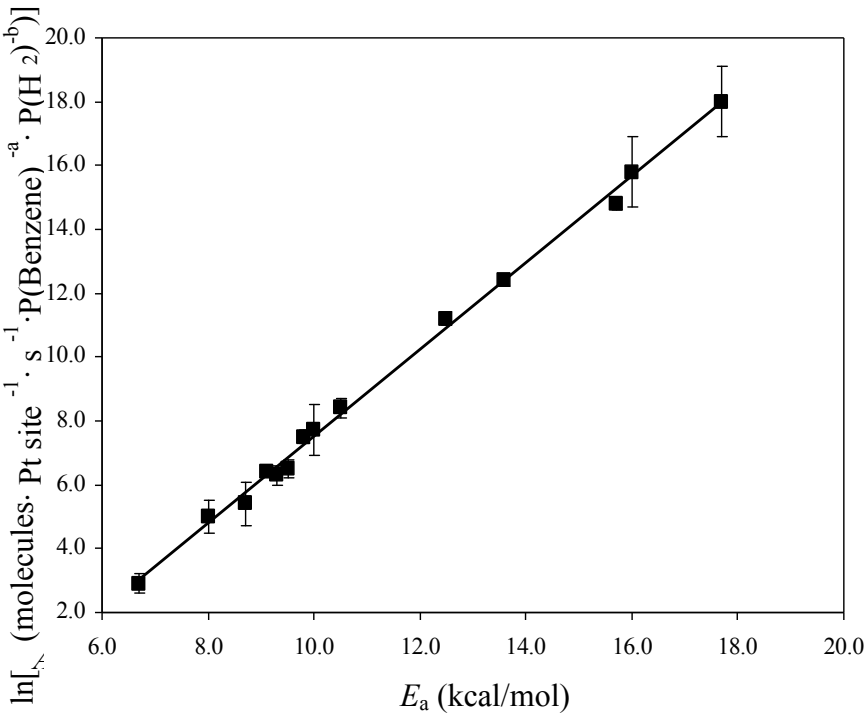

Figure 8.2. Constable plot for the hydrogenation of benzene to cyclohexane on Pt(111) and Pt(100).

The general idea of the SET model is that a molecule reacting in the condensed phase must have a continuous supply of energy. This supply of energy is thought to proceed via vibrational resonance[11] in the sense that a vibrator of the catalyst, ω, transfers its energy to a vibrator in the reacting molecule, ν, that has a frequency close to ω. Based on this model, the relation between the isokinetic temperature, the vibration frequency of the heat bath, and that of the reacting molecule is described by equation 8.5, as derived by Larsson,[8]

$$T_{iso} = NhcR^{-1}\left(v^2 - \omega^2\right)\omega^{-1}\left\{\pm\frac{1}{2}\pi - \arctan\left[0.5v\omega\left(v^2 - \omega^2\right)^{-1}\right]\right\}^{-1} \qquad (5)$$

where *N* is Avogadro's number, *h* is Planck's constant, and c is the speed of light.

The basic tenet of the SET model is that values of E_a, or rather the enthalpy of activation $\Delta H^{\ddagger}$, can be quantitized in that a specific number of vibrational quanta must be transferred from the catalyst to the adsorbed reactant in order to access the transition state.[10,12] One must, however, consider that vibrational modes in a molecule are anharmonic, resulting in an unequal spacing of the energy levels. The vibrational energy of a molecule, measured relative to the zero energy of the vibrational mode, is described (excluding higher order terms) by Herzberg[13] as

$$G_0(n) = n\nu_0 + \nu_0 x_0 n^2 \qquad (6)$$

where G_0 is the vibrational energy of the vibrator in excess of the zero energy vibrational level, n is the vibrational quantum number, x_0 is the anharmonicity constant (with negative sign) and ν_0, for small values of x_0, is twice the vibrational energy of the zero state. If the rest of the reacting molecule and all the non-reacting molecules are assumed to be in thermal equilibrium, then, following Benson,[14] the activation energy can be defined as the difference between the "average energy of the reacting molecules and the average energy of the molecules in the system." This excess energy, $G_0(n)$, is then equal to the activation enthalpy of the reaction

$$G_0(n) = \Delta H^{\ddagger}. \qquad (7)$$

Laidler[15] found that the following relation between activation energy and enthalpy of activation is approximately valid for reactions in the condensed phase

$$\Delta H^{\ddagger} = E_a - RT. \qquad (8)$$

Any energy term representing a possible pre-equilibrium, Q, must also be taken into consideration[7]

$$\Delta H^{\ddagger} = E_a - RT + Q. \tag{9}$$

Combining equations 8.6 – 9 leads to

$$E_a - RT + Q = n\nu_0 + \nu_0 x_0 n^2 . \tag{10}$$

The values of $\Delta H^{\ddagger} = E_a - RT$ are reported in table 8.2, using the mean of the experimental temperatures, 335 K. In table 8.2, we further report the consecutive differences between the E_a values. In the fifth column we estimate how many times a certain common factor (E_0) is appearing in the absolute values of those consecutive differences. By summing the absolute values of ΔE_a and dividing by the sum of *n'*, a relatively good value of E_0 is obtained (1.04 kcal/mol). It is our proposal that E_0 is related to the vibrational energy of the adsorbate leading to reaction. To determine appropriate values of the vibrational quantum number, n is set equal to the integer value of $(E_a - RT)/E_0$ by neglecting Q and the anharmonic term in equation 8.10. If Q is relatively large, it may have to be included. With these approximate values of n, a second-order polynomial is fitted to the data to give approximate values of M_0, M_1, and M_2

$$E_a - RT = M_0 + M_1 n + M_2 n^2 . \tag{11}$$

This procedure has been successfully used for a hydrodechlorination reaction of chlorobenzene over a series of nickel catalysts.[16]

In order to get a more precise, self-consistent value of M_1, however, one must use an iterative procedure, the aim of which is to obtain $E_0 = M_1$. For this purpose, it turned out best to use the differences of ΔE_a. Using equation 8.10 one can then write

$$\Delta E_a = E_{a_1} - E_{a_2} = \nu (n_1 - n_2) + x_0 \nu (n_1^2 - n_2^2) \tag{12}$$

$$n_1 = round\left[\left(E_{a_1} - RT\right)/E_0\right] \tag{13}$$

$$n_2 = round\left[\left(E_{a_2} - RT\right)/E_0\right] \tag{14}$$

For a set of activation differences, ΔE_a, given in table 8.2, the fitting problem is to find the best fitting parameters ν and $x_0\nu$, and to make sure the parameters are self-consistent by $E_0=\nu$. This means that for a specified value of E_0, equations 8.10 and 11 will have the same coefficient for the first and second order terms in n; thus, $M_1=\nu$. By a suitable iteration, one finds that E_0 = 1.13 kcal/mol is the value that gives a set of converged M_1 and M_2, as shown in table 8.3 and in figure 8.3.

Q (kcal/mol)	M_1 (kcal/mol)	M_2 ($\times 10^{-3}$ kcal/mol)	ν (cm^{-1})	$x_0\nu$ (cm^{-1})
-0.55 ± 0.39	1.13 ± 0.22	-4.4 ± 10.3	393 ± 77	-1.53 ± 3.59

Table 8.3. Fitting parameters M_0, M_1, and M_2 for the self-consistent iterative procedure and the vibrational energy (in cm^{-1}) and anharmonicity constant (in cm^{-1}) derived from the fitting parameters.

Comparison of equation 8.11 to equation 8.10 shows that the fitting parameter M_1 should correspond to the vibrational frequency of the adsorbate leading to reaction and M_2 should correspond to the anharmonicity term. From this comparison of equations 8.10 and 11, the self-consistent fit yields a value of 393 ± 77 cm^{-1} for the vibrational frequency of the adsorbate and an anharmonicity of -1.53 ± 3.59 cm^{-1}. This value of the

anharmonicity is quite reasonable for single bonded, low frequency vibrations. The vibrational frequency at 393 cm^{-1} is most likely related to the E_{2u} mode for free benzene, 404 cm^{-1}, described by Painter and Koenig,[17] implying a ring distortion and a C-H out of plane bending mode. This C-C distortion is expected to cause an anharmonicity of 1 – 2 cm^{-1}. It may be of interest to not that the out-of-plane C-H bending of benzene at 740 cm^{-1} has an anharmonicity of -0.7 cm^{-1}.[18,19]

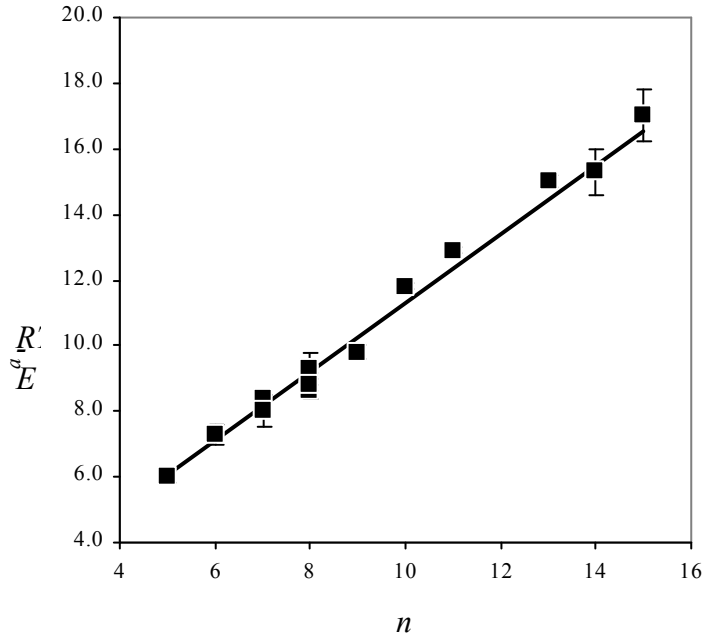

Figure 8.3. Plot of experimentally determined $E_a - RT$ against the vibrational quantum number, n,(cf Table 8.2) for Pt(111) and Pt(100).. The solid line is second order polynomial fit of the data.

In addition to yielding information regarding the vibration of the adsorbate leading to reaction, the SET model can also indicate the strength of adsorption of the reacting molecule, $M_0 = -Q$, from equations 8.10 and 11. The corresponding M_0 value for

the fit is -0.55 ± 0.39 kcal/mol, thus indicating that the heat of adsorption, Q, is 0.55 ± 0.39 kcal/mol.

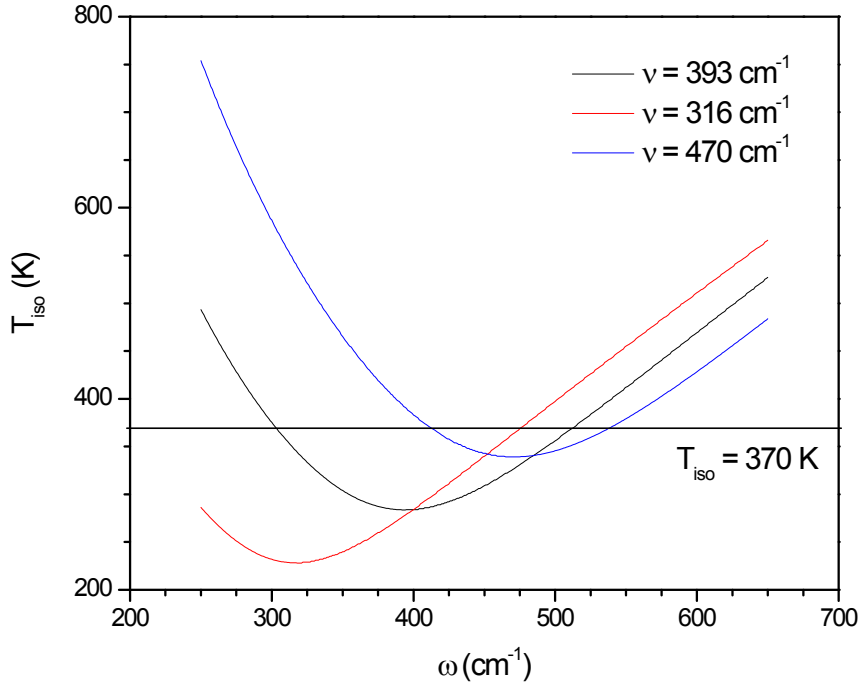

Figure 8.4. Isokinetic temperature, T_{iso}, calculated for ν = 393 ± 77 cm^{-1} using the full resonance formula. A line at T_{iso} = 370 K is drawn to obtain the vibration of the heat bath, ω.

After obtaining the vibrational frequency of the adsorbate leading to reaction, determining the frequency of the energy donating bath is necessary. To this end, the full resonance formula (equation 8.5) for ν = 393 ± 77 cm^{-1} is plotted in figure 4 along with the error limits. The value of T_{iso} obtained from figure 8.2 is 370 K and is drawn on the plot in figure 8.4 The point of intersection indicates an abscissa of 513 ± 33 cm^{-1}. Frequencies values of this magnitude have been reported for the Pt-H system. On

Pt(111), a mode at 470 cm^{-1} has been assigned to a Pt-H bend of an atop adsorbed hydrogen.[20] Baro *et al.*[21] have attributed a mode at 550 cm^{-1} on Pt(111) to the A_1 mode of hydrogen adsorbed to a three-fold hollow site. However, Zemlyanov *et al.*[22] observed a mode at 555 cm^{-1} on Pt(100)-(5 × 20) which was assigned to bridge bound hydrogen, displaying the ambiguity of the assignments. It is important to note that these measurements have a resolution of 60 – 90 cm^{-1}, indicating that the calculated frequency of the heat bath may correspond to any of these Pt-H modes.

The most striking result from employing the SET model is that the reacting molecules are not strongly adsorbed to the catalyst surface. Upon analysis of the step-wise change of the activation energies, the heat of adsorption is found to be quite low; not at all corresponding to what one instinctively considers the strength of adsorption of a molecule, severely disturbed by the adsorption and catalysis process. Nevertheless, the molecules have been assumed to be in thermal equilibrium. This must imply that most of the molecules are strongly adsorbed, as evidenced by previous vibrational spectroscopy studies.[23-25] In a mobile equilibrium, however, there must be at any given time a certain number of molecules that are far from being strongly adsorbed to the surface.[17] It may be possible that these weakly adsorbed molecules have the possibility to present an easy route for an approaching reactant than strongly adsorbed molecules have.

8.4. Conclusions

Benzene hydrogenation on Pt(100) and Pt(111) single crystal surfaces was carried out at low temperatures (310 – 360 K) and Torr pressures using gas chromatography. Indications of a compensation effect between activation energy and the pre-exponential

factor for cyclohexane production led to a detailed application of the SET model. A possible vibrational frequency of the adsorbate leading to reaction was attributed to the E_{2u} mode of free benzene. Further application of the SET model assigned the vibrational frequency of the catalyst to a Pt-H mode. The heat of adsorption of the reactant molecule was approximated as very small.

References

(1) Cooper, B. H.; Donnis, B. B. L. *Applied Catalysis A* **1996**, *137*, 203-223.

(2) Constable, F. H. *Proceedings of the Royal Society of London Series A* **1925**, *108*, 355-378.

(3) Cremer, E. *Advances in Catalysis* **1955**, *7*, 75-91.

(4) Galwey, A. K. *Advances in Catalysis* **1977**, *26*, 247-322.

(5) Keyes, R. W. *Journal of Chemical Physics* **1958**, *29*, 467-475.

(6) Barth, J. V.; Brune, H.; Fischer, B.; Weckesser, J.; Kern, K. *Physical Review Letters* **2000**, *84*, 1732-1735.

(7) Bond, G. C.; Keane, M. A.; Kral, H.; Lercher, J. A. *Catalysis Reviews-Science and Engineering* **2000**, *42*, 323-383.

(8) Larsson, R. *Catalysis Today* **1987**, *1*, 93-99.

(9) Bligaard, T.; Honkala, K.; Logadottir, A.; Norskov, J. K.; Dahl, S.; Jacobsen, J. H. *Journal of Physical Chemistry B* **2003**, *107*, 9325-9331.

(10) Larsson, R. *Catalysis Today* **1989**, *4*, 235-251.

(11) Larsson, R. *Journal of Molecular Catalysis* **1989**, *55*, 70-83.

(12) Larsson, R.; Jamroz, M. H.; Borowaik, M. A. *Journal of Molecular Catalysis A: Chemical* **1998**, *129*, 41-51.

(13) Herzberg, G. *Spectra of Diatomic Molecules*; 2nd ed.; Van Nostrand: New York, 1950.

(14) Benson, S. W. *Thermochemical Kinetics*; 2nd ed.; John Wiley & Sons: New York, 1976.

(15) Laidler, K. J. *Chemical Kinetics*; 3rd ed.; Harper & Row: New York, 1987.

(16) Keane, M. A.; Larsson, R. *Catalysis Communications* **2008**, *9*, 333-336.

(17) Painter, P. C.; Koenig, J. L. *Spectrochimica Acta* **1977**, *33*, 1019-1024.

(18) Maslen, P. E.; Handy, N. C.; Amos, R. D.; Jayatilaka, D. *Journal of Chemical Physics* **1992**, *97*, 4233-4254.

(19) Cane, E.; Miani, A.; Trombetti, A. *Journal of Molecular Spectroscopy* **1997**, *183*, 204-206.

(20) Parker, S. F.; Frost, C. D.; Telling, M.; Albers, P.; Lopez, M.; Seitz, K. *Catalysis Today* **2006**, *114*, 418-421.

(21) Baro, A. M.; Ibach, H.; Bruchmann, H. D. *Surface Science* **1979**, *88*, 384398.

(22) Zemlyanov, D. Y.; Smirnov, M. Y.; Gorodetskii, V. V. *Catalysis Letters* **1997**, *43*, 181-187.

(23) Bratlie, K. M.; Flores, L. D.; Somorjai, G. A. *Journal of Physical Chemistry B* **2006**, *110*, 10051-10057.

(24) Bratlie, K. M.; Kliewer, C. J.; Somorjai, G. A. *Journal of Physical Chemistry B* **2006**, *110*, 17925-17930.

(25) Bratlie, K. M.; Montano, M. O.; Flores, L. D.; Paajanen, M.; Somorjai, G. A. *Journal of the American Chemical Society* **2006**, *128*, 12810-12816.

Chapter 9

A Sum Frequency Generation Vibrational Spectroscopic Study of the Adsorption and Reactions of C_6 Hydrocarbons at High Pressures on Pt(100)

Sum frequency generation (SFG) vibrational spectroscopy was used to investigate the adsorption geometries and surface reactions of various C_6 hydrocarbons (*n*-hexane, 2-methylpentane, 3-methylpentane, and 1-hexene) on Pt(100). At 300K and in the presence of excess hydrogen, *n*-hexane, 3-methylpentane, and 2-methylpentane adsorb molecularly on Pt(100) mostly in "flat-lying" conformations. Upon heating the metal surface to 450K, the molecules underwent dehydrogenation to form new surface species in "standing-up" conformations, such as hexylidyne and metallacyclic species. 1-Hexene, however, dehydrogenated to form metallocycle $Pt_3{\equiv}C\text{-}(CH_2)_5\text{-}Pt$ at 300K in the presence of excess hydrogen and remained unreacted on the surface upon heating the metal surface to 450K. Dehydrogenation was enhanced in the absence of excess hydrogen in the cases of *n*-hexane, 2-methylpentane, and 3-methylpentane to form metallocycle $Pt_3{\equiv}C\text{-}(CH_2)_5\text{-}Pt$; 2-methyl-1-pentene and 4-methyl-1-pentene; and metallacyclohexane, respectively, at 300K. These surface species remained unreacted after increasing the surface temperature to 450K. The mechanisms for catalytic isomerization and dehydrocyclization of *n*-hexane were discussed on the basis of these results.

9.1. Introduction

The surface chemistry of alkanes on platinum surfaces is a central issue in understanding reforming reactions that produce high-octane gasoline.[1-3] Identifying reactive surface intermediates is key for understanding the mechanisms of isomerization and dehydrocyclization of *n*-hexane to benzene. Furthermore, understanding how surface reaction intermediates are affected by metal surface structure can extend our knowledge of chemical bonding on single crystals to industrial catalysts.

Various surface analytical techniques have been employed to probe surface species upon adsorption of alkane molecules on metal surfaces at low pressures ($< 10^{-6}$ Torr).[4-8] Among these are low energy electron diffraction (LEED), thermal desorption spectroscopy (TDS), high resolution electron energy loss spectroscopy (HREELS), and reflection absorption infrared spectroscopy (RAIRS).[4-8] However, at low pressures, only strongly bound adsorbates will exist on the surface, while weakly bound species desorb quickly. These weakly bound species may be key intermediates in high pressure reactions.

High pressure studies of C_6 alkane hydrocarbons on Pt(111) have been investigated using sum frequency generation (SFG) vibrational spectroscopy.[9] These studies have found that *n*-hexane and 3-methylpentane are inactive on Pt(111) at 296K in the presence of excess hydrogen. 2-Methylpentane and 1-hexene, however, readily dehydrogenate to form metallacyclobutane and hexylidyne. Heating the metal surface to 453K partially dehydrogenated *n*-hexane and 3-methylpentane to hexylidyne and metallacyclohexane. In the absence of excess hydrogen, *n*-hexane and 3-methylpentane dehydrogenate to form π-allyl c-C_6H_9 and metallacyclohexane at 296K. Heating the

metal surface to 453K caused π-allyl c-C_6H_9 to undergo irreversible dehydrogenation to benzene, whereas the hexylidyne and metallacyclic species remained unreacted. Since previous studies have been limited to Pt(111) single crystals, conducting these experiments on the Pt(100) single crystal will further our knowledge of this reaction, in particular how structure affects the reaction pathway.

In this study, sum frequency generation (SFG) vibrational spectroscopy is used to investigate adsorption geometries and surface reactions of C_6 alkane and alkene hydrocarbons on Pt(100) under 1.5 Torr hydrocarbon in the absence and presence of excess hydrogen at high temperatures (300 – 450 K). The C_6 hydrocarbons of interest in the study are *n*-hexane (C_6H_{14}), 2-methylpentane (C_6H_{14}), 3-methylpentane (C_6H_{14}), and 1-hexene (C_6H_{12}). *n*-Hexane is the simplest alkane molecule to undergo the full spectrum of skeletal rearrangement reactions involved in reforming: isomerization, dehydrogenation, cyclization, and dehydrocyclization.[10,11] Under the electric dipole approximation media with centrosymmetry and isotropic gases do not appear in the SFG spectrum. Since bulk platinum has a center of inversion, its contribution to the SFG signal is negligible. The symmetry at the surface of the platinum crystal is broken, giving rise to a surface specific signal. SFG is a more sensitive tool to study interfaces than infrared absorption and Raman spectroscopies since the SFG signal arises solely from the adsorbates. Electron spectroscopies typically cannot be employed under ambient pressure conditions necessary to perform catalytic reactions.

Here it will be shown that the surface species and their adsorption geometries change radically with temperature and the presence of excess hydrogen. At 300K and in the presence of excess hydrogen, *n*-hexane, 3-methylpentane, and 2-methylpentane are

inactive on Pt(100) while 1-hexene readily dehydrogenates to form metallocycle $Pt_3{\equiv}C\text{-}(CH_2)_5\text{-}Pt$. Upon heating, both *n*-hexane and 2-methylpentane dehydrogenate to form hexylidyne while 3-methylpentane forms metallacyclohexane. At 300K in the absence of excess hydrogen, all of the hydrocarbons readily dehydrogenate. *n*-Hexane, 1-hexene, and 3-methylpentane form metallacyclic species on Pt(100): both *n*-hexane and 1-hexene form metallocycle $Pt_3{\equiv}C\text{-}(CH_2)_5\text{-}Pt$ while 3-methylpentane forms metallacyclohexane. 2-Methylpentane is suggested to form 2-methyl-1-pentene and 4-methyl-1-pentene in the absence of excess hydrogen.

On the basis of the SFG results, I discuss the mechanisms of *n*-hexane catalytic reactions to form isomers and benzene on Pt(100) and we compare these mechanisms to those proposed for Pt(111). Our SFG results provide spectroscopic evidence that metallocycle $Pt_3{\equiv}C\text{-}(CH_2)_5\text{-}Pt$ is a reactive surface intermediate during dehydrocyclization of *n*-hexane on Pt(100), giving credence to previous studies[9] that suggest benzene formation does not occur through a five-member cyclic intermediate, as does isomerization, but through direct 1, 6-ring closure.

9.2. Experimental

All experiments were carried out in a high-pressure/ultrahigh-vacuum (HP/UHV) system on a prepared Pt(100) single-crystal surface. The HP/UHV system consists of a UHV chamber operating at a base pressure of 2×10^{-9} Torr and a high-pressure (HP) cell isolated from the UHV chamber by a gate valve. The UHV chamber is equipped with an Auger electron spectrometer (AES), quadrupole mass spectrometer (QMS) and Ar^+ ion sputter gun. Two CaF_2 conflat windows on the HP cell allow transmission of infrared

(IR), visible (VIS), and sum frequency radiation for SFG experiments. The reactant and product gases are constantly mixed via a recirculation pump.

The Pt(100) crystal was cleaned by sputtering with Ar^+ ions (1 keV) for 20 minutes, heating to 1123 K in the presence of 5×10^{-7} Torr O_2 for 2 minutes, and then annealing at 1123 K for 2 minutes. AES and LEED were used to verify the cleanliness of the Pt(100) surface after several cleaning cycles. The Pt(100) sample was then transferred into the HP cell for SFG reaction studies. 1-Hexene ($\geq$ 99.8 %, Fluka), *n*-hexane ($\geq$ 99.7 %, Fluka), 2-methylpentane ($\geq$ 97 %, Fluka), and 3-methylpentane ($\geq$ 99 %, Fluka) were purified by several freeze-pump-thaw cycles before introduction into the HP cell. Prior to the experiment, the hydrocarbons were checked for impurities by means of QMS. Such impurities were below 0.5 % and consisted of mostly light alkanes below C_6.

A Nd:YAG laser (1064 nm fundamental having a 20 ps pulse width operating at a 20 Hz repetition rate) was used to create a tunable IR (1800-4000 cm^{-1}, 5 cm^{-1} resolution) and a second harmonic VIS (532 nm) beam. The VIS beam (200 μJ) and the IR (200 μJ) beams were spatially and temporally overlapped on the Pt(100) surface with incident angles of 55º and 60º, with respect to the surface normal. All spectra were taken using a ppp polarization combination (SFG, VIS, and IR beams were all p-polarized). The generated SFG beam was sent through a monochromator and the signal intensity was detected with a photomultiplier tube and a gated integrator as the IR beam was scanned over the range of interest. Spectra were curve fit using a previously reported procedure[12,13] to a form of the equation

$$I_{SFG} \propto \left| \chi_{NR}^{(2)} e^{i\phi_{NR}} + \sum_q \frac{A_q}{\omega_{IR} - \omega_q + i\Gamma_q} e^{i\gamma_q} \right|^2 \qquad (8.1)$$

where $\chi_{NR}^{(2)}$ is the nonresonant nonlinear susceptibility, $e^{i\phi_{NR}}$ is the phase associated with the nonresonant background, A_q is the strength of the qth vibrational mode, ω_{IR} is the frequency of the incident infrared laser beam, ω_q is the frequency of the qth vibrational mode, Γ_q is the natural line width of the qth vibrational transition, and $e^{i\gamma_q}$ is the phase associated with the qth vibrational transition. Detailed descriptions on the HP/UHV system and SFG measurement can be found elsewhere.[14-19]

9.3. Results

9.3.1. SFG Spectra of Surface Species on Pt(100) at 300K in 1.5 Torr C_6 Hydrocarbons and 15 Torr Hydrogen.

The SFG spectra of surface species on Pt(100) at 300K in 1.5 Torr C_6 hydrocarbons and 15 Torr H_2 are shown in Figure 9.1. In order from the top in Figure 9.1 are *n*-hexane, 3-methylpentane, 2-methylpentane, and 1-hexene. The solid lines in Figure 9.1 correspond to fits using equation 9.1.

Hexane. There are two major bands at 2860 and 2915 cm^{-1}. The band at 2860 cm^{-1} is assigned to a mixture of unperturbed symmetric CH_2 and CH_3 stretches (CH_2(s) and CH_3(s)). The CH_2(s) and CH_3(s) stretches are typically located at ~2850 and ~2870 cm^{-1} making the assignment of the spectral feature located at 2860 cm^{-1} to either a CH_2 or CH_3 group difficult. Furthermore, the peak width of the observed mode is ~60 cm^{-1}, implying that multiple resonances are responsible for the spectral feature. The band at 2915 cm^{-1} is also assigned to a mixture of stretches: perturbed asymmetric CH_2 and CH_3

(CH_2(a, p) and CH_3(a, p)). Perturbed asymmetric CH_2 and CH_3 are generally centered at ~2900 and ~2920 cm^{-1}. Akin to the symmetric stretch discussed above, assignment of this mode to one functional group is not possible chiefly since the peak width is ~45 cm^{-1}.

Previous studies of *n*-hexane on Pt(111)[9] have been able to distinguish the peaks responsible for the CH_2 and CH_3 functional groups for both the symmetric and perturbed asymmetric cases. Based on the strong CH_3(a, p) peak, Yang and Somorjai[9] determined that the CH_3 groups align with their 3-fold rotational symmetry axis parallel to the surface, thus interacting with the metal surface. The CH_2 groups were also predicted to align with their 2-fold rotational symmetry axis parallel to the surface based on the strong CH_2(a, p) peak. The asymmetric perturbed CH_2 and CH_3 groups are characteristic of the "flat-lying" *n*-hexane in the trans-trans-trans (TTT) conformation (see scheme 9.1).[20,21] However, the presence of the symmetric CH_2 and CH_3 groups is not in line with this assessment. The metal surface selection rule (MSSR) forbids IR modes that are parallel to the metal surface. As seen in scheme 9.1, the dipole moment for the symmetric CH_2 and CH_3 stretches for an *n*- hexane molecule adsorbed on a metal surface will not be allowed. Based on the observation of symmetric CH_2 and CH_3 stretches in the sum frequency spectrum, the adsorbate must exist in different conformations on the surface.

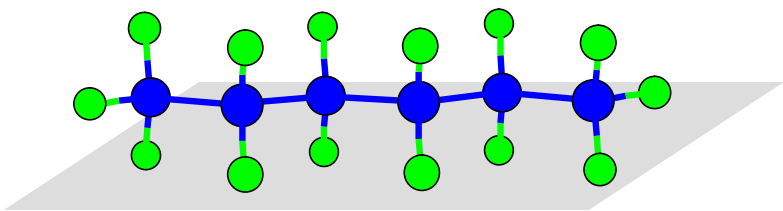

***n*-hexane (C_6H_{14})**

Scheme 9.1. Schematic diagram of *n*-hexane (C_6H_{14}) adsorbed on Pt(100) and Pt(111).

Conformational changes of *n*-alkanes on Pt(111) have been studied by RAIRS,[22] temperature programmed desorption (TPD),[23] laser induced thermal desorption (LITD),[24] and molecular dynamics (MD).[25-28] Theoretical calculations on the dynamics and equilibrium of *n*-alkanes on Pt(111) have stated that *n*-hexane adsorbs in the TTT conformation greater than 99% of the time at temperatures below 200K.[26] The fraction of conformational isomers in gauche states increases above 200K since torsional motions around the C-C bonds are thermally activated. Previous spectroscopic and theoretical studies on *n*-hexane conformers in the liquid and gas phases report the enthalpy change between the TTT conformer and the next stable conformers (TTG, TGT, TGG, and GTG) to be in the range of 0.4-2.0 kcal/mol.[29,30] At room temperature there will be sufficient energy to overcome this barrier and form conformational isomers of *n*-hexane. Based on the above information, the adsorbate present at 300K is suggested to be conformational isomers of "flat-lying" *n*-hexane.

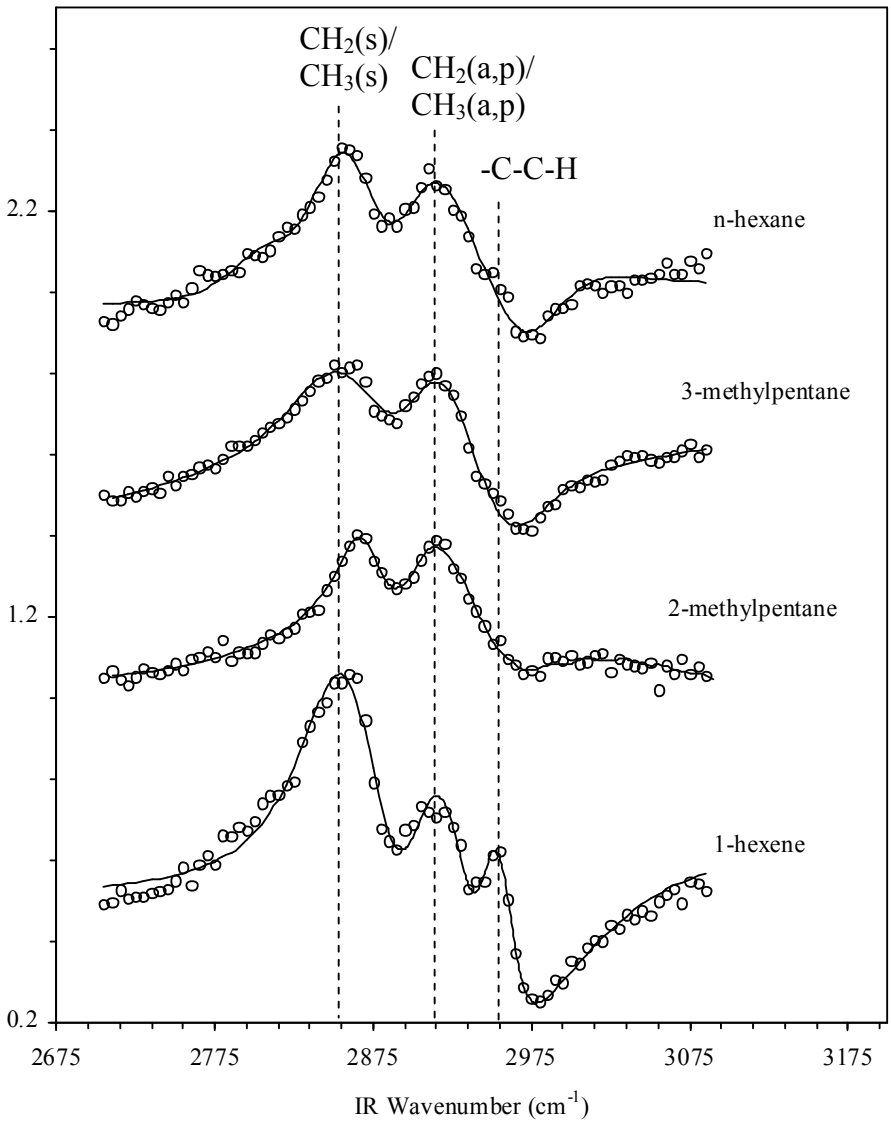

Figure 9.1. SFG spectra of surface species on Pt(100) at 300K in 1.5 Torr C_6 hydrocarbon and 15 Torr H_2. In order from the top are *n*-hexane, 3-methylpentane, 2-methylpentane, and 1-hexene, respectively. Markers represent experimental data and solid lines represent the curve fits using equation 9.1.

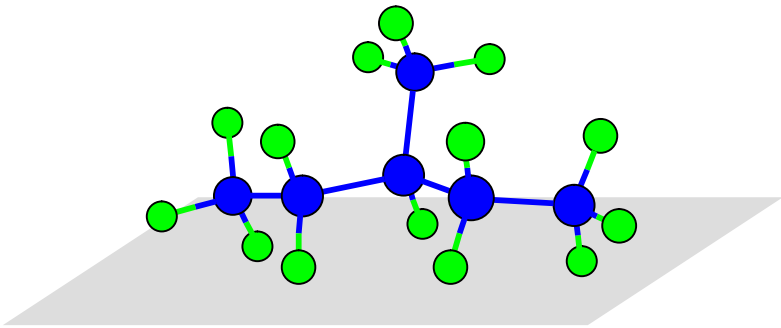

3-methylpentane (C_6H_{14})

Scheme 9.2. Schematic diagram of 3-methylpentane (C_6H_{14}) adsorbed on Pt(100).

3-Methylpentane. The SFG spectrum of 3-methylpentane is strikingly similar to that of *n*-hexane: two major bands appear at 2860 and 2915 cm^{-1}. As is the case of *n*-hexane, the mode at 2860 cm^{-1} is assigned to a mixture of CH_2(s) and CH_3(s) while the mode at 2915 cm^{-1} is assigned to a mixture of CH_2(a, p) and CH_3(a, p). Difference between the *n*-hexane and 3-methylpentane spectra can be observed when examining the relative intensities of the symmetric and perturbed asymmetric stretches. The asymmetric stretches in the *n*-hexane spectrum are less intense than the symmetric stretches as compared to the 3-methylpentane, which has comparable stretches for the symmetric and asymmetric stretches. This difference lends to the interpretation that two different adsorbates are being observed. Previous work by Yang and Somorjai[9] on the Pt(111) surface asseverated that physisorbed C_6 alkanes adsorb in a manner that will maximize the number of carbon chains bonding to the metal surface on Pt(111). Based on the presence of an unperturbed asymmetric CH_3 stretch, Yang and Somorjai[9] proposed an adsorption geometry which is illustrated in scheme 9.2. The proposed geometry involves the CH_2 and terminal CH_3 groups interacting with the metal surface while the central CH_3

group tilts away from the surface. The similarities between the spectra for Pt(111) and Pt(100) in the presence of 1.5 Torr 3-methylpentane and 15 Torr H_2 have led to the conclusion that similar surface species are present on both metal surfaces.

2-Methylpentane. The SFG spectrum of the surface species present in 1.5 Torr 2-methylpentane and 15 Torr H_2 is somewhat similar to *n*-hexane and 3-methylpentane. One noticeable difference from the 2-methylpentane spectrum and those of *n*-hexane and 3-methylpentane is that there appears to be a much weaker interaction between the nonresonant nonlinear susceptibility and the resonance at 2915 cm^{-1}. This may be explained by a weaker interaction between the adsorbate and the metal surface and implies that the surface species present upon adsorption of 2-methylpentane is different from those present when *n*-hexane and 3-methylpentane adsorbed.

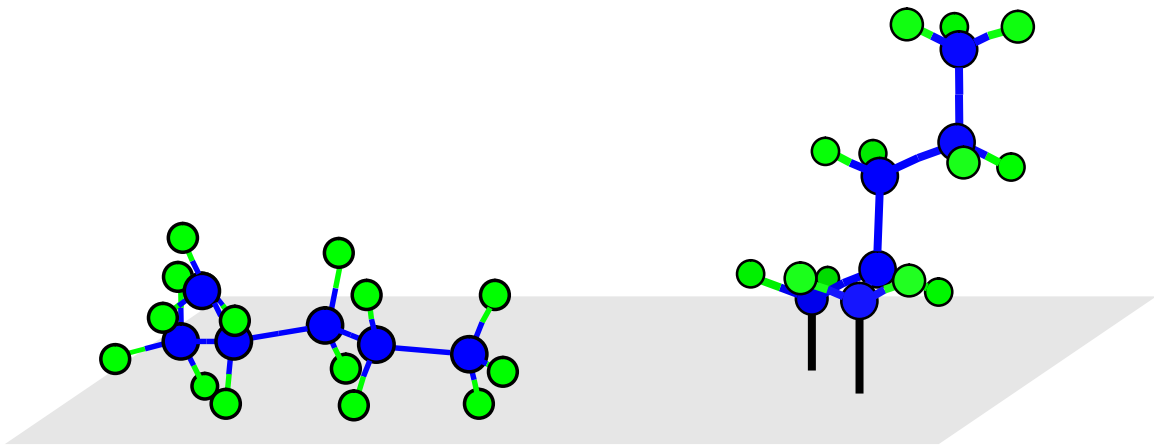

(a) 2-methylpentane (C_6H_{14}) **(b) metallacyclobutane (C_6H_{12})**

Scheme 9.3. Schematic diagram of (a) 2-methylpentane (C_6H_{14}) adsorbed on Pt(100) and (b) metallacyclobutane (C_6H_{12}) adsorbed on Pt(111).

Two major peaks are present at 2870 and 2915 cm^{-1}. As in the *n*-hexane and 3-methylpentane cases, the feature at 2870 cm^{-1} is assigned to a mixture of symmetric

CH_2 and CH_3 stretches while the feature at 2915 cm^{-1} is assigned to perturbed asymmetric CH_2 and CH_3 stretches. To determine the adsorption geometry of 2-methylpentane, we apply criterion proposed by Yang and Somorjai:[9] C_6 alkanes physisorb in such a way as to maximize the number of carbon chains bonding to the metal surface. This information coupled with the knowledge that the spectrum for 3-methylpentane is very similar to 2-methylpentane leads to the conclusion that 2-methylpentane adsorbs in a similar fashion as 3-methylpentane. As seen in scheme 9.3(a), the proposed adsorption geometry involves the two CH_2 and two of the terminal CH_3 groups interacting with the metal surface while the third terminal CH_3 group is tilted away from the surface.

This proposed adsorption geometry is quite different from the molecular geometry on Pt(111). A much stronger symmetric stretch is observed on Pt(111). Based on the strong symmetric stretch, the adsorbate is determined to be in a "standing-up" conformation on Pt(111) with two carbon atoms interacting with the surface to form a metallacyclobutane (see scheme 9.3(b)).

1-Hexene. The SFG spectrum in the case of 1-hexene is dissimilar to the cases of *n*-hexane, 3-methylpentane, and 2-methylpentane. Three strong bands are present in the SFG spectrum at 2860, 2915, and 2950 cm^{-1}. Previous RAIRS[31] studies on 1-hexene adsorption under UHV conditions on Pt(111) have shown three peaks at 2880, 2911, and 2938 cm^{-1}, which have been assigned as CH_2(s), CH_2(s) (bound to surface), and CH_2(a), respectively. Based on these assignments, Ilharco *et al.*[31] have proposed that the adsorbate present on the surface is metallocycle $Pt_3{\equiv}C\text{-}(CH_2)_5\text{-}Pt$, as illustrated in scheme 9.4. The similarity between the RAIRS and SFG spectra leads us to conclude that the

adsorbate present under 1.5 Torr 1-hexene and 15 Torr H_2 is metallocycle $Pt_3{\equiv}C\text{-}(CH_2)_5\text{-}Pt$.

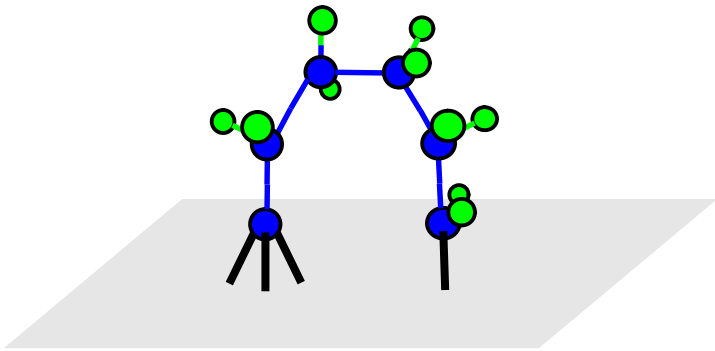

metallocycle $Pt_3{\equiv}C\text{-}(CH_2)_5\text{-}Pt$

Scheme 9.4. Schematic diagram of metallocycle $Pt_3{\equiv}C\text{-}(CH_2)_5\text{-}Pt$ adsorbed on Pt(100).

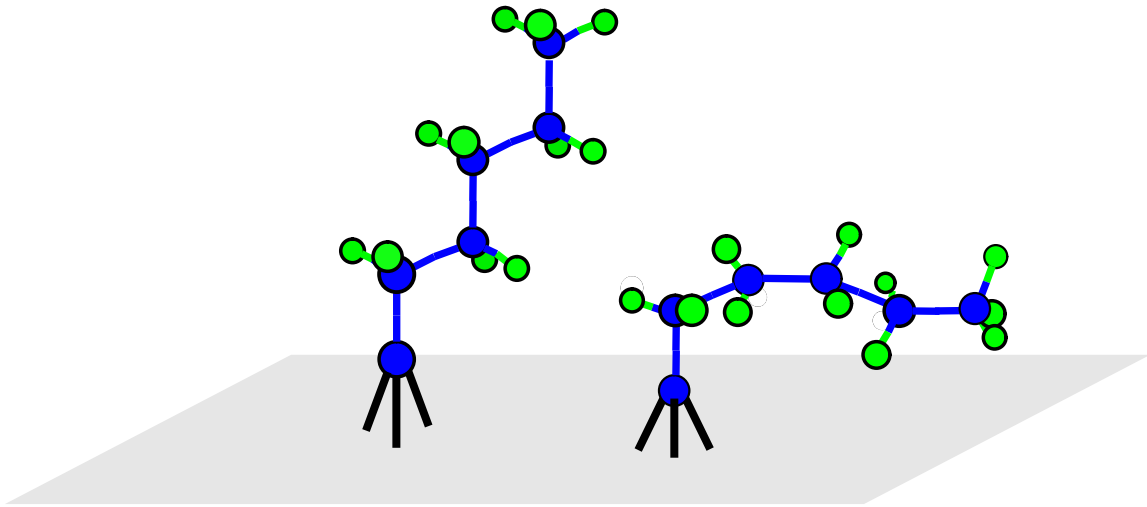

hexylidyne (C_6H_{11})

(a) TTT **(a) GTT**

Scheme 9.5. Schematic diagram of hexylidyne (C_6H_{11}) in the (a) TTT and (b) GTT conformations adsorbed on Pt(100) and Pt(111).

9.3.2. Temperature Dependent SFG Spectra of Surface Species in 1.5 Torr C_6 Hydrocarbons and 15 Torr Hydrogen.

The temperature dependent SFG spectra of the surface species on Pt(100) under 1.5 Torr C_6 hydrocarbon and 15 Torr H_2 are shown in figures 9.2-5. The crystal was initially held at 300K and sequentially heated for each SFG measurement. After reaching 450K, the crystal was cooled to 300K to examine the reversibility of the reaction and the surface chemistry during the heating/cooling cycle.

As described in the previous section, *n*-hexane adsorbs in a "flat-lying" geometry at 300K on Pt(100) with two major peaks at 2860 and 2915 cm^{-1}, which were assigned as CH_2(s)/CH_3(s) and CH_2(a, p)/CH_3(a, p). Upon heating the surface, the bands in the SFG spectra broaden. This is most likely the result of the thermal activation of the translational/rotational motions of the adsorbates giving rise to many adsorption structures, ultimately giving rise to inhomogeneous broadening of the observable SFG bands. At 375K a new band at 3000 cm^{-1} appears in the spectrum, most likely arising from a vinylic stretch.[31,32] This vinylic stretch has been assigned to the partial dehydrogenation of *n*-hexane. Further heating the surface increases the relative intensity of the peak at 2860 cm^{-1} and decreased the relative intensity of the peak at 2915 cm^{-1}. A shoulder is also observed at 2825 cm^{-1}. Previous studies on the Pt(111) surface[9] have shown a similar SFG spectrum, which was ascribed to hexylidyne (see scheme 9.5). RAIRS studies[31] have shown that hexylidyne exists in the TTT and GTT conformations. We have assigned the peaks as follows: 2825 cm^{-1} corresponds to CH_2(s) (GTT), 2860 cm^{-1} corresponds to CH_3(s) (TTT), and 2915 cm^{-1} corresponds to CH_2(a) (GTT/TTT). Heating the crystal to 450K and cooling to 300K reveals a similar spectrum to the initial spectrum at 300K; indicating that "flat-lying" *n*-hexane is present on the surface and indicates that hexylidyne was formed through a reversible pathway.

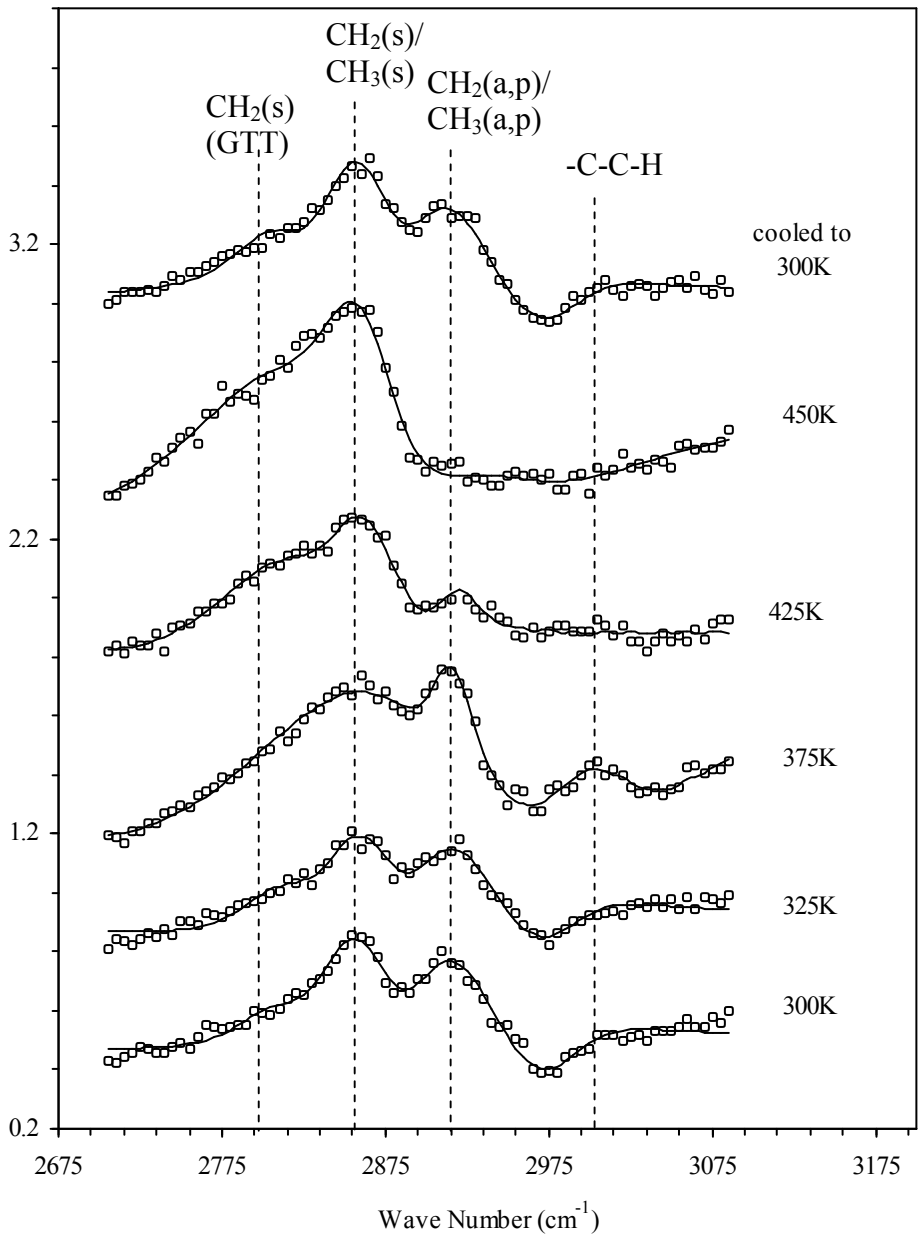

Figure 9.2. Temperature dependent SFG spectra of surface species on Pt(100) under 1.5 Torr *n*-hexane and 15 Torr H_2 in the temperature range of 300-450K. The top SFG spectrum was taken after the metal surface was cooled from 450 K to 300 K. Symmetric CH_2 and CH_3, perturbed asymmetric CH_2 and CH_3, and vinylic (-C=C-H) bands are identified. Markers represent experimental data and solid lines represent the curve fits using equation 9.1.

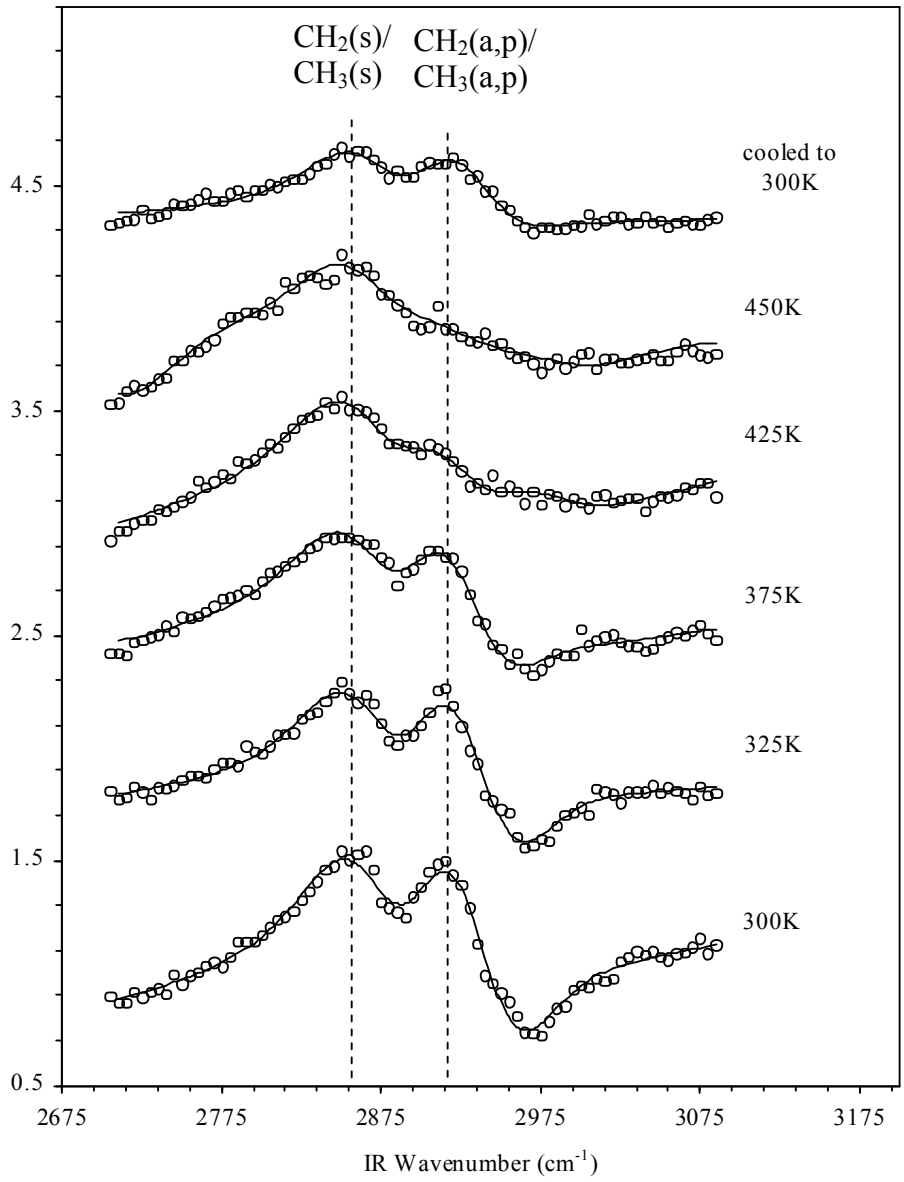

Figure 9.3. Temperature dependent SFG spectra of surface species on Pt(100) under 1.5 Torr 3-methylpentane and 15 Torr H_2 in the temperature range of 300-450K. The top SFG spectrum was taken after the metal surface was cooled from 450 K to 300 K. Symmetric CH_2 and CH_3 and perturbed asymmetric CH_2 and CH_3 bands are identified. Markers represent experimental data and solid lines represent the curve fits using equation 9.1.

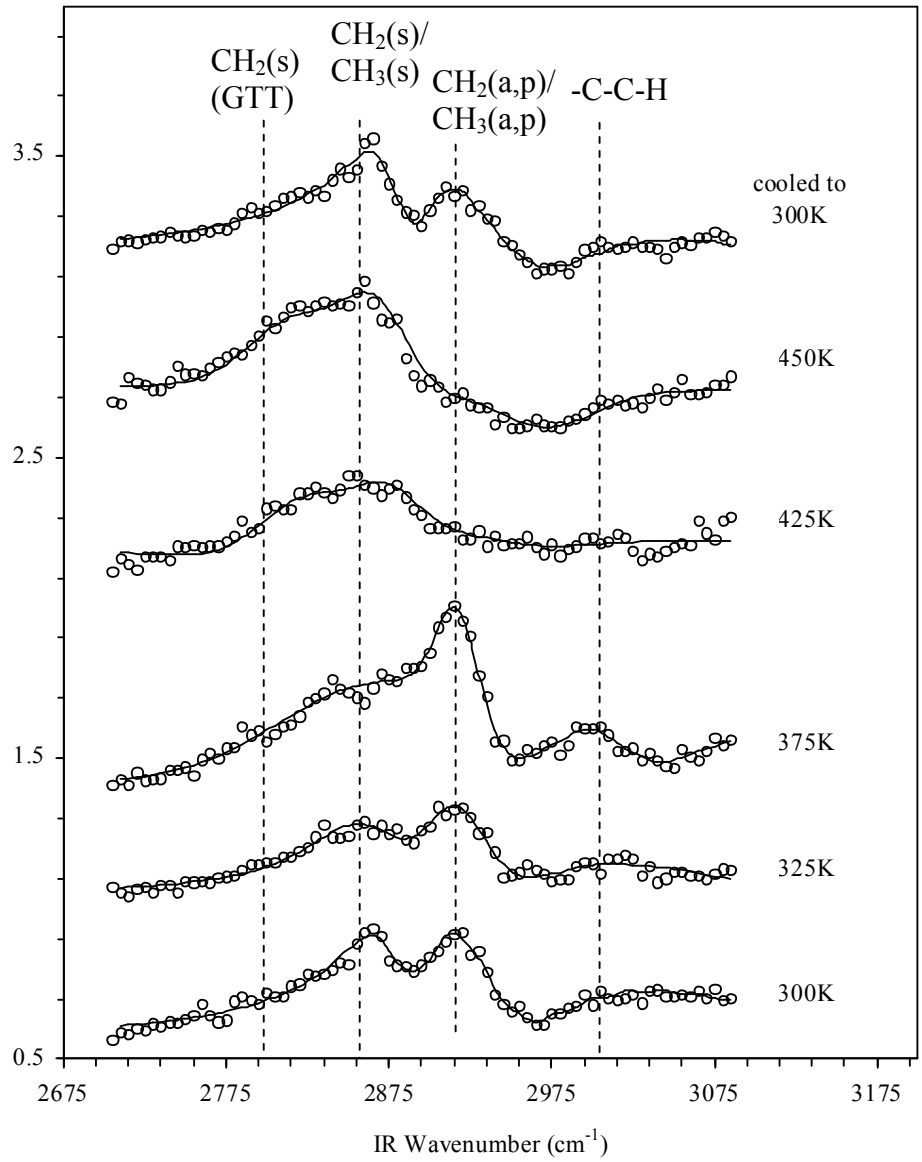

Figure 9.4. Temperature dependent SFG spectra of surface species on Pt(100) under 1.5 Torr 2-methylpentane and 15 Torr H_2 in the temperature range of 300-450K. The top SFG spectrum was taken after the metal surface was cooled from 450 K to 300 K. Symmetric CH_2 and CH_3; perturbed asymmetric CH_2 and CH_3; and vinylic CH bands are identified. Markers represent experimental data and solid lines represent the curve fits using equation 9.1.

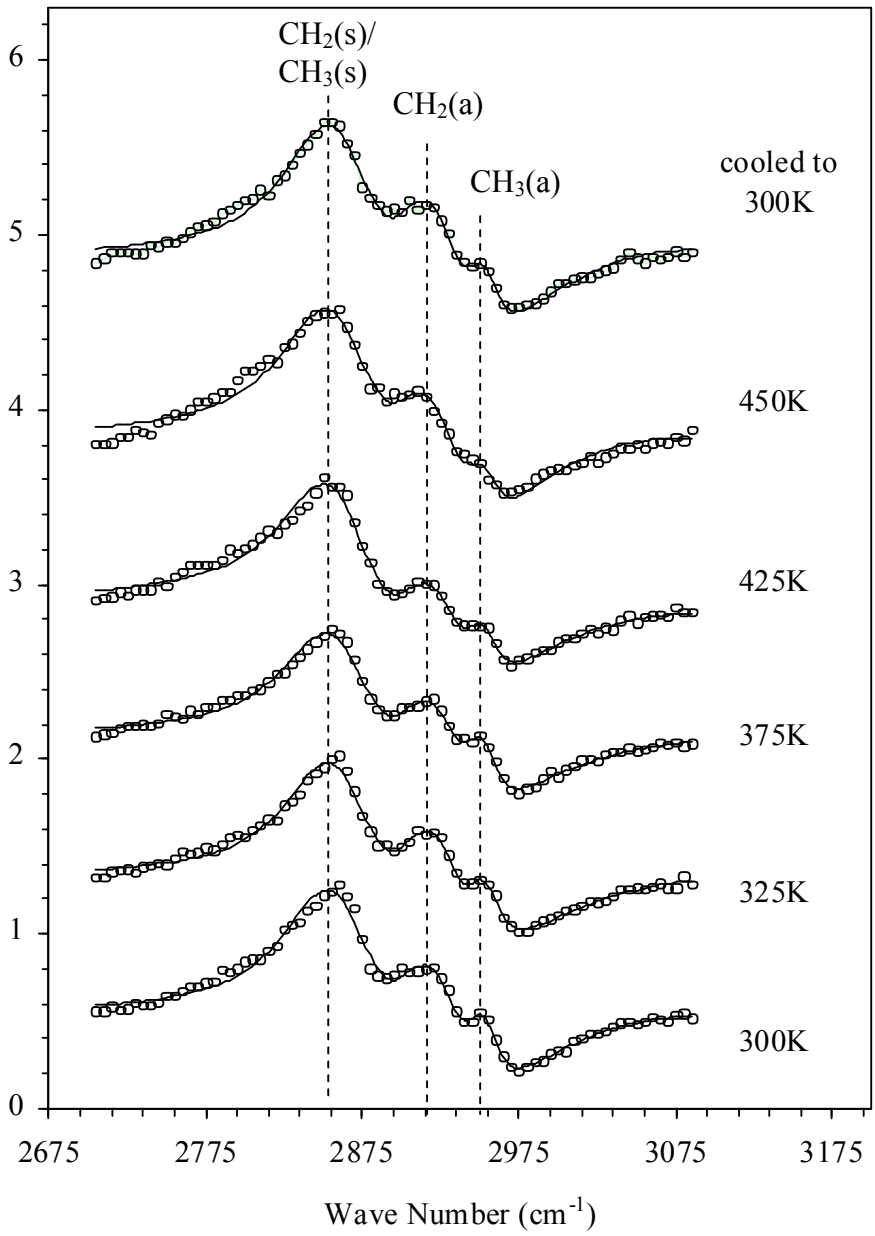

Figure 9.5. Temperature dependent SFG spectra of surface species on Pt(100) under 1.5 Torr 1-hexene and 15 Torr H_2 in the temperature range of 300-450K. The top SFG spectrum was taken after the metal surface was cooled from 450 K to 300 K. Symmetric CH_2 and CH_3 and asymmetric CH_2 and CH_3 bands are identified. Markers represent experimental data and solid lines represent the curve fits using equation 9.1.

The SFG spectra in the case of 3-methylpentane is remarkably similar to that of *n*-hexane. Increasing the surface temperature to 375K shows little change in the vibrational signature of the surface adsorbate, much like in the case of *n*-hexane. Upon heating to 425K, the relative intensities of the symmetric and asymmetric stretches change. This may be due to dehydrogenation of the adsorbed 3-methylpentane to metallacyclohexane since the CH_3 group is now aligned with the surface normal, thus increasing its relative intensity in the SFG spectrum as compared to the "flat-lying" 3-methylpentane whose methyl group is tilted toward the metal surface. Another alternative explanation for the spectra is that 3-methylpentane isomerizes to form *n*-hexane upon adsorption. This rearrangement is less likely since the relative intensities of the adsorbate observed during 3-methylpentane adsorption at 425K are not consistent with the relative intensities observed during *n*-hexane adsorption at the same surface temperature. Furthermore, in the case of *n*-hexane a vinylic stretch is observed at 3000 cm^{-1} after heating the crystal to 375K. No such stretch was observed in the case of 3-methylpentane, indicating that the adsorbate present under 1.5 Torr 3-methylpentane and 15 Torr H_2 is different that in the presence of 1.5 Torr *n*-hexane and 15 Torr H_2. Cooling the surface from 450K to 300K reveals that the temperature dependent changes in the adsorption of 3-methylpentane are reversible.

The SFG spectra in the case of 2-methylpentane show temperature dependences different from those in the cases of *n*-hexane and 3-methylpentane, as seen in figure 9.4. Increasing the surface temperature to 375K results in the increase of the CH_2(a, p)/CH_3(a, p) peak and the appearance of a stretch at 3000 cm^{-1}. The stretch at 3000 cm^{-1} has been attributed to a vinylic stretch.[32] Further heating the crystal surface to 425K results in the

disappearance of the vinylic stretch along with the CH_2(a, p)/CH_3(a, p). The vibrational spectrum observed at 425K bears striking resemblance to the case of 1.5 Torr *n*-hexane and 15 Torr H_2 at 425K. Therefore, the surface species present at 425K is determined to be hexylidyne. Upon cooling the surface to 300K, a spectrum similar to "flat-lying" *n*-hexane is observed. It should be noted that the peak positions of the cooled to 300K spectrum are very similar to the initial spectrum at 300K, however, the relative peak intensities are not similar. Based on the relative intensities of the CH_2(s)/CH_3(s) and CH_2(a, p)/CH_3(a, p), the adsorbate present after cooling to 300K is assigned as "flat-lying" *n*-hexane. Identifying the adsorbate responsible for the vibrational signature at 375K is difficult since there is a paucity of vibrational spectroscopic studies of 2-methylpentane. What can be said about the intermediate is that it is some intermediate in the rearrangement of 2-methylpentane to hexylidyne.

Contrary to the cases of *n*-hexane, 3-methylpentane, and 2-methylpentane, very little change is observed in the SFG spectra for 1-hexene during the heating/cooling treatment, as seen in figure 9.5. These results indicate that metallocycle $Pt_3{\equiv}C\text{-}(CH_2)_5\text{-}Pt$ is a thermally stable species on Pt(100) in the temperature range 300-450K. The proposed adsorption geometries and thermal chemistry of the C_6 hydrocarbons in the presence of excess hydrogen are summarized in Schemes 9.6-9.

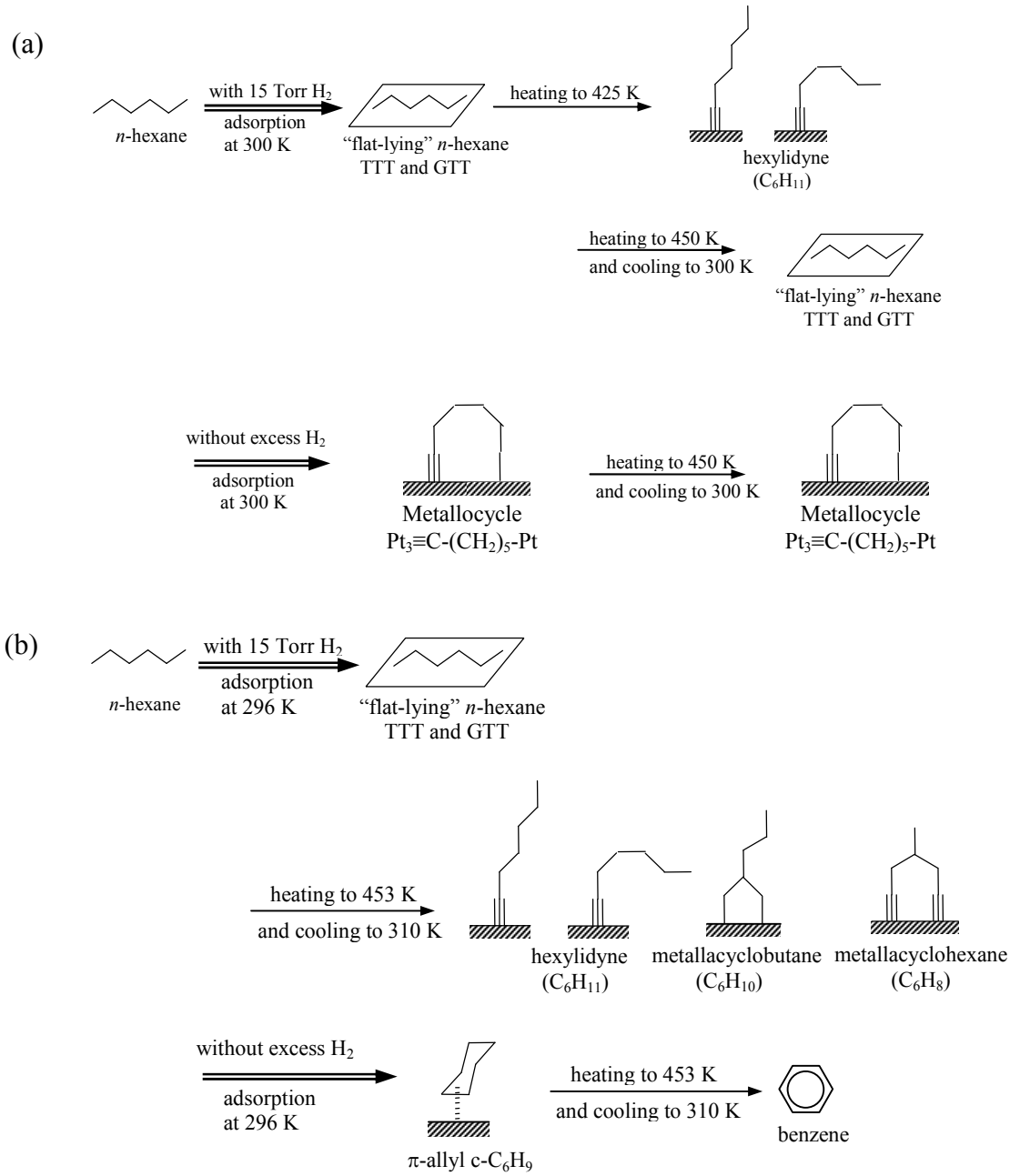

Scheme 9.6. Schematic diagram of observed surface species under 1.5 Torr *n*-hexane in the presence and absence of excess H_2 on (a) Pt(100) and (b) Pt(111)[9].

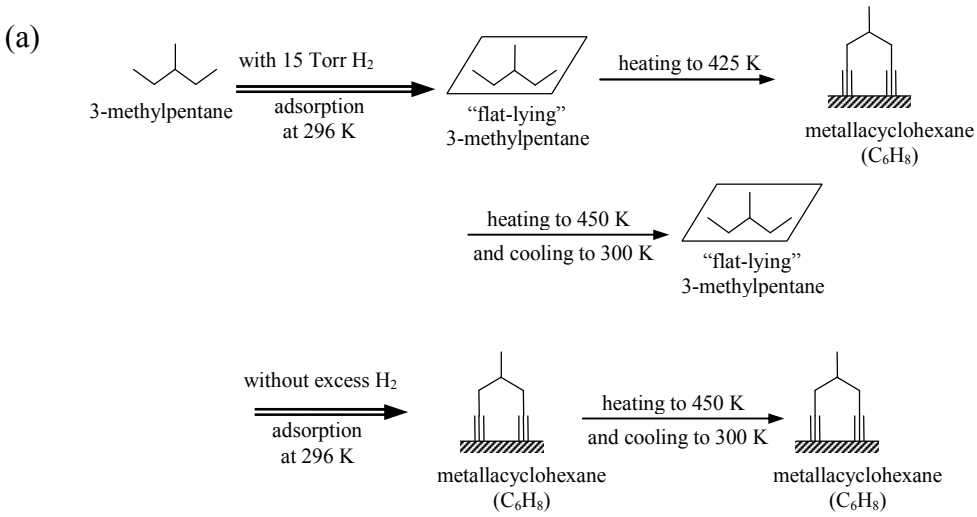

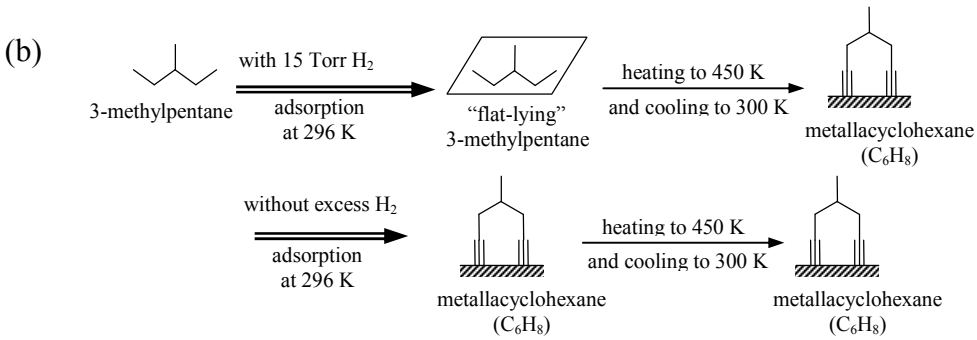

Scheme 9.7. Schematic diagram of observed surface species under 1.5 Torr 3-methylpentane in the presence and absence of excess H_2 on (a) Pt(100) and (b) Pt(111)[9].

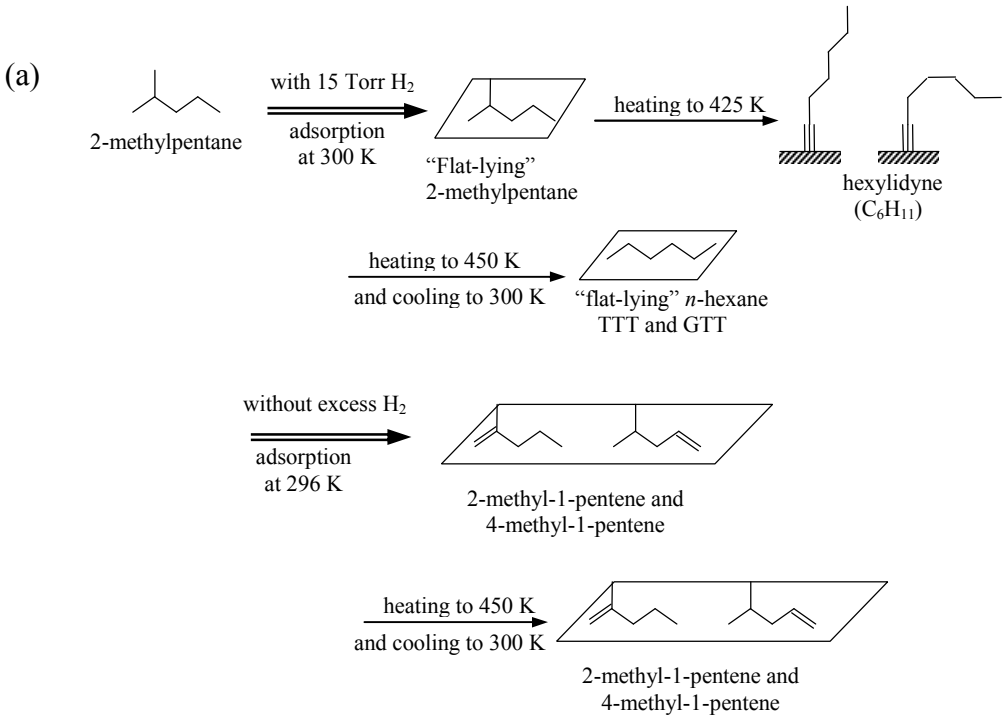

Scheme 9.8. Schematic diagram of observed surface species under 1.5 Torr 2-methylpentane in the presence and absence of excess H_2 on (a) Pt(100) and (b) Pt(111)[9].

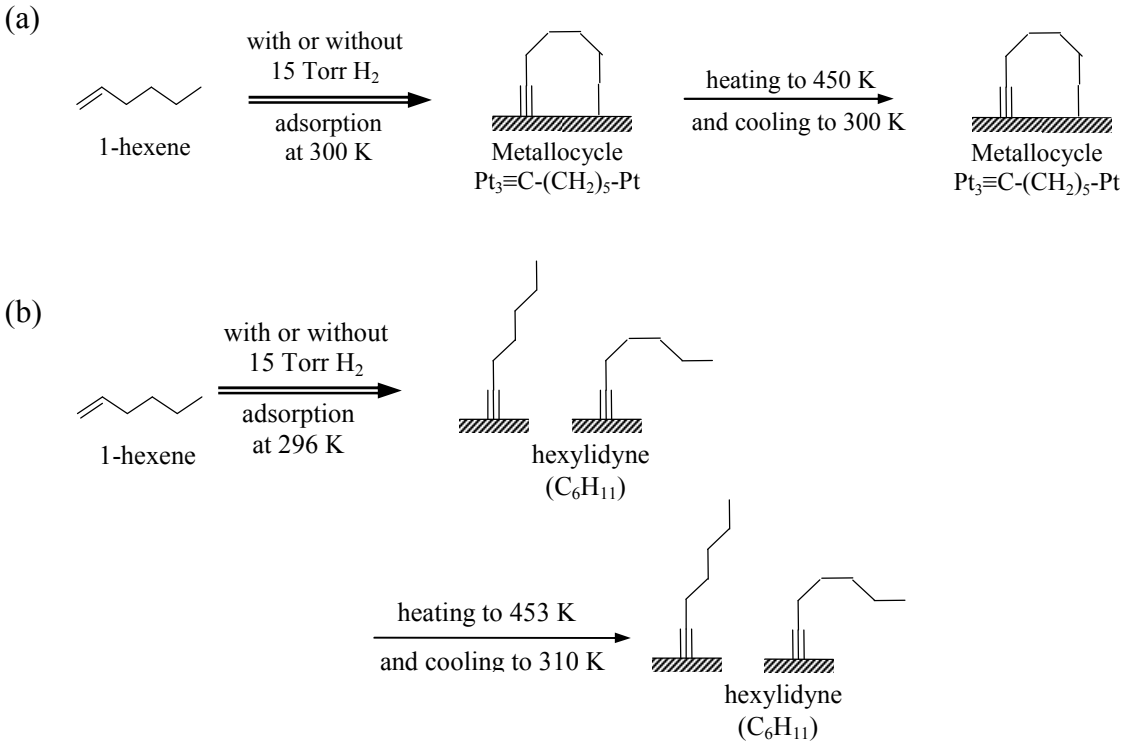

Scheme 9.9. Schematic diagram of observed surface species under 1.5 Torr 1-hexene in the presence and absence of excess H_2 on (a) Pt(100) and (b) Pt(111)[9].

9.3.3 SFG Spectra of Surface Species on Pt(100) at 300K under 1.5 Torr C_6 Hydrocarbons in the Absence of Excess Hydrogen.

The SFG spectra of the surface species on Pt(100) at 300K under 1.5 Torr C_6 hydrocarbons in the absence of excess hydrogen are shown in figure 9.6. The SFG spectrum for *n*-hexane features three bands at 2860, 2920, and 2955 cm^{-1}. The peak positions, relative intensities, and widths are very similar to the case of 1.5 Torr 1-hexene and 15 Torr H_2 (see figure 9.5). We propose that the surface species present in this case is also metallocycle Pt_3≡C-$(CH_2)_5$-Pt (see scheme 9.4).

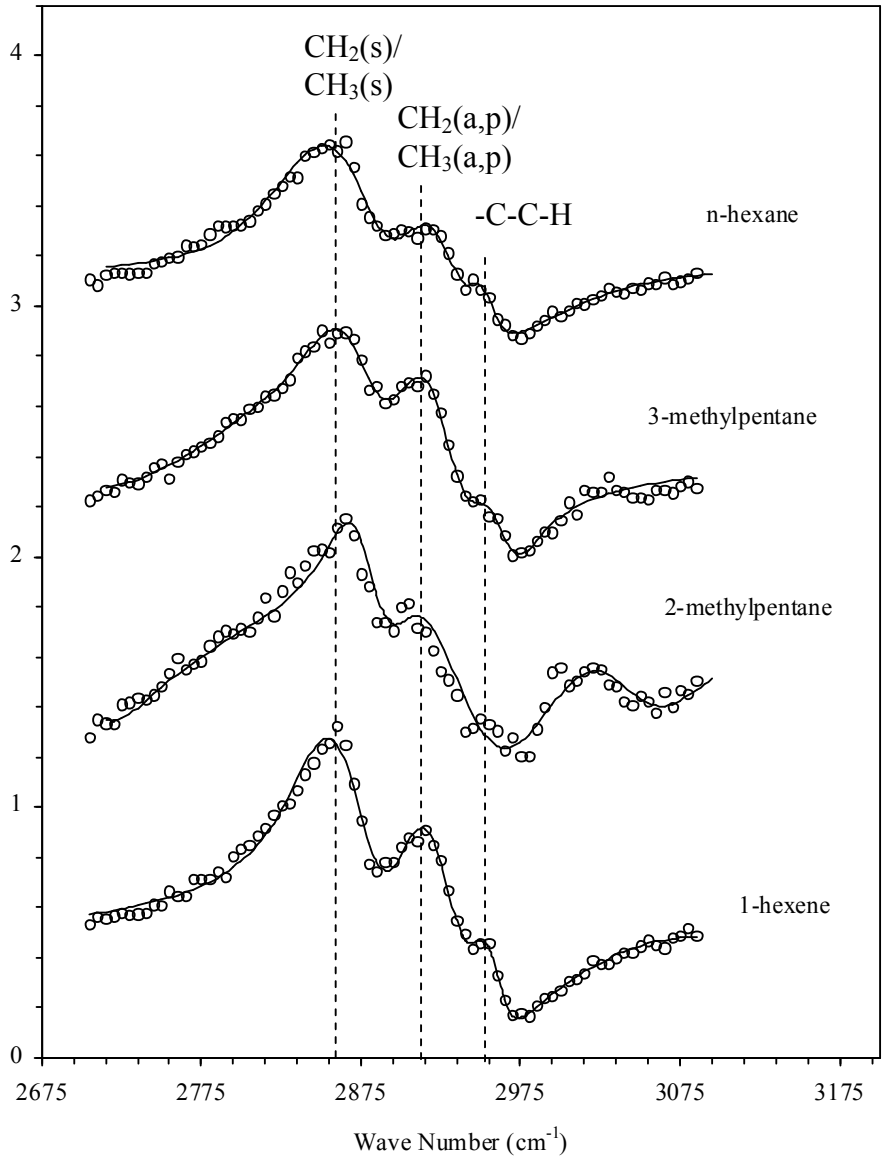

Figure 9.6. SFG spectra of surface species on Pt(100) at 300K under 1.5 Torr C_6 hydrocarbons in the absence of excess hydrogen. In order from the top are *n*-hexane, 3-methylpentane, 2-methylpentane, and 1-hexene. Markers represent experimental data and solid lines represent the curve fits using equation 9.1.

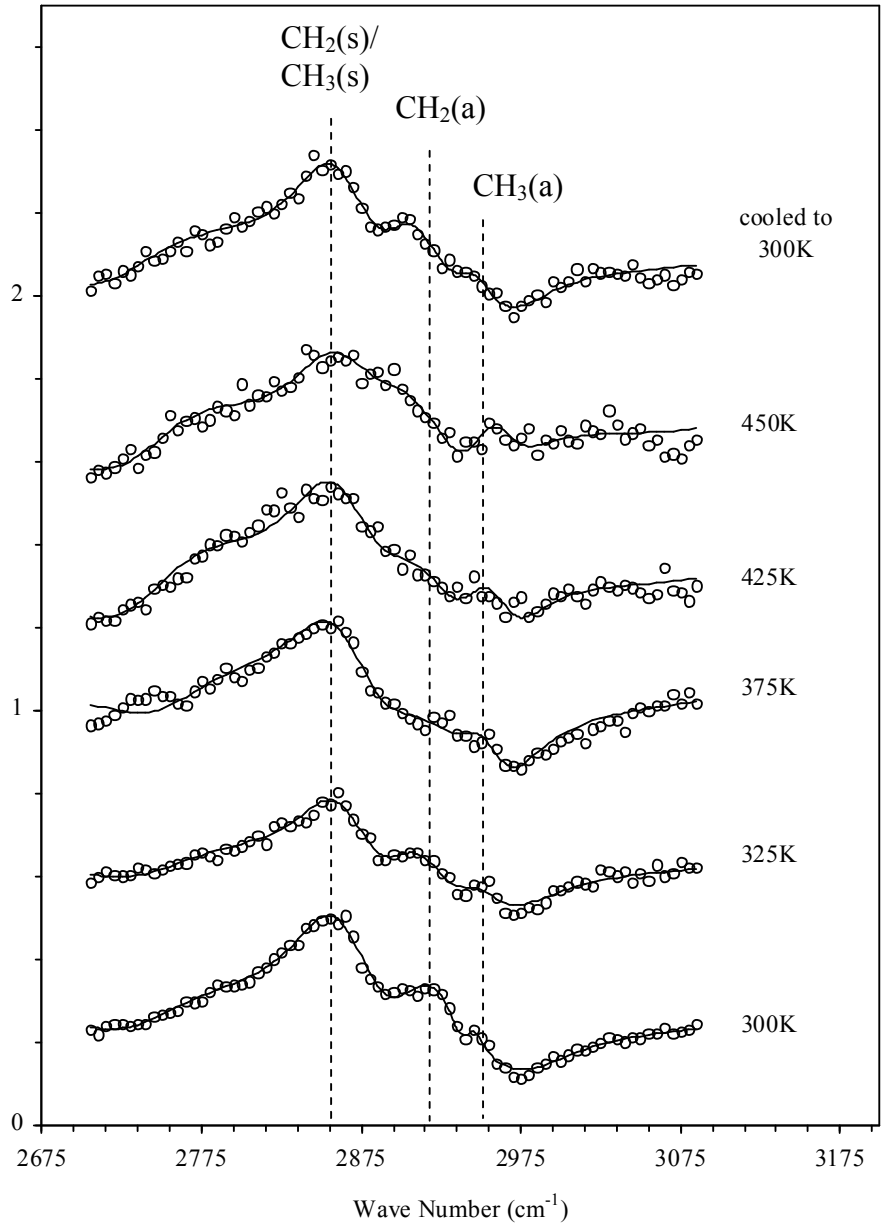

Figure 9.7. Temperature dependent SFG spectra of surface species on Pt(100) under 1.5 Torr n-hexane in the temperature range of 300-450K. The top SFG spectrum was taken after the metal surface was cooled from 450 K to 300 K. Symmetric CH_2 and CH_3 and asymmetric CH_2 and CH_3 bands are identified. Markers represent experimental data and solid lines represent the curve fits using equation 9.1.

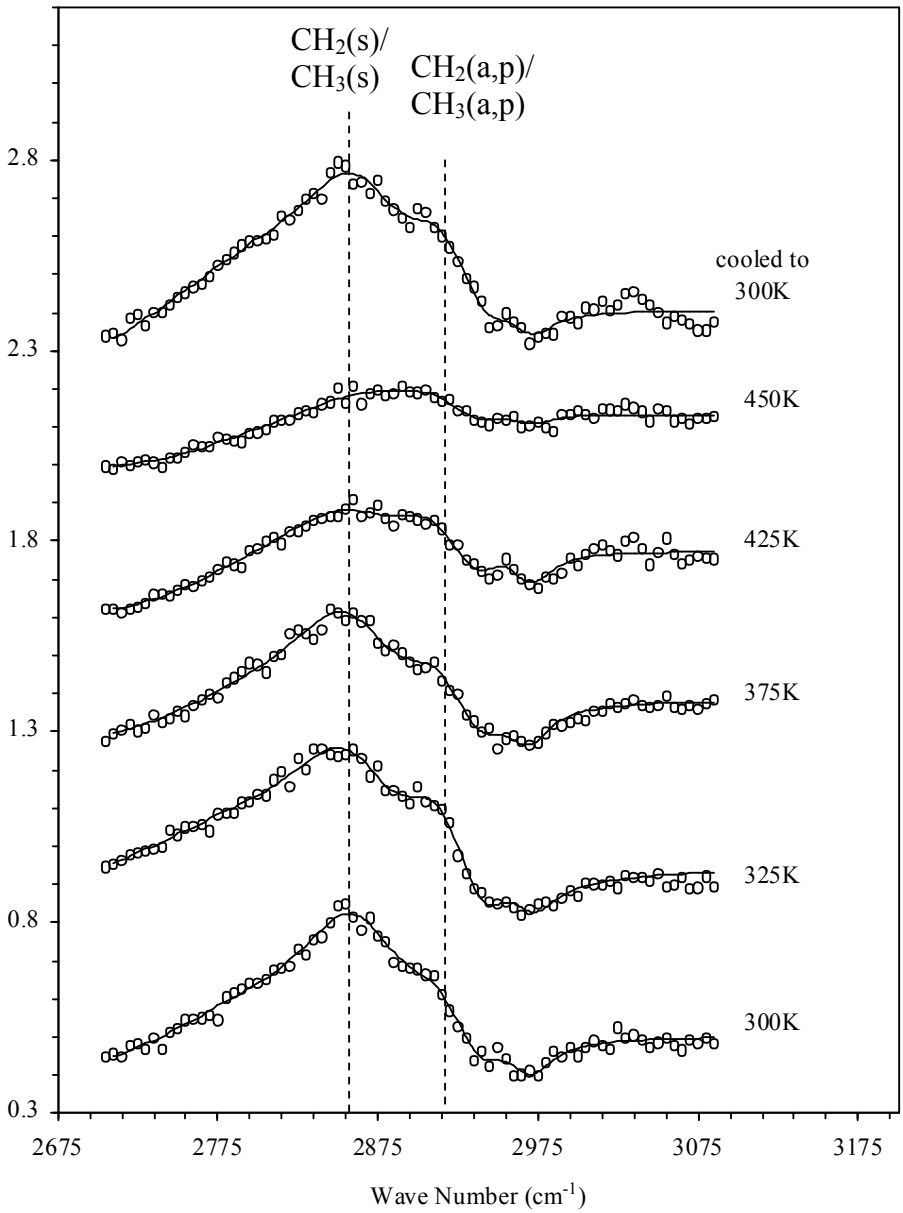

Figure 9.8. Temperature dependent SFG spectra of surface species on Pt(100) under 1.5 Torr 3-methylpentane in the temperature range of 300-450K. The top SFG spectrum was taken after the metal surface was cooled from 450 K to 300 K. Symmetric CH_2 and CH_3 and asymmetric CH_2 and CH_3 bands are identified. Markers represent experimental data and solid lines represent the curve fits using equation 9.1.

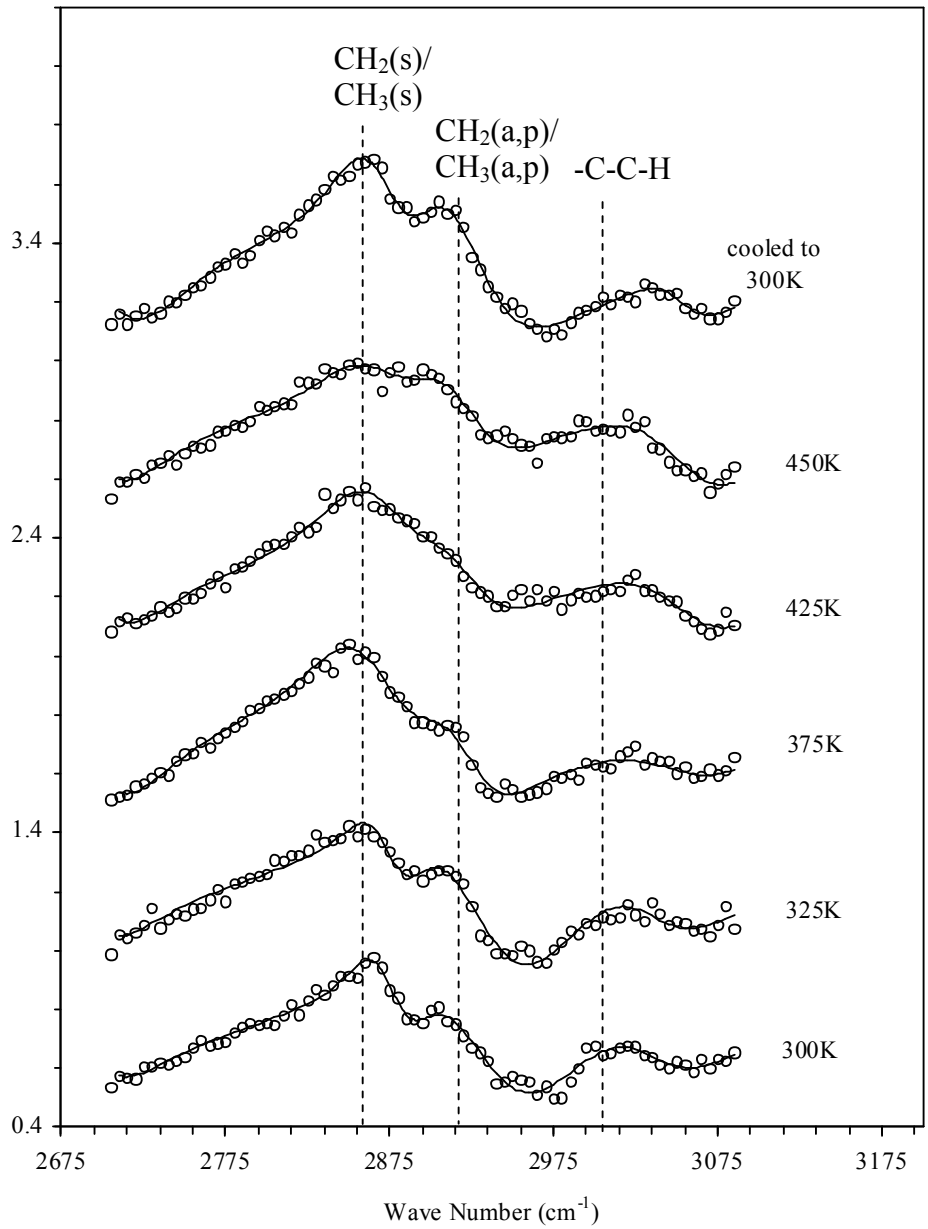

Figure 9.9. Temperature dependent SFG spectra of surface species on Pt(100) under 1.5 Torr 2-methylpentane in the temperature range of 300-450K. The top SFG spectrum was taken after the metal surface was cooled from 450 K to 300 K. Symmetric CH_2 and CH_3 and asymmetric CH_2 and CH_3 bands are identified. Markers represent experimental data and solid lines represent the curve fits using equation 9.1.

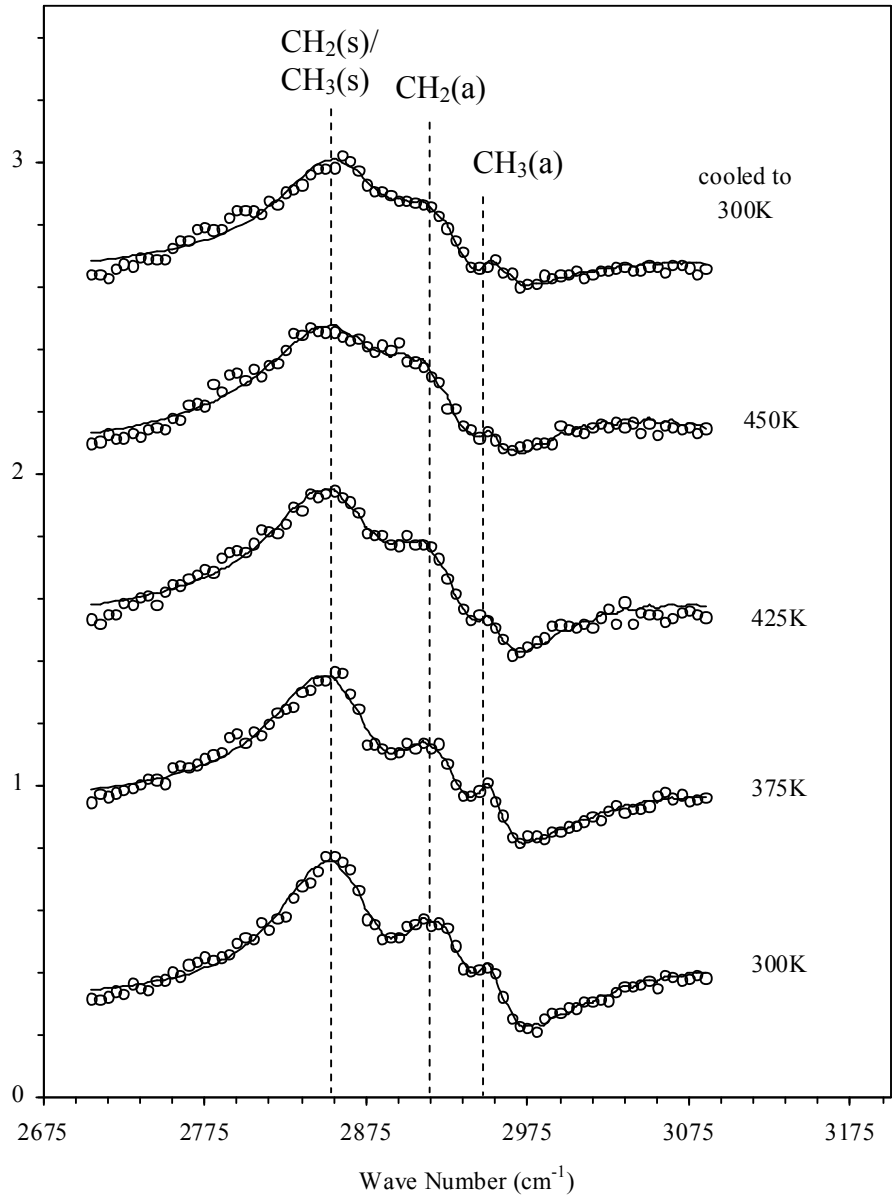

Figure 9.10. Temperature dependent SFG spectra of surface species on Pt(100) under 1.5 Torr 1-hexene in the temperature range of 300-450K. The top SFG spectrum was taken after the metal surface was cooled from 450 K to 300 K. Symmetric CH_2 and CH_3 and asymmetric CH_2 and CH_3 bands are identified. Markers represent experimental data and solid lines represent the curve fits using equation 9.1.

The SFG spectrum for 3-methylpentane features three bands at 2860, 2915, and 2955 cm^{-1}, which are assigned as $CH_2(s)/CH_3(s)$, $CH_2(a)$, and $CH_3(a)$, respectively. Previous studies on Pt(111)[9] have observed similar features of similar intensities to the spectrum shown in figure 9.6. Yang and Somorjai attributed the vibrational signature to metallacyclohexane (see scheme 9.10). Metallacyclohexane is believed to be a surface intermediate in the isomerization of 3-methylpentane to *n*-hexane and vice versa.[2] Another possible interpretation is that the adsorbate present under 1.5 Torr 3-methylpentane is metallocycle $Pt_3{\equiv}C\text{-}(CH_2)_5\text{-}Pt$ based on the peak positions. However, we believe that metallacyclohexane is the more likely surface adsorbate based on the relative intensities of the observed modes in the case of 3-methylpentane.

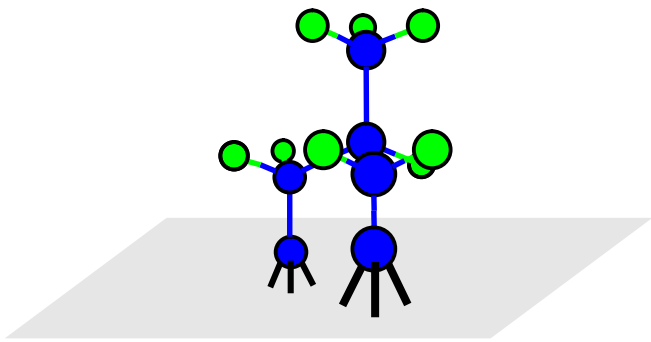

metallacyclohexane (C_6H_8)

Scheme 9.10. Schematic diagram of metallacyclohexane (C_6H_8) adsorbed on Pt(100) and Pt(111)[9].

The SFG spectrum in the case of 2-methylpenatane exhibits four peaks at 2860, 2905, 2955 and 3030 cm^{-1} that are assigned as CH_2(s)/CH_3(s), CH_2(a, p), and vinylic -C=C-H stretches. The vinylic stretch indicates that 2-methylpentane has dehydrogenated on the surface. The identification of this intermediate is difficult since there is a dearth of spectroscopic studies examining the surface intermediates present during 2-methylpentane adsorption. However, two possible candidates for the surface species are 2-methyl-1-pentene and 4-methyl-2-pentene based on infrared spectroscopy.[33] Both of these molecules have modes present at 2870, 2925, 2960, and 3070 cm^{-1}. In the case of 1-hexene, there is very little differences between the SFG spectra in the presence and absence of excess hydrogen (figures 9.1 and 9.6). Cooling the surface temperature from 450K to 300K shows that all of the reactive surface intermediates observed in the absence of excess hydrogen are reversible, indicating that they are thermally stable intermediates (see figures 9.7-10).

9.4. Discussion

The most important reactions in naphtha reforming processes are isomerization and dehydrocyclization because they produce the largest increase in octane number. Catalytic reactions of *n*-hexane on platinum based catalysts have been used as a model system to elucidate the reaction mechanisms.[1,2,4,34] Four classes of reactions occur during reforming of *n*-hexane on platinum based catalysts in the presence of excess hydrogen: (1) dehydrocyclization to form benzene, (2) cyclization to form methylcyclopentane, (3) isomerization to form 2- and 3- methylpentane, and (4) hydrogenolysis to form smaller hydrocarbons.[2,9,34] Extensive studies have investigated macroscopic information such as

reaction kinetics through the functionality of active sites and surface structure.[2,10] However, to have a detailed understanding of elementary reaction steps, the reactive surface intermediates must be identified. Yang and Somorjai[9] have made considerable progress in this arena by using SFG to investigate adsorbates present on the Pt(111) surface during *n*-hexane isomerization and dehydrocyclization. To further understand the catalytic reactions of *n*-hexane on platinum based catalysts, a molecular level understanding of the adsorbates present during reaction on other surface structures is necessary.

n-Hexane adsorption on Pt(111) and Pt(100) yields quite similar adsorbates in the presence of excess hydrogen, as summarized in scheme 9.7. Initially, *n*-hexane adsorbs in a "flat-lying" conformation. Increasing the surface temperature dehydrogenates the "flat-lying" species to form hexylidyne. In the absence of hydrogen, different adsorbates exist on the platinum surfaces: metallocycle $Pt_3{\equiv}C\text{-}(CH_2)_5\text{-}Pt$ on Pt(100) and π-allyl c-C_6H_9 on Pt(111).

Similar surface species are observed on Pt(100) and Pt(111) in the case of 3-methylpentane (see scheme 9.8). In the presence of excess hydrogen, "flat-lying" 3-methylpentane is observed which dehydrogenates to metallacyclohexane as the surface temperature is increased. Metallacyclohexane is also observed in the absence of hydrogen on both surfaces and is believed to be a surface intermediate when *n*-hexane isomerizes to 3-methylpentane and vice versa.[2] Furthermore, the rate of isomerization from *n*-hexane to 3-methylpentane has shown little dependence on surface structure,[10] which supports this theory.

Metallacyclobutane is believed to be an intermediate in the isomerization of *n*-hexane to 2-methylpentane[2] and is only observed on the Pt(111) surface. In the case of 2-methylpentane on Pt(100), "flat-lying" 2-methylpentane forms hexylidyne without forming metallacyclobutane. This may indicate that the isomerization of metallacyclobutane occurs so rapidly on Pt(100) that it can not be observed in the SFG spectrum. Without hydrogen, 2-methylpentane undergoes another different reaction pathway: through a dehydrogenated species speculated to be 2-methyl-1-pentene or 4-methyl-1-pentene (see scheme 9.9).

In the case of 1-hexene, the dehydrogenated products are observed on both Pt(111) and Pt(100) in the presence and absence of hydrogen: hexylidyne is formed on the Pt(111) surface while metallocycle $Pt_3{\equiv}C\text{-}(CH_2)_5\text{-}Pt$ is formed on Pt(100). Previous work[35] has suggested that the intermediate for dehydrocyclization of 1-hexene is a hexa-σ-bonded triene. This species is clearly not present on either surface since there is no vinylic mode observed. This may indicate that under the experimental conditions, benzene is not produced. Alternatively, the observation of metallocycle $Pt_3{\equiv}C\text{-}(CH_2)_5\text{-}Pt$ may indicate that cyclization occurs prior to dehydrogenation in the formation of benzene. Yang and Somorjai[9] found in the case of *n*-hexane, production of benzene occurs primarily through the formation of π-allyl c-C_6H_9 and proposed that direct 1, 6-ring closure occurs via formation of cyclohexane followed by consecutive dehydrogenation rather than consecutive dehydrogenation of *n*-hexane followed by cyclization. We have expanded upon the 1, 6-ring closure mechanism by purporting that metallocycle $Pt_3{\equiv}C\text{-}(CH_2)_5\text{-}Pt$ is the reactive intermediate in forming π-allyl c-C_6H_9, which in turn forms benzene. Furthermore, we suggest that the cyclization of

metallocycle $Pt_3{\equiv}C\text{-}(CH_2)_5\text{-}Pt$ to form π-allyl $c\text{-}C_6H_9$ is the rate determining step in *n*-hexane dehydrocyclization to benzene. This assertion is based on studies by Davis *et al.*[10] that investigated structure sensitivity of aromatization of *n*-hexane and found that the reaction is markedly maximized on Pt(111) surfaces. Combining the gas phase production data with the molecular level information provided by SFG leads us to the conclusion that the 1, 6-ring closure is faster on Pt(111) leading to a larger production of benzene.

9.5. Conclusions

Through the use of SFG I was able to probe reactive surface intermediates and elucidate reaction pathways in hydrocarbon reforming processes. *n*-Hexane, 3-methylpentane, and 2-methylpentane were inactive on Pt(100) at 300K in the presence of excess hydrogen. However, 1-hexene readily dehydrogenated to form metallocycle $Pt_3{\equiv}C\text{-}(CH_2)_5\text{-}Pt$, regardless of the presence of excess hydrogen. At high surface temperature, *n*-hexane and 2-methylpentane dehydrogenated to form hexylidyne in the presence of excess hydrogen. 3-Methylpentane also underwent dehydrogenation at elevated temperature to form metallacyclohexane. In the absence of excess hydrogen, dehydrogenation of each hydrocarbon was enhanced: *n*-hexane formed metallocycle $Pt_3{\equiv}C\text{-}(CH_2)_5\text{-}Pt$, 2-methylpentane formed 2-methyl-1-pentene and 4-methyl-1-pentene, and 3-methylpentane formed metallacyclohexane. These results support previous claims[9] that metallacyclohexane is a reactive surface intermediate in the isomerization of 3-methylpentane to *n*-hexane and vice versa. Additionally, metallocycle $Pt_3{\equiv}C\text{-}(CH_2)_5\text{-}Pt$

is suggested to be a reactive surface intermediate in the direct 1, 6-ring closure of *n*-hexane in the formation of benzene.

References

(1) *Catalytic naphtha reforming: science and technology*; 2nd ed.; Antos, G. J.; Aitani, A. M.; Parera, J. M., Eds.; Marcel Dekker: New York, 1995.

(2) Davis, B. H. *Catal. Today* **1999**, *53*, 443-516.

(3) Cooper, B. H.; Donnis, B. B. L. *Applied Catalysis A* **1996**, *137*, 203-223.

(4) Somorjai, G. A. *Introduction to Surface Science Chemistry and Catalysis*; Wiley: New York, 1994.

(5) Sheppard, N. *Annu. Rev. Phys. Chem* **1988**, *39*, 589-644.

(6) Sheppard, N.; Cruz, C. D. L. *Advances in Catalysis* **1998**, *42*, 181-313.

(7) Bent, B. E. *Chemical Reviews* **1996**, *96*, 1361-1390.

(8) Zaera, F. *Chemical Reviews* **1995**, *95*, 2651-2693.

(9) Yang, M.; Somorjai, G. A. *Journal of the American Chemical Society* **2004**, *126*, 7698-7708.

(10) Davis, S. M.; Zaera, F.; Somorjai, G. A. *J. Catal.* **1984**, *85*, 206-223.

(11) Zaera, F.; Godbey, D.; Somorjai, G. A. *Journal of Catalysis* **1986**, *101*, 73-80.

(12) Bain, C. D.; Davies, P. B.; Ong, T. H.; Ward, R. N.; Brown, M. A. *Langmuir* **1991**, *7*, 1563-1566.

(13) Moore, F. G.; Becraft, K. A.; Richmond, G. L. *Applied Spectroscopy* **2002**, *56*, 1575-1578.

(14) Bratlie, K. M.; Flores, L. D.; Somorjai, G. A. *Surface Science* **2005**, *599*, 93-106.

(15) Kung, K. Y.; Chen, P.; Wei, F.; Rupprechter, G.; Shen, Y. R.; Somorjai, G. A. *Review of Scientific Instruments* **2001**, *72*, 1806-1809.

(16) Yang, M.; Tang, D. C.; Somorjai, G. A. *Review of Scientific Instruments* **2003**, *74*, 4554-4557.

(17) Shen, Y. R. *Nature* **1989**, *337*, 519-525.

(18) Shen, Y. R. *Annual Review of Physical Chemistry* **1989**, *40*, 327-350.

(19) Shen, Y. R. *The Principles of Nonlinear Optics*; Wiley: New York, 2003.

(20) Chesters, M. A.; Gardner, P.; McCash, E. M. *Surface Science* **1989**, *209*, 89-99.

(21) Manner, W. L.; Bishop, A. R.; Girolami, G. S.; Nuzzo, R. G. *Journal of Physical Chemistry B* **1998**, *102*, 8816-8824.

(22) Bishop, A. R.; Girolami, G. S.; Nuzzo, R. G. *Journal of Physical Chemistry B* **2000**, *104*, 754-763.

(23) Paserba, K. R.; Gellman, A. J. *Physical Review Letters* **2001**, *86*, 4338-4341.

(24) Brand, J. L.; Arena, M. V.; Deckert, A. A.; George, S. M. *Journal of Chemical Physics* **1990**, *92*, 5136-5143.

(25) Fichthorn, K. A.; Miron, R. A. *Physical Review Letters* **2002**, *89*, 196103-196106.

(26) Huang, D.; Chen, Y.; Fichthorn, K. A. *Journal of Chemical Physics* **1994**, *101*, 11021-11030.

(27) Raut, J. S.; Fichthorn, K. A. *Journal of Chemical Physics* **1998**, *108*, 1626-1635.

(28) Cohen, D.; Zeiri, Y. J. *Journal of Chemical Physics* **1992**, *97*, 1531-1541.

(29) Mirkin, N. G.; Krimm, S. *Journal of Physical Chemistry* **1993**, *97*, 13887-13895.

(30) Harada, I.; Takeuchi, H.; Sakakibara, M.; Matsuura, H.; Shimanouchi, T. *Bulletin of the Chemical Society of Japan* **1977**, *50*, 102-110.

(31) Ilharco, L. M.; Garcia, A. R.; Hargreaves, E. C.; Chesters, M. A. *Surface Science* **2000**, *459*, 115-123.

(32) Bratlie, K. M.; Kliewer, C. J.; Somorjai, G. A. *Journal of Physical Chemistry B* **2006**, *110*, 17925-17930.

(33) Coblentz Society, I. In *NIST Chemistry WebBook, NIST Standard Reference Database Number 69*; Linstrom, P. J., Mallard, W. G., Eds.; National Institue of Standards and Technology: Gaitersburg, MD, 20899, 2005.

(34) Davies, P. B.; Zaera, F.; Somorjai, G. A. *J. Catal.* **1984**, *101*, 73.

(35) Teplyakov, A. V.; Bent, B. E. *Journal of Physical Chemistry B* **1997**, *101*, 9052-9059.

Chapter 10

Platinum Nanoparticle Shape Effects on Benzene Hydrogenation Selectivity

Benzene hydrogenation was investigated in the presence of a surface monolayer consisting of Pt nanoparticles of different shapes (cubic and cuboctahedral) and tetradecyltrimethylammonium bromide (TTAB). Infrared spectroscopy indicated that TTAB binds to the Pt surface through a weak C-H···Pt bond of the alkyl chain. The catalytic selectivity was found to be strongly affected by the nanoparticle shape. Both cyclohexane and cyclohexene product molecules were formed on cuboctahedral nanoparticles whereas only cyclohexane was produced on cubic nanoparticles. These results are the same as the product selectivities obtained on Pt(111) and Pt(100) single crystals in earlier studies. The apparent activation energy for cyclohexane production on cubic nanoparticles is 10.9 ± 0.4 kcal/mol, while for cuboctahedral nanoparticles, the apparent activation energies for cyclohexane and cyclohexene production are 8.3 ± 0.2 and 12.2 ± 0.4 kcal/mol, respectively. These activation energies are lower and corresponding turnover rates are three times higher than those obtained with single-crystal Pt surfaces.

10.1. Introduction

Structure insensitive reactions on Pt nanoparticles, such as ethylene hydrogenation, has been the main objective of numerous invstigations.[1-4] Extending

reaction studies to structure-sensitive reactions for which turnover rates and product selectivities change with both nanoparticle size and shape is essential for obtaining a molecular understanding of catalytic processes. Benzene hydrogenation is an ideal reaction for such studies because it has been investigated extensively on single-crystalline Pt surfaces.[5-7] Since this reaction has been shown to produce only cyclohexane on Pt(100) and both cyclohexene and cyclohexane on Pt(111),[6] it is suitable for probing nanoparticle dependent reaction selectivity in catalysis. The objective of this investigation was to examine the catalytic activity of benzene hydrogenation on surface monolayers consisting of cubic or cuboctahedral Pt nanoparticles and tetradecyltrimethylammonium bromide (TTAB) capping agent. Kinetic results for TTAB-stabilized Pt nanoparticles are contrasted with those of single-crystal Pt surfaces to elucidate nanoparticle shape effects on catalysis.

The stabilizing agent used to prevent nanoparticle aggregation can also have consequential effects on the catalytic activity. Strongly bound stabilizing agents may hinder or even prevent catalysis by blocking active surface sites and inducing steric effects. For example, previous work[8] has shown that certain stabilizers that strongly encapsulate Pd nanoparticles prevent catalysis. TTAB has recently been used as a stabilizing agent in Pt nanoparticle synthesis and was found to produce much higher catalytic activity for ethylene hydrogenation than polymeric stabilizing agent.[9] However, the interaction of TTAB with the Pt surface has not been studied yet. Infrared (IR) spectra provide insight into this interaction in a dry condition that is conducive to gas-phase reaction.

10.2. Experimental Procedures

10.2.1 Synthesis and Assembly of Platinum Nanoparticles

Nanoparticles stabilized with TTAB were prepared by mixing aqueous solutions of K_2PtCl_4 (99.9% pure, Alfa Aesar) and TTAB (99% pure, Aldrich) in a 20 mL vial at room temperature.[9] The mixture was heated at 323 K for ~5 min until the solution became clear. After the addition of ice-cold $NaBH_4$ (98% pure, Strem Chemicals), the vial was capped with a rubber septum and the H_2 gas pressure inside the vial was released through a needle in the septum for 10 min. After the removal of the needle, the solution was kept at 323 K for 6 h. For cuboctahedral nanoparticle synthesis, a solution of 150 mM TTAB and 1.5 mM K_2PtCl_4 was reduced with 7.5 mM $NaBH_4$ in mild H_2 flow. The cubic nanoparticles were prepared from a solution consisting of 100 mM TTAB and 1 mM K_2PtCl_4 reduced with 30 mM $NaBH_4$. The nanoparticles were centrifuged at 3 krpm for 30 min. The precipitates were discarded. The solution was centrifuged again at 14 krpm for 10min. The supernatant was discarded and the precipitates were re-dispersed in DI water by sonication. The solution was centrifuged at 14 krpm for 10 min once more, and the precipitates were collected and re-dispersed in DI water. The washed nanoparticles were used for transmission electron microscope (TEM) analysis and reaction studies. The nanoparticle shape and size distributions were studied in a TEM (JEOL 200CX) operated at 200 kV.

Nanoparticles were assembled and deposited on a silicon wafer by the Langmuir-Blodgett (LB) technique. Colloidal Pt solutions were dispersed on the surface of deionized water (18 MΩ·cm) sub-phase on a LB trough (type 611, NIMA Technology) at room temperature. The surface pressure was monitored with a Wilhelmy plate and

adjusted to zero before spreading the nanoparticles. The resulting surface layer was compressed by a mobile barrier at a rate of 20 cm^2/min. The nanoparticles were deposited by lifting up the silicon substrates, which had been immersed in water subphase before the nanoparticles were dispersed, at the surface pressure of ~15 mN/m. The surface coverage of the silicon wafer by the nanoparticles was observed in a scanning electron microscope (SEM) (Ultra-55, Zeiss Gemini).

10.2.2. Reaction Cell

Benzene hydrogenation studies were carried out in a custom-made reaction cell under continuous batch reactor conditions. A silicon wafer coated with a nanoparticle monolayer was pressed against a rubber O-ring by tightening a teflon block with two set screws. The temperature at the wafer surface was measured with a thermocouple placed directly onto the sample. Heating was applied at the top of the wafer by a Kapton resistive element (Omega Engineering). Temperature variations across the 20 × 20 mm^2 wafer area were insignificant. The reaction cell was connected to a stainless steel tubing gas manifold of diameter equal to 0.3175 cm. Benzene (≥99.0 wt%, EM Science) was purified by several freeze-pump-thaw cycles before being introduced into the reaction cell. Prior to each experiment, benzene was checked for impurities using gas chromatography (GC). Impurity levels were found to be less than 0.5 wt% and consisted of mostly light alkanes below C_6. A vacuum pressure of less than 1 mTorr was maintained in the reaction cell by mechanical and turbomolecular pumps.

The reaction cell is equipped with a recirculation loop that includes a diaphragm pump and a septum for GC analysis. The reactant and product gases were constantly

mixed by the recirculation pump, while kinetic data were acquired periodically by sampling the reaction mixture and measuring the relative gas phase composition. Kinetic measurements were obtained with GC system (HP 6890) using flame ionization detection and a 0.1% AT-1000 on Graphpac GC 80/100 packed column of 180 m length and 0.3175 cm outside diameter (Alltech). Helium was used as carrier gas and the oven temperature was maintained at 413 K. The reactant pressure was 10 Torr benzene, 100 Torr hydrogen, and 650 Torr argon. Prior to the collection of the kinetic data, the nanoparticles were treated in 100 Torr H_2 for 1 h to optimize cyclohexane formation at 310 K.

10.2.3. Single-crystal Pt surfaces

All single-crystal Pt experiments were carried out in a high-pressure/ultrahigh-vacuum (HP/UHV) system on prepared single-crystal Pt(100) or Pt(111) surfaces. This vacuum system consists of a UHV chamber operating at a base pressure of 2×10^{-9} Torr and a HP cell isolated from the UHV chamber by a gate valve. The UHV chamber is equipped with Auger electron spectrometer (AES), quadrupole mass spectrometer, and Ar^+ ion sputter gun. The HP cell is equipped with a re-circulation loop that includes a diaphragm pump and a septum for gas chromatographic analysis. The reactant and product gases are constantly mixed via a recirculation pump, while kinetic data are acquired by periodically sampling the reaction mixture and measuring the relative gas phase composition (FID detection and 0.1% AT-1000 on Graphpac GC 80/100 packed column (Alltech)).

The single-crystal Pt(100) and Pt(111) surfaces were cleaned by sputtering with Ar^+ ions (1 keV) for 20 min, heating to 1123 K in the presence of 5×10^{-7} Torr O_2 for 2 min, and then annealing at 1123 K for 2 min. AES and loss energy electron spectroscopy were used to verify the cleanliness of the Pt(100) and Pt(111) surfaces after several cleaning cycles. The Pt(100) or Pt(111) sample was then transferred into the HP cell for reaction studies. Cyclohexene (99.97%, EM Science) was purified by several freeze-pump-thaw cycles before introduction into the HP cell. Prior to the experiment, cyclohexene was checked for impurities by means of GC. The impurities were below 0.5% and consisted of mostly light alkanes below C_6. Detailed descriptions on the HP/UHV system can be found elsewhere.[10-12]

10.2.4. Infrared Spectroscopy. Diffuse reflectance IR Fourier transformed (DRIFT) spectra were obtained with a spectrophotometer (Nicolet Nexus-670) equipped with integrated diffuse reflectance optics (Spectra-Tech Collector II). Thin layers evaporated from TTAB-stabilized nanoparticles in H_2O on Al foils were used to obtain the IR spectra. The layer thickness was adjusted to render the samples partially IR transparent. This method has been described as a hybrid method of DRIFT and reflection absorption IR spectroscopy.[13]

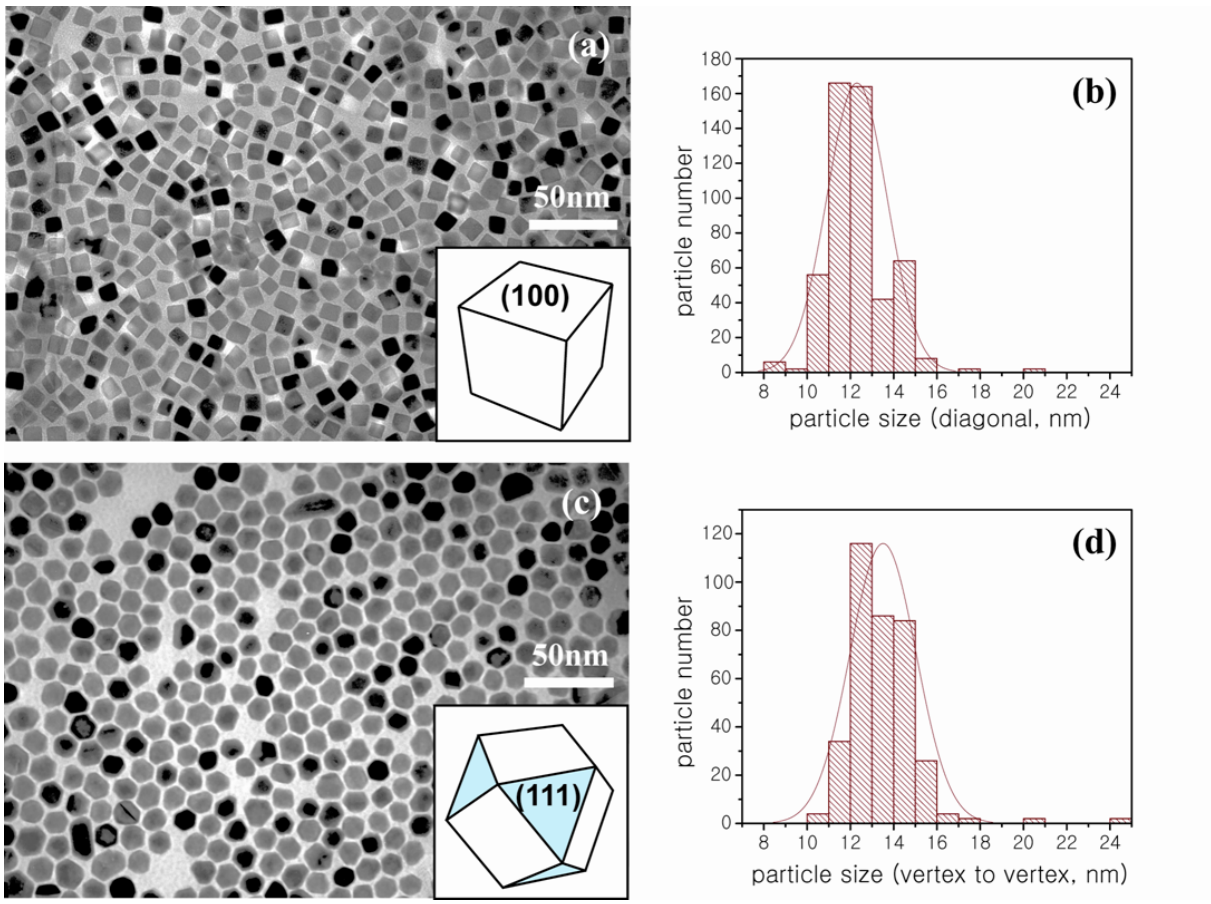

Figure 10.1. (a) TEM image and (b) size distribution of TTAB-stabilized cubic particles. (The average size: 12.3 ± 1.4 nm, 79% cubes, 3% triangles, and 18% irregular shapes). (c) TEM image and (d) size distribution of TTAB-stabilized cuboctahedral particles. (The average size: 13.5 ± 1.5 nm, 90% cuboctahedra and 10% irregular shapes).

10.3. Results and Discussion

The Pt nanoparticles used in the present reaction studies are shown in Figure 10.1. The synthesis of these particles has been reported in a previous study.[9] The cubic particles have a size of 12.3 ± 1.4 nm (diagonal, 79% cubes, 3% triangles, and 18% irregular shapes) and consist of only Pt(100), whereas the cuboctahedral particles have a

size of 13.5 ± 1.5 nm (vertex to vertex, 90% cuboctahedra and 10% irregular shapes) and consist of both Pt(100) and Pt(111). Unlike cubic nanoparticles, the (111) surface in cuboctahedral nanoparticles would promote the production of cyclohexene. Monolayers of these nanoparticles were prepared on Si wafers for reaction studies by the Langmuir-Blodgett technique, as illustrated in detail in the supporting information of this article. Figure 10.2 shows a comparison between kinetic data of TTAB-stabilized cubic and cuboctahedral Pt nanoparticles in the temperature range of 310–400 K for 10 Torr C_6H_6, 100 Torr H_2, and 650 Torr Ar. It is noted that only cyclohexane formed on cubic nanoparticles, as opposed to both cyclohexane and cyclohexene on cuboctahedral nanoparticles. The calculation of the turnover rates shown in Figure 10.2(a) was based on the nanoparticle coverage of the Si wafer surface determined from SEM images, assuming that each Pt atom at the monolayer surface is an active site. The error bars indicate the image-to-image scatter in the measurements. Figure 10.2(b) shows Arrhenius plots of cyclohexane and cyclohexene turnover rates in the 310–400 K temperature range. The deviation of both cyclohexane and cyclohexene turnover rates from the Arrhenius relationship above ~340 and ~360 K, respectively, is attributed to changes in the Pt surface coverage caused by gas-phase adsorbed species, as discussed previously.[10] The apparent activation energies for cyclohexane and cyclohexene formation on cuboctahedral nanoparticles in the temperature ranges of 310–340 and 330–360 K are respectively equal to 8.3 ± 0.2 and 12.2 ± 0.4 kcal/mol. For cubic nanoparticles, the apparent activation energy for cyclohexane formation in the temperature range of 330–370 K is equal to 10.9 ± 0.4 kcal/mol. The SEM images (Figure 10.3) obtained before and after reaction at 400 K reveal that nanoparticle aggregation did not occur under the

present reaction conditions. In addition, transmission electron microscopy (TEM) did not reveal any discernible changes in nanoparticle shape after reaction. Figure 10.4 shows representative TEM images of cubic and cuboctahedral Pt nanoparticles obtained after reaction at 400 K which confirm that the observed chemistry was a result of differences in the original nanoparticle shape, not a consequence of nanoparticle shape changes induced during the reaction.

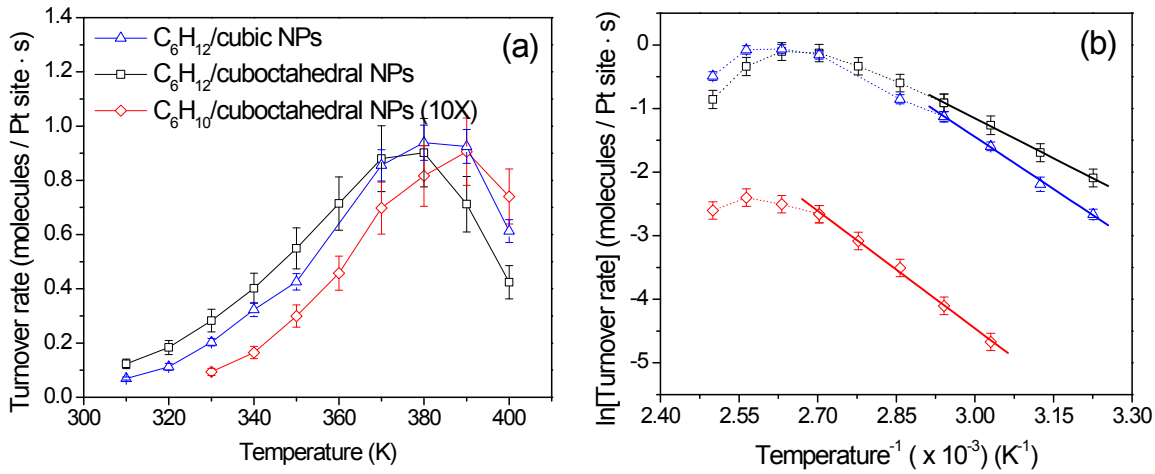

Figure 10.2. (a) Turnover rates of cyclohexane and cyclohexene formation on TTAB-stabilized cubic and octahedral Pt nanoparticles (NPs) for 10 Torr C_6H_6, 100 Torr H_2, and 650 Torr Ar, and (b) corresponding Arrhenius plots. The deviation from the Arrhenius behavior above 340 K for cyclohexane and above 370 K for cyclohexene formation is attributed to changes in the nanoparticle surface coverage caused by gas-phase adsorbates. The dotted lines are drawn as visual aides.

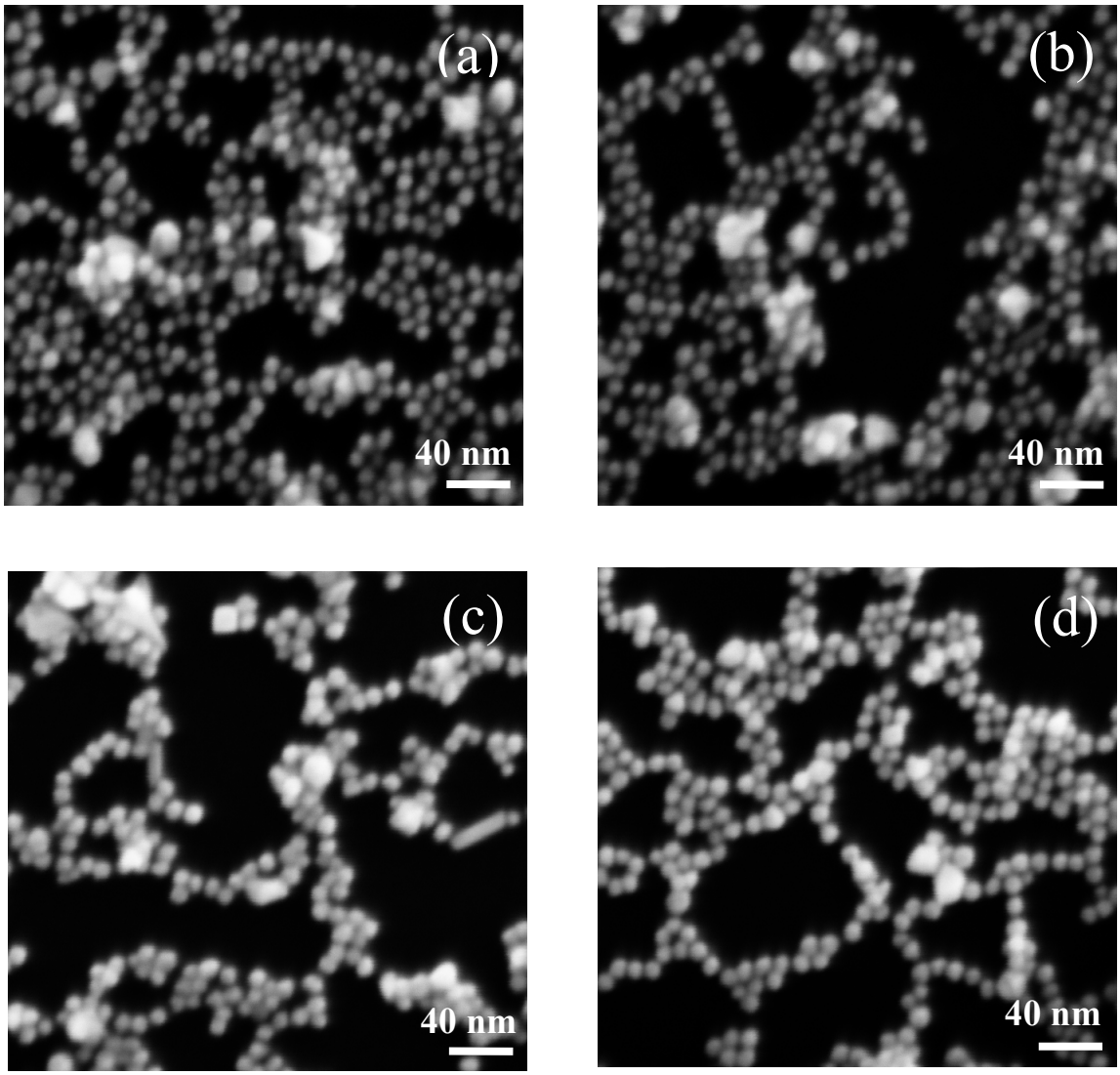

Figure 10.3. SEM images of TTAB-stabilized cube nanoparticles (a) before and (b) after reaction at 400 K and TTAB-stabilized cuboctahedra nanoparticles (c) before and (d) after reaction at 400 K for 10 Torr C_6H_6, 100 Torr H_2, and 650 Torr Ar.

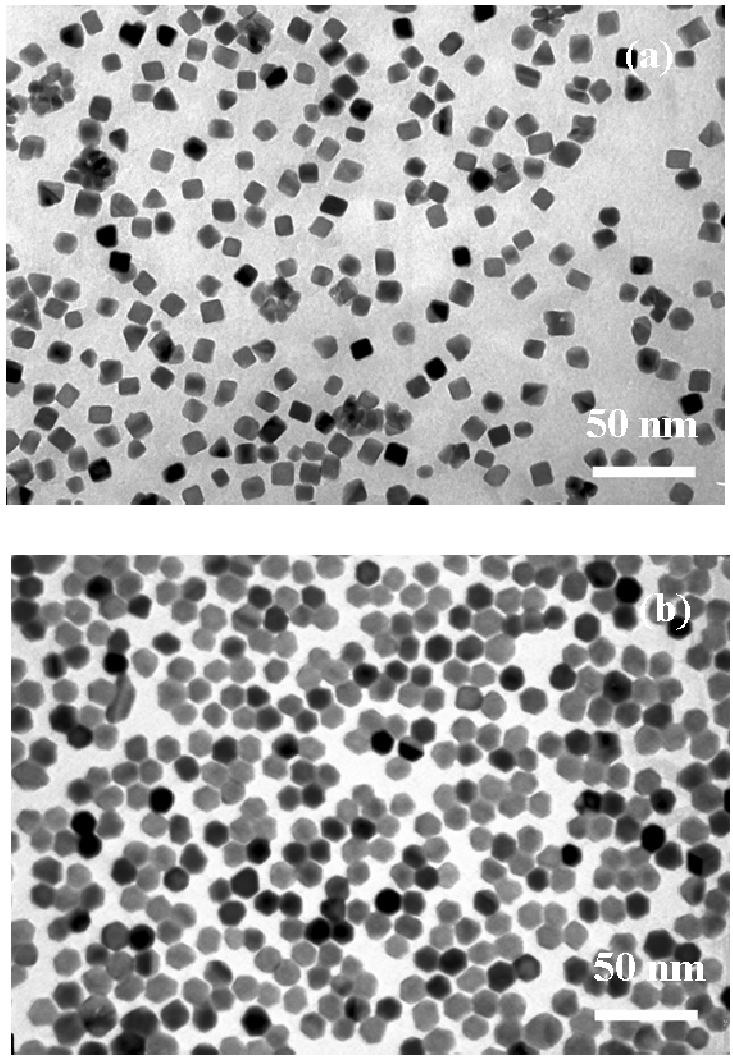

Figure 10.4. TEM images of TTAB-stabilized (a) cubic and (b) cuboctahedral Pt nanoparticles after reaction at 400 K for 10 Torr C_6H_6, 100 Torr H_2, and 650 Torr Ar.

Previous studies[5,6] of benzene hydrogenation on single-crystal Pt surfaces have demonstrated that, unlike cyclohexene, low-temperature production of cyclohexane is not structure sensitive, as evidenced by the formation of both cyclohexene and cyclohexane on Pt(111) and only cyclohexane on Pt(100). The formation of these products on TTAB-stabilized nanoparticles is in agreement with the former findings.

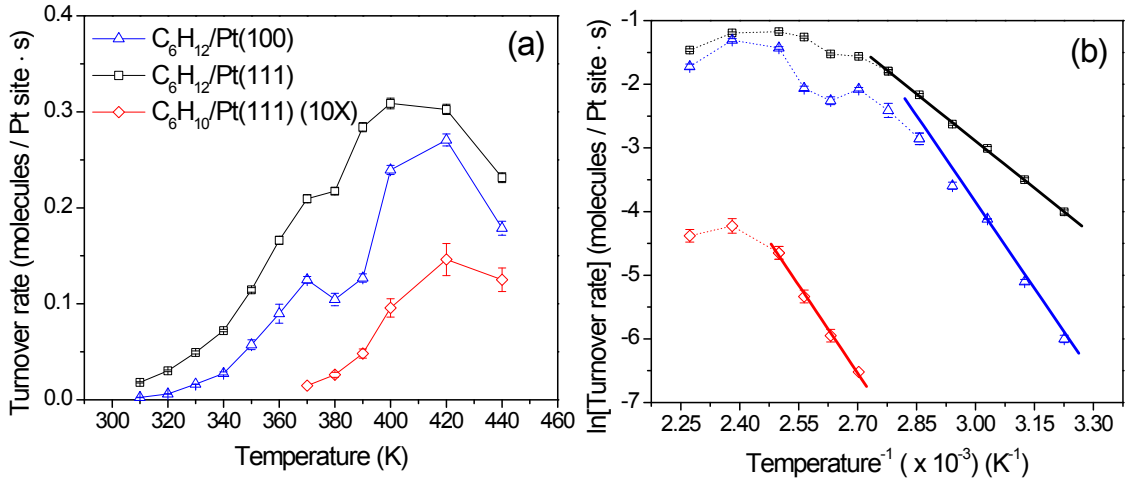

Figure 10.5. (a) Turnover rates of cyclohexane (C_6H_{12}) and cyclohexene (C_6H_{10}) formation on Pt(100) and Pt(111) single-crystals for 10 Torr C_6H_6, 100 Torr H_2, and 650 Torr Ar and (b) corresponding Arrhenius plots. The dotted lines are drawn as visual aides.

		TTAB-stabilized Pt NPs		Pt single crystals[5,6]	
		cube	cuboctahedra	Pt(100)	Pt(111)
Activation Energy[a]	C_6H_{12}	10.9 ± 0.4	8.3 ± 0.2	15.7 ± 0.1	9.8 ± 0.1
	C_6H_{10}	na	12.2 ± 0.4	na	18.3 ± 0.8
Maximum turnover rates[b]	C_6H_{12}	0.93 ± 0.06	0.90 ± 0.12	0.27 ± 0.01	0.30 ± 0.01
	C_6H_{10}	na	0.08 ± 0.01	na	0.015 ± 0.002

a. measured in the temperature range of 310-400K.

b. measured at 380K for Pt NPs, and measured at 420K for Pt single crystals.

Table 10.1. Apparent activation energies (in kcal · mol^{-1}) and maximum turnover rates (in molecules · Pt $site^{-1}$ · s^{-1}) for TTAB-stabilized Pt nanoparticles (NPs) and Pt single-crystals in the temperature range of 310–340 K.

Table 10.1 shows the effect of the nanoparticle shape on the apparent activation energy and maximum turnover rate of cyclohexane and cyclohexene. For comparison, similar data for single-crystal Pt(100) and Pt(111) surfaces reported previously[5,6] are also included in Table 10.1. The apparent activation energy for cyclohexane formation on the cubic nanoparticles comprising only {100} facets is less than that of Pt(100). Similarly the apparent activation energies for cyclohexane and cyclohexene formation on the cuboctahedral nanoparticles are less than that of Pt(111). A three-fold increase in the turnover rate was also observed for benzene hydrogenation on nanoparticles compared to single-crystal Pt surfaces. This can be seen by comparing the kinetic data and Arrhenius

plots for benzene hydrogenation on single-crystal Pt(100) and Pt(111) surfaces shown in Figure 10.5. The lower apparent activation energies and higher turnover rates obtained with nanoparticles than single crystals may be attributed to an increase in corner and edge sites. The ratio of corner and edge atoms to terrace atoms increases with the decrease of crystal domains.[14-17] Edge and corner atoms exhibit open coordination sites that may result in significantly different bond enthalpies, desorption energies, and adsorption geometries compared to adsorption on terrace sites. Another possible explanation is the change in the electronic structure with decreasing size. Electronic changes due to Pd nanoparticle size changes have been reported for formic acid oxidation.[18] The smallest particles were found to be the most active, which was attributed to an enhancement of the d-band hybridization that weakened the bond strength of the COOH intermediate with the surface of the Pd nanoparticles. Compared to single crystals, a three-fold increase in the turnover rate for benzene hydrogenation was also observed in the presence of nanoparticles. This increase is also attributed to an increase of the ratio of corner and edge atoms to terrace atoms or a change in electronic structure with decreasing crystal size. Benzene hydrogenation may be augmented at edge and corner sites, thus increasing the catalytic activity of the nanoparticles.

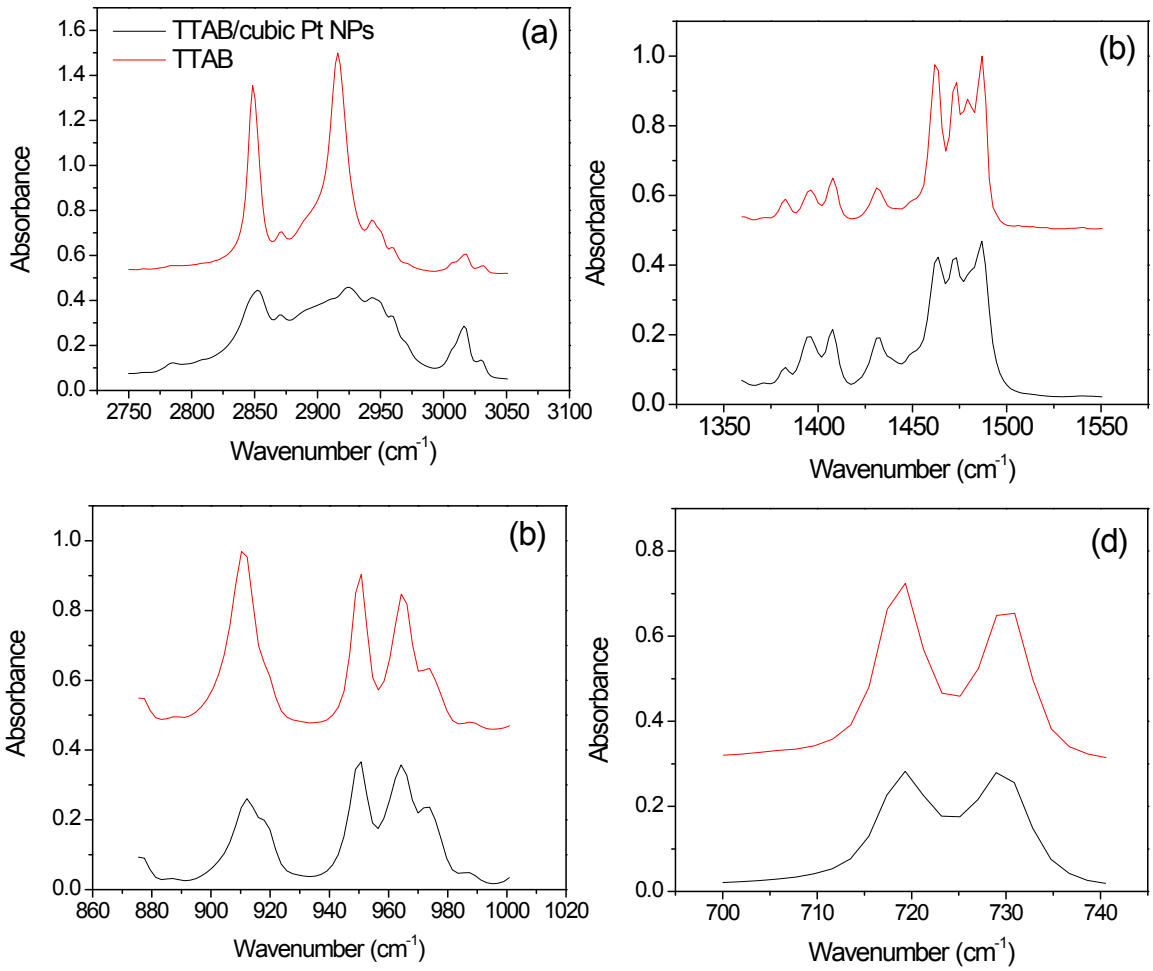

Figure 10.6. IR spectra of pure TTAB and TTAB-stabilized cube Pt nanoparticles (NPs) in the (a) C-H stretching, (b) C-H bending, (c) C-N+ stretching, and (d) C-H rocking regions. Mode assignments for each range (based on information from the literature) are given in Table 10.2.

IR mode stretches (cm^{-1})		IR assignment
TTAB	TTAB/Pt NPs	
3032	3032	$\nu_{as}(CH_3\text{-}N^+)$
3017	3016	$\nu_{as}(CH_3\text{-}N^+)$
2944		$\nu_{as}(CH_3)$
	2945	CH_3, $\nu(C\text{-}H_{distal})$
	2924	CH_3, $\nu(C\text{-}H_{distal})$
2915		$\nu_{as}(CH_2)$, $\nu_s(CH_3\text{-}N^+)$
	2896	CH_2, $\nu(C\text{-}H_{distal})$
2848	2852	$\nu_s(CH_3)$, $\nu_s(CH_2)$
	2783	$\nu(C\text{-}H_{proximal})$
1486	1488	$\delta_{as}(CH_3\text{-}N^+)$
1479	1480	$\delta_{as}(CH_3)$
1473	1474	} $\delta(CH_2)$, scissor doublet
1462	1464	
1432	1432	$\delta(CH_3\text{-}N^+)$
1407	1408	$\delta(CH_3\text{-}N^+)$
1395	1395	$\delta(CH_3\text{-}N^+)$
1384	1382	$\delta_s(CH_3)$
974	974	$\nu(C\text{-}N^+)$
965	964	$\nu(C\text{-}N^+)$
951	952	$\nu(C\text{-}N^+)$
919	919	$\nu(C\text{-}N^+)$
910	912	$\nu(C\text{-}N^+)$
730	730	$\gamma(CH_2)$
719	719	$\gamma(CH_2)$

Table 10.2. Mode assignments in IR spectra of pure TTAB and TTAB-stabilized cube Pt nanoparticles (NPs).[1-5]

IR spectra of pure TTAB and TTAB-stabilized cubic Pt nanoparticles revealed insignificant differences in the C-H rocking (700–740 cm^{-1}), C-H bending (1350–1550 cm^{-1}), and C-N^+ stretching (880–1000 cm^{-1}) regions. These spectra windows along with their peak assignments can be found in the supporting information (Figure 10.6 and Table 10.2). However, the IR spectra in the C-H stretching region shown in Figure 10.6 show significant differences in the spectra of pure TTAB and TTAB-stabilized nanoparticles. The IR spectrum of the TTAB-stabilized nanoparticles contains an additional mode at 2783 cm^{-1}, which is attributed to direct C-H···M (M = metal) interactions between Pt atoms on the nanoparticle surfaces and proximal C-H bonds [ν(C-$H_{proximal}$)][19] and is usually referred to as "softened" mode. This mode generally indicates a direct interaction of the alkyl chain with the metal surface.[19] The assignment of each peak in the spectra of Figure 10.6 can also be found in the supporting information (Table 10.2). Since the IR spectra of pure TTAB and TTAB-stabilized cubic Pt nanoparticles differ only in the C-H stretching region, it may be presumed that TTAB does not interact with the Pt surface through the trimethylammonium head group, but rather through the alkyl chain as indicated by the "softened" C-H mode in a dry condition. The different interaction of alkylammonium ions on Pt surfaces compared to Au surfaces[20] may be related to the catalytic activity of Pt toward alkanes, which allows Pt to more readily dehydrogenate alkanes than Au.

10.4. Conclusions

In this investigation, nanoparticle surface effects on benzene hydrogenation were studied by comparing kinetic results for cubic and cuboctahedral Pt nanoparticles. It was

found that the capping agent (TTAB) interacts with the Pt atoms through the alkyl chain forming C-H···Pt weak bonds. Benzene hydrogenation studies demonstrated that both cyclohexene and cyclohexane formed on cuboctahedral nanoparticles and only cyclohexane on cubic nanoparticles, consistent with previous results for single-crystal Pt surfaces. The significantly lower apparent activation energies and higher turnover rates obtained with Pt nanoparticles than Pt single crystals may be attributed to an increase of the corner and edge sites on the nanoparticles available for catalysis or changes in the electronic structure of the nanoparticles compared to the Pt single crystals.

References

(1) Chotisuwan, S.; Wittayakun, J.; Gates, B. C. *Journal of Physical Chemistry B* **2006**, *110*, 12459-12469.

(2) Contreras, A. M.; Grunes, J.; Yan, X. M.; Liddle, A.; Somorjai, G. A. *Topics in Catalysis* **2006**, *39*, 123-129.

(3) Gomez, R.; Solla-Gullon, J.; Perez, J. M.; Aldaz, A. *Chemphyschem* **2005**, *6*, 2017-2021.

(4) Rioux, R. M.; Song, H.; Grass, M.; Habas, S.; Niesz, K.; Hoefelmeyer, J. D.; Yang, P.; Somorjai, G. A. *Topics in Catalysis* **2006**, *39*, 167-174.

(5) Bratlie, K. M.; Flores, L. D.; Somorjai, G. A. *Journal of Physical Chemistry B* **2006**, *110*, 10051-10057.

(6) Bratlie, K. M.; Kliewer, C. J.; Somorjai, G. A. *Journal of Physical Chemistry B* **2006**, *110*, 17925-17930.

(7) Bratlie, K. M.; Montano, M. O.; Flores, L. D.; Paajanen, M.; Somorjai, G. A. *Journal of the American Chemical Society* **2006**, *128*, 12810-12816.

(8) Li, Y.; El-Sayed, M. A. *Journal of Physical Chemistry B* **2001**, *105*, 8938-8943.

(9) Lee, H.; Habas, S. E.; Kweskin, S. J.; Butcher, D.; Somorjai, G. A.; Yang, P. *Angewandte Chemie-International Edition* **2006**, *45*, 7824-7828.

(10) Bratlie, K. M.; Flores, L. D.; Somorjai, G. A. *Surface Science* **2005**, *599*, 93-106.

(11) Kung, K. Y.; Chen, P.; Wei, F.; Rupprechter, G.; Shen, Y. R.; Somorjai, G. A. *Review of Scientific Instruments* **2001**, *72*, 1806-1809.

(12) Yang, M.; Tang, D. C.; Somorjai, G. A. *Review of Scientific Instruments* **2003**, *74*, 4554-4557.

(13) Borodko, Y.; Habas, S. E.; Koebel, M.; Yang, P.; Frei, H.; Somorjai, G. A. *Journal of Physical Chemistry B* **2006**, *110*, 23052-23059.

(14) Burton, J. J. *Catalysis Reviews-Science and Engineering* **1974**, *9*, 209-222.

(15) Greegor, R. B.; Lytle, F. W. *Journal of Catalysis* **1980**, *63*, 476-486.

(16) Ladas, S. *Surface Science* **1986**, *175*, L681-L686.

(17) Van Hardeveld, R.; Hartog, F. *Surface Science* **1969**, *15*, 189.

(18) Zhou, W. P.; Lewera, A.; Larsen, R.; Masel, R. I.; Bagus, P. S.; Wieckowski, A. *Journal of Physical Chemistry B* **2006**, *110*, 13393-13398.

(19) Manner, W. L.; Bishop, A. R.; Girolami, G. S.; Nuzzo, R. G. *Journal of Physical Chemistry B* **1998**, *102*, 8816-8824.

(20) Nikoobakht, B.; El-Sayed, M. A. *Langmuir* **2001**, *17*, 6368-6374.

Chapter 11

Regeneration of Platinum Nanoparticles during Benzene Hydrogenation: A Kinetic and Sum Frequency Generation Spectroscopic Study

The regeneration of the catalytic activity of a monolayer consisting of cubic Pt nanoparticles and tetradecyltrimethylammonium bromide (TTAB) stabilizing agent for benzene hydrogenation was investigated using gas chromatography (GC) and surface-specific sum frequency generation (SFG) vibrational spectroscopy performed in total internal reflection (TIR) geometry. Kinetic studies demonstrated reproducible turnover rates after multiple oxidation/reduction cycles of the monolayer. Activation energies before and after oxidation were found to be 9.2 ± 0.1 and 9.5 ± 0.2 kcal/mol, respectively. TIR-SFG spectra revealed negligibly small changes in the TTAB layer before and after reduction, during benzene hydrogenation, and after oxidation. The obtained GC and TIR-SFG results suggest that combustion of benzene during the oxidation cycle removes the hydrocarbon species adsorbed on the nanoparticle surfaces, hence regenerating the catalytic activity of the nanoparticle monolayer.

11.1. Introduction

Since volatile organic compounds, such as benzene, have long been a major source of air pollution, catalytic reactions leading to their removal are of paramount

importance in both fuel reform and environment protection.[1-6] Regenerating catalysts that remove aromatics is an important aspect in reducing costs and energy consumption. Benzene is the simplest aromatic hydrocarbon and a volatile organic compound. Therefore, it is an ideal candidate for catalysis studies on Pt nanoparticle monolayers. Benzene hydrogenation has been extensively studied on Pt single crystals,[7-9] and recently on monolayers of Pt nanoparticles stabilized by a polymer binding agent.[10]

Low-coordination surface atoms, such as those at step and kink sites, are more reactive than terrace atoms on single crystals.[11-13] Edge and corner sites, which are mostly absent in single crystals, play a significant role in adsorption and reaction on nanoparticles. It has been reported[13] that the barrier for CO dissociation on the stepped Rh(211) surface is 28 kcal/mol less than that on the Rh(111) surface and, as a result, the dissociation is 9 orders of magnitude faster on Rh(211) than on Rh(111). However, single crystals are not representative of industrially relevant heterogeneous catalysts, which typically involve small metal particles (1-10 nm) on high-surface-area oxides. Therefore, fundamental studies of catalytic reactions and intermediates forming on nanoparticle surface assemblies are of high scientific and industrial importance.

Sum frequency generation (SFG) vibrational spectroscopy and gas chromatography (GC) were used in this study to investigate benzene hydrogenation at high temperatures (310–340 K). Media exhibiting centrosymmetry and isotropic gases do not appear in the SFG spectrum under the electric dipole approximation. Since bulk Pt has a center of inversion, its contribution to the SFG signal is negligible. However, a surface-specific SFG signal can be obtained because the symmetry at the surface of the Pt crystal is broken. Since the SFG signal is produced solely from the adsorbates, SFG is a

more sensitive tool to study interfaces than infrared absorption and Raman spectroscopies. Electron spectroscopy typically cannot be used under the ambient pressure conditions needed for catalytic reactions. SFG vibrational spectroscopy has been mainly used to study surface reactions on flat samples due to the relative ease of collection and analysis. However, in recent investigations SFG has been used to study Au nanoparticles,[14,15] Pd nanoparticles deposited on alumina,[16] and solutions containing submicrometer particles.[17]

The objective of the present study was to examine the regeneration of the catalytic activity of monolayers consisting of cubic Pt nanoparticles stabilized by a very thin layer of tetradecyltrimethylammonium bromide (TTAB) after benzene (C_6H_6) hydrogenation at 10 Torr C_6H_6, 100 Torr H_2, and 650 Torr Ar in the temperature range of 310–340 K. The effects of oxidation/reduction cycles on the kinetics of benzene hydrogenation were investigated in the light of GC measurements. SFG vibrational spectroscopy demonstrated that the effects of the oxidation/reduction and benzene hydrogenation reaction conditions on the TTAB capping agent were negligibly small.

11.2. Experimental Procedures

11.2.1. Synthesis and Assembly of Platinum Nanoparticles.

Nanoparticles stabilized with TTAB were prepared by mixing aqueous solutions of K_2PtCl_4 (99.9% pure, Alfa Aesar) and TTAB (99% pure, Aldrich) in a 20 mL vial at room temperature.[18] The mixture was heated at 323 K for ~5 min until the solution became clear. After the addition of ice-cold $NaBH_4$ (98% pure, Strem Chemicals), the vial was capped with a rubber septum and the H_2 gas pressure inside the vial was released through a needle in the septum for 10 min. After the removal of the needle, the solution

was kept at 323 K for 6 h. Cubic Pt(100) nanoparticles (79% cubes, 3% triangles, and 18% irregular shapes with an average size of 12.3 ± 1.4 nm (face diagonal)) were prepared from a solution consisting of 100 mM TTAB and 1 mM K_2PtCl_4 reduced with 30 mM $NaBH_4$. The nanoparticles were centrifuged at 3 krpm for 30 min, the precipitates were discarded, and the solution was centrifuged again at 14 krpm for 30 min. Then, the supernatant was discarded, the precipitates were redispersed in deionized (DI) water by sonication, the solution was again centrifuged at 14 krpm for 30 min, and the precipitates were collected and redispersed in DI water. The washed nanoparticles were used for transmission electron microscope (TEM) analysis and reaction studies. The nanoparticle shape and size distributions were studied in a TEM (JEOL 200CX) operated at 200 kV. Details of the Pt nanoparticles used in the present reaction studies and their synthesis can be found elsewhere.[10,18]

Nanoparticles were assembled and deposited on a Si wafer (for kinetic measurements) or a fused quartz prism (for spectroscopic measurements) by the Langmuir-Blodgett (LB) technique. Colloidal Pt solutions were dispersed on the surface of a DI water (18 MΩ·cm) sub-phase on a LB trough (type 611, NIMA Technology) at room temperature. The surface pressure was monitored with a Wilhelmy plate and adjusted to zero before spreading the nanoparticles. The resulting surface layer was compressed by a mobile barrier at a rate of 20 cm^2/min. The nanoparticles were deposited by lifting up the silicon substrate (immersed in water subphase before the nanoparticles were dispersed) when the surface pressure reached ~15 mN/m. The surface coverage of the silicon wafer by the nanoparticles was observed in a scanning electron microscope (SEM) (Ultra-55, Zeiss Gemini).

11.2.2. Reaction-Spectroscopy Cell

A special cell was used for *in-situ* SFG spectroscopy in total internal reflection (TIR) geometry under batch gas circulation.[19] A Si wafer or a fused quartz prism coated with a nanoparticle monolayer was pressed against a rubber O-ring by tightening a teflon block with two set screws. The temperature at the wafer or prism surface was measured with a thermocouple placed directly onto the sample. Heating was applied at the top of the wafer by a Kapton resistive element (Omega Engineering) and to the prism by wrapping the reactor cell with a heat tape and applying a variable voltage (McMaster-Carr). Temperature variations across the 20 × 20 mm^2 wafer or prism area were found to be insignificant. The reaction cell was connected to a 0.3175-cm-diameter stainless steel tubing gas manifold. Benzene (≥99.0 wt%, EM Science) was purified by several freeze-pump-thaw cycles before being introduced into the reaction cell. Prior to each experiment, benzene was checked for impurities using GC. Impurity levels were found to be less than 0.5 wt% and consisted of mostly light alkanes below C_6. A vacuum pressure of <1 mTorr was maintained in the reaction cell by mechanical and turbomolecular pumps.

The reaction cell is equipped with a recirculation loop that includes a diaphragm pump and a septum for GC analysis. The reactant and product gases were constantly mixed by the recirculation pump, while kinetic data were acquired periodically by sampling the reaction mixture and measuring the relative gas phase composition. Kinetic measurements were obtained with GC system (HP 6890) using flame ionization detection and a 0.1% AT-1000 on Graphpac GC 80/100 packed column of 180 m length and

0.3175 cm outside diameter (Alltech). Helium was used as carrier gas and the oven temperature was maintained at 413 K. The reactant pressure was 10 Torr C_6H_6, 100 Torr H_2, and 650 Torr Ar. Before collecting kinetic data, the nanoparticles were treated in 100 Torr H_2 for 1 h to optimize cyclohexane formation at 310 K.

11.2.3. Sum Frequency Generation Vibrational Spectroscopy

SFG measurements were performed using a mode-locked Nd:YAG laser (1064 nm fundamental wavelength, 20 ps pulses, 20 Hz repetition rate) to generate a tunable infrared (IR) beam (1800–4000 cm^{-1}) and a 532 nm second-harmonic visible (VIS) beam. The IR and VIS beams, both of energy equal to 200 μJ, were spatially and temporally overlapped on the fused quartz surface with incident angles of 55º and 60º with respect to the surface normal. Spectra were taken using *ssp* or *ppp* polarization combinations. The generated SFG beam was passed through a monochromator, and the signal intensity was detected with a photomultiplier tube and a gated integrator while the IR beam was scanned over the frequency range of interest. The sum frequency output was normalized by the intensity of the incident IR beam at the surface. This is necessary because gas molecules absorb some of the incoming radiation. Using a previously reported procedure,[20,21] the SFG spectra were curve fit according to the following equation:

$$I_{SFG} \propto \left| \chi_{NR}^{(2)} \, e^{i\phi_{NR}} + \sum_q \frac{A_q}{\omega_{IR} - \omega_q + i\Gamma_q} e^{i\gamma_q} \right|^2 \qquad (11.1)$$

where $\chi_{NR}^{(2)}$ is the nonresonant nonlinear susceptibility, ϕ_{NR} is the phase associated with the nonresonant background, A_q is the strength of the q^{th} vibrational mode, ω_{IR} is the frequency of the incident IR laser beam, ω_q is the frequency of the q^{th} vibrational mode,

Γ_q is the natural line width of the q^{th} vibrational transition, and γ_q is the phase associated with the q^{th} vibrational transition. Detailed descriptions of the SFG theory can be found elsewhere.[22-27]

11.3. Results and Discussion

11.3.1. Turnover Rates and Activation Energies for Cyclohexane Formation on Clean Platinum Nanoparticle Monolayers

Figure 11.1 shows turnover rates (expressed in units of molecules per Pt site per second) for a monolayer consisting of TTAB-stabilized cubic Pt nanoparticles exposed to 10 Torr C_6H_6, 100 Torr H_2, and 650 Torr Ar obtained at 310 and 340 K after cleaning. The calculation of the turnover rates was based on the surface coverage of the Si wafer by nanoparticles deduced from SEM images, assuming that each Pt atom at the monolayer surface is an active adsorption site. The error bars indicate the image-to-image scatter in the measurements. The nanoparticle monolayer was initially cleaned by flowing 100 Torr H_2 and 660 Torr Ar at 393 K for 1 h. All subsequent cleaning cycles involved monolayer exposure first to 100 Torr O_2 and 660 Torr Ar at 393 K for 20 min and then to 100 Torr H_2 and 660 Torr Ar at 393 K for 20 min. The turnover rate at 310 K was found equal to 0.08 ± 0.01 molecules $\cdot$ Pt site^{-1} $\cdot$ s^{-1}, which is very close to the value obtained after the first cleaning cycle. The turnover rate at 340 K was equal to 0.45 ± 0.07 molecules $\cdot$ Pt site^{-1} $\cdot$ s^{-1}, and differences after each oxidation/reduction cycle were within the experimental error. Hence, the increase of the temperature from 310 to 340 K resulted in a fivefold increase of the turnover rate and the effect of the cleaning process was secondary.

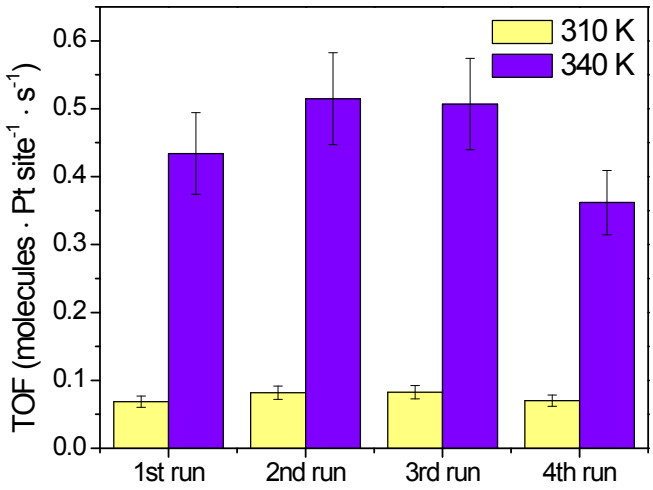

Figure 11.1. Turnover rates of cyclohexane formation on a monolayer consisting of TTAB-stabilized cubic Pt nanoparticles under reaction conditions of 10 Torr C_6H_6, 100 Torr H_2, and 650 Torr Ar obtained at 310 and 340 K after cleaning. In the first cleaning cycle the monolayer was treated in 100 Torr H_2 and 660 Torr Ar at 393 K for 1 h, whereas in all subsequent cleaning cycles the monolayer was treated first in 100 Torr O_2 and 660 Torr Ar at 393 K for 20 min and then in 100 Torr H_2 and 660 Torr Ar at 393 K for 20 min.

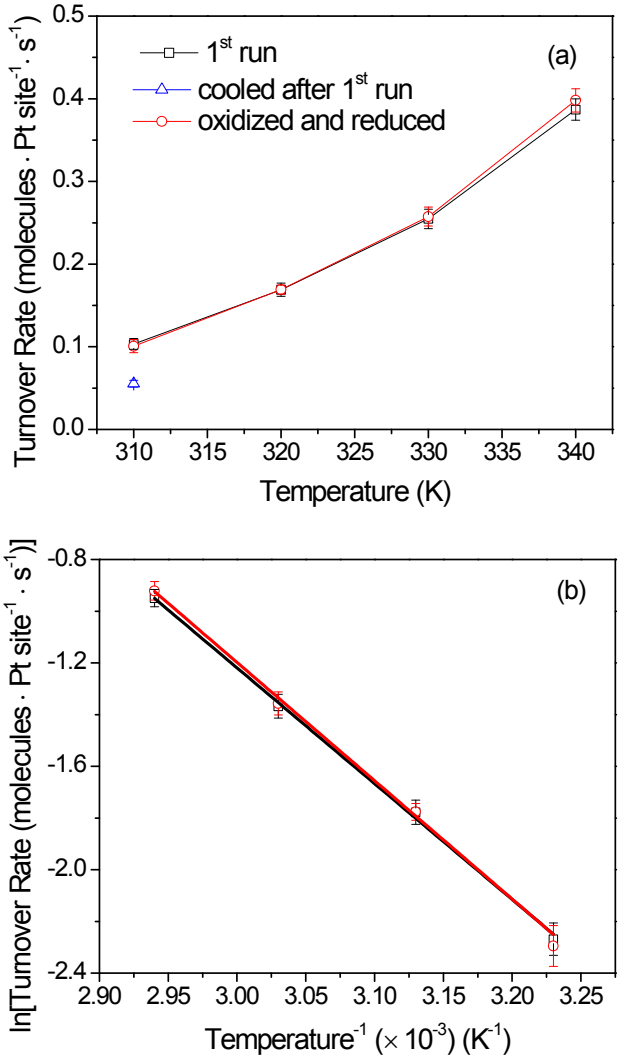

Figure 11.2. (a) Turnover rates of cyclohexane formation on a monolayer consisting of TTAB-stabilized cubic Pt nanoparticles under reaction conditions of 10 Torr C_6H_6, 100 Torr H_2, and 650 Torr Ar, and (b) corresponding Arrhenius plots. Turnover rates were obtained after cleaning the monolayer in 100 Torr H_2 and 660 Torr Ar at 393 K for 1 h (□), after cooling from 340 K under the reaction conditions (Δ), and after cleaning sequentially in 100 Torr O_2 and 660 Torr Ar at 393 K for 20 min and 100 Torr H_2 and 660 Torr Ar at 393 K for 20 min (○). All turnover rates were obtained with the same monolayer.

Figure 11.2 shows kinetic data for reaction conditions of 10 Torr C_6H_6, 100 Torr H_2, and 650 Torr Ar in the temperature range of 310–340 K. Estimated turnover rates of cyclohexane formation at different temperatures and corresponding Arrhenius plots are shown in Figures 11.2(a) and 2(b), respectively. Prior to benzene hydrogenation, the monolayer was cleaned by flowing 100 Torr H_2 and 660 Torr Ar at 393 K for 1 h. After benzene hydrogenation at 340 K, the sample was first cooled down to 310 K and then exposed again to the same reaction conditions. The turnover rate obtained at 310 K was approximately one-half of that obtained at the same temperature immediately after the first cleaning. However, subsequent cleaning of the monolayer by flowing first 100 Torr O_2 and 660 Torr Ar at 393 K for 20 min and then 100 Torr H_2 and 660 Torr Ar at 393 K for 20 min regenerated the catalytic activity of the monolayer over the entire 310–340 K temperature range. The activation energies obtained after the initial cleaning and after the oxidation/reduction treatment were found equal to 9.2 ± 0.1 and 9.5 ± 0.2 kcal/mol, respectively (Figure 11.2(b)). Previous studies[10] have shown that C_6H_6 hydrogenation on Pt nanoparticle monolayers exposed to 100 Torr H_2 and 660 Torr Ar at 393 K for 1 h does not change the shape of the nanoparticles. Since the turnover rates after the oxidation/reduction treatment were comparable to the initial rates, it may be inferred that the nanoparticle shape was not affected by the cleaning procedure used to regenerate the catalytic activity of the monolayer.

11.3.2. SFG Vibrational Spectroscopy of Platinum Nanoparticle Monolayers

Figure 11.3 shows IR and SFG (*ssp* and *ppp* polarization combinations) spectra of a monolayer consisting of TTAB-stabilized cubic Pt nanoparticles. Corresponding peak assignments are given in Table 11.1. Significant differences between the *ssp* and *ppp*

SFG spectra exist for the symmetric CH_2 stretching [CH_2(s)], asymmetric CH_2 stretching [CH_2(a)], and asymmetric CH_3 stretching [CH_3(a)] modes. The appearance of the CH_2(s) and CH_2(a) modes in the SFG spectra are a clear indication of gauche conformational defects of the TTAB ligand. This arises from a local centrosymmetry of the alkane chain in an all-trans conformation. The CH_2 transitions will effectively cancel with one another due to local inversion symmetry.[28,29] Gauche defects in the alkyl chain result in an SFG signal of these modes.[28-31] The CH_2 modes are typically less than 10% of the CH_3 modes for well-ordered self-assembled monolayers on planar Au, in which the alkyl chain is predominantly in an all-trans conformation.[28,30] These gauche defects may prevent TTAB from adsorbing to all possible sites on the Pt nanoparticles, leaving sites available for catalysis.

IR	SFG ssp	SFG ppp	assignment
3032			$\nu_{as}(CH_3\text{-}N^+)$
3016			$\nu_{as}(CH_3\text{-}N^+)$
2945	2955		CH_3, $\nu(C\text{-}H_{distal})$
2924	2930		CH_3, $\nu(C\text{-}H_{distal})$
2896	2900	2905	CH_2, $\nu(C\text{-}H_{distal})$
2852	2870	2870	$\nu_s(CH_2)$
2852	2845	2850	$\nu_s(CH_3)$

Table 11.1. Mode assignments in IR[32-35] and SFG spectra of a monolayer consisting of TTAB-stabilized cubic Pt nanoparticles.

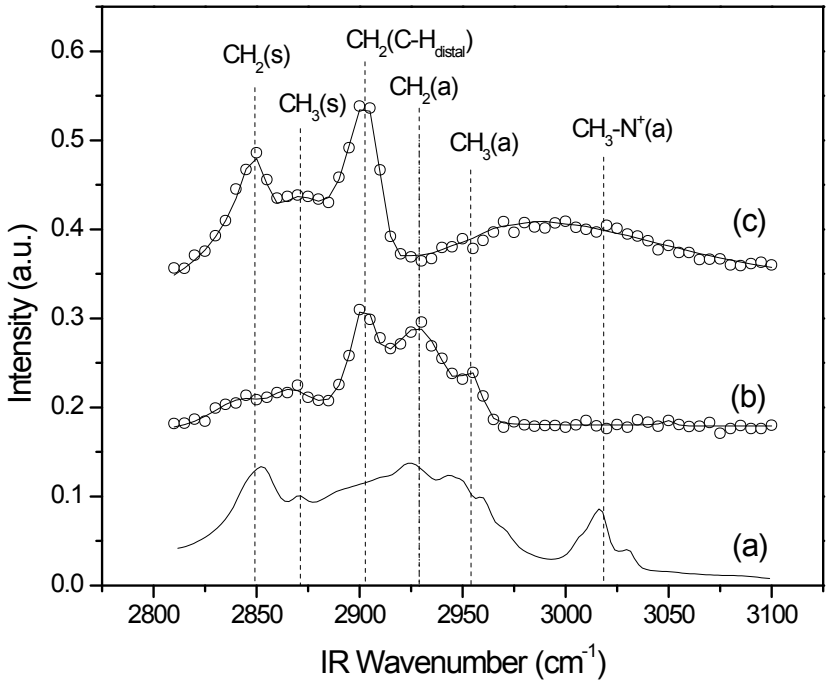

Figure 11.3. Spectra of a monolayer consisting of TTAB-stabilized cubic Pt nanoparticles obtained with (a) IR spectroscopy[10] and SFG spectroscopy in (b) *ssp* and (c) *ppp* polarizations.

Figure 11.4 shows SFG (*ppp* polarization combination) spectra of the TTAB stabilizing agent obtained before and after cleaning in 100 Torr H_2 and 660 Torr Ar at 393 K for 1 h, during C_6H_6 hydrogenation, and after cleaning in 100 Torr O_2 and 660 Torr Ar at 393 K for 20 min. The very similar spectral signatures observed in all four treatments indicate that chemical and molecular orientation changes in the stabilizing agent did not occur under any of these conditions. The SFG spectra shown in Figure 11.3 and the turnover rates shown in Figures 11.1 and 2 demonstrate that monolayers

consisting of TTAB-stabilized cubic Pt nanoparticles remain intact after several reactions and cleaning cycles.

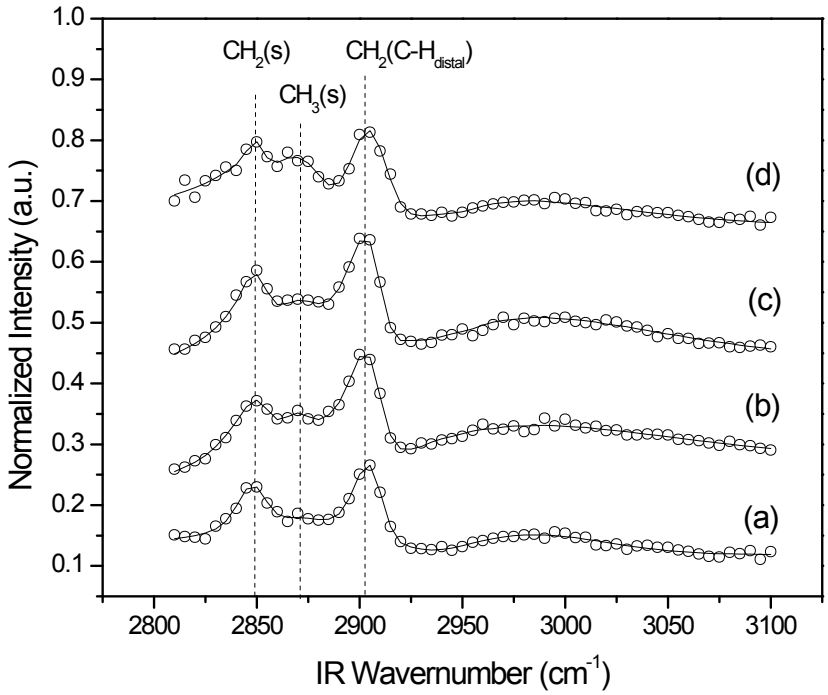

Figure 11.4. SFG spectra (*ppp* polarization) of the TTAB-stabilizing agent obtained (a) before and (b) after cleaning by flowing 100 Torr H_2 and 660 Torr Ar at 393 K for 1 h, (c) during C_6H_6 hydrogenation (10 Torr C_6H_6, 100 Torr H_2, and 650 Torr Ar at 300 K), and (d) after cleaning by flowing 100 Torr O_2 and 660 Torr Ar at 393 K for 20 min. Discrete points represent experimental data, whereas solid lines are curve fits based on equation 11.1. A different sample was used to obtain each spectrum.

The deactivation of the Pt nanoparticles demonstrated by the results shown in Figure 11.2 after cooling from 340 K most likely results from hydrocarbons blocking

active sites. In the case of a high surface coverage, benzene has been shown to adsorb transiently in a weakly bound state.[36] In the presence of excess hydrogen this weakly bound benzene may be desorbed intact. The ignition temperature of benzene on Pt powders has been found to be 423 K,[37] implying that benzene may be removed by combustion after reaction. The reproducible turnover data obtained before and after the oxidation/reduction treatment of the Pt nanoparticle monolayer suggest that the developed cleaning procedure is effective in regenerating the catalytic activity of the cubic Pt nanoparticles. This is corroborated by the SFG spectra obtained before and after reduction, under conditions of benzene hydrogenation, and after oxidation. These results also indicate that the removal of the TTAB stabilizing agent may require more aggressive protocols that those used in this study.

11.4. Conclusions

The regeneration of the catalytic activity of cubic Pt nanoparticles (~12 nm in average size) was investigated by GC and SFG vibrational spectroscopy. Oxidation and reduction of the Pt nanoparticles after benzene hydrogenation was effective in reproducing turnover rates and activation energies with scatter within experimental errors. Surface-specific SFG vibrational spectroscopy performed in TIR geometry enabled probing of the TTAB-stabilizing agent on the Pt nanoparticles before and after reduction, during benzene hydrogenation, and after oxidation. The very small differences in the SFG spectra of different treatment conditions indicated that the stabilizing agent remained intact. The regeneration of the catalytic activity of the Pt nanoparticle monolayer is attributed to both weakly bound benzene adsorbed to the nanoparticle surface and the combustion of benzene in oxygen.

References

(1) Cooper, B. H.; Donnis, B. B. L. *Applied Catalysis A* **1996**, *137*, 203-223.

(2) Noordally, E.; Richmond, J. R.; Tahir, S. F. *Catalysis Today* **1993**, *17*, 359-366.

(3) Heck, R. M.; Farrauto, R. J. In *Catalytic Air Pollution Control: Commercial Technology*; International Thomson Publishing: New York, 1995, p 435.

(4) Spivey, J. *Industrial and Engineering Chemical Research* **1987**, *26*, 2165-2180.

(5) Golodets, G. I. In *Heterogeneous Catalytic Reactions Involving Molecular Oxygen*; Elsevier: New York, 1983, p 234.

(6) Volter, J.; Lietz, G.; Spindler, H.; Lieske, H. *Journal of Catalysis* **1987**, *104*, 375-380.

(7) Bratlie, K. M.; Flores, L. D.; Somorjai, G. A. *Journal of Physical Chemistry B* **2006**, *110*, 10051-10057.

(8) Bratlie, K. M.; Kliewer, C. J.; Somorjai, G. A. *Journal of Physical Chemistry B* **2006**, *110*, 17925-17930.

(9) Bratlie, K. M.; Montano, M. O.; Flores, L. D.; Paajanen, M.; Somorjai, G. A. *Journal of the American Chemical Society* **2006**, *128*, 12810-12816.

(10) Bratlie, K. M.; Lee, H.; Komvopoulos, K.; Yang, P.; Somorjai, G. A. *Nano Letters* **2007**, *7*, 3097-3101.

(11) Somorjai, G. A. *Introduction to Surface Science Chemistry and Catalysis*; Wiley: New York, 1994.

(12) Boudart, M. *Advances in Catalysis* **1969**, *20*, 153.

(13) Mavrikakis, M.; Baumer, M.; Freund, H.-J.; Norskov, J. K. *Catalysis Letters* **2002**, *81*, 153-156.

(14) Tourillon, G.; Dreesen, L.; Volcke, C.; Sartenaer, Y.; Thiry, P. A.; Peremans, A. *Nanotechnology* **2007**, *18*, 415301-415307.

(15) Bordenyuk, A. N.; Weeraman, C.; Yatamara, A.; Jayathilake, H. D.; Stiopkin, I.; Liu, Y.; Benderskii, A. V. *Journal of Physical Chemistry C* **2007**, *111*, 8925-8933.

(16) Dellwig, T.; Rupprechter, G.; Unterhalt, H.; Freund, H.-J. *Physical Review Letters* **2000**, *85*, 776-779.

(17) Roke, S.; Roeterdink, W. G.; Wijnhoven, J. E. G. J.; Petukhov, A. V.; Kleyn, A. W.; Bonn, M. *Physical Review Letters* **2003**, *91*, 258302-258306.

(18) Lee, H.; Habas, S. E.; Kweskin, S. J.; Butcher, D.; Somorjai, G. A.; Yang, P. *Angewandte Chemie-International Edition* **2006**, *45*, 7824-7828.

(19) Kweskin, S. J.; Rioux, R. M.; Habas, S. E.; Komvopoulos, K.; Yang, P.; Somorjai, G. A. *Journal of Physical Chemistry B* **2006**, *110*, 15920-15925.

(20) Bain, C. D.; Davies, P. B.; Ong, T. H.; Ward, R. N.; Brown, M. A. *Langmuir* **1991**, *7*, 1563-1566.

(21) Moore, F. G.; Becraft, K. A.; Richmond, G. L. *Applied Spectroscopy* **2002**, *56*, 1575-1578.

(22) Kung, K. Y.; Chen, P.; Wei, F.; Rupprechter, G.; Shen, Y. R.; Somorjai, G. A. *Review of Scientific Instruments* **2001**, *72*, 1806-1809.

(23) Yang, M.; Tang, D. C.; Somorjai, G. A. *Review of Scientific Instruments* **2003**, *74*, 4554-4557.

(24) Bratlie, K. M.; Flores, L. D.; Somorjai, G. A. *Surface Science* **2005**, *599*, 93-106.

(25) Shen, Y. R. *The Principles of Nonlinear Optics*; Wiley: New York, 2003.

(26) Shen, Y. R. *Annual Review of Physical Chemistry* **1989**, *40*, 327-350.

(27) Shen, Y. R. *Nature* **1989**, *337*, 519-525.

(28) Bain, C. D. *Journal of the Chemical Society, Faraday Transactions* **1995**, *91*, 1281-1296.

(29) Guyot-Sionnest, P.; Hunt, J. H.; Shen, Y. R. *Physical Review Letters* **1987**, *59*, 1597-1600.

(30) Himmelhaus, M.; Eisert, F.; Buck, M.; Grunze, M. *Journal of Physical Chemistry B* **2000**, *104*, 576-584.

(31) Bordenyuk, A. N.; Jayathilake, H. D.; Benderskii, A. V. *Journal of Physical Chemistry B* **2005**, *109*, 15941-15949.

(32) Ihm, H.; Ajo, H. M.; Gottfried, J. M.; Bera, P.; Campbell, C. T. *Journal of Physical Chemistry B* **2004**, *108*, 14627-14633.

(33) Xia, Q.-H.; Hidajat, K.; Kawi, S. *Catalysis Today* **2001**, *68*, 255-262.

(34) Manner, W. L.; Bishop, A. R.; Girolami, G. S.; Nuzzo, R. G. *Journal of Physical Chemistry B* **1998**, *102*, 8816-8824.

(35) Nikoobakht, B.; El-Sayed, M. A. *Langmuir* **2001**, *17*, 6368-6374.

(36) Sikiric, M.; Smit, I.; Tusek-Bozic, L.; Tomasic, V.; Pucic, I.; Primozic, I.; Filipovic-Vincekovic, N. *Langmuir* **2003**, *19*, 10044-10053.

(37) Casal, H. L.; Mantsch, H. H.; Cameron, D. G.; Snyder, R. G. *Journal of Chemical Physics* **1982**, *77*, 2825-2830.